

PLANTATION STUDIES

Volume 1

Proceedings of the
3rd International Symposium on
One Health, One World (OHOW2024)

10 - 12 December 2024
Putrajaya, Malaysia



UPM
UNIVERSITI PUTRA MALAYSIA
BERILMU BERAKHYAT

PUTRA
PERTANIAN UNTUK RAKYAT

PLANTATION STUDIES

Volume 1

Proceedings of the
3rd International Symposium on One Health, One World
(OHOW2024)

10-12 December 2024
Putrajaya, Malaysia

Published by
Institut Kajian Perladangan (IKP)
Universiti Putra Malaysia
43400 UPM Serdang
Selangor Darul Ehsan

©Institut Kajian Perladangan (IKP), 2024

All rights reserved. No part of this book may be reproduced in any form without permission in writing from the publisher. Except by a reviewer who wishes to quote brief passages in a review written for inclusion in a magazine or newspaper.

First Print 2024.

e ISBN 978-629-95253-0-1



EDITORIAL BOARD

Editor-in-Chief

Siti Khairunniza Bejo

Deputy Editor-in-Chief

Wong Mui Yun

Associate Editors

Mohd Rafein Zakaria

Ganesan Vadamalai

Anas Mohd Mustafah

Editors

Siti Nooradzah Adam

Halimatun Saadiah Hafid

Kong Lih Ling

Erneeza Mohd Hata

Fariz Adzmi

Zailani Khuzaimah

Ahmad Faiz Mokhtar

PREFACE

Welcome to the inaugural volume of Plantation Studies. The first volume presents the proceedings of the 3rd International Symposium on One Health, One World (OHOW2024) held on December 10-12, 2024, in Putrajaya, Malaysia. This symposium brought together experts, researchers, and practitioners from various fields to discuss pressing issues related to plantation management, environmental sustainability, and public health.

Plantation Studies is published by the Institute of Plantation Studies (*Institut Kajian Perladangan* (IKP)) at Universiti Putra Malaysia, which has consistently been at the forefront of agricultural research and development. We are proud to provide a platform for the dissemination of knowledge that can influence policy, inform practices, and inspire future research.

In recent years, the interconnectedness of health, environment, and agriculture has become increasingly evident. The One Health concept emphasizes the importance of collaboration across disciplines to address complex challenges that affect both human and ecological health. This volume aims to contribute to that dialogue by featuring a diverse range of topics presented at the symposium, showcasing innovative research and practical solutions from around the globe.

The articles included in this volume cover a wide array of subjects that directly relate to plantation studies. The research presented in this volume highlights critical advancements in enhancing the sustainability and productivity of plantation systems. The integration of renewable energy solutions promotes sustainability while addressing energy needs. Insights into disease management are essential for maintaining crop health, and the application of technology strengthens the resilience of plantation ecosystems. Additionally, the emphasis on innovative strategies for water resource management and climate adaptation is vital for responding to environmental changes affecting productivity.

Moreover, the findings underscore the importance of aligning plantation practices with public health and environmental concerns, informing better management practices and supporting policy development. Addressing disaster management is also crucial, as understanding evacuation factors and urban planning can mitigate risks associated with natural disasters. Collectively, these outcomes provide a comprehensive overview of the current challenges and solutions in plantation management.

The editorial team has worked diligently to ensure a rigorous peer-review process, maintaining high academic standards. We are grateful to our contributors for their valuable insights and to our reviewers for their thoughtful evaluations. As we embark on

this journey, we invite readers to engage with the research presented in this volume. We hope that the findings and discussions will not only advance academic knowledge but also foster collaborative efforts toward sustainable plantation practices and improved health outcomes.

TABLE OF CONTENTS

Paper Title / Author (s)	Page	ID
CARBON EMISSION AND BIODIVERSITY		
MULTI-SCALE ASSESSMENT OF SOLAR FARM EXPANSION USING GEOSPATIAL DATA: A CASE OF TARLAC CITY AND TARLAC PROVINCE, PHILIPPINES J.A. Principe, N.A.H. Arca and C.J.G. Decena	1	101
MAPPING GANODERMA INFECTION IN OIL PALM PLANTATIONS ACROSS MALAYSIA AND INDONESIA USING PALSAR-2 TIME SERIES D.A.S. Daranagama and W. Takeuchi	3	102
DETECTION OF MANGROVE IN COASTAL AREA OF PENINSULAR MALAYSIA USING A MAXIMUM LIKELIHOOD CLASSIFIER Zhao Hengyang, Siti Khairunniza-Bejo, Abdul Rashid Mohamed Shariff and Mahirah Jahari	5	103
MACHINE LEARNING PERFORMANCE ON THE CLASSIFICATION OF BAGWORM INFESTATION AREA USING SMOTE METHOD Siti Nurul Afiah Mohd Johari, Siti Khairunniza-Bejo, Abdul Rashid Mohamed Shariff, Nur Azuan Hussin, Mohamed Mazmira Mohd Masri and Noorhazwani Kamarudin	9	104
ESTIMATED REVENUE CHARACTERISTICS FOCUSED ON THE LONG-TERM BENEFITS OF GREENING Yohei Kawaguchi, Kaori Isawa, Hiroko Hatanabe and Yudai Honma	14	105
A VOLUME PROJECTION MODEL EXPANDABLE TO CARBON SINK CAPACITY: A CASE STUDY ON SABAL FOREST PLOTS W.N.Z. Zainol @ Abdullah, O.F. Marzuki, M.F. Bohari and H. Omar	18	106
CLIMATE CHANGE AND WATER RESOURCES		
DROUGHTS AND DELUGES: NAVIGATING WATER RESOURCE IN SDG PERSPECTIVE AND SAVING WATER RESOURCE USING IOT K. Sivasubramaniyan, S.Tamilarasi, R.Latha, A.Loganathan, S.Vetrivel, J.Gajalakshmi and R.Vijayalakshmi	20	107
EXPLORING THE SURFACE WATER STATUS OF AWD IRRIGATED RICE PADDY FIELDS INTEGRATING SAR-UAV AND IOT TO CLIMATE CHANGE MITIGATION Md Rahedul Islam and Wataru Takeuchi	24	108
THE IMPACT OF LAND USE/COVER CHANGES ON HABITAT QUALITY IN JOHOR RIVER BASIN, MALAYSIA Y.S. Yong and K.D. Kanniah	25	109
CORRELATION AND TIMING BETWEEN REGIONAL WATER STRESS FACTORS AND OIL PALM YIELD USING 22-YEAR SATELLITE DATA IN MALAYSIA AND INDONESIA C. Naito and W. Takeuchi	31	110
ADAPTING TO CLIMATE CHANGE: MITIGATIVE AND ADAPTIVE APPROACHES IN INDONESIA'S PALM OIL INDUSTRY Nuzul Hijri Darlan, Iman Yani Harahap	33	111

REMOTE SENSING FOR CLIMATE CHANGE, GREEN RECOVERY AND SUSTAINABILITY	37	112
--	----	-----

Helmi Zulhaidi Mohd Shafri

INNOVATIVE SYSTEMS FOR A SUSTAINABLE BUILT ENVIRONMENT

SUSTAINABLE BUILT DEVELOPMENT AND CLIMATE CHANGE ADAPTION: A CASE STUDY FROM LEH, LADAKH, INDIA	38	113
---	----	-----

Surender K Negi, Kishor S. Kulkarni, Ajay Chourasia and P. K. Ramancharla

NON-CHLORINATED CELLULOSE EXTRACTION FROM AGRICULTURAL BIOMASS AND ITS POTENTIAL APPLICATION AS PACKAGING MATERIALS	41	114
---	----	-----

Hafid H.S. and Omar F.N.

SEISMIC RESILIENT & SUSTAINABLE CONSTRUCTION UTILISING STONES AND WOODS IN KATH KUNI CONSTRUCTION STYLE	43	115
---	----	-----

Ashish Pippal, Surender K Negi, Ajay Chourasia and Shaina Sachdeva

AUTOMATED EXTRACTION AND SEGMENTATION OF TUNNEL UTILITIES FOR ENHANCED DAMAGE DETECTION USING 3D LIDAR DATA	47	116
---	----	-----

A. Regmi and T. Mizutani

TESTING THE EFFECTIVENESS OF AN INCENTIVE-BASED BICYCLE REALLOCATION APPROACH IN A SHARED CYCLE SYSTEM	49	117
--	----	-----

Takashi Miyazawa and Kazuyuki Takada

SUSTAINABLE 3D CONCRETE PRINTING: ENHANCING MECHANICAL PROPERTIES WITH BAGASSE ASH AS A CEMENT REPLACEMENT	52	118
--	----	-----

A. Kapoor and A. Chourasia

CHEMICAL SENSORS FOR ONE HEALTH, ONE WORLD	57	119
--	----	-----

Tsuyoshi Minami

INTERNATIONAL PUBLIC HEALTH RESEARCH IN ASIA

PATTERN ANALYSIS OF CHANGES IN PRODUCTION ACTIVITIES IN THAI INDUSTRIAL COMPLEXES USING ALTERNATIVE DATA	59	120
--	----	-----

A. Kodaka, N. Leelawat and N. Kohtake

REGIONAL ESTIMATION OF FUTURE DEMAND FOR MEDICINES NEEDED IN THE EVENT OF A LARGE-SCALE EARTHQUAKE DISASTER: FOR A SMALL CITY IN A RURAL AREA IN JAPAN USING MEDICAL BIG DATA	61	121
---	----	-----

Ken Takakuwa, Yuma Morisaki, Makoto Fujiu and Yuta Baba

WHAT SDGS DON'T MEASURE: NON-ACTIONABLE URBAN WELL-BEING FACTORS THROUGH GISCIENCE	62	122
--	----	-----

G.Y. Yan, Y. Yue, W. Takeuchi, Y.Q. Chen and B.H. Li

TOTAL CARBON STOCK ESTIMATION FOR RUBBER PLANTATION USING UNMANNED AERIAL VEHICLE IMAGERY	64	123
---	----	-----

Zailani Khuzaimah, Hishamuddin Hashim and Nazmi Mat Nawi

THE IMPACT OF SPECTROSCOPY IN PLANT DISEASE DETECTION, ENVIRONMENTAL SUSTAINABILITY AND PUBLIC HEALTH	66	124
--	----	-----

Siti Nooradzah Adam, Siti Khairunniza Bejo and Nazmi Mat Nawi

SMART CITIES AND TRANSPORT

OPTIMAL LOCATION OF WIRELESS POWER TRANSFER SYSTEMS FOR URBAN RESILI- ENCE AND SUSTAINABLE TRANSPORTATION	68	125
--	----	-----

Yudai Honma

IMPACT ASSESSMENT OF FARE INCREASES AND CONSCIOUSNESS OF RAILWAY USERS' REGARDING THE HOKURIKU SHINKANSEN TSURUGA EXTENSION	72	126
---	----	-----

K. Nishioka, M. Fujiu and Y. Morisaki

RESAERCH ON APPROPRIATE USE OF DEMAND TAXIS FOR TRANSPORTATION PURPOSES	74	127
--	----	-----

Taiki Mukoyama and Kazuyuki Takada

FLOW OF PEOPLE USING SENSING DEVICES IN DILI, DEMOCRATIC REPUBLIC OF TIMOR-LESTE	77	128
---	----	-----

Y. Minematsu, M. Fujiu, Y. Morisaki and Y. Kon

INVESTIGATING THE RELATIONSHIP BETWEEN CITY COMPACTNESS AND LIVABILITY IN JAPAN	79	129
--	----	-----

T. Kondo and W. Takeuchi

PROPOSAL OF BASE LOOP STRATEGY FOR MULTI-RETAILER AND MULTI- CUSTOMER DE LIVERY SERVICE BY AUTOMATED DELIVERY ROBOTS	81	130
---	----	-----

Motoya Ueda, Hiroyuki Hasada, Kaori Isawa and Yudai Honma

ESTIMATION OF GROUND DEFORMATION IN SUZU CITY WITH ALOS-2/PALSAR-2 DATA	85	131
--	----	-----

Yifan Yang Hideomi Gokon and Wataru Takeuchi

ANALYSIS OF THE MEASUREMENT OF POPULATION FLOW BASED ON NON- CONTACT SENSING DEVICES IN PHITSANULOK PROVINCE, THAILAND	87	132
---	----	-----

H. Kawakami, M. Fujiu, Y. Morisaki, Y. Kon and Jaruan Daengbuppha

INFRASTRUCTURE MANAGEMENT

STUDY ON AN EARLY WARNING SYSTEM FOR DISASTER MITIGATION USING GROUND-BASED SAR	89	133
--	----	-----

Y. Izumi and M. Sato

EFFECT OF MIXING WITH STEEL SLAG ON MODIFICATION OF SIMULATED UNDER- SIEVE RESIDUE	91	134
---	----	-----

H. Hu and Y. Kikuchi

ANALYSIS OF SATISFACTION EVALUATION OF FOREIGNER TO JAPAN AT RESTAURANTS IN REGIONAL SIGHTSEEING CITIES: STUDY OF THE USING REVIEWS DATA FROM TRAVEL INFORMATION WEBSITE	96	135
--	----	-----

Y. Baba, M. Fujiu and Y. Morisak

AUTOMATION OF REBAR SEGMENTATION IN GPR USING BINARY IMAGES FOCUSING ON DIAGONAL CONVEXITY AND DOWNWARD SEARCH CLUSTERING ALGORITHM	98	136
S. Iwai and T. Mizutani		
ESTIMATING PAVEMENT CONDITION USING PUBLICLY AVAILABLE SATELLITE IMAGERY FOR DATA-DRIVEN ROAD MAINTENANCE PLANNING	100	137
Takuma Ooba, Angela Odera, Azam Amir and Michael Henry		
POTENTIAL ASSESSMENT OF VERTICAL SOLAR PV SYSTEMS FOR POWER PRODUCTION AND THERMAL PERFORMANCE IN TROPICAL BUILDING ENVELOPES	102	138
A.L. Marquez, J.A. Principe and J.J.L. Seranilla		
ECONOMIC IMPACT ANALYSIS CONSIDERING RECONSTRUCTION FOR ASSISTANCE DURING LARGE-SCALE EARTHQUAKE DISASTER FOCUSED ON CRUISE SHIPS PASSENGERS CALLING AT KANAZAWA PORT	104	139
K. Nakabayashi, M. Fujiu, Y. Morisaki and Y. Yamaya		
EFFECTIVE USE OF TUNNEL FACE OBSERVATION RECORDS DURING TUNNEL CONSTRUCTION FOR RENEWAL OF ABANDONED TUNNEL	106	140
Ami Shirai, Tomohisa Kosegawa and Shinji Konishi		
DISASTER AND POST DISASTER		
ANALYSIS OF WHAT SHOULD BE DONE AFTER A DISASTER AND THE CURRENT SITUATION IN JAPAN WHERE THIS IS DIFFICULT TO DO	108	141
Tetsuro Ito		
COMPREHENSIVE ASSESSMENT OF THE PERNOTE LANDSLIDE, RAMBAN DISTRICT, JAMMU & KASHMIR UNION TERRITORY (INDIA)	110	142
Debi Prasanna Kanungo, Rajesh Kumar Dash and Pradeep Kumar Ramancharla		
ANALYSIS OF EVACUATION FACTORS FOR FAMILIES WITH INFANTS AND TODDLERS CONSIDERING PRIVACY IN EVACUATION SHELTERS	112	143
D. Naoi, Y. Morisaki and M. Fujiu		
GIS CHARACTERISATION FOR FOREST WEATHER INDEX (FWI) IN PEATLAND FOREST	114	144
Nureen Natasya Mohd Saufi, Aduwati Sali and Sheriza Mohd Razali		
ANALYSIS OF CRUISE SHIP PASSENGERS' BEHAVIOR DURING EARTHQUAKE DISASTER: CASE STUDY OF KANAZAWA PORT	116	145
Y. Yamaya, M. Fujiu, Y. Morisaki and K. Nakabayashi		
ANALYSIS OF POPULATION DYNAMICS IN THE DISASTER AREA BEFORE AND AFTER THE 2024 NOTO PENINSULA EARTHQUAKE: EXAMINATION USING KDDI LOCATION ANALYZER	118	146
T. Mashio, Y. Morisaki and M. Fujiu		
FIELD INVESTIGATION OF THE 30TH JULY 2024 WAYANAD DEBRIS FLOW OF WESTERN GHAT, INDIA	119	147
R.K. Dash, A. Chourasia, R. Pradeep Kumar and D.P. Kanungo		

FROM LANDSLIDE SUSCEPTIBILITY TO HAZARD & RISK MODELING: A SPACE-TIME PERSPECTIVE	120	148
S. Das, D.P. Kanungo and S. Sarkar		
A FRAMEWORK FOR GEO-INTEGRATED RAINFALL THRESHOLDING AND UAV BASED LANDSLIDE MONITORING	122	149
R. Pati, R. Dash and D.P. Kanungo		
STRUCTURAL VULNERABILITY		
TSUNAMI EVACUATION RISK CHANGES IN BANDA ACEH AFTER 2004 INDIAN OCEAN TSUNAMI	124	150
O. Murao, M. Sato, K. Sugiyasu, H. Miura, M. Khoiriyah, R. Saito and M. Affan		
PREDICTING BUILDING RISK IN LAND SUBSIDENCE-PRONE AREAS: THE ROLE OF DECISION TREE REGRESSION MODEL IN URBAN SAFETY	126	151
K.S. Kulkarni, S.K. Negi, A. Chourasia and P. K. Ramancharla		
SIMPLIFIED VULNERABILITY ASSESSMENT FOR MASONRY BUILDINGS USING FRAGILITY CURVE	129	152
A. Chourasia, A. Pain, R. Pradeep Kumar and A. Minhas		
DEVELOPMENT OF A POTENTIAL INDEX FOR UTILIZATION OF VACANT HOUSES CONSIDERING DISASTER RISK: A CASE STUDY OF HATOYAMA TOWN, SAITAMA PREFECTURE	132	153
A. Sasaki, Y. Morisaki and M. Fujiu		
DEM STUDY ON THE STRESS DISTRIBUTION OF MUCK AND FOAM IN THE EPB SHIELD CHAMBER	134	154
J. Jiang and R. Kuwano		
ROBUSTNESS OF TRAFFIC NETWORKS: ANALYZING DAMAGE AND RECOVERY PROCESS AGAINST REPEATED DISASTERS	139	155
T. Tateishi, H. Hasada, H. Watanabe and Y. Honma		
DETECTION OF MILLIMETER-SCALE DEFORMATIONS AT JATILUHUR DAM USING PERSISTENT SCATTERER INSAR (PS-INSAR)	141	156
Arliandy P. Arbad and Wataru Takeuchi		
OUT-OF-PLANE BEHAVIOUR OF MASONRY WALL STRENGTHENED USING TEXTILE REINFORCEMENT	143	157
R. Siva Chidambaaram, S.Saranya, Ajay Chourasia and R. Pradeep Kumar		
SATELLITE IMAGERY METHOD FOR ESTIMATING CONSTRUCTION YEARS OF ROAD BRIDGES	146	158
K. Matsumoto and B. Hamunzala		
DEEP LEARNING BASED APPROACHES FOR LANDSLIDE DETECTION	148	159
P. Sharma, S. Das, A. Pain and D.P. Kanungo		

MULTI-SCALE ASSESSMENT OF SOLAR FARM EXPANSION USING GEOSPATIAL DATA: A CASE OF TARLAC CITY AND TARLAC PROVINCE, PHILIPPINES

J.A. PRINCIPE*, N.A.H. ARCA and C.J.G. DECENA

Department of Geodetic Engineering, University of the Philippines Diliman, Quezon City, Philippines

**Correspondence: japrincipe@up.edu.ph*

Keywords: Solar farm, Remote sensing, GIS, cropland, MOLUSCE

1. INTRODUCTION

Over the past decade, countries worldwide have significantly ramped up efforts to utilize renewable energy (RE) sources. This rapid increase in RE adoption is driven by global climate agreements, technological advancements, supportive government policies, and concerns over environmental and energy security. Due to its advantages in terms of being low carbon resource, scalability, and technological maturity, solar has become one of the most widely adopted RE sources playing a key role in enhancing energy security [1]. However, placing solar farms on former agricultural land raises concerns about food security and ecological impacts [2]. The objective of this study is to assess solar farm expansion impacts at both city and provincial levels using geospatial data.

2. DATA AND METHODS

This study used various satellite-derived data, including MODIS land cover (MCD12Q1), VIIRS nighttime lights, AHI-8/9 shortwave radiation, and the SRTM Digital Elevation Model. Additional geospatial layers, such as road networks, power lines, land use/land cover (LULC), and substation locations, are utilized to model solar farm expansion. To predict LULC changes, the study used several transition potential modeling (TPM) methods through CA-Markov simulations in QGIS's MOLUSCE plugin. For city-level analysis, land cover transitions to solar farm were generated from MCD12Q1 LC data only. In provincial level analysis, the different spatial variables were included for TPM and solar farm expansion modelling via the CA-Markov method in MOLUSCE plugin of QGIS (Figure 1).

3. RESULTS AND DISCUSSIONS

Results showed a gradual LULC shift from cropland to grassland, then to solar farms over 16 years in city-level analysis. However, the MCD12Q1 dataset's coarse resolution limits the accuracy of solar farm expansion modelling. In provincial-level analysis, the use of the NAMRIA LULC dataset and WoE TPM produced the highest F1 score (0.772) and IoU (0.628), making it the most

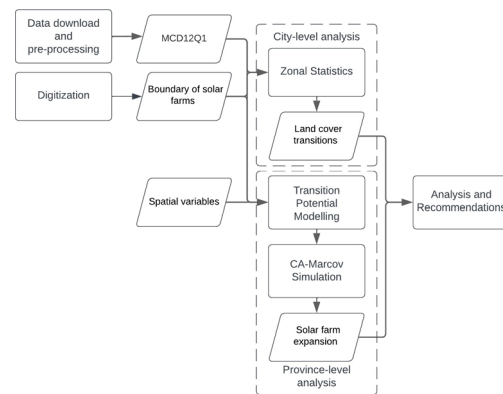


Figure 1. Methodology of this study

accurate for modelling solar expansion. By 2040, Tarlac Province is projected to lose approximately 135 ha of cropland due to solar farm expansion, yielding an estimated annual additional capacity of 877.75 MWh and a carbon emissions reduction of 24,105.28 tCO₂e (Figure 2).

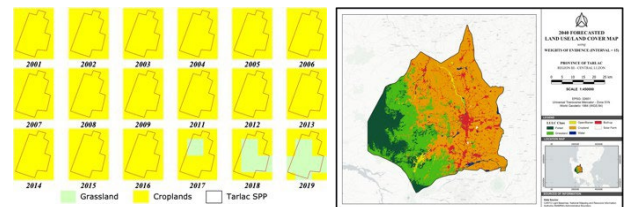


Figure 2. Left: LULC maps for Tarlac SPP (2001-2019); Right: 2040 forecasted LULC simulated using the NAMRIA LULC data WoE TPM approach

4. CONCLUSIONS

This study used geospatial data to analyze solar farm expansion in Tarlac, Philippines. While MCD12Q1's coarse resolution proved insufficient, decrease in canopy cover may signal land transitions to solar farms. Higher-resolution land cover data and machine learning enhanced model accuracy. Results of this study underscore the need for strategic planning to balance renewable energy growth with agricultural land preservation, supporting both energy and food security.

5. ACKNOWLEDGMENTS

DOST-SEI and ERDT Program for the research dissemination grant.

REFERENCES

- [1] D.L. Chandler, "Explaining the plummeting cost of solar power," 20 November 2018. [Online]. Available: <http://news.mit.edu/2018/explaining-dropping-solar-cost-1120>. [Accessed Nov 2024].
- [2] N. Gomez-Casanovas et al., "Knowns, uncertainties, and challenges in agrivoltaics to sustainably intensify energy and food production," *Cell Reports Physical Science*, 4(8) (2023).

MAPPING GANODERMA INFECTION IN OIL PALM PLANTATIONS ACROSS MALAYSIA AND INDONESIA USING PALSAR-2 TIME SERIES

D.A.S. DARANAGAMA¹ and W. TAKEUCHI^{2*}

¹ Department of Civil Engineering, The University of Tokyo, Tokyo, Japan

² Institute of Industrial Science, The University of Tokyo, Tokyo, Japan

*Correspondence: wataru@iis.u-tokyo.ac.jp

Keywords: Oil palm, Ganoderma, SAR, ALOS PALSAR, Linear regression

1. INTRODUCTION

The oil palm is a globally vital crop for vegetable oil production and is particularly crucial for Southeast Asia's economy specially in Malaysia and Indonesia. However, the sustainability of oil palm plantations in this region is under significant threat from Ganoderma disease, which can lead to severe yield loss. Current methods for managing and detecting the spread of this disease are inadequate [1]. This study utilizes 25 m resolution PALSAR-2 global mosaic time-series data (2015–2023) to identify Ganoderma-infected oil palm plantations in Malaysia and Indonesia through linear regression-based trend analysis.

2. METHODOLOGY

This study was, conducted in Google Earth Engine platform. The HV polarization backscatter values were extracted and masked to focus on oil palm plantations in Malaysia and Indonesia [2]. Linear regression-based trend analysis was applied to HV polarization backscatter data to identify pixels with significant negative slopes (threshold < -0.4) as potential indicators of infection. Following this, annual backscatter declines were analyzed for each pixel, and a cumulative decline count was computed to assess persistence, resulting in the creation of the Ganoderma age map. The findings were validated using field data, with accuracy assessed through precision, recall and F1 score metrics. Figure 1 shows the overall methodology.

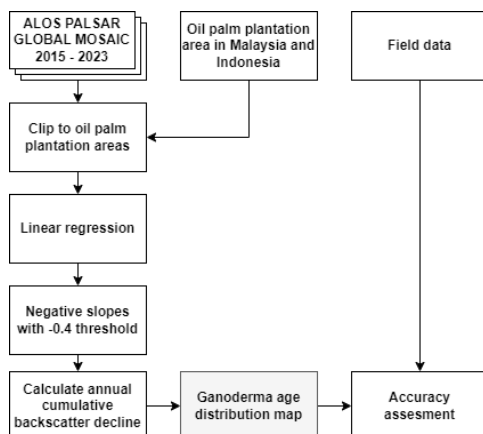


Figure 1. The overall study flow

3. RESULTS AND DISCUSSIONS

Figure 2 shows the Ganoderma age map across Malaysia and Indonesia indicating the duration of the HV backscatter decline.

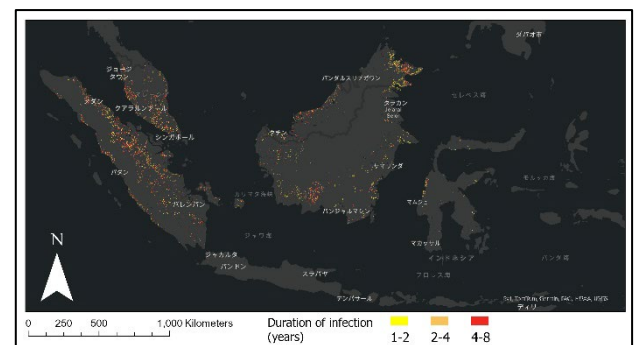


Figure 2. Ganoderma age map

Figure 3 illustrates the yearly variation in the number of pixels undergoing decline, providing insights into the dynamics of Ganoderma progression.

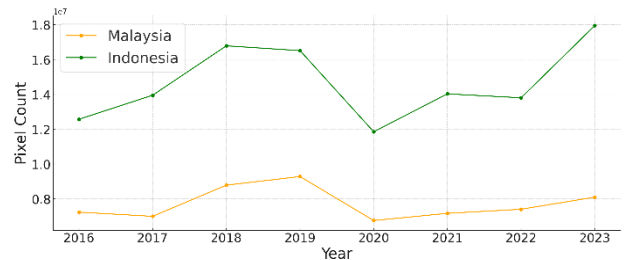


Figure 3. Yearly variation of Ganoderma disease

The accuracy assessment was conducted using field data, with precision, recall, and F1 score obtained as 0.76, 0.39, and 0.52 respectively.

4. CONCLUSION

The study identifies areas of Ganoderma infection, providing insights into disease dynamics. These findings support targeted and scalable disease management interventions to mitigate Ganoderma's impact on the oil palm industry.

REFERENCES

- [1] Jazuli, N.A., Kamu, A., Chong, K.P., Gabda, D., Hassan, A., Abu Seman, I. and Ho, C.M., 2022.

- A review of factors affecting Ganoderma basal stem rot disease progress in oil palm. *Plants*, 11 (19), 2462.
- [2] Descals, A., Wich, S., Meijaard, E., Gaveau, D.L., Peedell, S. and Szantoi, Z., 2020. High-resolution global map of smallholder and industrial closed-canopy oil palm plantations. *Earth System Science Data Discussions*, 2020, pp.1-22.

DETECTION OF MANGROVE IN COASTAL AREA OF PENINSULAR MALAYSIA USING A MAXIMUM LIKELIHOOD CLASSIFIER

ZHAO HENGYANG¹, SITI KHAIRUNNIZA-BEJO^{1,2,3,*}, ABDUL RASHID MOHAMED SHARIFF^{1,3}
and MAHIRAH JAHARI^{1,3}

¹*Department of Biological and Agricultural Engineering, Faculty of Engineering, Universiti Putra Malaysia, Malaysia*

²*Institute of Plantation Studies, Universiti Putra Malaysia, Malaysia*

³*Smart Farming Technology Research Centre, Universiti Putra Malaysia, Malaysia*

*Correspondence: skbejo@upm.edu.my

Keywords: Landsat-9, Mangrove extraction, OIF, MLC, Peninsular Malaysia

1. INTRODUCTION

Malaysia has the second largest mangrove cover area in Southeast Asia (approximately 11.7%) [1] with the estimated growth rate of 1% or 1,282 hectares per year since 1990s [4]. Mangrove studies have been conducted in Malaysia for many years to study and determine the extent of the existing mangrove forests [2-8].

Remote sensing technology has been used as a precedent for detecting and mapping mangrove distribution since the 1990s [9-11]. Combined with the fact that mangrove ecosystems mostly grow in muddy swamp areas or foreshore zones, it poses a huge challenge for field detection and measurement [12-16]. Sulong et al. [2] used aerial images and Landsat TM images to classify mangroves in Kemaman area of Peninsular Malaysia in 2002 and obtained 87.8% accuracy.

Meanwhile, Azian et al. [3] used SPOT 4 satellite images to detect and map the change of mangrove area in Perak from 1989 to 2000, with an overall classification accuracy of more than 70%. Kanniah et al. [4] used Landsat satellites series, including TM, ETM and OLI sensors, to study mangrove cover changes in Iskandar region of Malaysia over 25 years from 1989 to 2014 and demonstrated that the maximum likelihood has higher accuracy than the SVM classification.

Likewise, Ibrahim et al. [5], used series of Landsat images to analyze the land use change in Matang mangrove reserve from 1993 to 2011 by applying the MLC classification method. Satyanarayana et al. [6] used ALOS (Advanced Land Observation Satellite) and ground-based observation data to examine undisturbed mangrove forests in the Brunei Bay, which located in East Malaysia.

To date, most of the studies focused on mangrove cover and mangrove changes in parts of Malaysia, and did not involve the large-scale detection area in Malaysia except for Omar et al. [7] and Gopalakrishnan et al. [8]. However, the latest study on mangrove detection in Peninsular Malaysia and

Malaysia mentioned before was reported for year 2021 [7,8], and so far, none of the study used Landsat-9 which was released on September 27, 2021.

Meanwhile, Landsat-9 has great consistency and higher radiation resolution which can be complemented with other Landsat data to improve imaging temporal resolution [17]. Moreover, the data of Landsat-9 is no less capable than Landsat-8 in detecting coastal water bodies and extracting vegetation index such as NDVI, NDMI and etc [18,19].

2. MATERIAL AND METHODS

2.1 Study Area

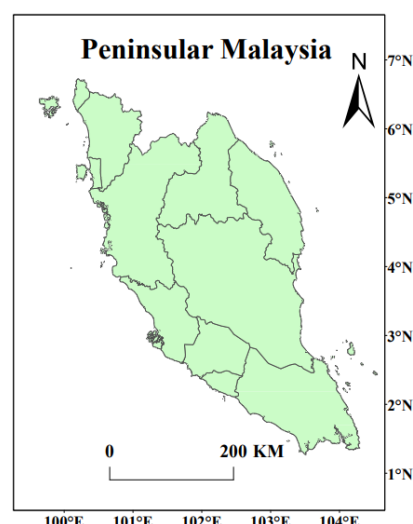


Figure 1. Peninsular Malaysia

The study area was located at Peninsular Malaysia as in Figure 1. It has a predominantly tropical rainforest climate with an average annual temperature between 26°C to 28.7°C [20,21]. Mangroves area in Peninsular Malaysia account for about 17% (0.58 ha) of the total mangrove forest in Malaysia [4,22], which have brought great ecological, economic and social benefits to its people [23].

2.2 Methodology

Figure 2 shows flowchart of the methodology for this study. Specific steps as follow: It starts with data collection of Landsat-9 satellite image and then followed by image processing, classification and finally data verification. ENVI5.6.3 software was used. Band fusion between a clean image after atmospheric correction and a panchromatic band was used to enhance the image. Seamless mosaic was used to synthesize multi-band images of target areas and Region of Interest (ROI) selection tool was used to select training samples for the six land cover types, namely tidal area, other vegetation, mangrove, water, build-up area and bare land. The most suitable bands used to make false composite was chosen based on Optimum Index Factor (OIF) index [24].

The separability analysis of the ROI sample was carried out. ROI separability values between the six land cover types were greater than 1.9, which indicated that the samples were suitable for the next step of classification [25]. The maximum likelihood method was used to class the study area. Meanwhile, data verification was based on Google Earth historical images by selecting verification points to verify the accuracy of the results of the classification map.

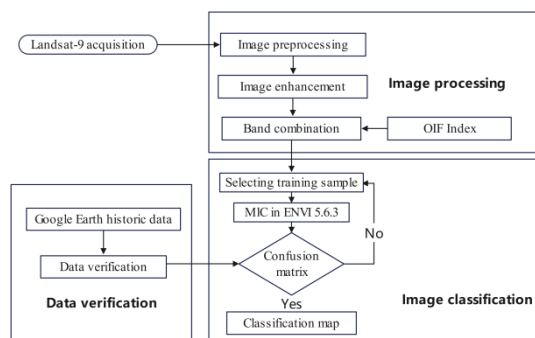


Figure 2. Flowchart of the methodology

More than 500 land cover areas were selected as ROI for each class. These samples of ROI are distributed as evenly as possible in the study area.

3. RESULTS AND DISCUSSIONS

Meanwhile, the result of the accuracy index is shown in Table 1. The accuracy of producers for the six classes for mangrove, water body, other vegetation, tidal area, built-up area and bare land is 100%, 99.53%, 99.44%, 100%, 99.96% and 98.91%, respectively. The accuracy of users for the six classes for mangrove, water body, other vegetation, tidal area, built-up area and bare land were 96.56%, 100%, 100%, 100%, 88.80% and 99.58%, respectively. Therefore, the extraction accuracy of mangroves is acceptable because the overall accuracy of those regions is greater than 90%, and the Kappa coefficient of the classification

results is also between 0.81 and 1, which can show excellent to perfect agreement [25,26].

Table 1. Accuracy indices estimated from the classification image

Indices	Mangrove	Water	Other vegetation	Tidal area	Built-up area	Bare land
Producer's Accuracy %	100	99.5	99.4	100	99.9	98.9
User's Accuracy %	96.5	100	100	100	88.8	99.5
Overall Accuracy %	99.787%					
Kappa Coefficient	0.983					

Total area of the six-land cover from the classification map is tabulated in Table 2. The highest area is the water body, which has reached 36805.4km²; It is followed by other vegetation (25440.2km²), built-up area (5829.4 km²), bare land (5451.1km²), tidal area (1197.5 km²) and mangrove area (950.7 km²).

Table 2. Total area of the six-land cover from the classification map

Attribute	Area(km ²)
Tidal area	1197.474
Other vegetation	25440.153
Mangrove	950.745
Water	36805.381
Built-up area	5829.386
Bare land	5451.123

4. CONCLUSIONS

The mangrove distribution in Peninsular Malaysia was successfully detected and extracted based on the latest Landsat-9 images. The result of our classification is that there are 950.7km² of mangroves in the target area, which is 95,075 hectares of mangroves spread over the coastal area of Peninsular Malaysia in recent years from 2023 to 2024. Compared with previous studies in 2018 there was 962.97km² of mangrove area [8], which can explain the changes in five years, and the mangrove area in Peninsular Malaysia basically remained unchanged sharply, but the rate of mangrove loss in Peninsular Malaysia is consistent with previous researchers' calculations of an overall decline of 1% per year [4]. Therefore, it can be shown that the mangrove protection measures in Malaysia in the past five years have played a positive effect.

REFERENCES

- [1] Giesen, W., Wulffraat, S., Zieren, M., & Scholten, L. (2007). Mangrove guidebook for Southeast Asia.
- [2] Sulong, I., Mohd-Lokman, H., Mohd-Tarmizi, K., & Ismail, A. (2002). Mangrove mapping

- using Landsat imagery and aerial photographs: Kemaman District, Terengganu, Malaysia. *Environment, Development and Sustainability*, 4, 135-152.
- [3] Hasmadi, I. M. (2009). The use of remote sensing for monitoring spatial and temporal changes in mangrove management. *The Malaysian Forester*, 72(1), 15-22.
- [4] Kanniah, K. D., Sheikhi, A., Cracknell, A. P., Goh, H. C., Tan, K. P., Ho, C. S., & Rasli, F. N. (2015). Satellite images for monitoring mangrove cover changes in a fast-growing economic region in southern Peninsular Malaysia. *Remote Sensing*, 7(11), 14360-14385.
- [5] Ibrahim, N. A., Mustapha, M. A., Lihan, T., & Mazlan, A. G. (2015). Mapping mangrove changes in the Matang Mangrove Forest using multi temporal satellite imageries. *Ocean & coastal management*, 114, 64-76.
- [6] Satyanarayana, B., Muslim, A. M., Horsali, N. A. I., Zauki, N. A. M., Otero, V., Nadzri, M. I., ... & Dahdouh-Guebas, F. (2018). Status of the undisturbed mangroves at Brunei Bay, East Malaysia: a preliminary assessment based on remote sensing and ground-truth observations. *PeerJ*, 6, e4397.
- [7] Omar, H., & Misman, M. A. (2020). Extents and distribution of mangroves in Malaysia. *Mangroves*, 2.
- [8] Gopalakrishnan, L., Satyanarayana, B., Chen, D., Wolswijk, G., Amir, A. A., Vandegehuchte, M. B., ... & Dahdouh-Guebas, F. (2021). Using historical archives and landsat imagery to explore changes in the mangrove cover of Peninsular Malaysia between 1853 and 2018. *Remote Sensing*, 13(17), 3403.
- [9] Das, S., & Crépin, A. S. (2013). Mangroves can provide protection against wind damage during storms. *Estuarine, Coastal and Shelf Science*, 134, 98-107.
- [10] Hu, W., Wang, Y., Zhang, D., Yu, W., Chen, G., Xie, T., ... & Chen, B. (2020). Mapping the potential of mangrove forest restoration based on species distribution models: A case study in China. *Science of The Total Environment*, 748, 142321.
- [11] Karmaker, S. (2006). Study of Mangrove Biomass. Net Primary Production & Species Distribution using Optical & Microwave Remote Sensing Data (Doctoral dissertation, Indian Institute of Remote Sensing).
- [12] Zhao, C., & Qin, C. Z. (2020). 10-m-resolution mangrove maps of China derived from multi-source and multi-temporal satellite observations. *ISPRS Journal of Photogrammetry and Remote Sensing*, 169, 389-405.
- [13] Wang, L., Jia, M., Yin, D., & Tian, J. (2019). A review of remote sensing for mangrove forests: 1956–2018. *Remote Sensing of Environment*, 231, 111223.
- [14] Zhang, J., Yang, X., Wang, Z., Zhang, T., & Liu, X. (2021). Remote sensing based spatial-temporal monitoring of the changes in coastline mangrove forests in China over the last 40 years. *Remote sensing*, 13(10), 1986.
- [15] Liu, X., Yang, X., Zhang, T., Wang, Z., Zhang, J., Liu, Y., & Liu, B. (2022). Remote sensing based conservation effectiveness evaluation of mangrove reserves in China. *Remote Sensing*, 14(6), 1386.
- [16] Hu, L., Li, W., & Xu, B. (2018). Monitoring mangrove forest change in China from 1990 to 2015 using Landsat-derived spectral-temporal variability metrics. *International Journal of Applied Earth Observation and Geoinformation*, 73, 88-98.
- [17] Li, X., Zhang, D., Jiang, C., Zhao, Y., Li, H., Lu, D., & Liu, S. (2022). Comparison of lake area extraction algorithms in Qinghai Tibet plateau leveraging google earth engine and landsat-9 data. *Remote Sensing*, 14(18), 4612.
- [18] Esendağlı, Ç., Selim, S., & Demir, N. (2022). Comparison of shoreline extraction indexes performance using Landsat 9 satellite images in the heterogeneous coastal area. *Intercontinental Geoinformation Days*, 4, 199-202.
- [19] Chen, J., Wang, Y., Wang, J., Zhang, Y., Xu, Y., Yang, O., & Hu, Z. (2024). The Performance of Landsat-8 and Landsat-9 Data for Water Body Extraction Based on Various Water Indices: A Comparative Analysis. *Remote Sensing*, 16(11), 1984.
- [20] Peel, M. C., Finlayson, B. L., & McMahon, T. A. (2007). Updated world map of the Köppen-Geiger climate classification. *Hydrology and earth system sciences*, 11(5), 1633-1644.
- [21] Tang, K. H. D. (2019). Climate change in Malaysia: Trends, contributors, impacts, mitigation and adaptations. *Science of the Total Environment*, 650, 1858-1871.
- [22] Omar, H. Mangroves threats and changes. In *Status of Mangroves in Peninsular Malaysia*; Omar, M., Aziz, K., Shamsudin, I., Raja Barizian, R.S., Eds.; Forest Research Institute Malaysia: Kuala Lumpur, Malaysia, 2012; pp. 89–110.
- [23] Azian, M.; Mubarak, H.T. Functions and values of mangroves. In *Status of Mangroves in Peninsular Malaysia*; Omar, M., Aziz, K., Shamsudin, I., Raja Barizian, R.S., Eds.; Forest Research Institute Malaysia: Kuala Lumpur, Malaysia, 2012; pp. 12–25.
- [24] Chavez, P. S., Berlin, G. L., & Sowers, L. B. (1982). Statistical method for selecting Landsat MSS ratios.

- [25]Ma, C., Ai, B., Zhao, J., Xu, X., & Huang, W. (2019). Change detection of mangrove forests in coastal Guangdong during the past three decades based on remote sensing data. *Remote Sensing*, 11(8), 921.
- [26]Landis, J. R. (1977). The Measurement of Observer Agreement for Categorical Data. *Biometrics*.

MACHINE LEARNING PERFORMANCE ON THE CLASSIFICATION OF BAGWORM INFESTATION AREA USING SMOTE METHOD

SITI NURUL AFIAH MOHD JOHARI¹, SITI KHAIRUNNIZA-BEJO^{1,2,3,*},
ABDUL RASHID MOHAMED SHARIFF^{1,2,3}, NUR AZUAN HUSSIN^{1,3},
MOHAMED MAZMIRA MOHD MASRI⁴ and NOORHAZWANI KAMARUDIN⁴

¹Department of Biological and Agricultural Engineering, Faculty of Engineering, Universiti Putra Malaysia, Malaysia,

²Institute of Plantation Studies, Universiti Putra Malaysia, Malaysia,

³Smart Farming Technology Research Centre, Universiti Putra Malaysia, Malaysia

⁴Malaysian Palm Oil Board (MPOB), Persiaran Institusi, Malaysia

*Correspondance: skbejo@upm.edu.my

Keywords: Bagworm infestation, Pest, Machine learning, SMOTE, Oversampling

1. INTRODUCTION

Bagworm, known as *Metisa plana* (Lepidoptera: Psychidae), is one of the serious pest threats to Malaysia oil palm plantation. They can appear in huge numbers and eventually spread like epidemic due to their rapid reproduction and brief life span with an average life span of 103.5 days. This allows them to consistently expand and cause major negative impact to oil palm yield due to 10% to 13% leaf defoliation and up to 40% crop losses [1-3].

According to Chung [4], first sign of the bagworm damage on the fronds are the smallest holes due to bagworm feeding, as they eat immediately upon hatching. The upper surface of the frond was scraped until it dried out and developed holes. The outbreaks are easier to spot when there are numerous dried fronds and holes. When holes in the foliage first appear, it is considered low infestation. However, when multiple holes and necrosis show up, it is considered mild infestation and needs to be treated immediately to avoid becoming severe. Once a palm has a serious infestation of bagworms, the fronds become completely dry and brown.

Pre-censuses were typically carried out manually every two weeks by chopping down a frond in the middle of the canopy that showed new damage symptoms to count the number of larvae on both sides of the frond. According to Malaysian Palm Oil Board's Standard Operating Procedure (SOP) for bagworm control (2016), 1% of the infested area is used for the census, and one palm out of every tenth palm in every tenth row is sampled.

The presence of ten larvae on each frond was deemed to be a critical early defoliation. Based on Kamarudin et al. [5], control measures ought to be initiated right away when the larval population is in its early stages and above the threshold (5–10 larvae per frond). Nevertheless, if more than 70% of the population is in the late instar stage, control

measures should not be implemented until the next generation of early larval stages emerges.

To cover a larger area, this manual method typically takes longer and requires more labor. Therefore, a fast and reliable manner would be helpful to determine the extent of the bagworm infestation in a using remote sensing as the decisions about controlling the outbreak could be made in a timely manner. Unmanned aerial vehicles (UAVs) have advanced to a new level due to their capacity to gather broad field data at low altitudes and produce crop images with astonishingly high spatial resolution by being equipped with a variety of sensor types, including visual RGB (red, green, and blue) cameras, multispectral cameras, hyperspectral cameras, and thermal cameras. UAVs are more effective than ground systems because they can quickly cover a large field and, most importantly, in a non-destructive manner, which is particularly useful for detecting crop pests and diseases [6,7].

According to Neupane & Baysal-Gurel [8], the most popular sensor for detecting pests and diseases is the multispectral camera which can collect the spectral data needed to calculate vital vegetation indices (VIs) such as normalized difference vegetation index (NDVI), the green normalized difference vegetation index (GNDVI), the normalized difference red edge (NDRE). The valuable features represented by these vegetation indices were subsequently processed using machine learning (ML), a widely recognized and efficient technique for crop parameter classification and prediction. Utilizing vegetation indices taken from UAV photos, machine learning (ML) has been applied extensively recently to estimate crop yield [9], chlorophyll content [10], and pest and disease detection [11-13].

However, there are times when UAV imagery data leads to an uneven dataset [14]. The unbalanced datasets commonly encountered in agricultural settings pose a major challenge, particularly in the

identification of pests and diseases. Thabtah et al. [15] state that because machine learning classifiers tend to favour a majority class, the class imbalance in the data presents a challenge. Resolving the imbalance issue is essential for machine learning to enhance classification performance since imbalances can produce subpar classification results, particularly for minority classes.

To address the issue of class imbalance, resampling techniques like under sampling and oversampling have been developed. For instances, by applying the resampling method known as random under sampling, the size of the majority class dataset is reduced to match the size of the minority class [16]. In the meantime, increasing the number of instances from the minority samples class is the practice of oversampling techniques like random oversampling (ROS) [17].

Synthetic minority oversampling technique (SMOTE), developed by Chawla et al., [18] is a widely used oversampling strategy for addressing imbalanced class issues. SMOTE is an oversampling method that generates new instances of the minority class by randomly interpolating between the existing instances of the minority class. According to Ghazouani et al., [19], synthetic samples from the minority classes that were created using SMOTE could improve the ability of the model to handle underrepresented classes and encouraged a more balanced representation of all classes. Macuácuá et al., [20] used sample balancing via SMOTE techniques with a KNN classifier to achieve 95% accuracy in classifying various seed varieties.

Previous research done by Mohd Johari et al., [21] revealed the ability of UAV images to identify various degrees of bagworm infestation severity in oil palm plantations using an unbalanced dataset. Results showed that NDVI was the most significant vegetation indices that could identify infestation levels at every stage. Besides, weighted KNN was determined to be the best model that consistently performed the best in classifying all infestation levels with an F1-score of more than 99.70%.

Since the prior study used an unbalanced dataset, it was unknown whether a balanced dataset give an impact toward the machine learning performance. Consequently, this study aims to explore the impact of altering the size of the dataset using SMOTE affects the machine learning performance in classifying all infestation levels as healthy, low, mild, and severe.

2. MATERIAL AND METHOD

2.1 Overview

The flowchart of the study is summarized in Figure 1.

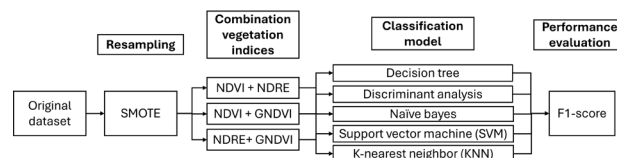


Figure 1. Flowchart of the study

This study began with the resampling techniques (SMOTE) to create a balance dataset using the original dataset obtained from Mohd Johari et al., [21]. Three combinations of vegetation indices (i.e. NDVI, NDRE and GNDVI) were developed and fed into the classification model. The performance of the classification model was evaluated using macro F1-score. The most insensitive model which could classify all infestation level with the highest F1-score was discovered to be the optimal model.

There were four categories of infestation level (i.e., healthy, low, mild and severe) covered by three district plantation area as summarized in Table 1.

Table 1. Study area of bagworm infestation

Type of infestation level	Location	Area (ha)	No. of tree
Healthy	Serdang, Selangor	6.0	750
Low	Pagoh, Johor	7.0	800
Mild		2.0	300
Severe	Ayer Kuning, Perak	10.0	1000

The dataset was captured using a DJI Inspire 2 UAV (DJI Sky City, Shenzhen, China) and equipped with a Micasense Altum-PT multispectral camera (Seattle, Washington, DC, USA). Multispectral orthomosaics was created using Agisoft Metashape Professional software (Agisoft LLC, St. Petersburg, Russia) that consists of all band imagery including blue, green, red, red edge and thermal. It was then exported and loaded into an open-source GIS program, QGIS version 3.28.2, for vegetation indices extraction. The vegetation indices were calculated using the reflectance value generated by the multispectral bands and three vegetation indices with standard errors lower than 0.002 were further used, as summarized in Table 2.

Table 2. Selection of vegetation indices

Infestation	NDVI	NDRE	GNDVI
Healthy (n=750)	0.9469 ± 0.00034 ^a	0.6853 ± 0.00130 ^a	0.8874 ± 0.00069 ^a
Low (n=800)	0.8892 ± 0.00082 ^b	0.4908 ± 0.00147 ^b	0.7717 ± 0.00095 ^b
Mild (n=300)	0.7816 ± 0.00042 ^c	0.3319 ± 0.00109 ^c	0.6380 ± 0.00090 ^c
Severe (n=1000)	0.5958 ± 0.00180 ^d	0.1524 ± 0.00088 ^d	0.5213 ± 0.00149 ^d

Data represents mean (± standard errors). Different letters within the same column indicate statistical differences by the Tukey's HSD test at p<0.05, and n indicates the original dataset.

2.2 SMOTE method

Synthetic Minority Oversampling Technique (SMOTE) was carried out to fix the issue of the imbalanced dataset. SMOTE is a well-known oversampling technique which creates synthetic samples of the minority class. It randomly selects a representative from minority class, then locates the nearest neighbor that belongs to that class by using linear combination of two samples from the minority class based on the equation (1) as follows:

$$\mathbf{x}_{new} = \mathbf{x}_i + (\mathbf{x}_{knn} - \mathbf{x}_i)\alpha \quad (1)$$

where \mathbf{x}_{new} is a new artificial instance; \mathbf{x}_i is the chosen initial instance of the minority class to create the synthetic sample; α is the value between 0 to 1 that indicates the gap between the chosen neighbour and the original instances. \mathbf{x}_{knn} is the k-nearest neighbour of original instance of the same minority class.

In this study, MATLAB 2021b (The MathWorks Inc., Natick, MA, USA) was used to perform SMOTE. The increment of each dataset was done by referring to the majority class (i.e., severe with 1000 tree data). All the levels were oversampled until reached balance data distribution (1000 trees), with the nearest neighbours set into five. The percentage of increment is summarized in Table 3.

Table 3. Percentage of increment of each infestation level using SMOTE

Infestation level	Original data	Percentage of increment (%)
Healthy	750	40
Low	800	30
Mild	300	250
Severe	1000	0

2.3 Classification model

One of the machine learning apps namely classification learner apps from MATLAB (2021b, The Mathworks Inc., Natick, MA, USA) were utilized to create the models for classification in this study. In this the classification learner apps, five machine learning default classifiers were used: k-nearest neighbor (KNN), decision tree (DT), discriminant analysis (DA), naïve bayes (NB), and support vector machine (SVM). As seen in Figure 2, each of these classifiers has a default kernel of its own.

The classification model was developed using three different combinations of significant vegetation indices: NDVI+NDRE, NDVI+GNDVI, and NDRE+GNDVI. The goal of merging two vegetation indices indicates to be to create more straightforward and cost-effective tools for future hardware advancements.

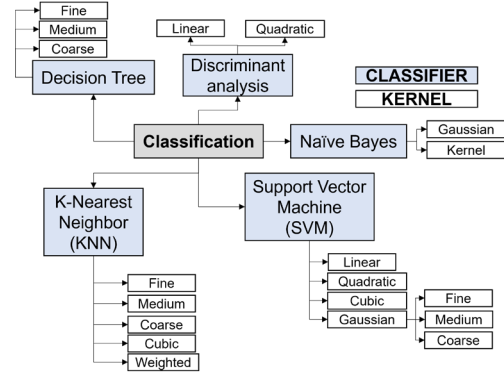


Figure 2. Type of classifier and kernel used for the classification.

A 30% portion was used for testing and the remaining 70% was used for model development across all the resampling datasets with various combinations of vegetation indices. The performance of the model was assessed via a five-fold cross-validation procedure employed by classification learner apps. After that, it was fed into the classification models, and the model with the highest F1-score was chosen as the best model.

2.4 Performance evaluation

The multiclass confusion matrix, which discloses the misclassifications and shows the accuracy of each class, was used to evaluate the performance of the model. The effectiveness of the model in identifying each level of infestation was assessed using the macro F1-score. Macro precision (Equation 2) and macro recall (Equation 3) were calculated by averaging each predicted class's precision and each actual class's recall to get the macro F1-score (Equation 4).

$$\text{Macro precision} = \frac{TP_{low}}{FP_{healthy low} + FP_{mild low} + FP_{severe low}} \quad (2)$$

$$\text{Macro recall} = \frac{TP_{low}}{FN_{healthy low} + FN_{mild low} + FN_{severe low}} \quad (3)$$

$$\text{Macro F1 score} = 2 \times \frac{(\text{macro precision} \times \text{macro recall})}{(\text{macro precision} + \text{macro recall})} \quad (4)$$

The macro F1-score was computed for each type of dataset at every level of infestation. The model with the highest macro F1-score was deemed to be the most effective one by evaluating its consistency in determining the level of infestation for each dataset type and each pair of vegetation indices.

3. RESULTS AND DISCUSSIONS

Figure 3 displays the model performance that achieved 100% F1-score in classifying every infestation level across all type of vegetation indices. There were 7 models able to perform with perfect score in the classification more than six times across

all combinations and levels of infestation namely fine gaussian SVM, medium gaussian SVM, fine KNN, medium KNN, coarse KNN, cubic KNN and weighted KNN.

Out of these seven models, only four models demonstrated consistencies in combinations of vegetation indices to classify each infestation as illustrated in Figure 4. Fine KNN consistently performed well in the NDVI-NDRE combination to categorize all infestation levels; similarly, medium KNN, coarse KNN, and cubic KNN classified all infestation levels in the NDVI-GNDVI combinations. Another three models such as fine gaussian SVM gained perfect score when classifying healthy and low infestation level in all combinations. Medium gaussian SVM performed well when classifying every infestation level using NDVI-NDRE and NDVI-GNDVI combinations except for healthy level, which the perfect score was achieved using NDRE-GNDVI combinations. Weighted KNN seems to perform well using NDVI-GNDVI combinations when classifying all level except for mild level.

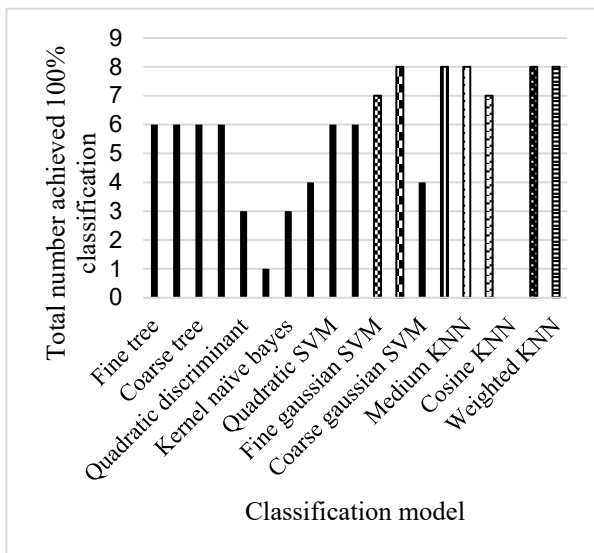
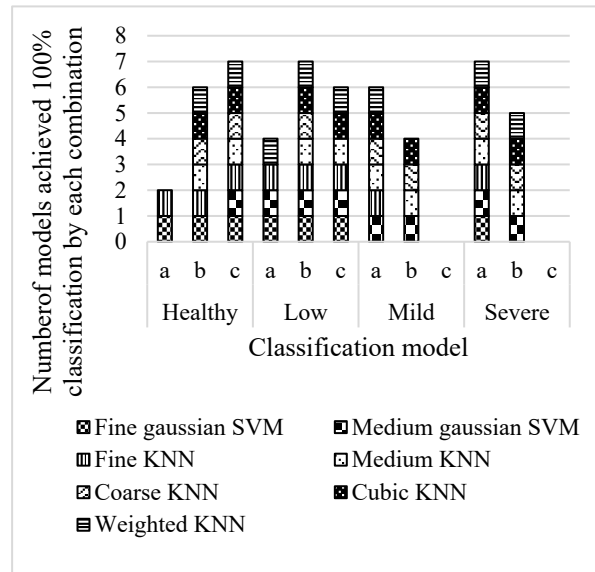


Figure 3. Overall model performance

Consequently, it can be inferred that the combination of NDVI-NDRE and NDVI-GNDVI yields optimal classification performance (100% F1-score) with SMOTE, since it successfully categorizes all levels of infestation. The NDRE-GNDVI model exhibited optimal performance for healthy and low level; however, none of the models achieved a perfect score in mild and severe level. In contrast to the previous study conducted by Mohd Johari et al., [21], which discovered these types of combinations could only classify certain infestation level, i.e., the NDVI-NDRE combination was the most suitable to classify mild and severe, as well as NDVI-GNDVI combination could classify healthy and low level. Nonetheless, by increasing and

balancing the size of dataset, both types of combinations could classify all the infestation level using fine KNN, medium KNN, coarse KNN, and cubic KNN.



a: NDVI+NDRE; b: NDVI+GNDVI; c: NDRE+GNDVI

Figure 4. Details classification across all combination and infestation level by each selected model

The success classification, achieving a 100% F1-score using SMOTE, improved to 46.05% compared to the 28% success classification using the original dataset. This clearly implies that the performance of classification was influenced by the size of the dataset.

Finding reveals that even the dataset needs to be extended and balanced, there is a greater possibility of classifying success utilizing the resampling technique without getting a larger dataset. This could expedite the execution of early control measures to stop the infestation from spreading and minimize the time required for sampling.

3. CONCLUSIONS

This study focuses on the potential of unmanned aerial vehicle (UAV) images for identifying and categorizing infestation levels using resampling dataset, SMOTE. Among the three types of vegetation index combinations, the NDVI-NDRE and NDVI-GNDVI combinations were essential since they could be employed by most models to classify each infestation level (100% F1-score).

The results indicate that the resampling technique may be helpful in the detection process. It would reduce the time required for sampling and speed up the implementation of early control actions to prevent the infestation from spreading. Experts could utilize it without obtaining a larger dataset to identify the infestation.

In the future, it may be possible to build more datasets using resampling techniques, which could improve the classification rate of detection.

REFERENCES

- [1] N. Benjamin, "Bagworm infestation in district causing palm oil production to drop," 2012. <https://www.thestar.com.my/news/community/2012/11/21/bagworm-infestation-in-district-causing-palm-oil-production-to-drop/> (accessed Jun. 12, 2020).
- [2] Y. L. Cheong and C. C. Tey, "Environmental Factors which Influence Bagworm outbreak," *Proceeding 5th MPOB-IOPRI Int. Semin.* 2013, pp. 1–15, 2011.
- [3] K. Norman and M. W. Basri, "Status of common oil palm insect pests in relation to technology adoption.," *Planter*, vol. 83, no. 975, pp. 371–385, 2007.
- [4] G. F. Chung, *Effect of Pests and Diseases on Oil Palm Yield*. AOCS Press, 2012.
- [5] N. Kamarudin, S. R. Ahmad Ali, M. M. Mohd Masri, M. N. Ahmad, C. A. H. Che Manan, and N. Kamarudin, "Controlling *Metisa plana* Walker (Lepidoptera: Psychidae) outbreak using *Bacillus thuringiensis* at an oil palm plantation," *J. Oil Palm Res.*, vol. 29, no. 1, pp. 47–54, 2017.
- [6] J. Kim, S. Kim, C. Ju, and H. Il Son, "Unmanned aerial vehicles in agriculture: A review of perspective of platform, control, and applications," *IEEE Access*, vol. 7, pp. 105100–105115, 2019.
- [7] P. Prabath, P. Nilusha, P. Ruwanpathirana, and J. GY, "Unmanned aerial vehicles (Uav) in precision agriculture: Applications and challenges," *Rajarata Univ. J.*, vol. 7, no. 1, pp. 36–48, 2022.
- [8] K. Neupane and F. Baysal-Gurel, "Automatic identification and monitoring of plant diseases using unmanned aerial vehicles: A review," *Remote Sens.*, vol. 13, no. 19, 2021.
- [9] F. Watson-Hernández, N. Gómez-Calderón, and R. P. da Silva, "Oil Palm Yield Estimation Based on Vegetation and Humidity Indices Generated from Satellite Images and Machine Learning Techniques," *AgriEngineering*, vol. 4, no. 1, pp. 279–291, 2022.
- [10] B. Boiarskii and H. Hasegawa, "Comparison of NDVI and NDRE Indices to Detect Differences in Vegetation and Chlorophyll Content," *J. Mech. Contin. Math. Sci.*, vol. spl1, no. 4, 2019.
- [11] D. B. Marin et al., "Detecting coffee leaf rust with UAV-based vegetation indices and decision tree machine learning models," *Comput. Electron. Agric.*, vol. 190, no. September, 2021.
- [12] J. Su et al., "Wheat yellow rust monitoring by learning from multispectral UAV aerial imagery," *Comput. Electron. Agric.*, vol. 155, no. October, pp. 157–166, 2018.
- [13] T. Wang, J. A. Thomasson, C. Yang, T. Isakeit, and R. L. Nichols, "Automatic classification of cotton root rot disease based on UAV remote sensing," *Remote Sens.*, vol. 12, no. 8, 2020.
- [14] M. Dian Bah, A. Hafiane, and R. Canals, "Deep learning with unsupervised data labeling for weed detection in line crops in UAV images," *Remote Sens.*, vol. 10, no. 11, pp. 1–22, 2018.
- [15] F. Thabtah, S. Hammoud, F. Kamalov, and A. Gonsalves, "Data imbalance in classification: Experimental evaluation," *Inf. Sci. (Ny).*, vol. 513, pp. 429–441, 2020.
- [16] A. Fernández, S. del Río, N. V. Chawla, and F. Herrera, "An insight into imbalanced Big Data classification: outcomes and challenges," *Complex Intell. Syst.*, vol. 3, no. 2, pp. 105–120, 2017.
- [17] R. Mohammed, J. Rawashdeh, and M. Abdullah, "Machine Learning with Oversampling and Undersampling Techniques: Overview Study and Experimental Results," 2020 11th Int. Conf. Inf. Commun. Syst. ICICS 2020, pp. 243–248, 2020.
- [18] N.V. Chawla, K. W. Bowyer, L. O. Hall, and W. P. Kegelmeyer, "SMOTE: Synthetic Minority Oversampling Technique," *J. Artif. Intell. Res.*, vol. 16, no. Sept. 28, pp. 321–357, 2002, [Online].
- [19] H. Ghazouani, W. Barhoumi, E. Chakroun, and A. Chehri, "Dealing with Unbalanced Data in Leaf Disease Detection : A Comparative Study of Hierarchical Classification , Clustering-based Undersampling and Reweighting-based Approaches," *Procedia Comput. Sci.*, vol. 225, pp. 4891–4900, 2023.
- [20] J.C. Macuácuá, J. A. S. Centeno, and C. Amisse, "Data mining approach for dry bean seeds classification," *Smart Agric. Technol.*, vol. 5, no. April, 2023.
- [21] S.N.A. Mohd Johari, S. Khairunniza-bejo, A. R. Mohamed Shariff, N. A. Husin, M. M. Mohd Masri, and N. Kamarudin, "Detection of Bagworm Infestation Area in Oil Palm Plantation Based on UAV Remote Sensing Using Machine Learning Approach," *Agric.*, vol. 13, no. 10, p. 1886, 2023.

ESTIMATED REVENUE CHARACTERISTICS FOCUSED ON THE LONG-TERM BENEFITS OF GREENING

YOHEI KAWAGUCHI¹, KAORI ISAWA², HIROKO HATANABE² and YUDAI HONMA^{2*}

¹ Graduate School of Engineering, the University of Tokyo, Tokyo, Japan

² IIS, the University of Tokyo, Tokyo, Japan

*Correspondence: yudai@iis.u-tokyo.ac.jp

Keywords: Greening, Building greening, Urban greening, Urban development, Mathematical analysis

1. INTRODUCTION

The SDGs were adopted by all 193 member states at the Sustainable Development Summit held at the United Nations in September 2015, and urban greening is gaining momentum around the world. For example, Bosco Verticale in Italy and Azabudai Hills in Japan are cases of proactive urban greening around the world (Figure 1). Urban greening, as described above, makes a significant social contribution in terms of combating global warming and contributing to community building, but real estate developers need to secure profits while promoting urban greening.

The benefits of greening for real estate developers can be divided into immediate and long-term benefits (Figure 2). Immediate benefits are those that are visible at the time of building planning. For instance, the greening of buildings can relax the floor-area ratio. Long-term benefits are those that are not visible at the time of building planning. For example, the attractiveness of greening, such as its healing effect on building users, may contribute to lower vacancy ratio and higher rents. On the other hand, one of the disadvantages of greening is the running cost as well as the initial cost. In actual development, it is expected that the above the disadvantages, immediate benefits and long-term benefits, which are difficult to translate into economic terms, are comprehensively taken into consideration.

The purpose of this study is to estimate the profit characteristics of long-term benefits by examining the problem of profit maximization by real estate developers. This study may provide a new perspective for evaluating the greening efforts of real estate developers in their development and the institutional design of greening by the government.

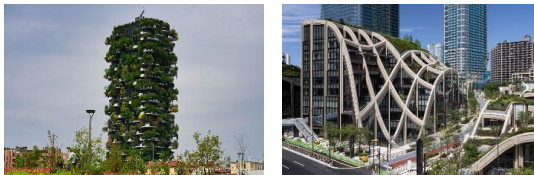


Figure 1. Bosco Verticale^[5] and Azabudai Hills^[6]

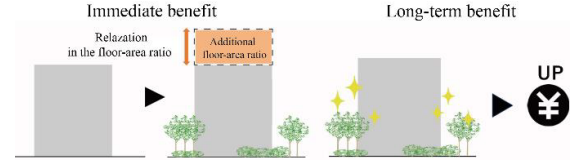


Figure 2. Immediate benefit and Long-term benefit

2. METHOD

This study focuses on office buildings to which the Tokyo Metropolitan Government's unique system for urban development, 'Comprehensive Design System', is applied. Under the 'Comprehensive Design System', the floor-area ratio is relaxed based on the greening ratio, up to 0.5 times the standard floor area ratio or 175%, whichever is lower (Figure 3). Also, the fixed numbers used in the following equations are shown in Table 1.

$$V_{add}(r) = \begin{cases} (r - P_0) \left(\frac{V_0}{4} + 1 \right) + (P - P_0) \left(\frac{V_0}{4} + 1 \right) (r - 0.35), & r \leq 0.35 \\ (r - P_0) \left(\frac{V_0}{4} + 1 \right) + \frac{(P - P_0) \left(\frac{V_0}{4} + 1 \right) (r - 0.35)}{2}, & 0.35 < r \end{cases} \quad (1)$$

$$s. t. V_{add}(r) \leq \min(0.5V_0, 1.75V_0) \quad (2)$$

We suppose that a real estate developer, in planning a building using 'Comprehensive Design System', tries to determine the greening ratio r by comprehensively considering the net profits over a 10-year period. First, using the sum of the immediate and long-term benefits from greening, $A(r)$ (Equation 3), and the sum of construction and greening costs, $C(r)$ (Equation 4), we formulate the net profits $F(r)$ (Equation 5) that the real estate developer will receive from greening.

$$A(r) = 12I_{office}V_{add}(r)SRtx_{interest}(1 - x_{operating})(1 + \alpha r^\beta) \quad (3)$$

$$C(r) = C_{building}V_{add}(r)S + C_{green}Sr \quad (4)$$

$$F(r) = A(r) - C(r) \quad (5)$$

The immediate benefits of greening are calculated by multiplying the site area S and unit price of income I_{office} by $V_{add}(r)$, a floor-area ratio

based on ‘the Comprehensive Design System’ for urban development. On the other hand, the long-term benefits are given as a general-purpose functional form using two revenue coefficients, α and β .

Table 1. Fixed numbers

V_0	Standard floor area ratio
P	Public open space ratio
P_0	Minimum public open space ratio
S	Site area [m^2]
I_{office}	Unit price of income per month [$¥/m^2$]
$C_{building}$	Unit construction cost [$¥/m^2$]
C_{green}	Unit greening cost [$¥/m^2$]
R	Rentable ratio
$x_{interest}$	Compound return ratio ($= 1/(1 + 0.03)^r$)
$x_{operating}$	Expense ratio
t	Years

The coefficient of return α represents the magnitude of the impact of greening on net profits, while the coefficient of return β represents the increasing trend of long-term benefits in relation to the greening ratio. Specifically, the sum of the immediate and long-term benefits from greening, $A(r)$ varies in a gradually decreasing when $-1 < \beta < 0$, linearly when $\beta = 0$, and gradually increasing when $0 < \beta < 1$. Finally, the construction cost is obtained by multiplying the floor area by the unit construction cost $C_{building}$, and the greening cost is obtained by multiplying the greening area Sr by the unit greening cost C_{green} . Under these equations, we consider the problem of maximizing $F(r)$ (Equation 6).

$$\max F(r) \quad (6)$$

$$s.t. \ 0 \leq r \leq 1 \quad (7)$$

To organize Equations 1, 3, 4, and 5, these Equations can be expressed using fixed numbers G_1 , G_2 , H_1 , H_2 , J_1 , J_2 , K_1 , K_2 , L_1 , L_2 , N_1 , N_2 as follows.

$$V_{add}(r) = \begin{cases} G_1 r + H_1, & r \leq 0.35 \\ G_2 r + H_2, & 0.35 < r \end{cases} \quad (8)$$

$$A(r) = \begin{cases} (L_1 r + N_1)(1 + \alpha r^\beta), & r \leq 0.35 \\ (L_2 r + N_2)(1 + \alpha r^\beta), & 0.35 < r \end{cases} \quad (9)$$

$$C(r) = \begin{cases} J_1 r + K_1, & r \leq 0.35 \\ J_2 r + K_2, & 0.35 < r \end{cases} \quad (10)$$

$$F(r) = \begin{cases} (L_1 - J_1)r + \alpha L_1 r^{\beta+1} + \alpha N_1 r^\beta + N_1 - K_1, & r \leq 0.35 \\ (L_2 - J_2)r + \alpha L_2 r^{\beta+1} + \alpha N_2 r^\beta + N_2 - K_2, & 0.35 < r \end{cases} \quad (11)$$

The fixed numbers in Equation 8, 9, 10 and 11 are placed as follows.

$$G_1 = \frac{V_0}{4} + \frac{PV_0}{4} + P + 1 - \frac{P_0 V_0}{4} - P_0 \quad (12)$$

$$G_2 = \frac{V_0}{4} + \frac{PV_0}{8} + \frac{P}{2} + 1 - \frac{P_0 V_0}{8} - \frac{P_0}{2} \quad (13)$$

$$H_1 = -\frac{P_0 V_0}{4} - P_0 - 0.35 \left(\frac{PV_0}{4} + P - \frac{P_0 V_0}{4} - P_0 \right) \quad (14)$$

$$H_2 = -\frac{P_0 V_0}{4} - P_0 - 0.35 \left(\frac{PV_0}{8} + \frac{P}{2} - \frac{P_0 V_0}{8} - \frac{P_0}{2} \right) \quad (15)$$

$$J_1 = C_{building} S G_1 + C_{green} S \quad (16)$$

$$J_2 = C_{building} S G_2 + C_{green} S \quad (17)$$

$$K_1 = C_{building} S H_1 \quad (18)$$

$$K_2 = C_{building} S H_2 \quad (19)$$

$$L_1 = 12 I_{office} S R t x_{interest} (1 - x_{operating}) G_1 \quad (20)$$

$$L_2 = 12 I_{office} S R t x_{interest} (1 - x_{operating}) G_2 \quad (21)$$

$$N_1 = 12 I_{office} S R t x_{interest} (1 - x_{operating}) H_1 \quad (22)$$

$$N_2 = 12 I_{office} S R t x_{interest} (1 - x_{operating}) H_2 \quad (23)$$

The optimal greening ratio r^* is then divided into cases by the revenue coefficient β .

$$\blacksquare -1 \leq \beta < 0$$

In this case, $F(r)$ is an upward convex function because $F''(r)$ is less than 0. For example, when $\alpha = 1.5$ and $\beta = -0.5$, $F(r)$ is as shown in Figure 4. So any $0 \leq r \leq 1$ is a candidate for the optimal greening ratio. By differentiating $F'(r)$, we obtain Equation 24.

$$F'(r) = \begin{cases} L_1 - J_1 + \alpha(\beta + 1)L_1 r^\beta + \alpha\beta N_1 r^{\beta-1}, & r \leq 0.35 \\ L_2 - J_2 + \alpha(\beta + 1)L_2 r^\beta + \alpha\beta N_2 r^{\beta-1}, & 0.35 < r \end{cases} \quad (24)$$

Putting r^{**} as the greening ratio such that $F'(r)=0$, we can derive the following relationship between α and β for r^{**} to be the optimal solution.

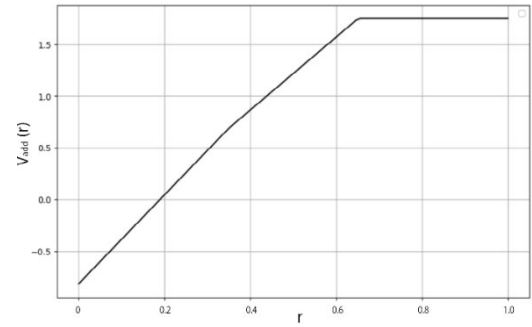


Figure 3. Relationship between $V_{add}(r)$ and r

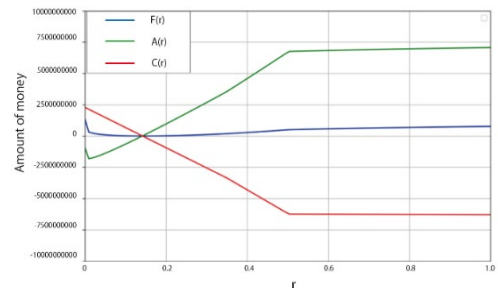


Figure 4. Relationship between $F(r)$, $A(r)$, $C(r)$ and r when $\alpha = 1.5$ and $\beta = -0.5$

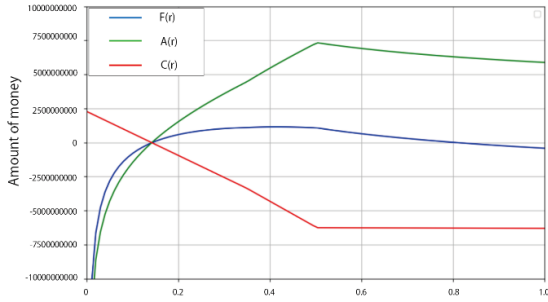


Figure 5. Relationship between $F(r)$, $A(r)$, $C(r)$ and r when $\alpha = 1.5$ and $\beta = 0.1$

$$\alpha = \begin{cases} \frac{J_1 - L_1}{(\beta + 1)L_1 r^{**\beta} + \beta N_1 r^{**\beta-1}}, & r \leq 0.35 \\ \frac{J_2 - L_2}{(\beta + 1)L_2 r^{**\beta} + \beta N_2 r^{**\beta-1}}, & 0.35 < r \end{cases} \quad (25)$$

■ $0 \leq \beta \leq 1$

In this case, $F(r)$ is a downward convex or linear function since $F''(r)$ is greater than 0 or $F''(r)$ is 0 respectively. For example, when $\alpha=1.5$ and $\beta=0.1$, $F(r)$ is as shown in Figure 5. So $r=0$ or $r=1$ is the optimal greening ratio (Equation 26).

$$r^* = \begin{cases} 0, & \alpha \leq \frac{(N_1 - N_2) - (K_1 - K_2) - L_2 + J_2}{L_2 + N_2} \\ 1, & \alpha \geq \frac{(N_1 - N_2) - (K_1 - K_2) - L_2 + J_2}{L_2 + N_2} \end{cases} \quad (26)$$

Here, using the data in Table 2 from 'Nihonbashi Honmachi 2-chome Project', which is an actual case of application of 'the Comprehensive Design System', we draw r^* contour lines in the phase plan of α and β (Figure 6).

For example, the optimal greening ratio is $r^*=0.5$ when the revenue coefficient is $\alpha=1.8$ and $\beta=-0.54$, as shown in the red dot in Figure 6.

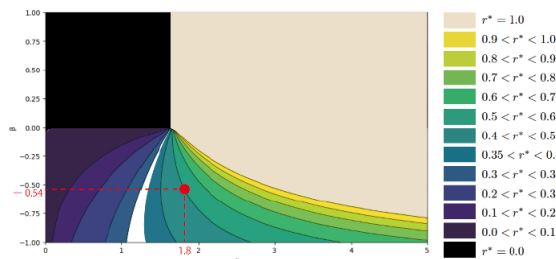



Figure 6. Relationship between r^* and α, β

3. CONCLUSIONS

Focusing on the challenges faced by real estate developers in developing buildings, this study attempts to actuarially quantify the optimal greening ratio r^* and the coefficients of return α and β for long-term profit.

In determining the optimal greening ratio, it was mathematically found that the coefficient of return β which represents the increasing trend of long-term benefits, has a significant impact.

Table 2. Target case data set

Photo of current condition (projected completion)	
Name	Nihonbashi Honmachi 2-chome Project
Date of permit	2010/4/13
Address	2-1-1 Nihonbashi-Honcho, Chuo-ku
Building use	Offices, stores, parking lots
Area zoned for use	business zone
Type of 'Comprehensive Design System'	Business commercial fostering comprehensive design
Standard floor area ratio	700%
Site area	2365.09m ²
Effective public open space ratio	66.2%
Minimum effective open space ratio	10%
Rental income per unit area per month	13,000 ¥/m ²
Construction cost per unit area	1,500,000 ¥/m ²
Greening cost per unit area	40,000 ¥/m ²

4. PROSPECTS

For prospects, we will extend this model to a mathematical model for estimating the coefficients of return α and β . We will attempt to estimate the coefficients of return α and β by overlaying and drawing the trajectory of the greening ratio for each case obtained by substituting five real case data. If the revenue coefficients α and β are successfully estimated, this model will help real estate developers to determine the optimal greening ratio, as well as help the government to design an appropriate greening system.

REFERENCES

- [1] Kaori Isawa, Hiroko Watanabe, Yudai Honma and Kotaro Imai. [Optimal Ratio for Renovating Historic Architectures into Profit-making Facilities with Conservation - Case study based on Kyoto city's ordinance on historic architectures -]. Journal of the City Planning Institute of Japan, Vol.56 No.3, October, 2021.
- [2] Hiroko Watanabe, Yudai Honma, Kentaro Honma and Kotaro Imai. [Effects of Height Restriction and Relaxation by Sky Factor Focusing on Digestion Floor Area Ratio and Building Height]. Journal of the City Planning Institute of Japan, Vol.52 No.3, October, 2017.
- [3] Kozo Okudaira, The Urban Engineering Reader - Analyzing Cities -, Japan, 1976.
- [4] Bureau of Urban Development, Tokyo Metropolitan Government, Tokyo Metropolitan

- Government Comprehensive Design Permit Outline, January, 2021.
- [5] Michael Moll, The globetrotters, 'Bosco Verticale - the green skyscrapers of Milan', <https://www.dieweltenbummler.de/reisen/sehen-swertes-europa/bosco-verticale-die-gruenen-hochhaeuser-von-mailand/>, July, 2020.
- [6] Built building × IT, 'Azabudai Hills, a 861,000 m² town with the tallest building in Japan, the 330-meter Mori JP Tower, will open in November.
- [7] Astellas Pharma Inc. and Mitsui Fudosan Co., Ltd, '2011 News Release', https://www.mitsui-fudosan.co.jp/corporate/news/2011/0228_01/ February, 2011.

A VOLUME PROJECTION MODEL EXPANDABLE TO CARBON SINK CAPACITY: A CASE STUDY ON SABAL FOREST PLOTS

W.N.Z. ZAINOL @ ABDULLAH^{1*}, O.F. MARZUKI^{1,2}, M.F. BOHARI³ and H. OMAR⁴

¹*Institute of Ecosystem Science Borneo (IEB), Universiti Putra Malaysia Bintulu Sarawak Campus, Malaysia*

²*Department of Science and Technology, Faculty of Humanities, Management and Science,
Universiti Putra Malaysia Bintulu Sarawak Campus, Malaysia*

³*Forest Department Sarawak Headquarters, Kuching, Sarawak, Malaysia*

⁴*Forest Research Institute Malaysia (FRIM), 68100 Kuala Lumpur*

*Correspondence: wnzz@upm.edu.my

Keywords: Volume projection, Carbon sink capacity, Forestry, CO₂ sequestration, Forest plots, Biomass

1. INTRODUCTION

Forests play a crucial role in the global carbon cycle by acting as natural carbon sinks, sequestering CO₂ from the atmosphere. They are essential for climate change mitigation, biodiversity conservation, and sustaining ecosystem services. With rising concerns over global warming and increasing carbon emissions, there is growing interest in accurately estimating the carbon sink capacity of forests to inform management strategies aimed at enhancing carbon sequestration. However, estimating carbon sink capacity is fraught with challenges, including the complexities of forest dynamics, land quality, and species composition [1, 2].

To address these challenges, recent advances have focused on refining models that predict tree growth, biomass, and carbon storage. These models incorporate factors such as tree height, diameter at breast height (DBH), and stand density, which are crucial for estimating forest volume and carbon sink potential. The development of such models is increasingly supported by advanced technologies like Light Detection and Ranging (LiDAR) and remote sensing, enabling the collection of detailed forest inventory data over large spatial scales [3,4].

2. METHODOLOGY

The data for this study were obtained from five forest plots at Sabal, Sarawak, Malaysia, each measuring 20m x 20m (Figure 1). These plots provide critical field measurements, including information on tree species, DBH, total tree height, and crown diameter—parameters that are essential for accurate tree volume and biomass estimation. The dominant species across these plots is *Rubroshorea leprosula*, alongside a mix of other species. Such detailed inventory data have been shown to improve the robustness of volume projections and carbon stock assessments [5,6].

Tree volume calculation is a critical step in estimating biomass and carbon sequestration

potential. For this study, a standard tree volume calculation formula was employed:

$$V = \frac{\pi}{4} \times (DBH)^2 \times H$$

Where V is the tree volume in cubic meters, DBH is the diameter at breast height in meters, and H is the total height of the tree in meters. This formula assumes a cylindrical shape for the tree, providing a reasonable approximation of tree volume [2].



Figure 1. Five forest plots at Sabal, Sarawak, Malaysia

Once tree volumes were calculated, biomass was estimated at approximately 50% of the tree volume, following established forestry practices [7]. The carbon content of the biomass was then estimated as 50%, and carbon sequestration capacity was calculated by multiplying the carbon content by 3.67, representing the molecular weight ratio of CO₂ to carbon [8].

3. RESULTS AND DISCUSSIONS

The results from the five forest plots show significant variation in CO₂ sequestration capacities, primarily driven by differences in tree volume and species composition. Plot 1 demonstrated the

highest potential with a sequestration capacity of 0.034 tons of CO₂, whereas Plot 5 exhibited the lowest with only 0.001 tons. This variation underscores the crucial role of site-specific factors such as tree density, species type, and age in determining the carbon sequestration capacity of a forested area [6, 8]

Biomass estimates across the five plots ranged from 0.0005m³ in Plot 5 to 0.0185m³ in Plot 1, reinforcing the link between tree volume and carbon storage potential. The findings emphasize the need for careful management to maximize biomass accumulation. Optimizing forest management practices, including selective tree harvesting and afforestation with high carbon-sequestering species, can further enhance the carbon sink potential of forests [4,9].

4. CONCLUSIONS

The volume projection model developed in this study offers a practical and scalable approach for estimating carbon sink capacity using standard forestry measurements such as tree height and diameter at breast height (DBH). By applying the model to five forest plots, its effectiveness in estimating tree volume, biomass, and CO₂ sequestration was demonstrated. The variability in carbon sequestration across the plots emphasizes the importance of site-specific factors like species composition, tree density, and environmental conditions, highlighting the need for tailored forest management practices.

This model's scalability makes it suitable for broader applications in forestry management, afforestation programs, and climate change mitigation efforts. Its ability to provide reliable estimates of forest carbon storage, even in small plots, aligns with the increasing focus on optimizing forest resources as a key strategy to meet global carbon neutrality goals. Future refinements to the model, including the incorporation of dynamic environmental factors and species-specific data, will further improve its utility in developing sustainable forest management strategies that contribute to global climate goals.

REFERENCES

- [1] Dong, Y., Yu, Z., Agathokleous, E., Zhou, G., & Liu, S. (2024). Pitfalls in forest carbon sink projection. *Journal of Forestry Research*, 35(1), 87.
- [2] Manso, R., Davidson, R., & McLean, J. P. (2022). Diameter, height and volume increment single tree models for improved Sitka spruce in Great Britain. *Forestry: An International Journal of Forest Research*, 95(3), 391–404.
- [3] Umami, K., & Inoue, A. (2024). A model for predicting mean diameter at breast height from mean tree height and stand density. *Journal of Forest Research*, 29(3), 186-195.
- [4] Zhao, S., Shi, W., Qiao, F., An, Y., Wang, W., & Zhang, G. (2023). Dynamic Analysis and Trend Forecast of China's Forestry Carbon Sink Benefits Based on Dual Carbon Targets.
- [5] Sharma, M. (2020). Increasing Volumetric Prediction Accuracy-An Essential Prerequisite for End-Product Forecasting in Red Pine. *Forests*, 11(10), 1050.
- [6] Huang, W., Wang, X., & Zhang, D. (2024). The Estimation of Forest Carbon Sink Potential and Influencing Factors in Huangshan National Forest Park in China. *Sustainability*, 16(3), 1351.
- [7] Peichl, M., & Arain, M. A. (2007). Allometry and partitioning of above- and belowground tree biomass in an age-sequence of white pine forests. *Forest Ecology and Management*, 253(1–3), 68–80.
- [8] Haripriya, G. S. (2000). Estimates of biomass in Indian forests. *Biomass and Bioenergy*, 19(4), 245-258.
- [8] Yu, Z., Liu, S., Li, H., Liang, J., Liu, W., Piao, S., Tian, H., Zhou, G., Lu, C., You, W., Sun, P., Dong, Y., Sitch, S., & Agathokleous, E. (2024). Maximizing carbon sequestration potential in Chinese forests through optimal management. *Nature Communications*, 15(1), 3154.
- [9] Qin, J., Liu, P., Martin, A. R., Wang, W., Lei, Y., & Li, H. (2024). Forest carbon storage and sink estimates under different management scenarios in China from 2020 to 2100. *Science of The Total Environment*, 927, 172076.

DROUGHTS AND DELUGES: NAVIGATING WATER RESOURCE IN SDG PERSPECTIVE AND SAVING WATER RESOURCE USING IOT

K. SIVASUBRAMANIYAN¹, S. TAMILARASI^{2*}, R. LATHA³, A. LOGANATHAN¹, S. VETRIVEL¹,
J. GAJALAKSHMI¹ and R. VIJAYALAKSHMI¹

¹Department of Economics, St. Peter's Institute of Higher Education and Research (SPIHER), Chennai, India

²Department of Information Technology, SPIHER, Chennai, India

³Department of Computer Application, SPIHER, Chennai, India

*Correspondence: ithod@spiher.ac.in

Keywords: Economic growth, Environmental sustainability, Water resources, Rural habitations, IoT

1. INTRODUCTION

Among all natural resources, water remains a critical input for survival of all living being on the earth. This point is easily understood if one visualised as the Indian economic growth has been largely facilitated by water resources gifted by the seasonal rainfall and thereby enabling the survival of both human and other living beings (animals, plants) on the earth. This water resource is harvested in both ways: i) Water bodies such as rivers, canals and tanks, assuming surface water source; and ii) Gradual percolation of rainwater under all the surface areas that forms the groundwater source. This natural environment system endures inevitable resources for survival of all living beings. Hence both the surface water and groundwater for distribution to community welfare remain as a gift of natural environment system.

1.1 Water for Agriculture

At the outset, it is pertinent to note that Indian economic growth has been primarily depending on agricultural activities in villages that has come a long way since independence. In turn water becomes an important supply oriented economic input for food production and the natural water is well regulated through surface water bodies like river and tank irrigation system. The past outcome from this natural phenomenon portrays that the food grains production increased from 50.8MT in 1950-1951 to 332.3MT in 2023-24 to feed an Indian population of [12] 1.44 billion without being driven to hunger in 2023 [13]. This apart towards challenging poverty, this primary sector provides employment to over 185 million workforces in 2006 that reduced to 158 million in 2022 [14]. Yet sustainability of this scenario that ensures food grains for future generation remains debatable one.

1.2 Water for Human Habitations

The provision of rural drinking water supply is primarily the responsibility of the states, yet government of India has had a significant role in

guiding sector reform by creating incentives and making significant financial contribution.

Under Bharat Nirman program, as a part of drinking water agenda, it targeted a total of 6 lakh habitations. In April 2009 Government of India launched National Rural Drinking Water Programme (NRDWP) to mainstream the 'demand responsive community participation' based approach.

In the case of Jal Jeevan Mission of central government, the goal is to assist, empower and facilitate States/UTs in planning of participatory rural water supply strategy for ensuring potable drinking water security on long-term basis to every rural household and public institution.

In the case of National Bank for Agriculture and Rural Development (NABARD) assisted Combined Water Supply Scheme (CWSS) in rural areas studied, it is observed that there are two stages of water supply system to rural habitations. In the first stage, Tamil Nadu Water Supply and Drainage (TWAD) Board takes the responsibility of arrangement of water supply from the main sources of water (mostly in river bed) to the respective beneficiary Panchayats; (Over Head Tanks OHT) while in the second stage, the accountability of the distribution of water from Panchayat OHT to the rural habitations ultimately at household level lies on the hands of the respective Panchayats.

2. CONTRIBUTORY VALUES OF WATER MANAGEMENT IN THE PATHWAYS TO SUSTAINABILITY

In the process of economic growth, leveraged by water resource system among others, the expected outcome would facilitate positive achievements of various SDGs as detailed below.

2.1 No Poverty and Zero Hunger (SDGs 1 & 2)

According to UN SDG web site "By managing our water sustainably, we are also able to better manage our production of food and energy and contribute to decent work and economic growth." Moreover, we can preserve our water ecosystems,

their biodiversity, and act on climate change. Among the three sectors of the economy – agriculture, industry and services – the primary sector is the key to several states as well as India’s economy, because it provides employment for a large chunk of the population even now.

2.2 Clean Water with Inclusive Concerns (SDG 6)

Developing countries face growing challenges linked to water scarcity, water pollution, degraded water-related ecosystems and interstate cooperation over Trans-boundary water transfers. A robust economic development process revolves around the trinity of Sustainability, Growth and Inclusion. Among others, the SDG no 6 ‘Clean water and sanitation’ highlights that in 2022, “2.2 billion people still lacked safely managed drinking water, including 703 million without a basic water service; 3.5 billion people lacked safely managed sanitation, including 1.5 billion without basic sanitation services; and 2 billion lacked a basic hand washing facility, including 653 million with no hand washing facility at all” (SDG-Featured news).

2.3 Critical Grey Areas in Water Management (SDG 3, 4 & 6)

Factors such as mismanagement of water bodies resulting to unauthorised encroachment, pollution, wastages and inequitable supply and distribution to tail end areas remain critical grey areas in surface water management arena. This is the potential area for providing employment to people that makes decent work (SDG 6). Once the above issues are sorted out by the government, one can get clean water for drinking and sanitation facilities will also improve (SDG 3).

3. NUANCES OF IRRIGATION MANAGEMENT AT GROUND LEVEL

3.1 Features of irrigation institutions

The quality of irrigation is not merely a function of the nature of the water source but of how well the source is institutionally managed. Partly this is a matter of engineering: For example, the ability to regulate the amount of water supplied to different segments of the canals depends on how well the canals and distributaries are designed and constructed, and whether they are equipped with regulatory devices. To regulate and manage the surface irrigation systems separate irrigation institutions (IIs) must build up. The early work on Irrigation Institutions was done by Wittfogel (1957), who concerned with the relation of irrigation with the emergence of strong centralised state systems. Subsequently, such system has been democratised down at user level.

3.2 Irrigation Management

3.2.1. Tank Irrigation Management

A.M. Michael in his book advocates “Scientific management of irrigation water provides the best instance against weather-induced fluctuations in total food production.” Towards effecting scientific management, an understanding of critical phases of irrigation management and of four vital tasks to be performed in each phase Figure 1. as defined by W.W. Kelly (1980), would be considered prudential for taking remedial action precisely and squarely in the respective command area of water bodies.

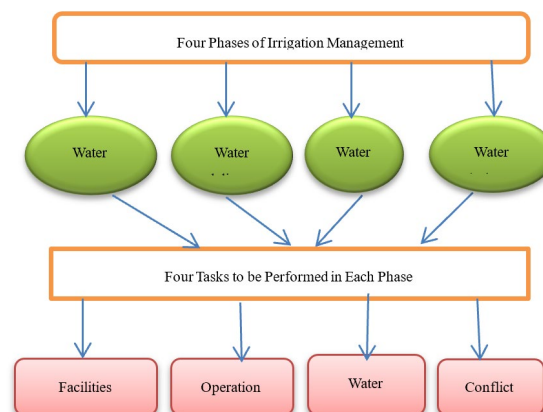


Figure 1. Different phases and tasks in irrigation management

3.2 Management of groundwater distribution for drinking to rural households

Supply and Distribution of Rural Drinking Water Supply: In Combined Water Supply System (CWSS), it is observed that there are two stages of water supply to rural habitations. In the first stage, Tamil Nadu Water Supply and Drainage (TWAD) Board takes the responsibility of arrangement of water supply from the main sources of water to the respective beneficiary. Panchayats: while in the second stage, the accountability of the distribution of water from Panchayat to the rural habitations ultimately at household level lies on the hands of the Panchayats. These supply systems are portrayed in Figure 2.

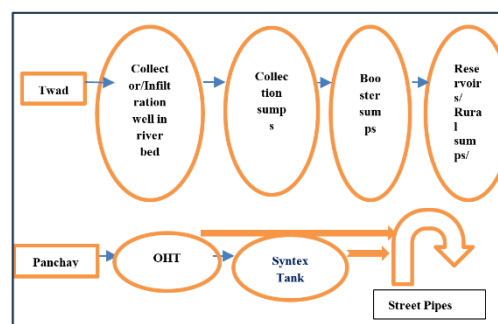


Figure 2. Supply and distribution of groundwater from main sources to rural households’ level in CWSS project areas

The main tasks of TWAD include pumping of required water from the main sources usually from the bore well erected in the riverbed, treatment of water to drinking status, supply of piped water to the OHT in the beneficiary Panchayats. Then the local Panchayats take the role of distribution of project water from their OHT along with local water through street pipes or syntax tanks at street level to the households in rural habitations covered in the project area.

4. IMPLEMENTATION OF IoT FOR WATER MANAGEMENT

From the perspectives of equitable distribution there are twin persisting concerns viz., pollution and wastages of natural water resources. Large-scale waste of water is a result of broken pipes that cause spills and overflowing water in overhead tanks. One of the main causes of water waste in both urban and rural regions is probably overflowing tanks and reservoirs.

Smart water management and automation can significantly alleviate the water crisis by removing the need for continuous pumping motor operation even when water tanks are fully filled. By analysing water levels at different times of the day, the smart management framework can help detect water spills. As such, a smart water management framework is an urgent necessity for our planet's transition to a green IoT.

As shown in Figure 3, the IoT laser water level sensor positioned at the topmost part of the OHT senses the water level in OHT and transmits the water level to the cloud through the transceiver. Data is transmitted using wireless technology such as Zigbee. Cloud service such as Adafruit IO is used as a bridge to facilitate exchange of data in real time. It displays the water level in OHT and if it is at the threshold value the dashboard transmits the message to the motor switch for “on” mode. Water level when reaches the desired height the sensor sends the message to the IoT dashboard, and the message is transmitted to the motor switch for “off”. By preventing overhead water tanks and reservoirs from overflowing repeatedly, this solution helps to prevent the waste of valuable water resources.

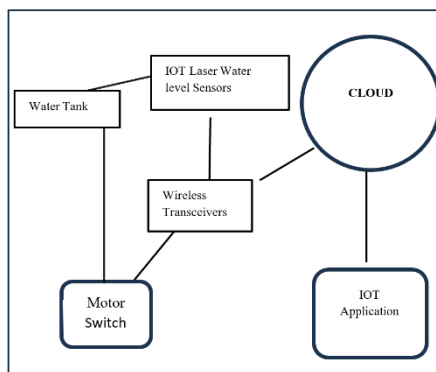


Figure 3. IOT based water management system

For consumers to always have access to water, it also automatically refills tanks.

5. IMPERATIVES FOR CHALLENGING NUANCES

All the above evidence-based observations on the nuances of natural water management at ground level remain critical one that need to be challenged from sustainable economic growth perspectives.

5.1 Maintenance of Data on Water Bodies

From the perspectives of equitable distribution there are twin persisting concerns viz., pollution and wastages of natural water resources. Therefore, it is essential to conduct a survey utilising Geographical Information System (GIS) for updating the details on the profile of existing ponds and tanks. Further it is essential to convert local ponds into full-fudged tanks and non-system tanks into system tanks for effective management.

5.2 Awareness Campaign on Maintenance of Water Resources

The users of the natural water resources need to be made aware of robust maintenance of tank for its proper maintenance and of street pipe connections for safe water supply without wastes and pollution. In this regard, involvement of local social capital such as Self-Help Group (SHG) and Farmers Club (FC), Joint Liability Group (JLG) is considered essential for making the local people to participate and to create an engaging ownership culture in protecting the natural resources at the tail end of distribution of water. Incentives such as prizes, cash award, cups, etc. may be considered annually as yet another imperative one for sustaining the spirit of ownership for the robust maintenance of distribution system at micro level.

6. CONCLUSIONS

For drinking water purpose, efficient water management both at surface and groundwater level need to be developed to avert drinking water scarcity throughout the nation. Future research studies need to cover such a holistic approach on the subject. Since this water subject is interconnected with each one of the sectors and sub-sectors, all sustainable development goals and their prosperity immensely depend on this fact. This paper also suggests an IoT based water management system. It has also been suggested that machine learning will be used in the future to address all these crucial characteristics and make predictions based on machine learning, which can boost the effectiveness of the smart water management system to save the most precious resource for livelihood.

REFERENCES

- [1] W.W. Kelly, Water Control in an Agrarian State; Irrigation Organisation in a Japanese River Basin, Ph.D. Thesis, London, University Microfilms International, 1980.
- [2] ICSSR, Report on Structure, Functioning and Impact of Irrigation Institutions: The Case of Tank Irrigation in Tamil Nadu, Project Report. Project Sanctioned by the Indian Council of Social Science Research (ICSSR), New Delhi, June, 2018.
- [3] NABARD, Report on Impact Evaluation Study of Rural Drinking Water Supply Project Assisted under Rural Infrastructure Development Fund (RIDF) in Tamil Nadu, Commissioned by National Bank for Agriculture and Rural Development (NABARD), September 2019.
- [4] RBI, Handbook of Statistics on the Indian Economy, 2022-23. September 15, 2023,
- [5] K. Sivasubramanian, Review of the book: Transforming Indian Agriculture - India 2040: Productivity, Markets and Institutions by Marco Ferroni (Ed). Review of Development & Change, Vol. XIX. No. 2, July-December, (2014) 117-120.
- [6] GoTN., Department of Evaluation and Applied Research (DEAR), Tamil Nadu – An Economic Appraisal, Various Issues.
- [7] GOI., Strategic Plan-2011-2022, Department of Drinking Water and Sanitation – Rural Drinking Water. Ministry of Rural Development, 2011-22, 9-10.
- [8] Julius Godslove Femi, Smart Water Management System, International Journal of Smart Sensor and Adhoc Network, March 2022,
- [9] Manmeet Singh, Suhaib Ahmed, IoT based Smart Water Management System: A Systematic Review, International Conference on Innovations in Clean Energy Technologies (ICET2020) Copyright ©2020 Elsevier Ltd.
- [10] P. Madhurima; Kirti Yadav; Ronit Gupta; Jitendra Singh Jadon, Real Time Smart Water Management System using IOT, 2022 International Mobile and Embedded Technology Conference (MECON), Publisher: IEEE
- [11] Babu, N., Suresh, T, Localized Distributed Secure Fast Neural Routing for QoS Maximization in WSN with IoT Using Machine Learning, SSRG International Journal of Electrical and Electronics Engineering, 2023, 10(11), pp. 33–44, IJECE-V10I11P104
- [13] <https://www.macrotrends.net/globalmetrics/countries/IND/india/population>
- [14] <https://www.statista.com/statistics/1284035/india-employment-in-agriculture-sector/>

EXPLORING THE SURFACE WATER STATUS OF AWD IRRIGATED RICE PADDY FIELDS INTEGRATING SAR-UAV AND IOT TO CLIMATE CHANGE MITIGATION

MD RAHEDUL ISLAM^{1*} and WATARU TAKEUCHI²

¹ Department of Geography and Environment, Pabna University of Science and Technology, Bangladesh

² Institute of Industrial Science, University of Tokyo, Japan

*Correspondence: rahe_ge@pust.ac.bd

Keywords: Synthetic Aperture Radar, Time series, Backscatter, Machine learning, Bangladesh

RESEARCH SUMMARY

Alternate wetting and drying (AWD) is a proven technique to reduce irrigated water, and methane emissions without yield reduction of rice cultivation. The effective and efficient ways to monitor paddy field surface water are significant to successfully implementing AWD to reduce water use and methane emissions. The aim of the study to monitoring AWD water status of rice paddy fields with remotely sensed data, Unmanned Aerial Vehicle (UAV) and IoT based low-cost water level monitoring devices. The experiment fields design with installation of IoT based water level devices and periodically UAV flight at the selected six plots in Bangladesh.

The vertically VV (vertical-vertical) polarization data, in comparison to VH (vertical-horizontal) polarization, show high sensitivity to soil moisture (Patel et al., 2006). The VH data, in its turn, has a higher sensitivity to volume scattering, which depends strongly on the geometrical alignment and characteristics of the vegetation. Thus, VH data has a limited potential for the estimation of soil moisture compared to VV data, but higher sensitivity to vegetation (Eweys et al., 2017; Gao et al., 2018; Gherboudj et al., 2011). As soil moisture of rice paddy field depends on irrigation, we use both VV and VH polarization data. In case of temporal resolution is very important to observe the AWD cycle, high temporal resolution required.

As a result, we used both ascending and descending data of the study area and the resolution becomes 3-7 days. Moreover, we used UAV flight to increases the high temporal observation in case of SAR images absence. The dataset has been collected from rice growing and AWD cycle practicing time from February to April 2024. The result found that the low cost IoT device-based water level data of six experimental field and farmer level manual data are good agreement. The AWD irrigation cycle varied based on the different agroclimatic variables.

The sensor-based detection also observed such variation like the maximum (06 times) AWD cycle duration observed in Naldanga, Natore district and minimum (04 times) in Pabna district. The AWD cycle length also varied as the maximum (8-10 days)

duration at Pabna and shortest duration (03-05) at Naldanga, Natore district. In Figure 1, the IoT device and device-based water level data showed with the clear irrigation cycle of the AWD irrigation schedule.

In case of SAR database water status monitoring case, the backscatter's coefficient value of VV and VH compared with water level data. The VV values are less sensitive than the VH value to watered condition of the rice paddy field. In Figure 2(a) shows the VV value fluctuate with response of the water level status. Similarly, in Figure 2(b) showed the variation of VH value fluctuated with water level condition. In the phase irrigated condition are comparatively more sensitive than the dry condition of the rice paddy field. The VV and VH both values slightly reduced and less responsive to IoT based water level data as the rice paddy growth stage, the canopy height and vegetation density increased.



Figure 1. Low cost IoT sensor based (left) water level monitoring device, and (right) water level data to monitor AWD irrigation practices

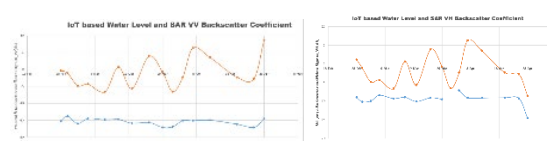


Figure 2. Low cost IoT sensor-based water level data (cm) comparison with SAR backscattered coefficient Sigma0 (left) VV (dB), (right) VH (dB)

This study provides a new paradigm for monitoring the water status of rice fields, which will be key to the precision irrigation of paddy fields in large regions in the future. As well as the accurate irrigated and non-irrigated conditions of rice paddy fields will help to monitoring AWD implantation and greenhouse gasses emission.

THE IMPACT OF LAND USE/COVER CHANGES ON HABITAT QUALITY IN JOHOR RIVER BASIN, MALAYSIA

Y.S. YONG¹ and K.D. KANNIAH^{2,3*}

¹*Faculty of Built Environment & Surveying, Universiti Teknologi Malaysia, Johor, Malaysia,*

²*Tropical Map Research Group, Faculty of Built Environment & Surveying, Universiti Teknologi Malaysia, Johor, Malaysia,*

³*Centre for Environmental Sustainability and Water Security (IPASA), Research Institute for Sustainable Environment, Universiti Teknologi Malaysia, Johor, Malaysia,*

**Correspondence: kasturi@utm.my*

Keywords: *Habitat quality, River basins, InVEST, Malaysia*

1. INTRODUCTION

The increasing benefits delivered by biodiversity to human welfare, essential living resources, and the global economy highlight its importance for human development [1,2]. Biodiversity encompasses not only the diversity of living organisms at the genetic and species levels but also the variety of ecosystem services—such as provisioning, regulating, supporting, and cultural services—provided by these organisms [1,3]. Unfortunately, the growing anthropogenic pressures on natural habitats are expected to exceed previous levels and continue rising in the future [4,5]. One of the major outcomes of anthropogenic activities is Land Use and Land Cover (LULC) change [6]. Human-induced landscape alterations driven by economic or political forces have significant impacts on key components of the Earth system, modifying habitat structure and disrupting the circulation of materials and the flow of energy between habitat patches [1,7]. Consequently, LULC change is a major risk factor for habitat quality (HQ). However, few studies have modeled the impact of LULC change on HQ. This study, therefore, focuses on the Johor River Basin (JRB) to explore the potential of using remote sensing approaches to model HQ in this region [8,9].

The JRB is one of Malaysia's most vital basins, both economically and for supplying natural resources to two metropolitan areas [10,11]. It is the primary source of freshwater for the southern Johor region and partially serves Singapore. However, Kang and Kanniah suggest that rapid changes in the JRB and its surrounding areas are primarily driven by fast-paced economic development and population growth [7]. Although anthropogenic activities, such as the construction of dams and barrages along the JRB, were intended to improve human welfare, they have severely degraded the ecological environment [12,13]. Therefore, the anthropogenic pressures within the JRB are considered a significant threat to the habitat stability of the river basin.

One approach to effective river basin management is the use of Decision Support Systems (DSSs), which can help managers protect the environment [1,14]. DSSs can be supported by indicators of ecosystem health and biological sustainability, such as habitat quality (HQ), which reflects the spatial relationship between ecological quality and human-induced threats [15,16]. HQ studies are typically conducted through two approaches: (1) field measurements of biodiversity, and (2) ecological process modeling and simulation [17]. Malaysia's unique geographical characteristics and accessibility challenges have limited field-based HQ studies. Therefore, modeling approaches are necessary to assess HQ in the JRB in relation to LULC changes [8,9].

In this study, HQ is estimated using the Integrated Valuation of Ecosystem Services and Tradeoffs (InVEST) model, which is widely used by researchers due to its broad applicability and the ability to provide high predictive accuracy with minimal data requirements [18]. Additionally, InVEST allows for spatial visualization of results, enhancing the understanding of outcomes [15,19]. The LULC data for the JRB and associated threat sources over the past 20 years were applied to the InVEST model to simulate changes in HQ related to LULC alterations. Increasing threats in areas of interest—such as population growth, agricultural expansion, and cultural transformation—have the potential to diminish ecosystem services in the JRB [10].

This study aims to help decision-makers better understand the conditions of habitat quality in the study area. Therefore, the objectives of this study are to: (1) analyze changes in habitat quality in the JRB from 2000 to 2020; (2) present spatiotemporal responses of HQ to LULC changes and impact factors; and (3) compare HQ responses with and without the presence of protected areas.

2. MATERIALS AND METHODS

2.1 Study Area

Johor is the second-largest state in the southern part of Peninsular Malaysia. The Johor River Basin as shown in Figure 1 is in the southeast of Johor (1.426°–2.080°N, 103.330°–104.075°E). It originates from Gunung Belumut, stretches for approximately 122.7km, and covers a water area of about 2,63km². The Johor River flows in a north-south direction toward the Straits of Johor, with the Lingui Dam serving as its main reservoir. Several major rivers are located within the basin, including the Sayong River, Lingui River, Tiram River, Semanggar River, Layang River, and Lebam River [20]. Malaysia has an equatorial climate, and the Johor River Basin experiences tropical monsoon influences, receiving rainfall throughout the year [21]. The primary land use and land cover (LULC) types in the basin are natural forests, followed by agricultural areas (oil palm and rubber plantations). Part of the river basin lies within Iskandar Malaysia, which has been undergoing rapid development since 2006 [3]. The major LULC transformations in the basin, driven by increasing urbanization and agricultural expansion, aim to accommodate population growth and meet the economic demands of the industrial and agricultural sectors.

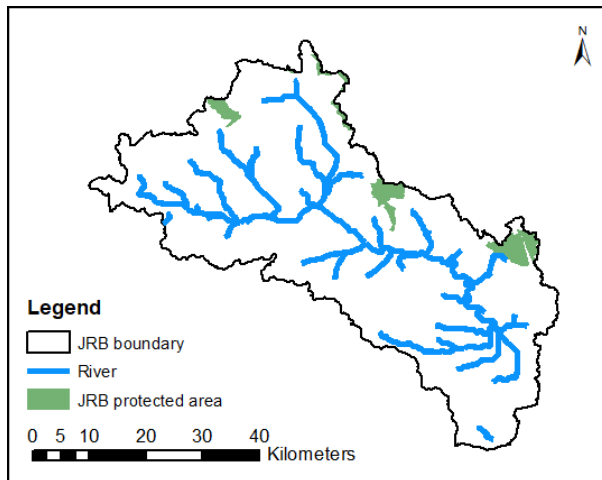


Figure 1. Johor river basin boundary containing river and protected areas

2.2 Data Sources and Processing

The LULC maps used in this study for the years 2000, 2005, 2010, 2015, and 2020 were obtained from a previous study conducted by Kang and Kanniah, which examined land use changes and alterations in river morphology within the Johor River Basin [7]. Six LULC classes were identified in the basin, based on the local land use map provided by the National Land Use Information Division, Department of Town and Country Planning, Malaysia. The *Kappa coefficients* for all land-use classifications from 2000 to 2020 are

greater than 85%, and therefore, the classifications are considered reliable for this study.

The remaining data required for model input are shown in Table 1. The socio-economic data presented in Table 1 represent key sources of negative impacts on habitat quality. These data were used as input raster layers for the threat sources affecting habitat quality in the study area. The respective impact weights and distances of these threats were adjusted based on expert knowledge and findings from similar studies. Environmental data, such as the digital elevation model (DEM), were used to generate elevation and slope information for the study area. These physical and geographical factors were then utilized as variables for correlating with the habitat quality scores generated later in the study.

Table 1. Source of model input

Type	Information	
	Name	Source
Environmental data	Digital Elevation Model	Department of Survey and Mapping Malaysia
Socio-economic data	Population Density	WorldPop
	Building Extent	
	Nighttime Lights	
	Roadmap	OpenStreetMap
	Protected Areas	World Database on Protected Areas

2.3 InVEST Model

InVEST is an open-source software model developed by the U.S. Natural Capital Project Team to map and value the goods and services from nature that sustain human life [15,22]. One of the models included in the software is the Habitat Quality Model that has been utilized in this study. The HQ is suitable for the measurement of anthropogenic impacts on the ecological environment; thus, the degree of habitat degradation was assessed through habitat suitability of different LULC types (H) and the sensitivity of LULC to external threat factors (D), with calculation from the HQI (Q) formulation [22] below:

$$Q_{xj} = H_j \left(1 - \left(\frac{D_{xj}^z}{D_{xj}^z + k^z} \right) \right) \quad (1)$$

where Q_{xj} and D_{xj} represent the HQI and degree of habitat degradation (total threat level) respectively at grid x in the LULC type j ; H_j is each LULC category assigned with a habitat score from 0 to 1 (1 = highest habitat suitability, 0 = no habitat); z

is an empirical model constant of 2.5 and k are scaling parameters (or constants).

Habitat degradation was assessed from the formulation below:

$$D_{xj} = \sum_{r=1}^R \sum_{y=1}^{Y_r} \left(\frac{w_r}{\sum_{r=1}^R w_r} \right) r_y i_{rxy} \beta_x S_{jr} \quad (2)$$

where R represents the index of all modeled degradation sources; Y_r is the set of grid cells for threat r 's raster maps; y indicates the index of all grid cells on r 's raster map; w_r is the weight parameters; β_x is the accessibility factor.

The InVEST model utilizes a half-saturation curve to show the correlation between habitat degradation scores and habitat quality scores, therefore threat decay is assigned as either a linear or exponential distance-decay function.

The impact of threat (i_{rxy}) was assessed from the formulation below:

$$i_{rxy} = 1 - \left(\frac{d_{xy}}{d_{rmax}} \right) \text{ if linear} \quad (3)$$

$$i_{rxy} = \exp \left(- \left(\frac{2.99}{d_{rmax}} \right) d_{xy} \right) \text{ if exponential} \quad (4)$$

where d_{xy} indicates the distance between raster x and y ; d_{rmax} shows the maximum distance of threat r acts.

The threat sources in this study were analyzed with a raster calculator tool through ArcGIS 10.8., and LULC-Threat sensitivities were determined from the InVEST model user's guide [22] and referred to similar studies [1,10,23].

3. RESULTS AND DISCUSSION

3.1 Land Use/Cover Change Analysis

The LULC data for the Johor River Basin (JRB) generated by Kang and Kanniah for the years 2000, 2005, 2010, 2015, and 2020 had Kappa values of 0.955, 0.886, 0.914, 0.940, and 0.957, respectively [7]. These values indicate significant LULC changes in the JRB over the twenty-year period. According to the previous study, the LULC in 2000 was dominated by agricultural land (68.1%), forest (20.7%), water (5.8%), and urban areas (2.3%) [7]. By 2020, urban and water land types had increased to 4.4% and 6.6%, respectively, due to residential expansion, while forest and agricultural land types had decreased to 19.0% and 67.7%, respectively. Particularly concerning is the mangrove land type, which covered less than 2.0% of the study area in 2000; over the past twenty years, nearly 30% of this area has been lost. These changes highlight a significant reduction in habitat-suitable land types, such as forests and mangroves, with a conversion to urban and water land types.

3.2 Habitat Quality Assessment

Changes in LULC and threat source density can directly or indirectly affect ecosystem stability. In

this study, habitat quality and degradation scores are used as quantitative measures to assess changes in ecosystem stability within the study area.

3.3 Changes in Habitat Quality

The spatial-temporal analysis of habitat quality (HQ) over 20 years in the Johor River Basin (JRB), shown in Figure 2, reveals a slight decrease in HQ from 2000 to 2020. From 2000 to 2015, HQ decreased from 0.2474 to 0.2353. However, it increased to 0.2417 from 2015 to 2020, resulting in an overall reduction in HQ from 0.2474 to 0.2417. A notable change in HQ was observed in 2015, likely due to the significant land use changes that occurred between 2010 and 2015. During this period, forest cover was converted into other land types, such as bare soil and agricultural land, leading to decreased habitat suitability in the study area [3]. Similar findings were reported by Zhang et al. (2024), who noted a gradual decline in HQ in the southern part of the Johor River due to land transformation from natural habitat to construction land [10]. The rapid land changes between 2010 and 2015 may have been driven by the development of the Iskandar Malaysia region, which had negative impacts on HQ [3]. Additionally, the loss of water bodies in 2015, particularly due to drought conditions associated with the El Niño climate phenomenon, contributed to the decline in HQ [3,24]. Water bodies, forests, and mangroves are land types with the highest habitat quality in the study area, so the reduction in forest cover and water bodies in 2015 resulted in the lowest HQ scores for the Johor River Basin. On the other hand, the increase in HQ in 2020 compared to 2015 can be attributed to the changes in LULC during the five-year interval. Between 2016 and 2020, the construction of the Seluyut Dam within JRB led to a significant conversion of other land types into water bodies, which improved HQ scores [25]. Additionally, forest cover in 2020 showed a net gain compared to its loss, further reducing the habitat degradation score for that year.

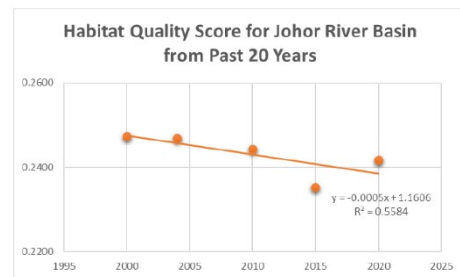


Figure 2. The JRB habitat quality score graph comparison for different years

3.4 Correlation of Impact Factor to Habitat Quality

The impact factors, such as physio-geographical factors (elevation, slope) and anthropogenic

activities (population density, building extent), were applied to statistical analysis (R 4.4.1) to identify their influence on the spatial patterns of habitat quality in the river basin. The results indicated that elevation was significantly correlated with the distribution of habitat quality scores ($p \leq 0.01$) in the Johor River Basin (JRB) over 20 years, as shown in Table 2. The uniform elevation and gentle slopes in the southwestern part of the river basin provided an opportunity for agricultural development, which influenced both LULC distribution and the corresponding habitat quality scores [26]. Population density, on the other hand, was found to have a significant correlation with habitat quality for the reference years ($r_{2020} = -0.33$, $r_{2015} = -0.23$, $r_{2000} = -0.31$, $p \leq 0.01$), but a non-significant correlation for 2010 and 2005 ($r_{2010} = -0.16$, $r_{2005} = -0.17$), indicating that anthropogenic activities increasingly impacted the fragmentation of biodiversity and habitat quality within the river basin. Furthermore, due to high elevation, rising slopes, and the implementation of protected areas, habitat suitability was relatively high in the northeastern part of the study area. The Panti, Seluyut, Kluang, and Ulu Sedili Water Catchment Forests, located in this area, contributed to conserving biodiversity and creating a favourable habitat.

Table 2. Correlation coefficient of impact factors and habitat quality from different years

Year	Impact Factors			
	Elevation	Population Density	Slope	Building Extent
2020	0.59**	-0.33**	0.37**	-0.23*
2015	0.48**	-0.23*	0.18 _{NS}	-0.31*
2010	0.50**	-0.16 _{NS}	0.28*	-0.17 _{NS}
2005	0.51**	-0.17 _{NS}	0.18 _{NS}	-0.35**
2000	0.52**	-0.31*	0.41**	-0.21*

ns: not significant at $p > 0.05$, *significant at $p \leq 0.05$, **significant at $p \leq 0.01$

3.5 Comparing HQ With and Without Protected Areas

Protected areas are crucial for biodiversity conservation, and their effectiveness was analyzed within the study area by comparing habitat quality (HQ) for specific land covers (forests). The input for protected areas in the model was modified by either including or excluding the protected areas vector file. The change analysis of HQ with and without protected areas for forest cover showed a 10.27% difference. The HQ score with protected areas was 0.56, whereas without protected areas, the forest cover scored only 0.51. This indicates the importance of implementing protected areas to reduce the influence of threat sources on natural

habitats. The study also highlights the effectiveness of the protected areas already implemented in the study area.

3.6 Limitations of the Study

The InVEST habitat quality model, while widely applied in biodiversity conservation and landscape management, still has several limitations [1]. One major limitation is the insufficient spatial and temporal data on species distribution, which is essential for habitat quality studies [10, 27]. Obtaining ecologically acceptable and sufficient information for species distribution across the study area typically requires field-based assessments. Therefore, combining field-based habitat suitability assessments with the InVEST habitat quality model could improve its accuracy [28]. Additionally, the InVEST model does not account for the impacts of soil, climate, vegetation differences, and other abiotic factors that are closely linked to habitat suitability [29]. Different vegetation types and forest edge effects can provide distinct habitat conditions for biodiversity. Furthermore, the model relies heavily on the maximum distance and weighting of threat sources to generate habitat quality scores, which can be influenced by expert judgment and modifications to the input parameters [1,16]. To address these issues, correlation analyses should be conducted to compare model outputs with actual conditions in the study area's habitats. Further research is needed to incorporate more detailed physio-geographical and anthropogenic threat sources to enhance the accuracy of habitat quality simulations using this modeling approach.

4. CONCLUSIONS

This study utilized remote sensing and GIS techniques to investigate habitat quality changes within the Johor River Basin over the period 2000–2020. While minor changes in habitat quality scores were observed, there was a significant decline in habitat quality in 2015, with the impacts of climate change and anthropogenic activities being particularly highlighted. The correlation analysis of physio-geographical factors revealed that land elevation influenced the extent of anthropogenic activity in the area. Additionally, the increasing significance of anthropogenic activities on habitat quality indicates that human impacts are increasingly affecting the habitat suitability of the study area. This study underscores how these anthropogenic modifications impact the ecosystem and environment.

In contrast, the positive role of environmental protection efforts in mitigating anthropogenic impacts is also evident in this study. The implementation of protected areas helped reduce habitat degradation, particularly in forest cover

within the study area. To improve overall habitat quality in the Johor River Basin, it is recommended that land management strategies be tailored to address the extent of habitat degradation. A key contribution of this study is that regional habitat quality assessments can serve as guidelines for future policy development and modification. Modeling approaches to habitat quality can assist decision-makers and practitioners in better understanding habitat conditions through visualized outcomes. Ultimately, understanding the role of anthropogenic and abiotic factors in habitat quality will become increasingly important for sustainable development and future human welfare.

REFERENCES

- [1] A.B. Aneseyee, T. Noszczyk, T. Soromessa, E. Elias, "The InVEST Habitat Quality Model Associated with Land Use/Cover Changes: A Qualitative Case Study of the Winike Watershed in the Omo-Gibe Basin, Southwest Ethiopia," *Remote Sens.* 12 (2020) 1103.
- [2] L. Dai, "The influence of land use change on the spatial-temporal variability of habitat quality between 1990 and 2010 in Northeast China," *J. For. Res.* 30 (2019) 2227–2236.
- [3] E.C. Ellis, U. Pascual, O. Mertz, "Ecosystem services and nature's contribution to people: negotiating diverse values and trade-offs in land systems," *Curr. Opin. Environ. Sustain.* 38 (2019) 86–94.
- [4] A.K. Mashizi, F.J. Escobedo, "Socio-ecological assessment of threats to semi-arid rangeland habitat in Iran using spatial models and actor group opinions," *J. Arid Environ.* 177 (2020) 104136.
- [5] M. Gaglio, M. Lanzoni, G. Nobili, D. Viviani, G. Castaldelli, E.A. Fano, "Ecosystem services approach for sustainable governance in a brackish water lagoon used for aquaculture," *J. Environ. Plan. Manag.* 62 (2019) 1501–1524.
- [6] X. Zhang, W. Song, Y. Lang, X. Feng, Q. Yuan, J. Wang, "Land use changes in the coastal zone of China's Hebei Province and the corresponding impacts on habitat quality," *Land use policy.* 99 (2020) 104957.
- [7] C.S. Kang, K.D. Kanniah, "Land use and land cover change and its impact on river morphology in Johor River Basin, Malaysia," *J. Hydrol. Reg. Stud.* 41 (2022) 101072.
- [8] Y. Wang, "Impact of climate change on dengue fever epidemics in South and Southeast Asian settings: A modelling study," *Infect. Dis. Model.* 8 (2023) 645–655.
- [9] Y. Yang, P. Li, "Scene-and pixel-level analysis of Landsat cloud coverage and image acquisition probability in South and Southeast Asia," *Int. J. Appl. Earth Obs. Geoinf.* 123 (2023) 103477.
- [10] J. Zhang, F. Yan, F. Su, V. Lyne, X. Wang, X. Wang, "Response of habitat quality to land use changes in The Johor River Estuary," *Int. J. Digit. Earth.* 17 (2024) 2390439.
- [11] A. Najah, A. Elshafie, O.A. Karim, O. Jaffar, "Prediction of Johor River water quality parameters using artificial neural networks," *Eur. J. Sci. Res.* 28 (2009) 422–435.
- [12] L. Qicai, "Influence of dams on river ecosystem and its countermeasures," *J. Water Resour. Prot.* 2011 (2011).
- [13] X.G. Wang, F.Z. Su, J.J. Zhang, F. Cheng, W.Q. Hu, Z. Ding, "Construction land sprawl and reclamation in the Johor River Estuary of Malaysia since 1973," *Ocean Coast. Manag.* 171 (2019) 87–95.
- [14] J.K. Kazak, J. van Hoof, "Decision support systems for a sustainable management of the indoor and built environment," vol. 27, no. 10. SAGE Publications Sage UK: London, England, 2018, pp. 1303–1306.
- [15] B. Xie, M. Zhang, "Spatio-temporal evolution and driving forces of habitat quality in Guizhou Province," *Sci. Rep.* 13 (2023) 6908.
- [16] M. Terrado, S. Sabater, B. Chaplin-Kramer, L. Mandle, G. Ziv, V. Acuña, "Model development for the assessment of terrestrial and aquatic habitat quality in conservation planning," *Sci. Total Environ.* 540 (2016) 63–70.
- [17] L.T. Beumer, F.M. van Beest, M. Stelvig, N.M. Schmidt, "Spatiotemporal dynamics in habitat suitability of a large Arctic herbivore: Environmental heterogeneity is key to a sedentary lifestyle," *Glob. Ecol. Conserv.* 18 (2019) e00647.
- [18] Z. Niu, "A Process-Based Model Integrating Remote Sensing Data for Evaluating Ecosystem Services," *J. Adv. Model. Earth Syst.* 13 (2021) e2020MS002451.
- [19] X. He, J. Tian, Y. Zhang, Z. Zhao, Z. Cai, Y. Wang, "Attribution and driving force of nitrogen losses from the Taihu Lake Basin by the InVEST and GeoDetector models," *Sci. Rep.* 13 (2023) 7440.
- [20] M.B. Kia, S. Pirasteh, B. Pradhan, A.R. Mahmud, W.N.A. Sulaiman, A. Moradi, "An artificial neural network model for flood simulation using GIS: Johor River Basin, Malaysia," *Environ. Earth Sci.* 67 (2012) 251–264.
- [21] M.L. Tan, A.L. Ibrahim, Z. Yusop, Z. Duan, L. Ling, "Impacts of land-use and climate variability on hydrological components in the Johor River basin, Malaysia," *Hydrol. Sci. J.* 60 (2015) 873–889.
- [22] R. Sharp et al., *InVEST User's Guide.* (2018).
- [23] C. Chen, J. Liu, L. Bi, "Spatial and Temporal Changes of Habitat Quality and Its Influential

- Factors in China Based on the InVEST Model,” *Forests*, 14 (2023) 374.
- [24]F. Tangang, L. Juneng, E. Salimun, A. Jamaluddin, “Scientific understanding of El Niño-Southern Oscillation (ENSO) and its climatic impacts in Malaysia and surrounding region,” (2019) 5–31.
- [25]H. Heng, W. Pan, J. Siaw Fei Lu, C. Hii, “Coastal and Estuary Reservoir: Case Studies for Johor River Basin,” *J. Civ. Eng. Sci. Technol.* 8 (2017) 25–40.
- [26]M. Hashim et al., “Analysis of Water Yield Changes in the Johor River Basin, Peninsular Malaysia Using Remote Sensing Satellite Imagery,” *Remote Sens.* 15 (2023) 3432.
- [27] S. Polasky, E. Nelson, D. Pennington, and K.A. Johnson, “The impact of land-use change on ecosystem services, biodiversity and returns to landowners: a case study in the state of Minnesota,” *Environ. Resour. Econ.* 48 (2011) 219–242.
- [28]X. Guo, N.C. Coops, P. Tompalski, S.E. Nielsen, C.W. Bater, J.J. Stadt, “Regional mapping of vegetation structure for biodiversity monitoring using airborne lidar data,” *Ecol. Inform.* 38 (2017) 50–61.
- [29]Y. Zhang et al., “Spatial and temporal variability in the net primary production of alpine grassland on the Tibetan Plateau since 1982,” *J. Geogr. Sci.* 24 (2014) 269–287.

CORRELATION AND TIMING BETWEEN REGIONAL WATER STRESS FACTORS AND OIL PALM YIELD USING 22-YEAR SATELLITE DATA IN MALAYSIA AND INDONESIA**C. NAITO^{1,2*} and W. TAKEUCHI²**¹*Graduate School of Engineering, The University of Tokyo, Tokyo, Japan*²*Institute of Industrial Science, the University of Tokyo, Tokyo, Japan***Correspondence: chihiro-naito807@g.ecc.u-tokyo.ac.jp***Keywords:** *Precipitation, Temperature, Evaporation, Transpiration, Soil moisture, VOD***1. INTRODUCTION**

Palm oil is globally used in various products and industries, mostly produced in Malaysia and Indonesia across millions of hectares. However, climate change is projected to negatively impact oil palms due to water stress. Generally, oil palms prefer consistent precipitation throughout the year, high temperatures, and a balance between precipitation and soil evaporation for optimal growth. The risk of water stress varies among regions because multiple climate factors, including soil moisture and other water-related variables, influence palm growth. The importance of these climate factors varies by region, as several studies have found different factors significant for oil palm production [1,2]. Additionally, the timing of stress is crucial for oil palms to form fruits [1]. Since it is important to implement adaptation actions based on local situation, identifying region-specific influential factors, their timing, and their long-term changes can help develop effective strategies. Therefore, this study investigated 1) the important climate factors and their crucial timing, and 2) changes in these important factors over 22 years to discuss the impact of climate change on palm production at the state or provincial level in Malaysia and Indonesia.

2. METHODOLOGY

Annual yield of fresh fruit bunch (FFB) (ton/ha) in Malaysia and Indonesia from 2002 to 2023 was collected. Satellite data of water components included temperature at 2 meters above the surface, precipitation, evaporation, transpiration, soil moisture, vegetation optical depth (VOD), and vapor pressure deficit (VPD). VPD was calculated based on [3]. All data was on a 0.1-degree grid and aggregated to monthly data. An oil palm distribution data with planted year [4] was also used to extract pixels containing palm planted before 2002. There were 37 regions where oil palms have been cultivated since 2002.

The Pearson correlation coefficient between FFB and each water variable for each month of the year and the previous year was calculated. The most negative Pearson correlation coefficient was selected to identify the risk variable and its month.

Long-term changes in the risk variables for the specific month were analyzed to assess climate change impacts on the variable, using the standard deviation (Std) and the Mann-Kendall trend slope.

3. RESULTS AND DISCUSSIONS

Soil moisture and VOD were selected as risk variables in 11 and 18 regions, respectively. However, some regions had both negative and positive correlations with soil moisture or VOD in different months, indicating that the importance of these variables depends on the season. Figure 1(a) presents the 22-year trend of soil moisture in August in Kelantan state, where soil moisture had the most negative correlation with FFB among the seven water components. Figure 1(b) shows the trend of soil moisture in regions where soil moisture was selected as the risk variable. The red bars represent a positive annual FFB trend, while the blue bars indicate a negative trend. Figure 1(b) shows that some regions had a negative FFB trend as soil moisture increased, which may indicate a decline in FFB due to surplus water. On the other hand, other regions had a positive FFB trend with an increase in soil moisture. High fluctuations in soil moisture also indicated a similar tendency for a decline in FFB.

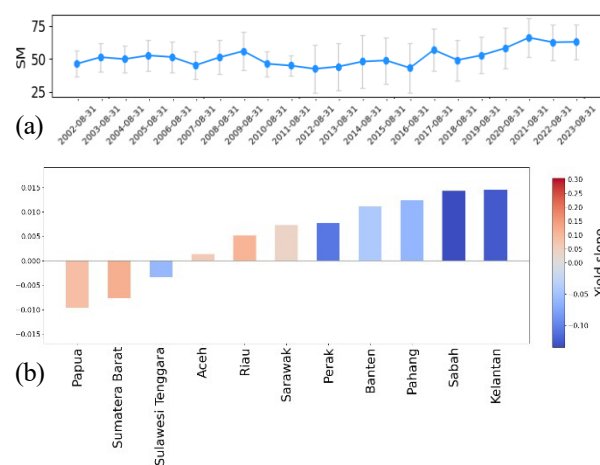


Figure 1. (a) Soil moisture in August from 2002 to 2023 in Kelantan state. (b) Soil moisture trends among regions where soil moisture is identified as a risk variable.

4. CONCLUSIONS

Increased soil moisture and its fluctuation, indicating waterlogged condition, might be caused by seasonal change of water cycle, which leads decline of palm yield. Long-term variable change analysis found future risk areas in Malay peninsula and some provinces in Indonesia.

REFERENCES

- [1] P. Oettli, et al. Sci Rep. 8 1 (2018) 2271.
- [2] J. P. Monzon et al., Agric. For. Meteorol. 314 (2022) 108789.
- [3] Y. Liu, et al. Ecol. Indic. 161 (2024) 111976.
- [4] A. Descals, et al. Earth Syst. Sci. Data Discuss. (202 4) 1–24

ADAPTING TO CLIMATE CHANGE: MITIGATIVE AND ADAPTIVE APPROACHES IN INDONESIA'S PALM OIL INDUSTRY

N.H. DARLAN^{1*}, I. PRADIKO¹ and I.Y. HARAHA²

¹Research Division, Indonesian Oil Palm Research Institute, Medan, Indonesia

²PT Riset Perkebunan Nusantara, Bogor, Indonesia

*Correspondence: nuzulhijri@gmail.com

Keywords: Sustainable palm oil, Climate resilience, Emission reduction

1. INTRODUCTION

The palm oil industry is a cornerstone of Indonesia's economy, contributing approximately 11% of national export earnings and supporting millions of livelihoods. However, this sector faces mounting challenges due to climate change, which threatens its productivity and long-term viability. Rising global temperatures, more frequent extreme weather events, and shifting rainfall patterns are disrupting the growth cycles of oil palms and increasing vulnerability to pests and diseases. The industry is also under scrutiny for its environmental footprint, as it accounts for 12% of Indonesia's GHG emissions, primarily through land-use changes, deforestation, fertilizer application, and methane emissions from POME. Addressing these challenges requires a dual approach that integrates mitigation and adaptation. Mitigation strategies aim to reduce emissions and environmental impacts, while adaptation measures focus on enhancing the sector's resilience to climate variability. This paper explores these strategies, supported by empirical research and case studies, to outline a sustainable path forward for Indonesia's palm oil sector.

2. CLIMATE CHANGE IMPACTS ON THE PALM OIL SECTOR

The impacts of climate change on the palm oil sector are both immediate and long-term, affecting productivity, smallholder livelihoods, and the broader economy. Rising temperatures, altered rainfall patterns, and the proliferation of pests and diseases highlight the need for urgent action. A combination of mitigation and adaptation strategies—such as efficient water management, resilient crop varieties, and sustainable land-use practices—is essential to address these challenges and secure the future of Indonesia's palm oil sector in a rapidly changing climate. Indonesia's palm oil sector is particularly vulnerable to the multifaceted impacts of climate change, which threaten both the productivity of plantations and the livelihoods of millions of smallholders and workers. These impacts stem from rising temperatures, altered rainfall patterns, increased drought frequency, and the proliferation of pests and diseases, each of which is

explored in greater detail below. Rising Temperatures and Heat Stress As global temperatures rise, oil palms face increasing heat stress, which disrupts their physiological processes. Oil palms have an optimal temperature range of 24–28°C, and prolonged exposure to temperatures exceeding 30°C can impair photosynthesis. This leads to reduced fruit formation and lower yields.

Research has shown that a 1°C increase in average temperature can reduce yields by 10–15%. In areas like Sumatra and Kalimantan, where annual average temperatures are already high, further increases could push conditions beyond the tolerance limits of oil palms. Additionally, heat stress accelerates evapotranspiration rates, leading to greater moisture loss from the soil and plant surfaces. This increases the water demand of oil palms, exacerbating the stress on water resources.

2.1 Rainfall Variability and Water Stress

Rainfall patterns in Indonesia have become increasingly erratic, with significant implications for oil palm productivity. Oil palms require a minimum annual rainfall of 1,800–2,500 mm, evenly distributed throughout the year, to thrive. Deviations from these norms—either in the form of droughts or excessive rainfall—can disrupt plantation operations.

The Droughts often associated with El Niño events, limit the availability of water for irrigation and reduce soil moisture with prolonged dry spells. This impedes the development of fruit bunches, leading to lower yields. Historical data shows that during the 2015–2016 El Niño, drought conditions reduced palm oil yields in Sumatra and Kalimantan by up to 30%, translating into billions of dollars in economic losses.

Meanwhile, the excessive rainfall with heavy and prolonged rains lead to waterlogging, root damage, and increased susceptibility to fungal diseases. Waterlogged soils also hinder nutrient uptake, reducing tree health and productivity. Flooding in low-lying plantations often disrupts harvesting and transportation, increasing costs by an estimated 15–20%.

2.2 Increased Frequency of Extreme Weather Events

Extreme weather events such as tropical storms and floods have become more frequent and severe, directly impacting plantations. Strong winds can cause physical damage to palms, particularly younger ones, while floods can erode topsoil, reducing land fertility. The combination of these factors not only reduces yields but also increases the cost of replanting and recovery.

2.3 Pests and Diseases

Climate change has altered the ecological balance in plantations, leading to the proliferation of pests and diseases. Warmer temperatures and shifting humidity levels create favourable conditions for several pests, for example bagworm (*Metisa plana*) which defoliates oil palms, reducing yield potential by up to 43% in heavily infested plantations.

Diseases such as *Ganoderma boninense* — a fungal pathogen causing basal stem rot — are also exacerbated by changing climatic conditions. *Ganoderma* affects approximately 50% of plantations in high-humidity areas and is responsible for yield losses of 15–20% annually. As climate conditions become more conducive to its spread, the disease could further threaten productivity.

2.4 Soil Erosion and Degradation

Erratic rainfall patterns, combined with deforestation and poor land management, have intensified soil erosion in oil palm plantations. Heavy rains wash away the fertile topsoil, reducing the availability of essential nutrients for palm growth. Soil erosion also increases sedimentation in rivers, disrupting local water ecosystems and reducing water quality.

A study in Sumatra found that plantations without adequate soil conservation measures experienced an average annual soil loss of 20 tons per hectare, significantly reducing long-term land productivity.

2.5 Impact on Smallholder Farmers

Smallholders, who manage nearly 40% of Indonesia's oil palm plantations, are disproportionately affected by climate change. Lacking access to advanced farming techniques, irrigation infrastructure, or financial safety nets, smallholders are particularly vulnerable to yield fluctuations.

The climate change impact the smallholder farmers in income volatility, which the lower yields will directly translate into reduced incomes; and in increased costs, because the extreme weather events force smallholders to invest in costly recovery measures such as replanting or pest control.

2.6 Economic Consequences

The cumulative impacts of climate change on palm oil production have significant economic implications. Yield reductions from droughts, pests, and diseases lower export revenues and increase the price of palm oil on global markets. For Indonesia, which relies on palm oil for 11% of its export earnings, these challenges could undermine economic stability, particularly in rural areas dependent on the industry.

2.7 Broader Environmental Implications

Climate change's feedback loops amplify its impacts on the palm oil sector. For example, deforestation for plantation expansion contributes to GHG emissions, which accelerate global warming and intensify climate change impacts. Without intervention, these cycles will continue to threaten the sustainability of Indonesia's palm oil industry.

3. MITIGATION STRATEGIES

Mitigation efforts in the palm oil sector focus on reducing GHG emissions through innovative practices and technologies. One of the most effective strategies is the recovery of biogas from POME, which accounts for approximately 50% of methane emissions from palm oil mills. Methane, a potent GHG, has a global warming potential 25 times greater than CO₂. By installing anaerobic digesters, mills can capture this methane and convert it into biogas for renewable energy use. For instance, a mill in Sumatra reduced its emissions by 40,000 tons of CO₂e annually, while simultaneously generating energy to power mill operations, reducing diesel consumption by 60%.

Biomass energy offers another sustainable solution. Residues such as empty fruit bunches (EFB), kernel shells, and palm fibers are often discarded or burned, contributing to pollution. However, these materials have high calorific values, making them ideal for energy production. The Wilmar Group in East Kalimantan demonstrated the potential of biomass energy by using these residues in combined heat and power (CHP) systems, reducing fossil fuel dependency by 50% and producing nutrient-rich ash for use as fertilizer.

Solar energy integration is also gaining traction. Indonesia's vast solar potential, estimated at 207 GW, remains underutilized. Solar photovoltaic (PV) systems installed on mill rooftops can provide clean electricity, while solar-powered pumps improve irrigation efficiency in remote plantations. A pilot project in Jambi produced 120 kW of clean energy annually, reducing grid dependency by 20% and lowering operational costs.

Additionally, Indonesia's commitment to biofuel production is reflected in its B35 program, which mandates a 35% blend of biodiesel in diesel fuel.

This initiative reduced 40 million tons of CO₂e emissions in 2023 alone, positioning palm-based biodiesel as a key contributor to national energy security and global GHG reduction efforts.

4. ADAPTATION STRATEGIES

Adaptation strategies in oil palm plantations are essential to address the multifaceted impacts of climate change, such as rising temperatures, irregular rainfall, prolonged droughts, and the proliferation of pests and diseases. One critical approach is improving water management. This includes deploying drip irrigation systems that deliver water directly to plant roots, significantly reducing waste and ensuring consistent moisture even during dry spells. Additionally, rainwater harvesting systems can capture excess rainfall during wet seasons for use during drought periods, while efficient drainage systems prevent waterlogging and soil erosion during heavy rains. Together, these methods enhance the resilience of plantations to both drought and excessive rainfall.

Developing and adopting drought-resistant oil palm varieties is another crucial strategy. These varieties are specifically bred to tolerate reduced water availability and higher temperatures, ensuring stable yields under challenging climatic conditions. For example, trials conducted by the Indonesian Oil Palm Research Institute (IOPRI) demonstrated that drought-resistant varieties could maintain yields even with 25% lower-than-average rainfall. Providing smallholders with access to these improved varieties through subsidies or distribution programs is vital to scaling their adoption.

Agroforestry integration is also gaining traction as an adaptive measure. By combining oil palms with shade-providing trees or food crops, agroforestry systems create microclimates that reduce heat stress, improve soil stability, and enhance biodiversity. Research in Kalimantan revealed that agroforestry increased yields by 10–15% and boosted soil moisture retention by 30%, while also providing additional income streams for farmers through the cultivation of secondary crops.

Maintaining soil health is another foundational adaptation strategy. Practices such as mulching with organic residues and applying biochar enhance soil fertility, improve water retention, and mitigate the effects of drought. For instance, plantations employing biochar reported a 20% improvement in productivity during prolonged dry periods. Additionally, contour planting and terracing in hilly areas reduce erosion and increase water infiltration, further supporting the long-term viability of plantations.

Integrated pest and disease management is necessary to address the increased prevalence of pests and diseases driven by changing climatic

conditions. Biological controls, such as introducing natural predators to manage pest populations, and the use of disease-resistant palm varieties can reduce yield losses while minimizing the need for chemical interventions. Regular monitoring systems also help in the early detection and containment of outbreaks, reducing their impact on productivity.

Empowering smallholders through training programs, financial aid, and access to climate information is critical for inclusive adaptation. Smallholders, who manage nearly 40% of Indonesia's oil palm plantations, often lack the resources and knowledge needed to implement advanced adaptation measures. Capacity-building initiatives can equip them with skills in water management, pest control, and agroforestry, while financial support through microloans or subsidies can lower the barriers to adoption.

Finally, policy and institutional support play a pivotal role in scaling adaptation strategies. Governments can provide incentives for adopting climate-smart practices, such as subsidies for drip irrigation systems or grants for soil health improvement projects. Public-private partnerships can also mobilize funding and technical expertise to develop and implement large-scale adaptation programs. These combined efforts ensure that oil palm plantations are better equipped to withstand the challenges posed by climate change, safeguarding both productivity and livelihoods.

5. SOCIO-ECONOMIC AND POLICY DIMENSIONS

Smallholder farmers play a pivotal role in Indonesia's palm oil sector, managing nearly half of the country's plantations. Empowering these farmers with access to sustainable practices and renewable technologies is vital for achieving climate resilience. Training programs initiated by the Roundtable on Sustainable Palm Oil (RSPO) have improved smallholder yields by 18% and reduced fertilizer costs by 12%.

Policy support is equally important. Indonesia's Nationally Determined Contributions (NDCs) target a 29% reduction in emissions by 2030, with the palm oil sector identified as one of focus area. Government incentives for biogas systems, solar PV installations, and biodiesel production are driving the transition to green energy. Public-private partnerships and green bonds have provided critical funding for renewable energy projects for biogas and biomass initiatives in 2022.

6. CONCLUSIONS

Indonesia's palm oil industry is at a crossroads, where sustainability and resilience must be prioritized to ensure its long-term viability. By integrating mitigation strategies such as biogas

recovery, biomass energy, and solar PV systems with adaptation measures like agroforestry and drought-resistant crops, the sector can reduce its environmental footprint while safeguarding livelihoods. Collaborative efforts among governments, businesses, and communities are essential to realizing this vision. These strategies not only align with Indonesia's climate goals but also position the palm oil industry as a global leader in sustainable agriculture.

REFERENCES

- [1] Agus, F., Gunarso, P., Sahardjo, B. H., & Killeen, T. J. (2013). "Oil Palm and Land Use Change in Indonesia, Malaysia, and Papua New Guinea." Reports from the Technical Panels of the 2nd Greenhouse Gas. Working Group of the Roundtable on Sustainable Palm Oil.
- [2] Fitzherbert, E. B., Struebig, M. J., Morel, A., Danielsen, F., Brühl, C. A., Donald, P. F., & Phalan, B. (2008). "How will oil palm expansion affect biodiversity?" *Trends in Ecology & Evolution*, 23(10), 538-545. *Nature Sustainability*.
- [3] Germer, J., & Sauerborn, J. (2008). "Estimation of the impact of oil palm plantation establishment on greenhouse gas balance." *Environment, Development and Sustainability*
- [4] Hansen, S., & Surya, D. (2020). "Mitigating Methane Emissions in Palm Oil Processing: A Case Study in Sumatra." *Journal of Clean Production*, 258, 120947. Vermeulen, S. J., Campbell, B. M., & Ingram, J. S. I. (2012). "Climate Change and Food Systems" *Annual Review of Environment and Resources*, 37(1), 195-222.
- [5] Wicke, B., Dornburg, V., Junginger, M., & Faaij, A.P.C. (2008). "Different palm oil production systems for energy purposes and their greenhouse gas implications." *Biomass and Bioenergy*, 32(12), 1322-1337.

REMOTE SENSING FOR CLIMATE CHANGE, GREEN RECOVERY AND SUSTAINABILITY

H. Z. M. SHAFRI

Department of Civil Engineering, Faculty of Engineering, Universiti Putra Malaysia, Selangor, Malaysia

Keywords: Remote sensing, climate change, green recovery, sustainability, geospatial, mapping, monitoring

1. INTRODUCTION

The increasing severity of climate change, marked by rising temperatures, extreme weather events, and shifting ecosystems, necessitates immediate and effective responses. Remote sensing, defined as the acquisition of information about an object or area from a distance (typically via satellite or aerial sensors), provides critical data that can inform climate action and sustainability initiatives. This technology enables scientists and policymakers to monitor environmental changes, assess natural resources, and evaluate the effectiveness of mitigation and adaptation strategies. By leveraging remote sensing data, countries can enhance their green recovery efforts - initiatives aimed at rebuilding economies in ways that are environmentally sustainable and resilient to climate impacts [1].

2. STATUS AND CHALLENGES

Remote sensing technologies, such as satellites, drones, and ground-based sensors, play a crucial role in monitoring climate change and supporting sustainable development [2]. These technologies provide accurate and timely data on parameters like land use, deforestation, carbon emissions, sea level rise, and glacier melt. Platforms like NASA's Earth Observing System and the European Space Agency's Sentinel satellites offer global datasets crucial for environmental policy and action. Recent advancements in AI and big data analytics further enhance the processing and interpretation of remote sensing data, making it more actionable for addressing climate challenges.

Remote sensing aids in tracking ecosystem restoration efforts, identifying areas for afforestation, and monitoring renewable energy projects like solar and wind farms. It supports precision agriculture by optimizing resource use and reducing emissions [3]. During the post-pandemic recovery, remote sensing has helped assess environmental changes and guide green economic strategies.

Despite advancements, remote sensing faces several challenges that hinder its full potential. Limitations in spatial and temporal resolution persist, particularly in remote or developing regions, creating significant data gaps. The high costs of

sophisticated remote sensing tools and data further restrict accessibility, especially for low-income countries. Additionally, integrating remote sensing data with ground-based observations and socio-economic information remains complex, requiring advanced methodologies and expertise [4]. Moreover, translating remote sensing insights into actionable policies demands robust interdisciplinary coordination, which is often insufficient, delaying effective implementation and decision-making.

3. CONCLUSIONS

Remote sensing plays a pivotal role in addressing climate change, fostering green recovery, and promoting sustainability. By providing accurate, timely data on environmental changes, it supports informed decision-making for mitigation and adaptation strategies. This technology enables the monitoring of deforestation, urban expansion, carbon emissions, and renewable energy potential, contributing to sustainable land use and resource management. As we aim for a green recovery, remote sensing helps track progress toward climate goals, assess ecosystem health, and identify areas needing restoration. Its integration with policy and community initiatives is essential for creating a resilient, sustainable future in the face of global challenges.

REFERENCES

- [1] Hsieh, YL., Yeh, SC. The trends of major issues connecting climate change and the sustainable development goals. *Discov Sustain* 5, 31 (2024).
- [2] Shaohua Z., Min L., Minghui T., Wei Z., Xiaoyan L., Yujiu X., Feng L., Qiao W. The role of satellite remote sensing in mitigating and adapting to global climate change, *Science of The Total Environment*, 904 (2023).
- [3] Han, H., Liu, Z., Li, J. Challenges in remote sensing-based climate and crop monitoring: navigating the complexities using AI. *J Cloud Comp* 13, 34 (2024).
- [4] Wang, X. Remote Sensing Applications to Climate Change. *Remote Sens.* 15 (2023).

SUSTAINABLE BUILT DEVELOPMENT AND CLIMATE CHANGE ADAPTION: A CASE STUDY FROM LEH, LADAKH, INDIA

SURENDER K NEGI¹, KISHOR S. KULKARNI^{1*}, AJAY CHOURASIA² and P. K. RAMANCHARLA²

¹Architecture Planning and Energy Efficiency, CSIR-Central Building Research Institute, Roorkee, India

²CSIR-Central Building Research Institute, Roorkee, India

*Correspondence: kishorsk@cbri.res.in

Keywords: Climate change, Climate resilient building design, Sustainable built environment

1. INTRODUCTION

One of the greatest challenges of the twenty-first century is climate change, which has negative effects on the environment, human health, and the economy. The most prominent effects of climate change include: an increase in extreme weather events like droughts, hurricanes, heat waves, heavier rainfall events leading to flooding and landslides; rise sea level etc. Due to climatic instability, climatic variables like wind, precipitation, solar irradiance, and humidity vary a lot. Intergovernmental Panel on Climate Change (IPCC) confirms that the main causes of climate change are the emissions of anthropogenic greenhouse gases (GHG), which include nitrous oxide, methane, and carbon dioxide (CO₂).

A building provides protection from external environment, space for household activities and opportunity to foster human health against the extreme outdoor environment. The major impact of climate change on buildings are thermal discomfort, increase in heating-cooling demand, and/or GHG emissions. In extreme conditions, the building becomes thermally uncomfortable to live for the occupants. Buildings' heating and cooling requirements are increasing significantly because of climate change, with geographical and climatic variations determining the amount of increase. Hence, it is very eminent to construct the buildings with such a design criterion so that the building become thermally comfortable for living and the outdoor temperature did not affect the occupants living inside the building. The proper building envelope design combined with passive building designs will ensure better performance of the structures.

For the better performance of the buildings in extreme climatic areas, the passive design strategies need to be opted. To provide an accurate representation of the functionality of a climate-responsive structure, full-scale field testing must be conducted. Also, in a climate responsive building, energy utilization can be thought of as a possible cost savings. In extreme cold weather, the outdoor environmental temperature has potential to deal with such conditions while the indoor environmental

conditions act as a buffer against the outside temperature. In the present study a sustainable climate resilient building design is proposed for the cold region of India.

2. STUDY AREA (LEH)

Leh, a region among the highest mountains in the world, is an area in which past, present, and future are fundamental aspects in a constant relationship. The region of Leh falls in the rain shadow area of the Himalayas. Scarce precipitation (< 100mm per year) characterized this land and therefore influenced the house form. Leh is a high-altitude cold desert that can reach temperatures down to -30 to -40 °C during winter. On the other hand, summer temperatures can also rise to 30-35 °C. Similarly, the region has the highest solar radiation available and the soil temperature below ground remains stable at a depth of about 10m from ground level that is not fully exploited in building usage.

The construction of Leh houses can perish quickly if not properly maintained, even if the dry climate and scarce rainfall in Leh permit better conservation of buildings as compared to other regions. The construction of the house is influenced by the place, not only because of the availability of materials. Masons might be specialized in one construction technique- e.g. stone works.

3. BUILT ENVIRONMENT

Historically, Leh buildings have been constructed using locally available materials like stone, mud and wood. Most are well-preserved traditional Tibetan city in the world. These traditional techniques include thick walls and small windows that can help retain heat as well as flat roofs to withstand heavy snow. Increased tourism and economic development in Leh need to change the building construction. Leh buildings face several issues due to extreme cold temperatures which can affect their structural integrity, comfort and energy efficiency.

Traditional Leh buildings retain heat better than modern materials, but they can still lose warmth quickly due to the prolonged sub-zero temperatures, making the interiors uncomfortably cold. In extreme

cold, buildings without proper insulation rely on continuous heating, increasing fuel consumption and costs. As the wood is scarce and importing fuel is costly in Leh, so buildings must minimize reliance on external heating sources and therefore emphasize should be on the need for passive solar heating and building insulation. Traditional buildings with mud walls are vulnerable to moisture retention which can weaken the structural integrity over time and lead to cracks or erosion in the walls [1].

With the arrival of new technology and materials, contemporary construction practices in Leh have evolved but often face challenges adapting to the extreme climate. Modern buildings increasingly use concrete, bricks, and steel, which are less suitable for Leh environment due to low thermal mass and poor insulation properties. These materials are also not locally sourced, adding to transportation costs and environmental impact. Glass is now more common, and many new buildings incorporate large windows for aesthetics and views. Due to a lack of insulation in walls, roofs, and windows, modern structures often struggle with thermal comfort, requiring more energy for heating. Figure 1 shows an example of the present construction in Leh.



Figure 1. Present construction in Leh

From Figure 1, it is observed that the orientation of the building is not planned which results in less exposure to sunlight. The windows couldn't allow significant sunlight, which is beneficial in a cold climate, as it provides passive solar heating. When sunlight enters, it can warm up the interior spaces during the day. The simplicity of the structure, with fewer complex forms or shapes, may make it more affordable and quicker to construct. This might also mean less surface area for heat loss. There are single-pane windows which leads to substantial heat loss during the night and cold days, as single panes are not effective insulators. Double or triple glazing would be more suitable for insulation.

The walls and roof lacks insulation, which is crucial for extreme climates like Leh, where winters are harsh. The lack of proper insulation means the building lose heat rapidly, leading to uncomfortable

indoor temperatures and increased heating costs. The roof is simple, flat, possibly metallic structure. Without proper insulation, this type of roof could allow significant heat loss, as heat naturally rises and escapes through poorly insulated roofs. The walls are built from standard masonry without thermal insulation, they will absorb heat during the day but also release it quickly when temperatures drop at night. In Leh climate, materials with high thermal mass or appropriate insulation are essential to retain heat longer.

4. CASE STUDY: PROPOSED CONSTRUCTION TECHNIQUE IN LEH

In the present study, sustainable building envelope with improved thermal mass and Low-energy building designs have been proposed for the climate resilient building in Leh. The proposed construction practice considers modern building materials and techniques. The structure is consisting of masonry wall having entrance from East facing and large window openings towards South direction. Figure 2(a) shows the proposed building plan having built-up area is 76 sqm. The building plan consists of one living room, one bedroom, kitchen and toilet.

In substructure, the foundation of the building is majorly made up of stone masonry. In super-structure outer walls are made up of EPS (Expanded polystyrene) sandwiched between the layers, outer layer being made up of stone masonry and inner layer is made up of rammed bricks which Thermal Transmittance having U value $0.289 \text{ W/m}^2\text{K}$ (Figure 2(b)). The inner walls are made up of rammed earth. The trombe walls are also provided in toilets and bedroom, orienting southward and westward side, which is a passive solar design element. The walls consist high thermal mass and wall painted with dark colour to absorb thermal energy from direct sunlight.

Figure 2(c) shows, roof of the building is made up of four different materials acting as a single composite material. Bottom layer of the roof is made up of XPS insulation wool. Above the insulation wool, 0.9 mm thick decking sheet is provided. The upper layer of the roof consists of 100 mm thick RCC slab in which (Thermal transmittance (U) $0.178 \text{ W/m}^2\text{K}$). All the four layers are connected by using tie rods penetrated in between these layers. The proposed building features include climate-resilient planning, the use of locally available materials, hybrid envelope systems, passive solar heating, earthquake resistance, water-resistant envelopes, and enhanced thermal properties.

5. SIMULATION RESULTS

Figure 3 shows the render view of the proposed building for Leh using the Design Builder simulation software. By applying the various required inputs (building orientation, building

materials, lighting properties, HVAC system, etc.) during the peak seasons of the year. The monthly energy consumption for present construction is shown in Figure 4(a) and for proposed building is shown in Figure 4(b). The simulation results show that it is more energy efficient as compared to the present construction as the heating and cooling loads are minimized in proposed building than in present construction.

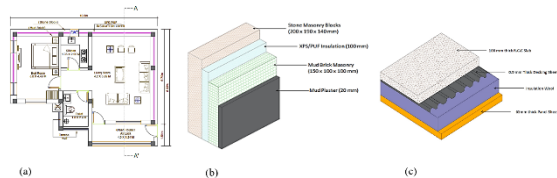


Figure 2. Proposed climate resilient building in Leh
(a) building plan (b) walling envelope (c) roofing envelope

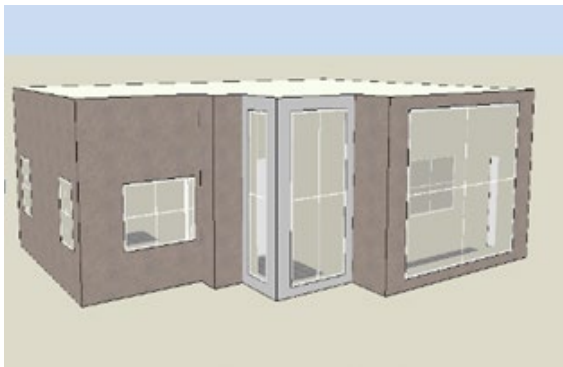


Figure 3. Rendered view of building in design builder

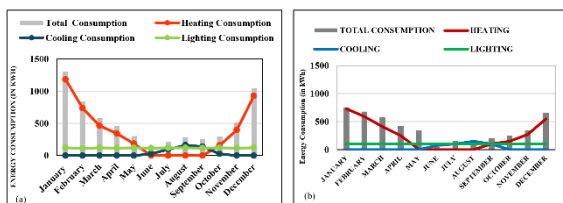


Figure 4. Monthly energy consumption
(a) present construction practice building
(b) proposed building

Figure 5 shows the daylight simulation results for proposed building using Design Builder Software. The red coloured area depicts the presence of maximum lux level i.e., the area having maximum heat due to the openings. This simulation result shows that the south direction is best direction of building for a cold region which allow the entrance of maximum sunlight during winters and keep the building warmer.

6. CONCLUSION AND WAY FORWARD

A vast study on the Leh present construction as well as modern technologies conclude various points

for the energy efficient buildings under harsh climatic conditions. Buildings should be located on the south slope (in the northern hemisphere) of a hill or mountain for better access to solar radiation. Ventilation should be carefully planned and air-lock lobbies at the entrance and exit points of a building should be used to reduce heat loss.

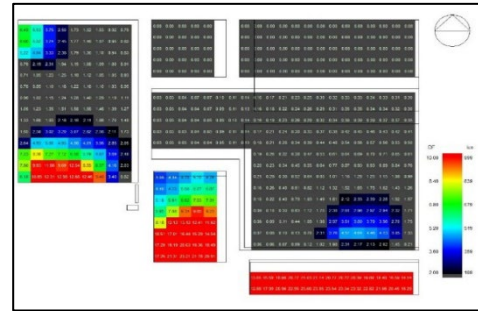


Figure 3. Daylight simulation for peak winter day

Additionally, heat generated by appliances in rooms such as kitchens may be used to heat the other parts of a building, so placing them in a more central part of the building can be beneficial.

Insulation decreases the transfer of heat and cold and provides for a more energy efficient building. Openings should be provided towards the southward direction to gain more sunlight. In a cold climate, insulation should have a vapour barrier that is sufficient to prevent moisture on the warm side from passing through and causing condensation.

For buildings in cold-dominated areas, the external surfaces of the walls should be dark in colour so that they absorb heat from the sun during the day. The trombe wall which soaks up the heat from the sun and radiates it out when the temperature is cooler. Double-glazing windows with low-E glass or double clear glass performs better than a single layer (pane) glass.

REFERENCE

- [1] R. Gupta, M. Vahanvati, J. Häggström, J.S. Halcomb, The Practical Guide to Climatic Resilient, United States, (2021).

NON-CHLORINATED CELLULOSE EXTRACTION FROM AGRICULTURAL BIOMASS AND ITS POTENTIAL APPLICATION AS PACKAGING MATERIALS

HAFID H.S.^{1*} and OMAR F.N.²

¹*Institute of Plantation Studies, Universiti Putra Malaysia, 43400 UPM Serdang, Selangor*

²*Preparatory Center for Science and Technology (PPST), Universiti Malaysia Sabah, Jalan UMS, 88400 Kota Kinabalu, Sabah, Malaysia*

*Correspondence: halimatun@upm.edu.my

Keywords: Cellulose, Non-chlorine, Agricultural biomass, Nitric acid, Starch, Packaging

1. INTRODUCTION

The conversion of untapped agricultural biomass into value-added products has a huge potential particularly due to its lignocellulosic component which makes it suitable as a raw material in various field such as textile industry, biomaterials composite, and food packaging [1]. Due to the high demand of cellulose materials, it is crucial to explore new sources of cellulose and its effective extraction process. Currently, cellulose is extracted using mechanical and chemical process which high energy consumption needed and cause leakage especially using chlorine method which is corrosive. Chlorine is known for its toxicity and harmful to the health and environment [2]. In addition, inappropriate extraction process may cause disruption of the cellulose structure make it not suitable for further application.

2. RESULTS AND DISCUSSION

In this study, cellulose was extracted from agricultural biomass using nitric acid hydrolysis in comparison with commercial chlorine method for lignocellulosic biomass dissolution. The cellulose quality through analysis of lignocellulosic content, mechanical properties, and surface morphology were assessed. The effect of treatment on the agricultural biomass is shown in Figure 1.



Figure 1. Cellulose extract using different method

HNO₃ treatment showed an increment (2.01–fold) in the cellulose content and some enhancement in the crystallinity of cellulose (up to 40.8%) and comparable with chlorine extraction method (Table 1).

Table 1. Chemical composition after treatment process

Treatment	Composition	
	Cellulose	Lignin
Untreated biomass	32.56	25.00
Chlorine treated	68.96	2.79
HNO ₃ treated	65.51	15.90

Starch-cellulose rice husk composites were prepared after surface modification of cellulose with phosphoric acid mediated hydrolysis and followed by reinforcing process with starch polymer.

The results of surface hydrophobicity and mechanical strength were found to be a function of an improvement of hydrophobicity (16 and 5.2%) (Figure 2) and tensile strength (3.6 and 23.2 MPa) (Figure 3), for both starch-rice husk chlorine and starch-rice husk nitric acid, respectively, as compared to neat starch.

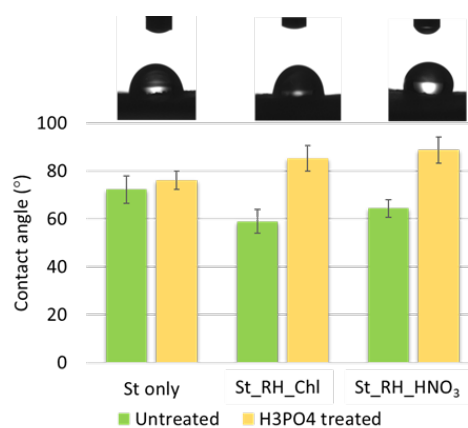


Figure 2. Hydrophobicity properties of cellulose-starch composite

Both starch-rice husk composites show an increment in crystallinity to 41.9% and 54.5% indicates the effectiveness of the reinforcement in improving the quality of the film.

In determining the optical and UV-shielding properties, transparency analysis using spectrophotometer transmittance (T) is carried out.

Transparency of the packaging materials is depending on the diffuse transmittance of wide and narrow-angle light scattering which plays a role in customer's visual inspection and appearance of the products. The starch films had high transparency as compared to starch cellulose films due to cellulose fiber dispersion block the light transmittance which is one of the disadvantages of its application as packaging materials (Figure 4).

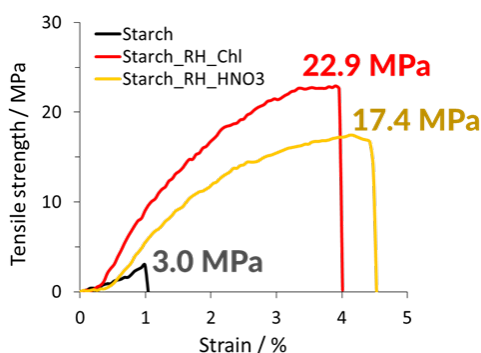


Figure 3. Mechanical properties of cellulose-starch composite

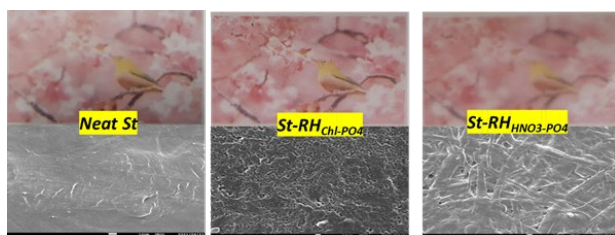


Figure 4. Transparency analysis of starch and starch-cellulose composite film

3. CONCLUSIONS

Cellulose extraction using proposed nitric acid extraction method is promising as an environmentally friendly method without compromising the quality as packaging materials and provide advantage compared to commercial chlorine method.

REFERENCES

- [1] Z. Kassab, Y. Abdellaoui, M.H. Salim, R. Bouhfid, A.E.K. Qaiss, M.E. Achaby, Carbohydr Polym. 245 (2020) 116506.
- [2] S. Boufi, A. Chaker, Ind Crops Prod. 93 (2016) 39-47.

SEISMIC RESILIENT & SUSTAINABLE CONSTRUCTION UTILISING STONES AND WOODS IN KATH KUNI CONSTRUCTION STYLE

ASHISH PIPPAL^{1,2}, SURENDER K NEGI¹, AJAY CHOURASIA^{1,2} and SHAINA SACHDEVA¹

¹CSIR- Central Building Research Institute, Roorkee- 247667, India

²Academy of Scientific and Innovative Research (AcSIR), Ghaziabad-201002, India

Keywords: Traditional construction, Himachal Pradesh, Kath Kuni, Seismic resiliency, Sustainability

1. INTRODUCTION

India is a country characterized by diverse geo-climatic conditions and varying geo-hazard risks. Vulnerabilities such as earthquakes, cyclones, landslides, floods, and tsunamis pose significant threats to different regions across the country. Over a period, habitants of these different regions learned the art to construct structures that can withstand the hazards of the region. One such construction practice is Kath Kuni, in which only wood and stone is required for the construction of sub, as well as superstructure. This traditional construction system is very prevalent in the region of Himachal Pradesh. Himachal Pradesh is a hill state, located in the Himalayan region of India, and is severely prone to earthquakes [1]. Being a cold climatic region, Himachal also requires sufficient thermal comfort to maintain.

A sound seismic resilient construction system requires features that include symmetrical configuration, improved integrity, and confinement of the masonry by ductile members [2]. Past earthquakes in the region have showcased that, construction with modern materials and techniques such as bricks and concrete have failed terribly in the region, causing a huge loss of money, infrastructure and life. This raised a serious question onto the modern construction practices. However, it is not the material that failed, the study suggested that reason of failure majorly is because of negligence in the factors mentioned above such as structural integrity and sufficient ductile detailing. This phenomenon thus, suggests the importance of construction techniques and skilled manpower.

On the other hand, structures made from Kath Kuni technique, withstood seismic events without any serious sign of distress. Many of currently existing structures of Kath Kuni style are more than 200-300 years old and yet look fascinating without any major maintenance.

However, in recent years, the evolution of modern construction materials and techniques has led to a neglect of traditional construction practices, despite their proven effectiveness over time. The aim of this paper is to highlight that a seismic-resilient structure can be constructed using local materials like wood and stone, even without mortar,

provided that integrity, ductility, and symmetry are maintained through quality workmanship.

2. BUILDING LAYOUT IN KATH KUNI

A typical Kath Kuni house is usually two or three stories tall, as shown in Figure 1 [3], although some structures can reach four to seven stories. The foundation typically consists of a strip footing made of stone, and the plinth is elevated to avoid high flood levels and minimize exposure to external cold conditions. The ground floor is designated for cattle, while the upper floors are used for living, storage, and cooking. The body heat from the cattle on the ground floor helps maintain warmth on the upper levels. Openings are kept to a minimum and are small, which reduces thermal exchange and ensures a thermally comfortable indoor environment.



Figure1. Typical section of Kath Kuni style house

The cantilevered balconies on the top floor are typically constructed using wooden projections. Kath Kuni houses exemplify a green housing system, as they are in harmony with nature. The primary construction materials are stone and wood, and thermal comfort is achieved by trapping the natural body heat of both cattle and humans within the heavy thermal mass of the stone-wood walls.

3. CONSTRUCTION MATERIAL

The primary construction materials in this style are wood and stone, both of which are abundantly available locally in the hills. Stones for construction

are typically sourced from the excavation of the foundation site, with any additional stones obtained from nearby locations. The wood used is usually Cheer or Deodar, which are plentiful in the higher elevations. Recently, split bamboo has also been utilized when wooden planks are unavailable. Stones can be used in both dressed and natural conditions as in Figure 2.

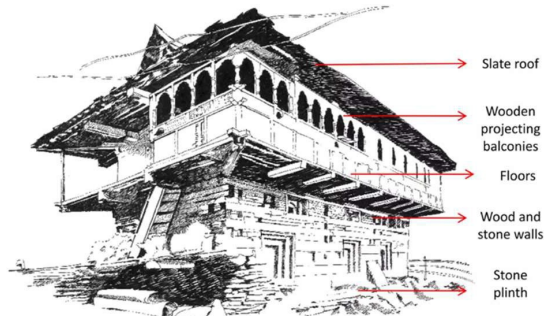


Figure 2. Components of Kath Kuni style construction

Dressed stones are usually utilized for the construction of walls, whereas small stones in natural undressed forms are used to fill in the gap inside the wooden beams or runners. This helps in keeping the wall dense and maintain sufficient thermal mass required for capturing the heat inside the house.

Wood is used in the form of planks to confine the stone structure and to impart ductility to the building. All the beams, purling and rafters are made up of wood. The balcony at the top floor also rests on the wooden cantilevered beams [4]. It can be said that the flexibility of this beautiful structure is primarily due to the wood, while rigidity is provided by the stones. However, since the structure does not use any mortar, all components have enough room to move and dissipate seismic energy during an earthquake [5]. These features make Kath Kuni an ideal construction method in areas where wood and stone are readily available and where earthquakes pose a significant risk.

4. CONSTRUCTION TECHNIQUE

In this construction style, foundation is typically made up in strip footing type with stones. Once the foundation is laid, the plinth using stones is raised to accommodate high flood levels of that region.

Over it walls using stones and wooden beams are constructed with alternate course of dry-stone masonry and wood without any cementing mortar. This type of wall construction involves laying of two wooden beams longitudinally parallel to each other and having a gap in between as in Figure 3. The wooden beams are held together by a dovetailed spacer termed as “Maanvi” as in Figure 4. These spacers are kept at every 3-4 feet to secure the space

and hold the beams firmly in place. The space between these beams is then filled with small natural stones. These wooden beams are placed at every alternate layer or at every two layers of stone masonry and are secured specifically at edges by wooden nails termed as “Kadil.”

These Kadil, provide necessary continuity to the wooden beams vertically. This arrangement ensures integrity of wall. The depth of these wooden beams is usually governed by the stone sizes and number of course. It is usually ensured that wooden beams are running continuously horizontally as well as vertically, considering alternate or two-layers of dry-stone masonry. Sometimes corner stones are also placed to protect wooden edges.

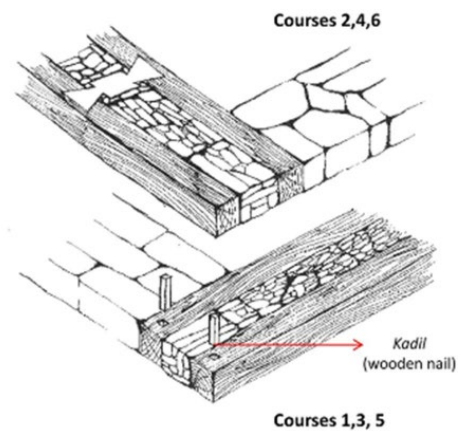


Figure 3. Wall construction with stones and wooden beams

Openings are constructed in walls using solid wooden shutters on all four sides and are usually kept very small and minimal in number (Figure 5). This is done to avoid much ventilation, as higher ventilation means higher heat loss, which is undesirable condition in these high altitude cold climatic areas). The openings are then carved beautifully on the outside to make them aesthetically pleasing.

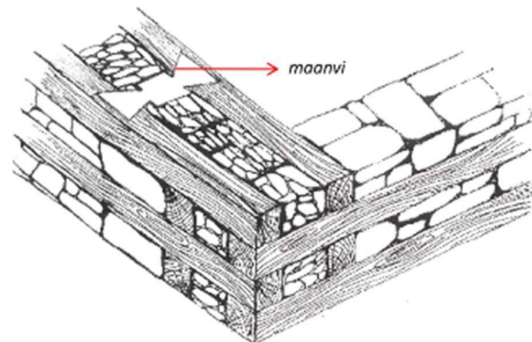


Figure 4. Wall construction in Kath Kuni style

Slate is used for roofing, with tiles typically cut in a 1:2 ratio (width to length). Wooden joists are installed, upon which wooden purlins are laid and

securely fastened with wooden nails. Layers of slate tiles are then placed on top and secured with nails to ensure that each tile is integrated with the purlins, which are connected to the wooden joists. These joists connect to a wooden beam running along the top of the wall, creating a continuous connection between the walls and the roof as in Figure 6.



Figure 5. Openings in the Kath Kuni wall

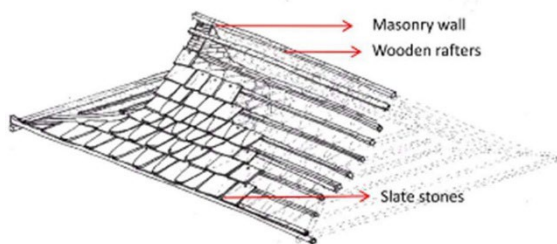


Figure 6. Laying of roof in Kath Kuni

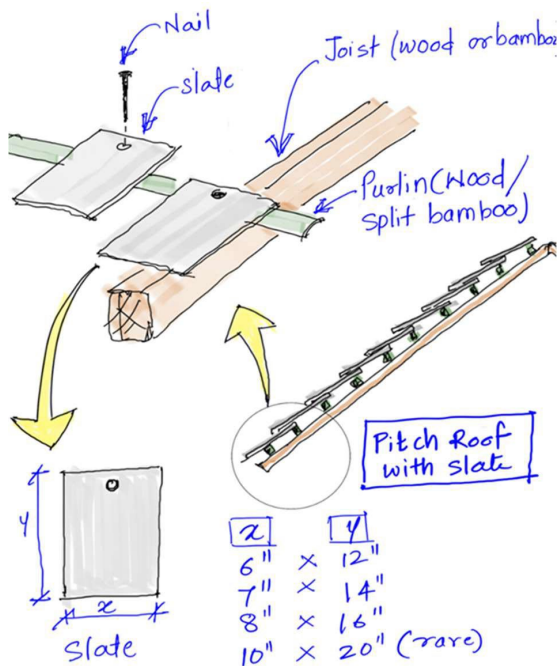


Figure 7. Fixing of slate tiles in roof

5. SEISMIC PERFORMANCE

Kath Kuni style structures have showcased their capability to withstand seismic event on many occasions, be it Kangra earthquake (1905), Chamba Earthquake (1945, 1994 and 1995), Kinnaur Earthquake (1975), Dharmashala earthquake (1986), Uttarkashi earthquake (1991), and Sundernagar earthquake (1997). These amazing structures made it through time without any significant sign of damage [6].

The secret of this lies in the construction style and materials. As we know that, a seismic resilient structure demands integrity, strength, flexibility, confinement and continuity [7]. This structure made in Kath Kuni style fulfills all these aspects, making them seismic resilient. The wooden beams used imparts flexibility and shock absorbent capability to the structure. Walls with mortar remain free to dissipate seismic energy and at the same time confinement of the same through wooden beams and corner stone provides strength to the structure. Maanvi and Kadil hold the structure together in the seismic event. The alternate layers of wood and stone connected at every level ensures integrity of the structure from foundation to the roof.

This style evolved through traditional wisdom of residents of these regions, covers all the verticals of an earthquake resilient structure, which they have proved at multiple times over these years.

6. CONCLUSION

Kath Kuni construction style is a need of the hour, as it is disaster resilient, energy efficient and sustainable in nature. It utilizes local material available in the vicinity and doesn't load the hills with foreign material such as bricks and RCC, which is being imported to hills from the plain regions.

It helps in generation of local employment and can help in even tackling the burning issues of migration in hilly regions. These structures are perfect examples of how simple materials like wood and stone, if utilized correctly, can create structures that are disaster resilient.

This paper aims to highlight the abundance of resources provided by nature to create safe, sustainable, and comfortable habitats. It emphasizes the importance of learning to utilize these resources effectively.

REFERENCES

- [1] Sharma AK, Kumar A and Sarhosis V (2024), Kath-Kuni architecture: field investigations and material characterization. Proceedings of the Institution of Civil Engineers – Structures and Buildings 177(8): 712–727
- [2] Jitendra Bothara, Jason Ingham, Dmytro Dizhur, Qualifying the earthquake resilience of vernacular masonry buildings along the Himalayan arc, Journal of Building Engineering 52 (2022)
- [3] Survesh Chetival, Sanjay Chikermane, Experimental investigation of traditional Kath-Kuni wall system and traditional joints, Engineering Structures 318 (2024)
- [4] Ashwani Kumar, Pushplata, Vernacular practices: as a basis for formulating building regulations for hilly areas, International Journal of Sustainable Built Environment (2013) 2, 183–192
- [5] K. Raju, S. Ravindhar, Detailed review on natural stone materials in architecture, Materials Today: Proceedings 45 (2021) 6341–6347

- [7] Antonio Murano, Javier Ortega, Graça Vasconcelos, Hugo Rodrigues, Influence of traditional earthquake-resistant techniques on the out-of-plane behavior of stone masonry walls: Experimental and numerical assessment, Engineering Structures 201 (2019)
- [8] Earthquake Hazard Risk Assessment Report Part-I & II, HP-SDMA

AUTOMATED EXTRACTION AND SEGMENTATION OF TUNNEL UTILITIES FOR ENHANCED DAMAGE DETECTION USING 3D LIDAR DATA

A. REGMI and T. MIZUTANI*

Department of Civil Engineering, The University of Tokyo, Tokyo, Japan

Correspondence: mizu-t@iis.u-tokyo.ac.jp

Keywords: 3D point cloud, Utility detection, Segmentation, Damage detection

1. INTRODUCTION

Regular monitoring of highway tunnels is important for safe and smooth operation. In Japan, mostly the tunnel inspections are human-intensive. The increasing number of ageing tunnels and reduction in manpower is being a major challenge in tunnel maintenance. To address this problem, in this research, we focus on automatizing the tunnel monitoring using the 3D point cloud data obtained from the on-vehicle LiDAR system [1]. We utilized the 3D coordinates for the extraction and segmentation of utilities. Along with it we used intensity information to detect the tunnel defects such as seepage, peeling and floating. The utility free tunnel data made the damage estimation more efficient.



Figure 1. Manual inspection



Figure 2. On-vehicle

2. MATERIALS AND METHODS

Curvature based analysis [2] followed by convex hull was used for extracting the tunnel utilities. Region growing method based on curvature was then used to segment the extracted utilities. Intensity based analysis was used to identify the seepage and joint information. Finally, the curve fitting strategy was used to extract the floating and peeling information.

3. RESULTS AND DISCUSSIONS

The extracted utilities in Figure 5 were

segmented based on the dimensional features as shown in Figure 6. The seepage and joint information obtained is shown in Figure 7. Extraction of tunnel utilities has helped in the application of intensity-based detection of seepage and joint information. Figure 8 shows the detection of floating and peeling damage on one of the 2D cross sections.

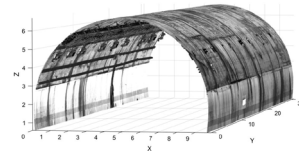


Figure 3. 3D Point cloud of a tunnel

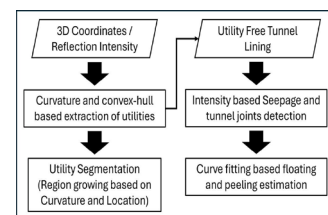


Figure 4. Methodology

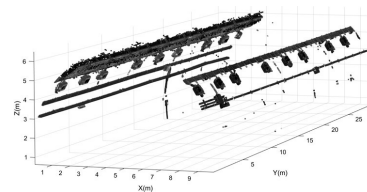


Figure 5. Extracted utilities

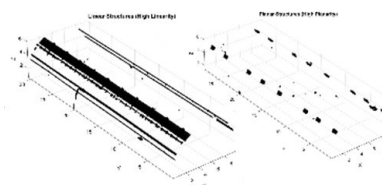


Figure 6. Segmenting as linear and planar objects

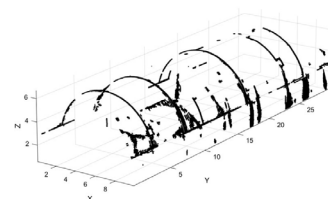


Figure 7. Seepage and joints detection

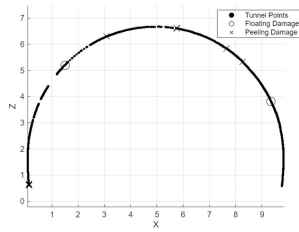


Figure 8. Floating and peeling detection



Figure 9. Condition of the tunnel being measured

Comparison of seepage and utilities results with the actual condition of the tunnel as shown in Figure 9 demonstrates the reliability of the method being used.

4. CONCLUSIONS

This research utilizes computational geometry and intensity information from the point cloud to extract the utilities and damage information. Testing in some other tunnels also has been done. This technique can be helpful in the smooth functionality and prevention of tunnel failures. However further testing and more improvement related to damage detection is needed.

REFERENCES

- [1] T. Mizutani, T. Yamaguchi, T. Kudo, et al., Quantitative evaluation of peeling and delamination on infrastructure surfaces by laser signal and image processing of 3D point cloud data, *Autom. Constr.* 133 (2022) 104023.
- [2] I. Jovančević, H.H. Pham, J.J. Orteu, et al., 3D Point Cloud Analysis for Detection and Characterization of Defects on Airplane Exterior Surface, *J. Nondestruct. Eval.* 36 (2017) 74.

TESTING THE EFFECTIVENESS OF AN INCENTIVE-BASED BICYCLE REALLOCATION APPROACH IN A SHARED CYCLE SYSTEM

TAKASHI MIYAZAWA and KAZUYUKI TAKADA *

Tokyo Denki University, Saitama, Japan

*Correspondence: takada@g.dendai.ac.jp

Keywords: Share bike, Real location, Incentive, Multi-agent simulation

1. INTRODUCTION

In recent years, bicycles have become increasingly popular in Japan. Bicycles are attracting attention as an environmentally friendly means of transportation, and efforts to reduce CO₂ emissions and ease traffic congestion in urban areas are gaining momentum.

A shared cycle service offers locations, referred to as "ports," where multiple bicycles can be rented or borrowed. Users can freely return their bicycles at these ports. However, due to uneven user demand, there are times when certain ports may have no bicycles available, as rental demand can become concentrated at specific locations. Additionally, when demand for returning bicycles peaks, the capacity of a port may be exceeded, making it impossible to park additional bicycles as in Figure 1.

To address the spatial mismatch in supply, operators utilize trucks to relocate bicycles, which constitutes a significant portion of their operating costs. This study aims to eliminate the need for trucks by testing a system that provides incentives to users, encouraging them to change their destinations to stations where bicycles are in short supply. Multi-agent simulation will be employed to compare the costs and availability of this incentive-based system with the current operational model.

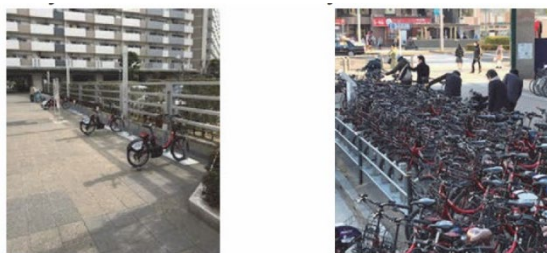


Figure 1. The bicycle bias situation, highlighting the uneven distribution of bicycles across different ports due to varying user demand

2. DATA

This study focuses on shared bicycles in Nerima Ward, located in the northwestern part of Tokyo's 23 wards. As shown in Figure 2, the demand density is not as high as in central Tokyo, but the number of users is increasing. This study uses actual usage data for the month of September 2019.

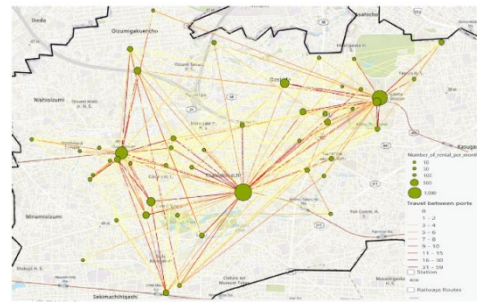


Figure 2. The origin-destination (OD) information, depicting the flow of users between various ports and illustrating the patterns of bicycle rental and return within the study area

3. METHODOLOGY

The objective of this study is to evaluate the effectiveness of user guidance measures based on incentives and reallocation by trucks, etc., in terms of cost and utilization through simulations based on actual utilization data. Specifically, a lending model and a destination choice model are incorporated into the simulation. The destination choice model stochastically represents the destination choice process based on the user's utility, and while the lending model often uses a Poisson regression model, this study incorporates a hurdle model due to the large amount of zero data.

By doing so, the simulation can reflect dynamic changes in the frequency of lending per port. At the time the usage data was recorded, there were 47 ports in the district, but in this study, we first built a simulation of a 10-port network to check the system performance.

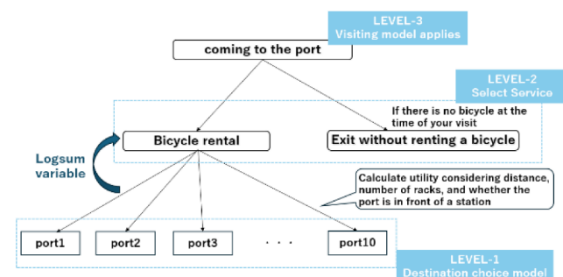


Figure 3. The simulation flow, detailing the processes involved in modeling user behavior, bicycle lending, and the distribution of incentives within the shared cycle system

4. SIMULATION OVERVIEW

4.1 Network

It will consist of ten ports. The ports are connected by a network graph obtained from OpenStreetMap data. Each port has information on the number of racks, number of initially placed units, latitude and longitude, user arrival rate, and surrounding environment.

4.2 Operator Agent

The operator agent continuously updates port information. When the number of bicycles available at a port fall below a specified threshold, the agent will identify eligible users who can change their destination to a port with a short supply. These users will receive incentives, such as financial rewards, for agreeing to alter their destination. Only one user will be accepted for each incentive proposal.

Conditions for User Eligibility for Incentives:

- The user must not have received any prior incentive requests.
- The new destination must be within 700 meters of the original destination.

4.3 User Agent

User arrivals are modeled using a hurdle approach based on arrival rates for each port, as indicated at Level 3. The hurdle model accounts for both lending behavior and the likelihood of arriving at a port. If bicycles are available, users can borrow Figure4. Response rate for distance and incentive amount; if not, the attempt is recorded, and the user exits the network. After borrowing, the destination is determined according to the utility function U_{ij} (Level 1), as shown in Equation (1),

$$U_{ij} = \beta_1 \times capacity_j + \beta_2 \times distance_{ij} + \beta_3 \times dummy_station_j \dots (1)$$

which is influenced by various factors.

The estimation results presented in Table 2 indicate the parameters affecting destination choice. The response rate for changing destinations in response to operator requests is determined probabilistically, following the logistic function described in Equation (2). This function illustrates how the response rate decreases with increasing distance while increasing with higher incentive amounts, as illustrated in Figure 4.

Response Ratio

$$= \frac{1}{1 + e^{-(\alpha \times distance + \beta \times Incentive\ amount)}} \dots (2)$$

Table1. Hurdle model result

	Hurdle model		Poisson regression model
	zero-hurdle	count part	
	-3.36***	-2.61***	-8.32***
dummy	0.226***	0.327***	0.357***
her	0.0972*	0.0755	0.107***
Commuting to work and back home dummy	0.896***	0.674***	1.01***
Population density (10,000 people/km ²)	0.603***	0.755***	0.642***
Distance from nearest station (km)	-0.0004***	-0.0005***	-0.0002***
Number of passengers at the nearest station (ten thousands)	0.144***	0.215***	0.165***
Number of ports within a 500m radius	-0.154***	-0.200***	-0.213***
variable	1.22***	1.24***	1.65***
number	34968		34968
Degrees of freedom	0.10		0.16
adjusted likelihood ratio	47798		51319
Intentional Level of Statistics: ***p<0.001, **p<0.01, *p<0.05			

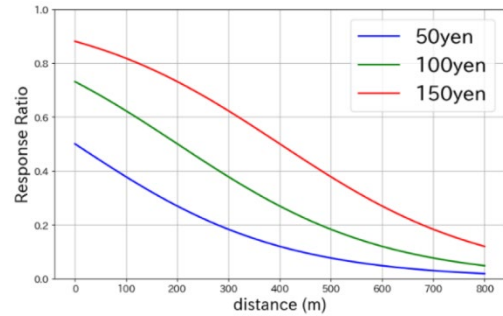


Figure 4. Response rate for distance and incentive amount

4.4 Truck Agent

The actual utilization data showed that the frequency of truck relocation was once a day. Therefore, the simulation also assumes that the trucks are relocated once a night.

Assume only one truck and two workers. The travel routes are route-optimized using the solution of the traveling salesman problem (TSP). The reallocation cost associated with the reallocation work is calculated from the previous study as follows:

$$\text{Cost} = W + g L \dots (3)$$

where:

g is gasoline price,

L is distance travelled by pickup or delivery trucks

W is labour cost

5. RESULTS AND DISCUSSIONS

This study constructed a simulation of a system that maintains bicycle equilibrium by adjusting users' destinations through incentives based on actual usage data. Currently, the response rate of users to incentives is set based on the author's rule of

thumb. However, future efforts will aim to improve the accuracy of this system by estimating the response rate more precisely through questionnaire surveys and field data collection.

The simulation results indicate that implementing an incentive-based approach can effectively address the spatial mismatch in bicycle supply, thereby reducing operational costs associated with truck relocations. Additionally, the analysis revealed significant insights from the Poisson regression and hurdle models, demonstrating the factors influencing user behavior and lending patterns. In the future, the network will be expanded to more accurately reproduce the situation at that time.

REFERENCES

- [1] Guidelines for the Introduction and Operation of Shared Cycle Business, Ministry of Land, Infrastructure, Transport and Tourism, 2023.9
- [2] AI-Based Bicycle Relocation Work Optimization at Docomo Bikeshare, 2021
- [3] Verification of Shared Cycle Operation System for Social Experiments on Incentive Systems: A Case Study of Tsukuba City's Shared Cycle Demonstration Project "Tsukuchari", Proceedings of the 44th Annual Meeting of the Japan Society of Transportation Engineering, 2024

SUSTAINABLE 3D CONCRETE PRINTING: ENHANCING MECHANICAL PROPERTIES WITH BAGASSE ASH AS A CEMENT REPLACEMENT

A. KAPOOR^{1,2} and A. CHOURASIA^{1*}

¹Structural Engineering Department, CSIR-CBRI, Roorkee, India

²CSIR- Academy of Scientific and Innovative Research, Roorkee, India

*Correspondence: ajaycbri@gmail.com

Keywords: 3D concrete printing, Sustainability, Sugarcane bagasse ash, Extrudability, Buildability

1. INTRODUCTION

3D concrete printing is recognized for its ability to minimize construction waste, optimize material usage, and expedite project timelines. Despite its benefits, 3DCP's reliance on fine aggregates leads to heightened cement demand, which contributes to significant CO₂ emissions. Cement production currently accounts for around 7% of global emissions. By exploring alternative materials like BA, a by-product of sugarcane processing, this study aims to curb cement consumption while preserving or enhancing concrete's mechanical properties.

2. MATERIALS AND METHODS

2.1 Material Composition and Mix Design

Bagasse ash was used as a partial cement substitute in varying percentages to evaluate its effects on 3D printable concrete's strength and workability. Fine aggregates with a maximum particle size of 2.36 mm were used. BA was calcined at 650°C and had similar particle characteristics to cement, with an 83.997% SiO₂ content enhancing pozzolanic activity. The mix design for fresh concrete aimed for high workability and low thixotropic behavior, essential for extrudability and shape retention.

2.2 Experimental Procedures

3DCP specimens were subjected to compressive and flexural strength tests as per ASTM standards. Rheological properties were assessed to determine the extrudability and buildability by optimizing viscosity-modifying agents (VMAs) and superplasticizers (SPs). The flow table test was employed to measure open time and printability, targeting optimal flow values of 160 ± 10 mm.

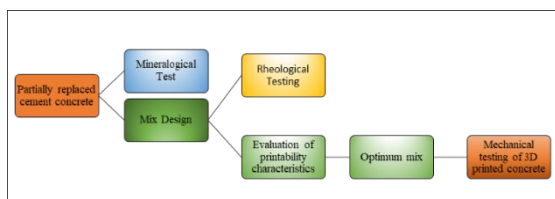


Figure 1. Schematic representation of experimental procedure

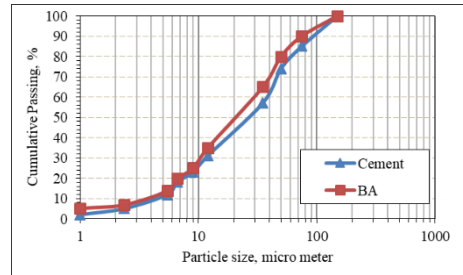


Figure 2. Particle size distribution for bagasse ash (BA) and cement

Table 1. The chemical composition of cement, bagasse ash and flyash (based on experimental test result of XRD analysis data)

Ingredients	Quantity (wt.%)		
	Cement	Bagasse Ash	Flyash
SiO ₂	20.34	83.997	36.1
Al ₂ O ₃	4.47	4.219	25.03
CaO	62.91	2.719	3.1
MgO	1.24	2.674	1
P ₂ O ₅	0	2.194	1.24
K ₂ O	0.29	1.942	1.08
Fe ₂ O ₃	4.58	1.154	0
FeO	0	0	8.66
SO ₃	2.58	0.818	0.59
TiO ₂	0	0.169	0.91
MnO	0	0.047	0
Na ₂ O	0.31	0.19	0
Mn ₂ O ₃	0	0	0
ZnO	0	0.019	0
SrO	0	0.013	0
Cr ₂ O ₃	0	0.009	0
S ⁺	0	0	0
S ²⁻	0	0	0
CuO	0	0.009	0
Rb ₂ O	0	0.004	0
Y ₂ O ₃	0	0.001	0
LOI	3.27	0	0
IR	0	0	0
C	0	0.1	23.29
Cl	0	0	0

3. RESULTS AND DISCUSSION

3.1 Printability and Rheology

BA-augmented concrete demonstrated enhanced printability with optimized open time and shape retention due to thixotropic adjustments from the VMA. The extrudability tests showed that mixtures with up to 40% BA had a suitable filament length before tearing, validating the BA's impact on maintaining dimensional stability during extrusion.



Figure 3. Flow table test

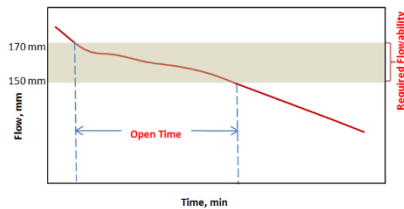


Figure 4. Graphical representation of open time



Figure 5. Measurement of printed filament

$$SRF = \frac{\text{Width of extruded filament}}{\text{Width of nozzle}}$$

3.2 Compressive and Flexural Strength

The BA content influenced both compressive and flexural strengths, with an optimal strength recorded at 40% cement replacement. A decrease in strength was noted beyond this threshold, likely due to BA's reduced binding capacity. Compressive strength varied across orientations (X, Y, Z axes), indicating anisotropy—a critical consideration in structural applications. Flexural strength tests aligned with the observed anisotropic behavior, with strength reductions seen along the Z-axis, perpendicular to the extrusion direction.

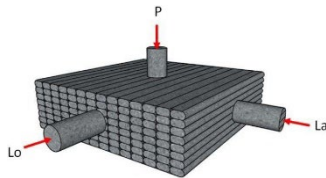


Figure 6. Extraction of cores from printed sample in various direction



Figure 7. Printed concrete bed and extracted core samples

Table 2. Composition of 3D printing concrete mix

Mix	Cement (%)	Bagasse Ash (%)	Sand: Binder	Water: Binder	SP (%)	VMA (%)
M0	100	0	1.4	0.44	1	0.5
M1	90	10	1.4	0.44	1	0.5
M2	80	20	1.4	0.44	1	0.5
M3	70	30	1.4	0.44	1	0.5
M4	60	40	1.4	0.44	1	0.5
M5	50	50	1.4	0.44	1	0.5

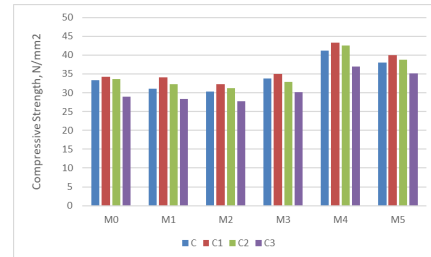


Figure 8. Compressive strength of mould cast specimen and printed specimen loaded in X, Y and Z direction

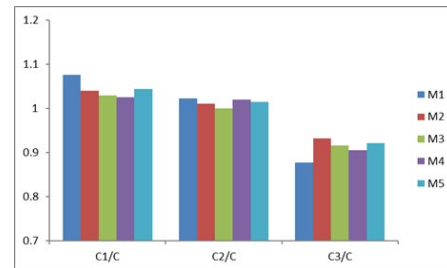


Figure 9. Anisotropy in compressive strength of 3D printed concrete

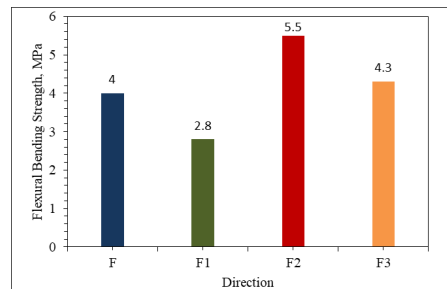


Figure 10. Flexure strength of mould cast specimen and printed specimen loaded in X, Y and Z direction

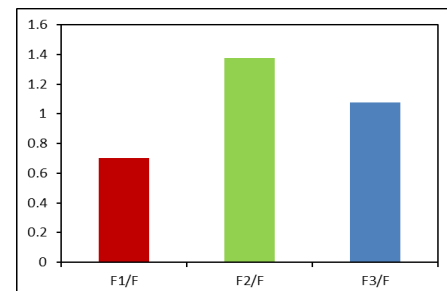


Figure 11. Anisotropy in flexure strength of 3D printed concrete

4. CONCLUSION

Bagasse ash provides a sustainable alternative for cement in 3DCP, enhancing mechanical properties and reducing environmental impact. The optimal mix design achieved notable printability and strength while addressing the structural integrity needed for multi-layer builds. This study supports BA's potential in large-scale 3D printing applications, contributing to eco-friendly construction solutions. Further research is warranted to explore the long-term durability of BA-enhanced 3D-printed structures.



Figure 12. Printing of Pie shape seater with optimized mix



Figure 13. Printed Pie shape seater with optimized mix (30layers)

REFERENCES

- [1] Liu Z, Li M, Weng Y, Qian Y, Wong TN, Tan MJ. Modelling and parameter optimization for filament deformation in 3D cementitious material printing using support vector machine. *Compos B Eng* 2020;193:108018.
- [2] Xu J, Ding L, Love PED. Digital reproduction of historical building ornamental components: from 3D scanning to 3D printing. *Autom Construct* 2017;76:85e96.
- [3] Jeon, K.H.; Park, M.-B.; Kang, M.-K.; Kim, J.-H. A study on the development of an automated freeform fabrication system and construction materials. *J. Korean Soc. Civ. Eng.* 2013, 33, 1665–1673.
- [4] Roussel, N. Rheological requirements for printable concretes. *Cem. Concr. Res.* 2018, 112, 76–85.
- [5] H. Okamura, M. Ouchi, Self-compacting concrete, *J. Adv. Concr. Technol.* 1 (2003) 5–15.
- [6] S.A. Austin, P. Robins, C.I. Goodier, The rheological performance of wet-process sprayed mortars, *Mag. Concr. Res.* 51 (1999) 341–352.
- [7] Khan, R.; Jabbar, A.; Ahmad, I.; Khan, W.; Khan, A.N.; Mirza, J. Reduction in environmental problems using rice-husk ash in concrete. *Constr. Build. Mater.* 2012, 30, 360–365.
- [8] Liew, K.M.; Sojobi, A.O.; Zhang, L. Green concrete: Prospects and challenges. *Constr. Build. Mater.* 2017, 156, 1063–1095.
- [9] Jensen, O.M.; Hansen, P.F. Autogenous deformation and RH-change in perspective. *Cem. Concr. Res.* 2001, 31, 1859–1865.
- [10] Thorpe, D.; Zhuge, Y. Advantages and disadvantages in using permeable concrete as a pavement construction material. In *Proceedings of the 26th Annual ARCOM Conference, Leeds, UK, 6–8 September 2010*; pp. 1341–1350.
- [11] Woodward, R.; Du_y, N. Cement and concrete flow analysis in a rapidly expanding economy: Ireland as a case study. *Resour. Conserv. Recycl.* 2011, 55, 448–455.
- [12] Frías, M.; Rodríguez, O.; De Rojas, M.I.S.; Villar, E.; Rodrigues, M.S.; Savastano, H. Advances on the development of ternary cements elaborated with biomass ashes coming from different activation process. *Constr. Build. Mater.* 2017, 136, 73–80.
- [13] Khan, A.; De Jong, W.; Jansens, P.; Splietho_, H. Biomass combustion in fluidized bed boilers: Potential problems and remedies. *Fuel Process. Technol.* 2009, 90, 21–50.
- [14] Pereira, A.; Akasaki, J.L.; Melges, J.L.; Tashima, M.; Soriano, L.; Borrachero, M.V.; Monzó, J.; Payá, J. Mechanical and durability properties of alkali-activated mortar based on sugarcane bagasse ash and blast furnace slag. *Ceram. Int.* 2015, 41, 13012–13024.
- [15] Cook JD. Rice husk ash. In: Swamy RN, editor. *Concrete technology and design. Cement replacement material*, 3. London: Surrey University Press; 1986. p. 171–95.
- [16] Mehta PK. Technology alternatives for use of rice husk. *Approp Tech* 1983;7.
- [17] Mehta PK. Properties of blended cement made from rice husk ash. *ACI Mater J* 1977;74(9):440–2.
- [18] Mehta PK. Rice husk ash – A unique supplementary cementing material. In: Malhotra VM, editor. *Proceeding of the international symposium on advances in concrete tech*, Athens, Greece; 1992. p. 407–30.
- [19] Moayad N, Al-Khalaf, Yousiff HA. Use of rice husk ash in concrete. *The Int J Cem Compo Lightweight Concr* 1984;6(4):241–8.
- [20] Mehta PK. Rice hull ash cement. . . high quality acid resisting. *ACI Mater J* 1975;72(5):235–6.

- [21] Smith RG, Kamwanga GA. The use of rice husk for making a cementitious material. Use of vegetable plants and fibres as building materials. Joint symposium RILEM/CIB/CCL. Baghdad; 1986. p. E85–94.
- [22] Zhang MH, Malhotra V. High-Performance concrete incorporating rice husk ash as supplementary cementing material. *ACI Mater J* 1996;93(6):629–36.
- [23] Biricik H, Akoz F, Berkay I, Tulgar AN. Study of pozzolanic properties of wheat straw ash. *Cem Concr Res* 1999;29:637–43.
- [24] Demirbas A, Asia A. Effect of ground hazel nutshell, wood and tea waste on the mechanical properties of cement. *Cem Concr Res* 1998;28(8):1101–4.
- [25] Akram T, Memon SA, Obaid H. Production of low cost self compacting concrete using bagasse ash. *Constr Build Mater* 2009;23:703–12.
- [26] Ganesan K, Rajagopal K, Thangavel K. Evaluation of bagasse ash as supplementary cementitious material. *Cem Concr Compos* 2007;29:515–24.
- [27] Ganesan, K., Rajagopal, K. and Thangavel, K., 2007. Evaluation of bagasse ash as supplementary cementitious material. *Cement and concrete composites*, 29(6), pp.515-524.
- [28] Rukzon, S. and Chindaprasirt, P., 2012. Utilization of bagasse ash in high-strength concrete. *Materials & Design*, 34, pp.45-50.
- [29] Kumar, M.V. and Lemessa, K., 2017. Behavior of Concrete with Agro and Industry Waste as a Replacement for Constitutive Materials. *Am. J. Eng. Res*, 6, pp.79-85.
- [30] Ismail, M.S.;Waliuddin, A. Effect of rice husk ash on high strength concrete. *Constr. Build. Mater.* 1996, 10, 521–526.
- [31] Qian Y, Kawashima S. Distinguishing dynamic and static yield stress of fresh cement mortars through thixotropy. *Cement Concr Compos* 2018;86:288-96.
- [32] Kolawole JT, Combrinck R, Boshoff WP. Rheo-viscoelastic behaviour of fresh cement-based materials: cement paste, mortar and concrete. *Construct Build Mater* 2020;248:118667.
- [33] Zhang Y, Zhang Y, She W, Yang L, Liu G, Yang Y. Rheological and harden properties of the high-thixotropy 3D printing concrete. *Construct Build Mater* 2019;201:278e85.
- [34] Yuan Q, Li Z, Zhou D, Huang T, Huang H, Jiao D, et al. A feasible method for measuring the buildability of fresh 3D printing mortar. *Construct Build Mater* 2019;227:116600.
- [35] Kruger J, Zeranka S, Zijl Gv. An ab initio approach for thixotropy characterisation of (nanoparticle-infused) 3D printable concrete. *Construct Build Mater* 2019;224:372e86.
- [36] Buswell RA, Leal de Silva WR, Jones SZ, Dirrenberger J. 3D printing using concrete extrusion: a roadmap for research. *Cement Concr Res* 2018;112:37e49.
- [37] Mechtcherine, V.; Nerella, V.N.;Will, F.; Näther, M.; Otto, J.; Krause, M. Large-scale digital concrete construction—CONPrint3D concept for on-site, monolithic 3D-printing. *Autom. Constr.* 2019, 107, 102933.
- [38] Soltan, D.G.; Li, V.C. A self-reinforced cementitious composite for building-scale 3D printing. *Cem. Concr. Compos.* 2018, 90, 1–13.
- [39] Zhu, B.; Pan, J.; Nematollahi, B.; Zhou, Z.; Zhang, Y.; Sanjayan, J. Development of 3D printable engineered cementitious composites with ultra-high tensile ductility for digital construction. *Mater. Des.* 2019, 181, 108088.
- [40] Lee, H.; Kim, J.-H.J.; Moon, J.-H.; Kim, W.-W.; Seo, E.-A. Evaluation of the Mechanical Properties of a 3D-Printed Mortar. *Materials* 2019, 12, 4104.
- [41] Weng, Y.; Li, M.; Tan, M.J.; Qian, S. Design 3D printing cementitious materials via Fuller Thompson theory and Marston-Percy model. *Constr. Build. Mater.* 2018, 163, 600–610.
- [42] Bong, S.H.; Nematollahi, B.; Nazari, A.; Xia, M.; Sanjayan, J.G. Fresh and hardened properties of 3D printable geopolymer cured in ambient temperature. In *Proceedings of the RILEM International Conference on Concrete and Digital Fabrication*, Zurich, Switzerland, 9–12 September 2018; pp. 3–11.
- [43] Tay, Y.W.D.; Qian, Y.; Tan, M.J. Printability region for 3D concrete printing using slump and slump flow test. *Compos. Part B Eng.* 2019, 174, 106968.
- [44] Weng, Y.; Lu, B.; Li, M.; Liu, Z.; Tan, M.J.; Qian, S. Empirical models to predict rheological properties of fiber reinforced cementitious composites for 3D printing. *Constr. Build. Mater.* 2018, 189, 676–685.
- [45] Chen, M.; Li, L.; Zheng, Y.; Zhao, P.; Lu, L.; Cheng, X. Rheological and mechanical properties of admixtures modified 3D printing sulphoaluminate cementitious materials. *Constr. Build. Mater.* 2018, 189, 601–611.
- [47] Ferraris, C.F. Measurement of the Rheological Properties of High Performance Concrete: State of the Art Report. *J. Res. Natl. Inst. Stand. Technol.* 1999, 104, 461–478.
- [48] Ferraris, C.F. Measurement of the Rheological Properties of High Performance Concrete: State of the Art Report. *J. Res. Natl. Inst. Stand. Technol.* 1999, 104, 461–478.
- [49] Roussel, N. A thixotropy model for fresh fluid concretes: Theory, validation and applications. *Cem. Concr. Res.* 2006, 36, 1797–1806.

- [50] Kruger, J.; Zeranka, S.; van Zijl, G. An ab initio approach for thixotropy characterisation of (nanoparticle-infused) 3D printable concrete. *Constr. Build. Mater.* 2019, 224, 372–386.
- [51] Reiter, L.; Wangler, T.; Roussel, N.; Flatt, R.J. The role of early age structural build-up in digital fabrication with concrete. *Cem. Concr. Res.* 2018, 112, 86–95.
- [52] Perrot, A.; Rangeard, D.; Pierre, A.J.M. Structural built-up of cement-based materials used for 3D-printing extrusion techniques. *Mater. Struct.* 2016, 49, 1213–1220.
- [53] Kolawole, J.T.; Combrinck, R.; Boshoff, W.P. Measuring the thixotropy of conventional concrete: The influence of viscosity modifying agent, superplasticiser and water. *Constr. Build. Mater.* 2019, 225, 853–867.
- [54] Le, T.T.; Austin, S.A.; Lim, S.; Buswell, R.A.; Gibb, A.G.; Thorpe, T.J.M. Mix design and fresh properties for high-performance printing concrete. *Mater. Struct.* 2012, 45, 1221–1232.
- [55] Rehman, A.U.; Lee, S.-M.; Kim, J.-H. Use of municipal solid waste incineration ash in 3D printable concrete. *Process. Saf. Environ. Prot.* 2020, 142, 219–228.
- [56] Brunori, F.; Penzo, M.C.; Torri, D. Soil shear strength: Its measurement and soil detachability. *CATENA* 1989, 16, 59–71.
- [57] Koehler, E.P.; Fowler, D.W.; Ferraris, C.F.; Amziane, S. A new, portable rheometer for fresh self-consolidating concrete. *ACI Spec. Publ.* 2005, 233, 97.
- [58] Chen, M.; Liu, B.; Li, L.; Cao, L.; Huang, Y.; Wang, S.; Zhao, P.; Lu, L.; Cheng, X. Rheological parameters, thixotropy and creep of 3D-printed calcium sulfoaluminate cement composites modified by bentonite. *Compos. Part B Eng.* 2020, 186, 107821.
- [59] Panda, B.; Unluer, C.; Tan, M.J. Investigation of the rheology and strength of geopolymer mixtures for extrusion-based 3D printing. *Cem. Concr. Compos.* 2018, 94, 307–314.
- [60] Manikandan, K.; Wi, K.; Zhang, X.; Wang, K.; Qin, H. Characterizing cement mixtures for concrete 3D printing. *Manuf. Lett.* 2020, 24, 33–37.
- [61] Hernandez JM, Middendorf B, Gehrke M, Budelmann H. Use of wastes of the sugar Industry as pozzolana in lime-pozzolana binders: study of the reaction. *Cem Concr Res* 1998;28(11): 1525–36.
- [62] Singh NB, Singh VD, Sarita Rai. Hydration of bagasse ash – blended Portland cement. *Cem Concr Res* 2000; 30:1485–8.
- [63] Hernandez JM, Rodriguez BS, Middendorf B. Pozzolanic properties of residues of sugar industries (first part). *Mater de Construction* 2000;50(260):71–8.
- [64] Hernandez JM, Rodriguez BS, Middendorf B. Pozzolanic properties of residues of sugar industries (second part). *Mater de Construction* 2001;51(261):67–72.
- [65] Paya J, Monzo J, Borrachero MV, Pinzon DL, Ordonez LM. Sugarcane bagasse ash (SCBA): studies on its properties for reusing in concrete production. *J Chem Tech Biotech* 2002;77(3):321–5.
- [66] Cordeiro. Influence of mechanical grinding on the pozzolanic activity of residual sugarcane bagasse ash. In: Vzquez E, Hendricks ChF, Janssen GMT, editors. *Proceeding of international RILEM conference on the use of recycled materials in building structures; 2004.* Nb reference 18.

CHEMICAL SENSORS FOR ONE HEALTH, ONE WORLD**T. Minami***Institute of Industrial Science, The University of Tokyo, Tokyo, Japan**Correspondence: tminami@g.ecc.u-tokyo.ac.jp***Keywords:** Paper, Chemosensor array, Imaging analysis, Pattern recognition, Multi-sensing**1. GENERAL INTRODUCTION**

Sensors of our human bodies play important roles in detecting invisible physical and chemical stimuli, which change (or control) our behaviors nonconsciously or consciously. Inspired by such sophisticated sensors endowed into our bodies, the development of various sensor platforms has promoted to detection of physical and chemical stimuli “instead of ourselves.” The requirements of sensor abilities are favorable sensitivity, selectivity, quick response, wide response ranges, reusability, repeatability, suppression ability of interference effects, etc., which have been desired to be “beyond the inherent recognition abilities of biological sensing systems.”

Sensors consist of receptors to detect invisible stimuli, and transducers (or reporters) to amplify the sensor signals [1]. Physical sensors have already been well established in practical situations, while chemical sensors have not been fully used because their development is still at the frontiers. Motivated by this, the author has focused on chemical sensor devices that can easily be fabricated using office printers.

2. PAPER-BASED CHEMOSENSOR ARRAYS

Paper substrates have been widely used as chemical sensor platforms owing to their eco-friendliness and high processability. Conventional paper-based analytical devices such as pH test stripes and virus test kits allow single analyte detection, whereas real samples contain multiple analytes at wide concentration ranges [2]. Although multi-sensing devices are required in real-world scenarios, the realization is still challenging. To develop multi-sensing devices, the author has focused on the cross-reactive recognition principle observed in the mammalian olfactory system for simultaneous sensing [1]. Cross-reactive chemical sensor elements (i.e., chemosensors) show various optical responses including colorimetric or fluorescence changes upon analyte capture.

Such various optical patterns, which are referred to as fingerprint-like responses, contain multi-dimensional chemical information corresponding to types of analytes and their concentrations. With pattern recognition techniques, various analyte information can be determined qualitatively and

quantitatively [3]. To date, the author has expanded the concept of the pattern recognition-driven chemical sensing approach to paper-based analytical devices for on-site sensing without using stationery instruments [4]. Chemosensor elements with cross-reactivity can be uniformly printed on the paper substrate using office apparatuses (Figure 1). In addition, optical responses of the paper substrate are rapidly detected using digital recorders, followed by data processing using imaging analysis and pattern recognition techniques [4]. Therefore, paper-based chemosensor array devices allow not only the simultaneous detection of multiple chemical information but also accurate analysis comparable to stationary analytical methods [5]. Indeed, the author has performed multi-sensing using paper-based chemosensor array devices and revealed their applicability to real-sample analysis for human body fluids [6], food and drink samples [4,7], and environmental water [5,8]. In this presentation, the sensor design, the optimization of device fabrication, and sensor performance will be introduced.

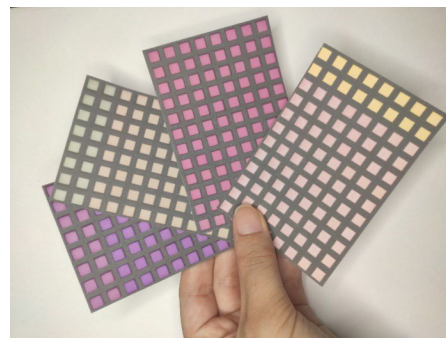


Figure 1. Manufactured paper-based chemosensor array devices. The chemosensor solutions as inks were uniformly printed using office apparatuses

REFERENCES

- [1] Y. Sasaki, R. Kubota, T. Minami, Coord. Chem. Rev. 429 (2021) 213607.
- [2] B. Mohan, Y. Sasaki, T. Minami, Anal. Chim. Acta 1313 (2024) 342741.
- [3] Y. Sasaki, S. Kojima, V. Hamedpour, R. Kubota, S. Takizawa, I. Yoshikawa, H. Houjou, Y. Kubo, T. Minami, Chem. Sci. 11 (2020) 3790–3796.

- [4] X. Lyu, V. Hamedpour, Y. Sasaki, Z. Zhang, T. Minami, *Anal. Chem.* 93 (2021) 1179–1184.
- [5] Y. Sasaki, X. Lyu, T. Kawashima, Y. Zhang, K. Ohshiro, K. Okabe, K. Tsuchiya, T. Minami, *RSC Adv.*, 14 (2024) 5159–5166.
- [6] Y. Sasaki, X. Lyu, T. Minami *Anal. Sens.* 3 (2023) e202200097.
- [7] X. Lyu, Y. Sasaki, K. Ohshiro, W. Tang, Y. Yuan, T. Minami, *Chem. Asian J.* 17 (2022) e202200597.
- [8] Y. Sasaki, X. Lyu, T. Minami, *Front. Chem.* 11 (2023) 1134752.

PATTERN ANALYSIS OF CHANGES IN PRODUCTION ACTIVITIES IN THAI INDUSTRIAL COMPLEXES USING ALTERNATIVE DATA

A. KODAKA^{1,2*}, N. LEELAWAT^{1,2,3} and N. KOHTAKE¹

¹Graduate School of System Design and Management, Keio Univ., Yokohama, Japan

²Disaster and Risk Mgmt. Info. Systems Research Unit, Chulalongkorn Univ., Bangkok, Thailand

³Dept. of Industrial Engineering, Faculty of Engineering, Chulalongkorn Univ., Bangkok, Thailand

*Correspondence: akira.kodaka@keio.jp

Keywords: Air quality, Google Earth Engine, Production activities, Alternative data, Industrial complex, Thailand

1. INTRODUCTION

Our socio-economic activities are vulnerable to disruptions from incidents such as natural disasters. Among these, extensive research has focused on the impact of COVID-19, including studies assessing its effects on air pollution improvements [1]. Additionally, research has evaluated the extent to which government measures, such as lockdowns and curfews, have contributed to these improvements [2]. While these studies primarily focus on quantitative analyses within relatively fixed timeframes, limited research captures the ongoing transformations in socio-economic activities on a continuous timescale due to the pandemic. Therefore, this study aims to provide new insights into the timescales at which production activities of businesses and other entities were affected by the pandemic, using industrial complexes in Thailand as a case study.

2. DATA AND METHODS

This study focused on the Rojana Industrial Park (RIP) in Phra Nakhon Si Ayutthaya Province, Thailand. Using data from the Copernicus Atmosphere Monitoring Service, we extracted time-series data of PM2.5 atmospheric concentrations over the RIP from January 1, 2018, to December 31, 2023. This was accomplished by loading the Particulate_matter_d_less_than_25_um_surface band on Google Earth Engine using the method developed by the authors [3]. Additionally, wavelet coherence analysis was conducted on the PM2.5 time-series data. Specifically, we treated the concentration variations for each year as signals in the frequency domain and performed continuous wavelet transform using the Morlet mother wavelet (see Equation 1) to analyze correlations between the annual patterns of PM2.5 concentration changes.

$$\psi(t) = \pi^{-1/4} e^{-t^2/2} (e^{-i\omega_0 t} - e^{-\omega_0^2/2}) \quad (1)$$

where $w_0 = \sqrt{2/\ln 2}$

3. RESULTS AND DISCUSSIONS

Figure 1 presents the results of the wavelet coherence analysis, comparing PM2.5 concentration changes in 2023 with those in 2019 and 2020. The vertical axis represents frequency, with higher values indicating correlations at lower frequencies (longer periods) and lower values indicating correlations at higher frequencies (shorter periods). The horizontal axis represents the daily timeline over a year. Given the observed correlation between PM2.5 atmospheric concentrations and changes in activity levels within industrial complexes [3], the analysis revealed that activity levels in the RIP during 2020 displayed a higher correlation with the patterns in 2023 (post-pandemic) than with those of 2019 (pre-pandemic). Notably, strong correlations were observed at lower frequencies corresponding to cycles of 2 to 4 months, as well as at relatively higher frequencies with cycles of up to approximately 2 weeks.

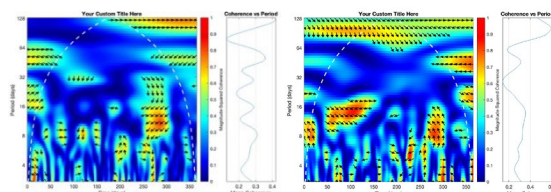


Figure 1. WCA results of PM2.5 concentration changes: 2019 vs. 2023 (left), 2020 vs. 2023 (right)

4. CONCLUSIONS

This study, using an industrial complex in Thailand as a case example, demonstrated the potential of wavelet coherence analysis of atmospheric compound time-series changes to capture shifts in industrial activity across varying timescales. Moving forward, validating these findings with on-site activity data and other relevant information will be essential.

REFERENCES

- [1] L. Li, et al., "Air quality changes during the COVID-19 lockdown over the Yangtze River Delta Region: An insight into the impact of human activity pattern changes on air pollution

- variation,” *Sci. Total Environ.*, vol. 732, 2020, 139282.
- [2] G. Carla, et al, “The impact of COVID-19 confinement measures on the air quality in an urban- industrial area of Portugal,” *Atmosphere*, vol. 12(9), 2021, 1097.
- [3] A. Kodaka, et al., “Influential factors on aerosol change during COVID-19 in Ayutthaya, Thailand,” *Eng. J.*, vol. 25(8), 2021, pp. 187-196.

REGIONAL ESTIMATION OF FUTURE DEMAND FOR MEDICINES NEEDED IN THE EVENT OF A LARGE-SCALE EARTHQUAKE DISASTER: FOR A SMALL CITY IN A RURAL AREA IN JAPAN USING MEDICAL BIG DATA

KEN TAKAKUWA¹, YUMA MORISAKI^{2*}, MAKOTO FUJII² and YUTA BABA¹

¹Faculty of Geosciences and Civil Engineering, Kanazawa University, Kanazawa, Japan

²Institute of Transdisciplinary Sciences for Innovation, Kanazawa University, Kanazawa, Japan

Correspondence: morisaki@staff.kanazawa-u.ac.jp

Keywords: Medical big data, Future estimation, Pharmaceutical demand, Large-scale earthquake disaster

1. INTRODUCTION

In Japan, the risk of earthquakes is high, and when a disaster occurs, there will be a huge demand for local medical resources, which can lead to a significant shortage of medical resources. Under such circumstances, the risk of deterioration in the health conditions of disaster victims, especially those with chronic diseases is increased. Therefore, it is necessary to estimate the demand for medications required by patients with chronic diseases during normal times. This study focuses on Hakui City in Ishikawa Prefecture, and national health insurance data (KDB data) of Hakui is used. In addition, Hakui city is divided into 10 areas, and the study aims to estimate the number of prescriptions for medications that are critically needed by patients with chronic diseases during normal times in each of these areas. Figure 1 shows the division of Hakui City into regions.

2. PHARMACEUTICALS ANALYZED

In this study, the prescribing status of nine types of medicines were analyzed: antithrombotic agents, antihypertensive drugs, antiepileptic drugs, psychotropic drugs, hypnotic-sedative drugs and anxiolytics, antiparkinsonian drugs, antidiabetic drugs, respiratory drugs, and heart failure drugs. Only psychotropic drugs are shown due to space limitation. In addition, SARIMA model, a statistical model used to analyze and forecast time series data with seasonality was applied to estimate the number of prescriptions of the target drugs.

3. ANALYSIS RESULTS

In this analysis, the number of prescriptions for psychotropic drugs in Hakui under normal circumstances was estimated for five years from June 2022 to May 2027. Figure 2, the result of the estimation shows that the number of prescriptions for psychotropic drugs decreased in eight regions over a 15-year period, while the number increased in two regions. In one of the regions, the number increased by 85.3% over the 15-year period,

indicating that the demand for neuropsychiatric drugs is rapidly increasing in this region.

4. SUMMARY AND FUTURE ISSUE

In this study, Hakui City was divided into 10 regions, and the future demand for psychotropic drugs was clarified for each region. The results show that while demand is expected to decrease in many areas, high demand is expected in some areas in the future. As a future issue, it is necessary to perform an extended estimation using the results of this analysis to estimate the situation of drug prescriptions, including those for people who are not enrolled in the national health insurance system.

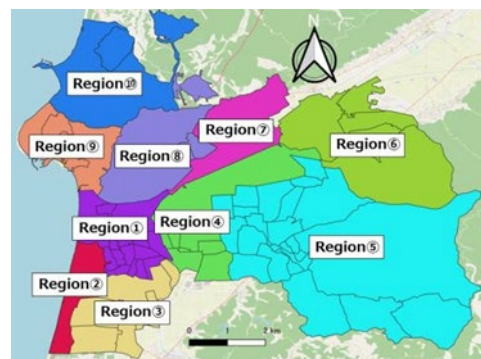


Figure 1. Regional division of Hakui, Ishikawa prefecture

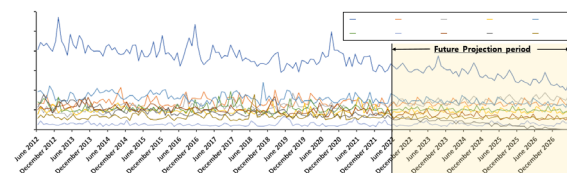


Figure 2. Estimated numbers of prescriptions for psychotropic drugs from June 2012 to May 2027

WHAT SDGS DON'T MEASURE: NON-ACTIONABLE URBAN WELL-BEING FACTORS THROUGH GISCIENCE

G.Y. YAN^{1*}, Y. YUE¹, W. TAKEUCHI², Y.Q. CHEN¹ and B.H. LI¹

¹Researcher, Department of Urban Informatics, Shenzhen University, Shenzhen, China

²Professor, Department of Civil Engineering, The University of Tokyo, Tokyo, Japan,

*Correspondence: guanyu.yan@szu.edu.cn

Keywords: *Quality of life, Urban sustainability, Global South, Urban well-being, Geospatial analysis*

1. INTRODUCTION AND METHODOLOGY

As global urbanization surpasses 50%, urban sustainable development and well-being have become crucial for humanity, especially in the Global South where the urbanization process burgeons [1]. While the UN Sustainable Development Goals (SDGs) [2] provide a common framework for urban development dialogue, their design principles of global-facing actionable goals inevitably ignore elements resistant to direct policy intervention, a gap more pronounced in the Global South [3].

The study identifies critical non-actionable factors influencing urban well-being that are often overlooked. Through a multi-disciplinary literature review spanning health science, psychology, and environmental research—beyond the traditional scope of urban studies—key omissions in the SDG framework are identified, including climate patterns, natural landscape features, cultural infrastructure, and food systems.

Employing meta-analysis, statistical and semantic analysis, we systematically categorize and rank non-actionable factors based on their prevalence in literature and impact magnitude.

The approach can be summarized as the following formula:

Filtered Factors = { $U_i \in \text{Urban Wellness Factors} \mid U_i \notin \text{SDG Factors and } U_i \text{ is measurable in GIScience}$ }

And the literature survey search term keywords are:

((*"urban well-being"* OR *"city well-being"* OR *"urban quality of life"* OR *"metropolitan livability"*) AND (*factor** OR *determinant** OR *indicator**) AND (*emerging* OR *novel* OR *understudied* OR *overlooked* OR *"beyond SDG"* OR *"not included in SDG"*))

The complete search term and search results are available upon reasonable requests to the corresponding author.

2. RESULTS AND DISCUSSION

The most influential and often ignored factors are summarized in Table 1. This preliminary qualitative report highlights several critical non-actionable factors affecting urban well-being that fall outside conventional policy frameworks (Table 1). Among these, urban shadow aesthetics emerges as a particularly significant factor due to its direct impact on human circadian rhythms and thermal comfort, yet its fundamental physical nature makes it resistant to policy intervention.

As cities expand, wildlife habitats are increasingly encroached upon during the urbanization process, leading to a worsening of human-animal conflicts—an issue that is somewhat overlooked in the current UN SDG agenda.

Notably, while the socio-cultural evolution category shows a relatively lower immediate impact in the analysis, its significance may be substantially underestimated in the context of contemporary global trends. As societies navigate post-modern realities—characterized by unprecedented migration flows, intensifying identity politics, growing polarization, and the pervasive influence of social networks—these seemingly background factors are becoming increasingly central to urban social stability.

3. CONCLUSIONS

Nature, urban built-up and socio history are the major categories of factors affecting human well-being discovered in this study. Non-actionable factors fill the missing gaps in designing localized SDG and ESG approaches.

REFERENCES

- [1] United Nations, World Urban. Prosp.: 2018 Rev., New York (2018).
- [2] United Nations, Transform. World: 2030 Agenda Sustain. Dev., New York (2015).
- [3] Z. Patel, et al., Sustain. Sci. 12 (2017) 785-797.

Table 1. Non-actionable factors affecting urban well-being outside of UN SDGs Framework

Category	Factor	Applicability
Ecology	Human-Animal Conflict	Regional
Built Environment	Urban Shadow Aesthetics	Global
Socio-Cultural Evolution	Urban Legends and Folklore	Global
	Family Name Diversity	Global
	Demographic Shift	Global

TOTAL CARBON STOCK ESTIMATION FOR RUBBER PLANTATION USING UNMANNED AERIAL VEHICLE IMAGERY

ZAILANI KHUZAIMAH^{1*}, HISHAMUDDIN HASHIM¹, SITI NOORADZAH ADAM¹ and NAZMI MAT NAWI²

¹Institute of Plantation Studies, Universiti Putra Malaysia, 43400 Selangor Darul Ehsan, Malaysia

²Faculty of Engineering Universiti Putra Malaysia, 43400 Selangor Darul Ehsan, Malaysia

*Correspondence: zailani@upm.edu.my

Keywords: Total rubber carbon stock, UAV, Rubber plantation, Plant biomass, Digital terrain model

1. INTRODUCTION

The establishment of rubber plantation has been proposed as an option to improve physical and chemical properties of the soil by protecting the soil from erosion and recycling nutrients through leaf litterfall. These plantations, as a monoculture or combined with other crops in agroforestry systems, may also sequester carbon from the atmosphere.

Plant biomass estimates in rubber plantations of different ages and grown in potentially dissimilar conditions in Malaysia and Asia have revealed a large range of Aboveground carbon accumulation rates, from 1.4 to 6.7 Mg C ha⁻¹ yr⁻¹. However, fewer studies have investigated changes in the Total carbon accumulation rates in rubber plantations. Estimating Total Rubber Biomass (TRB) is the key factor for calculating the Total Rubber Carbon Stock (TRCS).

Based on previous studies measuring TRB via remote sensing, there is a need for quicker, more reliable, and precise methods to quantify TRB and TRCS. Utilizing 3D data from images captured by Unmanned Aerial Vehicles (UAVs) has shown great potential for reducing costs and improving estimates. While many studies have focused on estimating above-ground rubber biomass using remote sensing data, few have employed UAV data or compared its accuracy with other remote sensing methods to assess TRB and TRCS in Malaysia. The UAV-based estimation of TRCS depends on the availability of accurate Digital Terrain Models (DTMs). The primary aim of this research is to illustrate the application of 3D data generated from UAV imagery in the calculation of TRCS and to evaluate the impacts of produced DTMs based on different approaches and parameters on developed models. The expected result will be to develop a statistic model and produce TRB and TRCS maps accurately.

2. METHODOLOGY

As in Figure 1, TRCS evaluation in rubber plantation sites will be performed as two years of desk research. The first stage is to measure the TRCS per plot in each rubber site; above ground carbon

stock, below ground carbon stock, deadwood carbon stock, litter carbon stock, and soil organic matter.

The second stage is UAV imagery and satellite data collections, in addition to data pre-processing. The third stage is to establish the TRCS model depending on UAV data, whilst the final stage in this research is the accuracy and validity assessment of the developed modeling techniques.

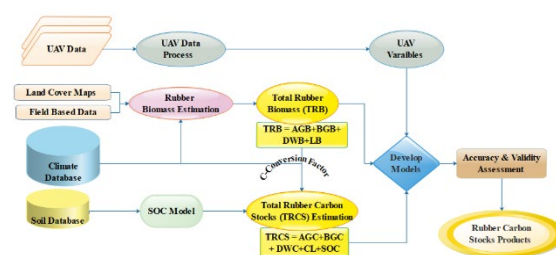


Figure 1. TRCS assessment

3. RESULTS AND DISCUSSIONS

The goal of this project is to identify the capability of 3D images from LiDAR sensors taken using drones in measuring carbon stocks in rubber plantations. From the data obtained it was found that we can measure all the rubber tree data by using the obtained 3D images which are:

- Tree height data
- DBH t
- Tree canopy size

From the data obtained, then all the data needed to measure the carbon stock is sufficient.

Figure 2 (a) – (j) showed the 3D image and data processed from the data obtained from the sensor.

4. CONCLUSIONS

Rubber plantations are vital to the agro-economy and play an indirect role in international public health, particularly in Asia. By sequestering atmospheric carbon, rubber plantations help mitigate climate change effects linked to health risks such as vector-borne diseases, heat stress, and respiratory ailments. Sustainable plantation management enhances soil quality, promotes food security in

agroforestry systems, reduces malnutrition, and fosters community health.

The development of drone technology for rubber surveying can contribute to wealth creation by reducing survey costs and improving the quality of ground rubber survey data, including information about rubber biomass, carbon, and tree structure properties. This technology also supports the creation and strengthening of new industries like rubber mapping and monitoring systems. Drones can serve as a novel method for conducting rubber ground surveys, collecting information on rubber tree structures, TRB, and TRCS. They will provide medium-sized maps for monitoring rubber plantation cover and change at regular intervals, offering insights into where and how changes occur on a biannual or annual basis.

Climate Risk Management, vol. 27, p. 100203, 2020.

- [2] S. Vrignon-Brenas *et al.*, "Nutrient management of immature rubber plantations. A review," *Agronomy for sustainable development*, vol. 39, no. 1, p. 11, 2019.
- [4] J. Fox, J.-C. Castella, A. D. Ziegler, and S. B. Westley, "Rubber plantations expand in mountainous Southeast Asia: what are the consequences for the environment?," 2014.
- [5] W. Ni, J. Liu, Z. Zhang, G. Sun, and A. Yang, "Evaluation of UAV-based forest inventory system compared with LiDAR data," in *2015 IEEE International Geoscience and Remote Sensing Symposium (IGARSS)*, 2015, pp. 3874-3877: IEEE.

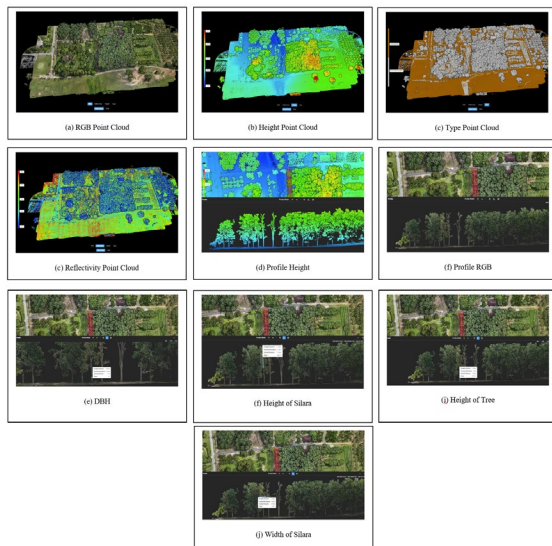


Figure 2 (a)-(j). The 3D image and data processed from the data obtained from the sensor

Table 1. Biomass of rubber tree

No.	Plantation Age	DBH (cm)	Height of Tree (m)	Rubber Biomass (DBH x Height)
1	15 years	16.2	4.7	76.28
2		16.2	5.1	82.77
3		20.1	6.3	126.32
4		26.7	6.9	184.51
5		29.6	7.5	222.00
6		33.4	7.4	247.31
7		36.9	7.2	265.82
8		37.2	8.4	312.82
9		38.2	9	343.80
10		38.2	9.6	366.72
Average		29.3	7.2	222.8

REFERENCES

- [1] M. H. M. Hazir, R. A. Kadir, E. Gloor, and D. Galbraith, "Effect of agroclimatic variability on land suitability for cultivating rubber (*Hevea brasiliensis*) and growth performance assessment in the tropical rainforest climate of Peninsular Malaysia,"

THE IMPACT OF SPECTROSCOPY IN PLANT DISEASE DETECTION, ENVIRONMENTAL SUSTAINABILITY AND PUBLIC HEALTH

SITI NOORADZAH ADAM^{1*}, SITI KHAIRUNNIZA BEJO¹ and NAZMI MAT NAWI²

¹*Institute of Plantation Studies, Universiti Putra Malaysia, UPM Serdang, Selangor, Malaysia*

²*Faculty of Engineering, Universiti Putra Malaysia, UPM Serdang, Selangor, Malaysia*

**Correspondence: snadzah@upm.edu.my*

Keywords: Plant disease, Spectroscopy, Disease detection, NIR, MIR, Fluorescence

1. INTRODUCTION

The increasing prevalence of plant diseases poses significant threats not only to agricultural productivity and environmental sustainability but also to public health. Traditional methods of disease detection often rely on visual inspection, which can be time-consuming and prone to human error.

Spectroscopy, a technique that analyzes the interaction between light and matter, offers a promising alternative for early and accurate detection of plant diseases. This study explores how the application of spectroscopy in plant disease detection contributes to environmental sustainability and ultimately benefits public health.

2. SPECTROSCOPY TECHNIQUES IN PLANT DISEASE DETECTION

Spectroscopy encompasses a range of techniques, including near-infrared (NIR), mid-infrared (MIR), and fluorescence spectroscopy, each exploiting the unique spectral signatures of plant materials to identify biochemical changes associated with disease.

2.1 Near-Infrared (NIR) Spectroscopy

NIR spectroscopy is particularly effective in detecting subtle changes in moisture content and chemical composition in plant tissues before visible symptoms manifest. This technique utilizes the absorbance of near-infrared light by molecular vibrations, providing insights into the water, protein, and carbohydrate levels in plants. Early detection through NIR allows for timely intervention, which is crucial for preventing the spread of pathogens that can adversely affect crop yields and human health. By identifying disease signatures early, farmers can implement targeted treatments, reducing the reliance on broad-spectrum pesticides.

2.2 Mid-Infrared (MIR) Spectroscopy

MIR spectroscopy offers a deeper analysis of plant biochemical composition by examining the vibrational transitions of molecular bonds. This technique can reveal specific functional groups in plant tissues, providing information about the presence of disease-related compounds such as

phenolics or other secondary metabolites. The detailed molecular information obtained through MIR allows for more precise diagnostics, enhancing the ability to differentiate between healthy and diseased plants.

2.3 Fluorescence Spectroscopy

Fluorescence spectroscopy focuses on the emission of light by chlorophyll and other pigments in response to excitation by light. This technique can detect changes in the fluorescence spectra of plants, which may indicate stress or disease. By analyzing the fluorescence characteristics, researchers can assess plant health and identify specific stressors, including pathogen infections. Fluorescence spectroscopy is not only non-invasive but also highly sensitive, making it a valuable tool for real-time monitoring of plant health.

2.4 Integration of Spectroscopic Techniques

Combining these spectroscopy methods can enhance disease detection capabilities. For example, integrating NIR and MIR data can provide a comprehensive view of both moisture content and biochemical changes, leading to more accurate assessments of plant health. Additionally, advancements in machine learning and data analysis techniques can further improve the interpretation of spectral data, enabling the development of predictive models for disease outbreaks.

Overall, spectroscopy techniques offer significant advantages in plant disease detection by enabling early diagnosis and intervention. This proactive approach not only enhances crop management strategies but also contributes to food security and public health by minimizing the spread of plant pathogens that could impact human health.

3. BENEFITS OF EARLY DETECTION

Early detection of plant diseases through spectroscopy allows for targeted management strategies, reducing the need for broad-spectrum pesticide applications. This precision agriculture approach minimizes chemical runoff into surrounding ecosystems, thereby protecting biodiversity and water quality. Moreover, timely

interventions can lead to less crop loss, enhancing food security while reducing the need for land expansion into natural habitats.

Healthy crops also mean safer food products, reducing the risk of foodborne illnesses linked to contaminated or diseased plants.

4. ENVIRONMENTAL SUSTAINABILITY

The integration of spectroscopy in agriculture has far-reaching implications for environmental sustainability, which in turn supports public health:

4.1 Biodiversity Conservation

Healthier crops require fewer resources, allowing for the preservation of surrounding ecosystems and wildlife habitats. Biodiversity is essential for ecosystem resilience and the prevention of disease outbreaks that can affect humans.

4.2 Soil Health Improvement

Minimizing chemical usage helps maintain soil biodiversity and structure, promoting long-term agricultural viability. Healthy soils contribute to the production of nutritious food, which is vital for human health.

4.3 Water Resource Management

Reducing chemical runoff protects aquatic ecosystems and ensures cleaner water supplies for both human and ecological communities. Access to clean water is a fundamental aspect of public health.

4.4 Carbon Footprint Reduction

Efficient disease management through spectroscopy can lead to lower greenhouse gas emissions associated with the production and application of agrochemicals. Mitigating climate change has direct benefits for public health by reducing the incidence of heat-related illnesses and vector-borne diseases.

5. CASE STUDIES AND APPLICATIONS

Several case studies have demonstrated the effectiveness of spectroscopy in detecting diseases such as late blight in potatoes and powdery mildew in cereals. These studies highlight the potential for spectroscopy to serve as a rapid diagnostic tool, enabling farmers to identify and manage diseases promptly, thus supporting sustainable agricultural practices. Reduced reliance on chemical treatments also lessens the risk of pesticide residue in food, contributing to safer consumption.

6. CONCLUSION

The application of spectroscopy in detecting plant diseases not only enhances agricultural productivity but also significantly contributes to environmental sustainability and public health. By

facilitating early detection and targeted interventions, spectroscopy minimizes the environmental impact of agriculture, supports biodiversity, and promotes healthier ecosystems. As advancements in spectroscopy technology continue to evolve, its integration into agricultural practices holds great promise for sustainable food production systems that prioritize both environmental and human health.

7. FUTURE DIRECTIONS

Future research should focus on improving the accessibility and affordability of spectroscopy technologies for smallholder farmers. Additionally, integrating machine learning algorithms with spectroscopic data can enhance predictive capabilities, further supporting sustainable agricultural practices. Public health initiatives should also consider the role of agricultural technology in improving food safety and reducing disease transmission. Through collaborative efforts between technologists, agronomists, public health officials, and policymakers, the potential of spectroscopy to transform plant disease management and promote environmental and public health can be fully realized.

REFERENCE

- [1] Saletnik, A., Saletnik, B., Zagula, G., & Puchalski, C. (2024). Raman Spectroscopy for Plant Disease Detection in Next-Generation Agriculture. *Sustainability*, 16(13), 5474.
- [2] Buja I, Sabella E, Monteduro AG, Chiriaco MS, De Bellis L, Luvisi A, Maruccio G. Advances in Plant Disease Detection and Monitoring: From Traditional Assays to In-Field Diagnostics. *Sensors (Basel)*. 2021 Mar 18;21(6):2129.
- [3] Fang Y, Ramasamy RP. Current and Prospective Methods for Plant Disease Detection. *Biosensors (Basel)*. 2015 Aug 6;5(3):537-61.

OPTIMAL LOCATION OF WIRELESS POWER TRANSFER SYSTEMS FOR URBAN RESILIENCE AND SUSTAINABLE TRANSPORTATION

YUDAI HONMA

University of Tokyo, Tokyo, Japan
Correspondence: yudai@iis.u-tokyo.ac.jp

Keywords: *Wireless power transfer, Sustainable transportation, Urban resilience, Disaster preparedness*

1. INTRODUCTION

In recent years, expectations for low-carbon alternative fuel vehicles, particularly electric vehicles (EVs), have risen rapidly. For the widespread adoption of these alternative vehicles, infrastructure development is essential to improve their convenience; in the case of EVs, this requires an extensive and efficient charging infrastructure network [1]. However, EVs face inherent challenges, such as limited driving range due to battery capacity constraints and long charging times. As a new power supply solution to address these issues, in-motion Wireless Power Transfer Systems (WPTS) have gained attention [2]. WPTS can charge EVs on the move by transferring power through coils embedded under the road, allowing EVs to recharge without waiting at charging stations and enabling continuous driving.

In addition to extending EV range, WPTS also has the advantage of potentially reducing the required battery capacity in vehicles, especially in urban areas. A promising scenario is the installation of WPTS near major intersections, where vehicles slow down, enabling more frequent charging opportunities and thus reducing the necessary onboard battery capacity.

The effectiveness of support infrastructure such as charging stations and WPTS greatly depends on their location. Optimal facility location, particularly in urban settings, is widely studied using discrete optimization methods, especially within geography and operations research fields [3]. Numerous studies have examined optimal location strategies for charging stations [4,5]; however, few have focused on WPTS, particularly on highways and in cities. Therefore, the authors have also conducted research examining the optimal location of WPTS for use on highways and in urban areas [6,7].

In this study, we investigate how optimally located WPTS in urban environments could minimize the necessary battery capacity for EVs. First, we introduce an optimal location model based on discrete optimization, designed to meet urban EV travel demand while minimizing the total length of WPTS required. We then verify the feasibility of various battery capacities using a traffic simulation

model conducted in Kawagoe City, Saitama Prefecture.

This research offers two primary innovations. First, it demonstrates that the feasibility of EV travel demand is highly dependent on WPTS location. Optimal location results in a significantly reduced total WPTS length compared to uniform intersection placement. Second, assuming optimal WPTS location, EVs may require only around 5 kWh of battery capacity—significantly lower than current standard capacities, demonstrating WPTS's potential to support "Infinite Driving" with reduced EV investment.

2. OPTIMAL LOCATION MODEL

2.1 Frameworks

In this section, we focus on everyday urban mobility and introduce a mathematical model for deriving the optimal location of WPTS to meet EV travel demand.

The urban mobility model in this section assumes that each EV follows various routes, with routes being determined exogenously; EVs do not intentionally alter their routes to pass through locations with WPTS. We explicitly consider EV acceleration and deceleration, as urban mobility frequently involves speed changes due to traffic signals and traffic conditions. To represent these factors in a mathematical model, we divide the road network into small segments of 7 meters each and express various EV behaviours as motions within each segment. The probability distribution for each EV motion is also exogenously determined and calculated separately. The notations used in the model are listed below:

qq Index of flow demands

ii Index of link segments

mm Index of motions

Sets:

QQ Set of flow demands

II Set of link segments in the entire network

MM Set of motions

Parameters:

ff_{qq} Flow volume of flow demand qq

dd_{ii} Length of the segment ii [m]

cc^{mm} Required electric power to pass through

segment ii by the motion mm [kWh]
 rr^{mm} Electric power transfer from WPTS at
segment ii by the motion mm [kWh]
 $pp(mm)^{qq}$ Probability of the motion mm for the
demand qq at the segment ii
 RR_{qq} Expected power consumptions for the
demand qq
 $\alpha\alpha$ Safety Coefficient
Decision Variables:
 xx_{ii} 1 if the WPTS is installed on ii , 0
otherwise

2.2. Optimal Location Problem for In-motion WPTS

We formulated a flow-capturing location problem for in-motion WPTSs. A flow demand is captured when an EV with a certain battery capacity can reach its destination using its battery capacity and energy transferred via WPTS.

$$\text{Min. } \sum_{ii \in II} dd_{ii} xx_{ii} \quad (1)$$

subject to:

$$RR_{aa} = \sum_{ii \in II} \sum_{mm \in MM} pp(mm)^{aa} \times (rr^{mm} xx_{ii} - \alpha\alpha cc^{mm}) \forall aa \in QQ \quad (2)$$

$$\sum_{aa \in QQ} ff_{aa} RR_{aa} \geq 0 \quad (3)$$

$$xx_{ii} \in \{0,1\} \quad \forall ii \in II \quad (4)$$

3. NUMERICAL EXAMPLES

3.1. Networks and Flow Volumes

Using the methods presented in Section 2, we applied our model to Japanese typical middle-sized city. First, as for the network data, we extracted detailed road information from OpenStreetMap. Then, based on the actual building data and road network data, its travel demand and routes were estimated, and motion data was created. The flow demand data is shown in Figure 1.



Figure 1. Example of OD flow in Kawagoe-city

3.2. Parameter settings

We summarize the parameter settings for the energy consumption. In this study, we used Equation (5) to calculate the motor power [kW], based on the

studies by Tanaka et al. (2008), Wu et al. (2015), and Fiori et al. (2016).

$$P(v, a, \theta) = \frac{1}{\eta} v \left(ma + mg \cos \theta f_{rl} + \frac{1}{2} \rho A_f C_D v^2 + mg \sin \theta \right) \quad (5)$$

Equation (5) expresses the motor power P when the EV has a velocity v [m/s], acceleration a [m/s²], and road gradient θ [°]. The parameters used in this study, based on Tanaka et al. [10], Wu et al. [11], Fiori et al. [12], and The Engineering ToolBox [13], are summarized in Table 1. In these parameters, we assumed a Nissan Leaf as the EV.

Next, we assumed the transfer power of the WPTS. Although there is no global standard amount of power to be transferred by an WPTS, existing studies assumed a power output of 20 – 25 kW [2]. In addition, when a vehicle is stationary, a wireless power transfer, such as that of WPT4, has been proposed [14]. In this study, the transfer capacity was set to 22 kW with a transfer efficiency of 85%, resulting in a power output of 18.7 kW.

Table 1. Parameters for calculating motor power

Parameters	Values
Efficiency of the electric motor η [%]	90
Vehicle weight (with drivers), m [kg]	1640
Gravitational acceleration g [m/s ²]	9.8066
Rolling resistance coefficient f_{rl}	0.015
Air mass density ρ [kg/m ³]	1.2256
Frontal area of the vehicle A_f [m ²]	2.34
Aerodynamic drag coefficient C_D	0.32

3.3. Optimal locations

Figure 2 and 3 shows the optimal location results for WPTS with a safety factor of 1.1. While it is intuitively clear that intersections are favorable locations, the analysis confirms that this is indeed the mathematically optimal strategy. The total road length in the target area is approximately 150 km, with 127 intersections; however, the total length of WPTS installation required is 2,359 meters, covering 56 intersections. The average WPTS installation length per location is 14.77 meters.

4. CONCLUSIONS

This study discusses the required battery capacity for urban mobility under the assumption of an optimally located WPTS. The findings reveal that even with a relatively small battery capacity, urban travel can be successfully completed, highlighting the promising potential of WPTS as a supportive EV infrastructure toward achieving "Infinite Driving."

5. ACKNOWLEDGMENT

This research was supported by Grants-in-Aid for Scientific Research (Project Numbers: 21H01563 and 24K01109), research grants from the

Kajima Foundation for the Promotion of Science, and the ENEOS TonenGeneral Research Encouragement and Scholarship Foundation.

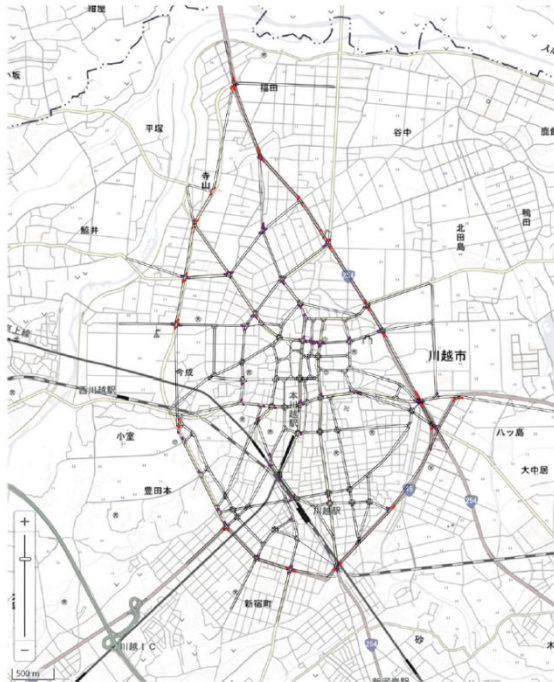


Figure 2. Optimal location of WPTS (overview)



Figure 3. Optimal location of WPTS (Enlarged)

REFERENCES

- [1] Ministry of Land, Infrastructure, Transport and Tourism, Japan, "Long-term Road Policy Vision: Transforming the Road Landscape by 2040," 2020.
- [2] K. Hata, T. Imura, H. Fujimoto, Y. Hori, and D. Gunji, "Charging Infrastructure Design for In-motion WPTS Based on Sensorless Vehicle Detection System," 2019 IEEE PELS Workshop
- on Emerging Technologies: Wireless Power Transfer (WoW), 2019.
- [3] Yukio Sadahiro, Ikuho Yamada, and Yoshimitsu Ishii (Eds.), Introduction to Spatial Analysis, Asakura Publishing Co., Ltd., 2018.
- [4] M.J. Kuby and S. Lim, "The Flow-refueling Location Problem for Alternative-fuel Vehicles," Socio-Economic Planning Sciences, vol. 39, pp. 125-145, 2005.
- [5] M. Coffman, P. Bernstein, and S. Wee, "Electric Vehicles Revisited: A Review of Factors that Affect Adoption," Transportation Reviews, vol. 37, no. 1, pp. 79-93, 2017.
- [6] Y. Honma, D. Hasegawa, K. Hata, and T. Oguchi, "Locational Analysis of In-motion Wireless Power Transfer System for Long-distance Trips by Electric Vehicles: Optimal Locations and Economic Rationality in Japanese Expressway Network," Networks and Spatial Economics, vol. 24, no. 1, pp. 261-290, 2024.
- [7] Y. Honma, D. Hasegawa, K. Hata, and T. Oguchi, "Optimal Location Model of In-motion Wireless Power Transfer System for Trips in Urban-scale Region by Electric Vehicles," In Proceedings of The 6th International Electric Vehicle Technology Conference (EVTec 2023), Yokohama, Japan, 2023.A. Author, B. Author, and C. Author, vol. 5, no. 12, pp. 12-15, May 2017.
- [8] Manshadi SD, Khodayar ME, Abdelghany K, Uster H (2018) Wireless charging of electric vehicles in electricity and transportation networks. IEEE Transactions on Smart Grid 9:4503-4512.
- [9] Liu H, Zou Y, Chen Y, Long J (2021) Optimal locations and electricity prices for dynamic wireless charging links of electric vehicles for sustainable transportation. Transportation Research Part E: Logistics and Transportation Review 152.
- [10] Tanaka D, Ashida T, Minami S (2008) An analytical method of EV velocity profile determination from the power consumption of electric vehicles. 2008 IEEE Vehicle Power and Propulsion Conference.
- [11] Wu X, Freese D, CabreraA, Kitch WA (2015) Electric vehicles' energy consumption measurement and estimation. Transp Res Part D: Transp Environ 34:52-67.
- [12] Fiori C, Ahn K, Rakha HA (2016) Power-based electric vehicle energy consumption model: Model development and validation. Appl Energy 168:257-268.
- [13] The Engineering ToolBox, 2008. https://www.engineeringtoolbox.com/rolling-friction-resistance-d_1303.html (Accessed November 10, 2024).

- [14] SAE J2954 standard, 2020. Wireless Power Transfer for Light-Duty Plug-in/Electric Vehicles and Alignment Methodology. https://www.sae.org/standards/content/j2954_202010/ (Accessed November 10, 2024).

IMPACT ASSESSMENT OF FARE INCREASES AND CONSCIOUSNESS OF RAILWAY USERS' REGARDING THE HOKURIKU SHINKANSEN TSURUGA EXTENSION

K. NISHIOKA¹, M. FUJIIU^{2*} and Y. MORISAKI²

¹*Division of Geosciences and Civil Engineering, Kanazawa University, Ishikawa Prefecture, Japan*

²*Faculty of Transdisciplinary Sciences for Innovation, Kanazawa University, Ishikawa Prefecture, Japan*

*Correspondence: fujiiu@se.kanazawa-u.ac.jp

Keywords: Hokuriku Shinkansen Tsuruga extension, Questionnaire survey, Fare increase, Survival analysis

1. INTRODUCTION

The Hokuriku Shinkansen is one of Japan's five high-speed railway lines. As shown in Figure 1, it serves as a crucial transportation route that starts in Tokyo, and passes through the Hokuriku region, which includes major cities such as Nagano, Toyama, and Kanazawa, before finally reaching the Kansai region, including cities as Kyoto and Osaka. The construction of the Hokuriku Shinkansen is important not only reducing travel time and increasing the number of people traveling and interacting, but also strengthening transportation networks as a countermeasure against disasters and providing alternative emergency transport routes.

The extension of the Hokuriku Shinkansen between Kanazawa and Tsuruga opened on Saturday, March 16, 2024. However, the opening of Tsuruga Station has required passengers to transfer to a local railway line when traveling to the Kansai and Chukyo regions, reducing transportation convenience due to the closure of direct through operations. Additionally, fares have increased compared to before the Tsuruga extension, with an increase of 1,950 yen for travel between Kanazawa and Osaka, and 1,680 yen for travel between Fukui and Osaka. The effect of fare increases on users' willingness to travel are not clear due to the ambiguous nature of travel behavior consciousness.

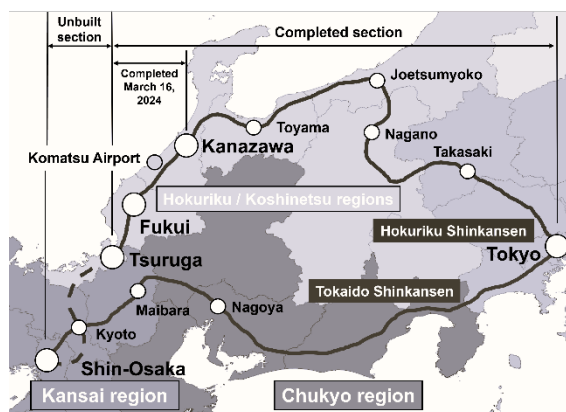


Figure 1. Route map of Hokuriku Shinkansen

2. OUTLINE OF THIS STUDY

In this study, a questionnaire survey was conducted to collect data on the awareness and behavior of high-speed railway users in Ishikawa and Fukui prefectures, as well as to identify factors related to fare increases. The fare increase of the Tsuruga extension is primarily due to the shift from conventional limited express trains to the higher-cost Shinkansen service. In addition, the decline in users and changes in transportation choices were analyzed using survival analysis to identify contributing factors. The purpose of this study is to explore appropriate fare levels to better understand the status of fare setting that promotes the use of the Hokuriku Shinkansen.

In this study, the dependent variable was the acceptable fare increase, while the independent variables included Hokuriku Shinkansen usage, annual income, perception of travel time changes, perception of transportation convenience, and acceptable transfer time. Results of the survival analysis showed that all variables were statistically significant. In particular, the Hokuriku Shinkansen utilization rate and perceived convenience of transportation were shown to be influential in determining the acceptable increase in fare. Additionally, the acceptable fare increase was analyzed for respondents who do not use the Hokuriku Shinkansen and have negative perceptions of travel time changes and transportation convenience. Figure 2 shows the result of analysis based on variations in annual income. Among higher-income respondents only about 25% found a 500-yen increase acceptable, and only about 5% accepted a 1,000-yen increase. In contrast, approximately 40% of lower-income individuals tolerated a 500-yen increase, while around 14% accepted a 1,000-yen increase. These findings suggest that limiting fare increases to around 500 - 1,000 yen, compared to the current 1,950-yen increase, could potentially boost ridership through adjusted fare settings or discounts.

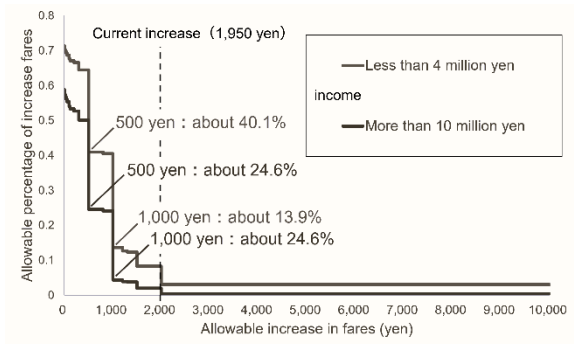


Figure 2. Analysis result (residents of Kanazawa City)

3. CONCLUSIONS

This study provided insights into the impact of fare increases on users' willingness to travel and identified which fare levels were most effective in encouraging the use of the Hokuriku Shinkansen.

RESEARCH ON APPROPRIATE USE OF DEMAND TAXIS FOR TRANSPORTATION PURPOSES

TAIKI MUKOYAMA and KAZUYUKI TAKADA*

Tokyo Denki university, Saitama, Japan
**Correspondence: takada@g.dendai.ac.jp*

Keywords: Demand taxi, Area with no traffic flow, Public transportation

1. INTRODUCTION

Demand responsive transport has attracted much attention in recent years. Multiple factors, including the aging of society, the lack of transportation infrastructure in rural areas, and the need to reduce costs, are driving this development. Demand responsive transport is characterized by its flexibility to meet the needs of users, making it an extremely important means of transportation for the elderly and people with limited mobility.

Ensuring transportation for the elderly is a serious issue. As the population ages, an increasing number of elderly people have given up driving cars, and in many cases, it is difficult for them to use local buses and other means of transportation. Demand responsive transport is therefore a valuable means of enabling the elderly to move freely when they need to. Demand taxis also play a role in improving the quality of daily life, such as hospital visits, shopping, and social activities, because they can be reserved by phone or through an app, and travel to where they are needed when they are needed. The need for demand responsive transport is especially acute in rural areas, where public transportation options are limited. In many rural areas, buses are infrequent, and their hours of operation are limited, leaving residents with few means of transportation.

The introduction of demand responsive transport in these situations will allow residents to move around more flexibly and will also help revitalize the local economy. In this study, to improve the sustainability of the demand taxis, we used data on the actual use of demand taxis to determine whether they are being used more than necessary. Specifically, the use of demand taxis before shopping, for example.

Appropriate use was defined, and the extent to which the financial burden would be reduced if it were applied was evaluated.

2. DATA

In this study, the “Higashimatsuyama City Demand Taxi” in Higashimatsuyama City, located in the central part of Saitama Prefecture, was the subject of research. Higashimatsuyama City has been in full-scale operation since December 2015. This study analyzes the impact of the demand taxis

on the choice set using actual usage data from December 2015, after the start of full-scale operation, to the present.

3. OVERVIEW OF “HIGASHIMATSYUYAMA CITY DEMAND TAXI”

This section outlines the “Higashimatsuyama City Demand Taxi” that has been in operation since December 1, 2015. Citizens who have completed user registration can use the service. Taxis are available at designated pick-up and drop-off points (519 as of October 2024), or in front of the user's home. The bus runs from 8:30a.m. to 5:00p.m., except on Sundays, national holidays, and during the year-end and New Year holidays. Reservations can be made by phone three days in advance. The fare paid by the user varies according to the cab meter rate, as shown in the table below. Fares were revised in July 2020.

The purpose of use of the “Higashimatsuyama City Demand Taxi” was examined. Figure 1 shows the total number of taxi trips by destination (excluding home). As shown in this figure, the most common destinations are hospitals and clinics, followed by commercial facilities. Since this study focuses on the round-trip use of demand taxis, the possibility of one-way use is discussed. In the case of hospitals, there are many people who are not in good health or have difficulty walking. On the other hand, if they are traveling to a commercial facility, it is possible for them to choose a public transportation method other than a demand taxi for the outward trip when they do not have much baggage. Based on this, this study analyzes users who travel between their homes and commercial facilities.

Table 1. “Higashimatsuyama City Demand Taxi” fees

Total amount of freight and pick-up/drop-off charges	Fees (before revision)	Fees (after revision)
Less than 1,000 yen	500 yen	500 yen
1,000 yen or more, but less than 2,000 yen	500 yen	800 yen
2,000 yen or more, but less than 3,000 yen	1,000 yen	1,000 yen

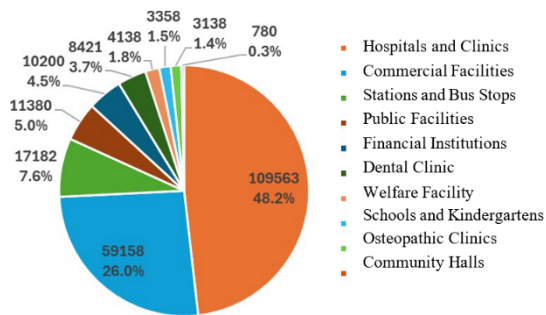


Figure 1. Cumulative total number of visits by destination type (excluding home)

4. APPROPRIATE USE

4.1 Definition of appropriate use

Demand taxis are an important means of transportation for residents living in areas with no traffic flow. Because the “Higashimatsuyama City Demand Taxis” can travel throughout the city and are very convenient, it is possible that demand taxis are used even when public transportation such as local buses can be used for transportation. Therefore, in this study, appropriate use is defined as the case where the point of boarding or alighting from a demand cab is in a traffic void area.

In rural areas, “vacant areas are defined as areas with a radius of 1,000 m or more from a station and 500 m or more from a bus stop.” However, with today's aging population, it is becoming increasingly difficult to define a vacant transportation area by this definition. Therefore, in this study, we decided to treat vacant public transportation areas in the manner described in the next section.

4.2 How to identify appropriate available trips

This section describes a method for identifying trips that can be made appropriate. We verify whether other means of public transportation can be used according to the definition just described. In this study, given that the users of the “Higashimatsuyama City Demand Taxi” are elderly people, we assumed a walking speed of 40 m/min. and set the area within a radius of 200 m, which can be reached in 5 minutes on foot from a station or bus stop, as an area where public transportation can be used.

As mentioned in the previous section, since this study targets round-trip use between home and commercial facilities, the decision is based on whether there is a bus stop within 200 meters around the home of the round-trip user.

4.3 Appropriate available trip extraction results

In 2023, there were 677 people who traveled back and forth between their homes and commercial facilities. Figure 2 shows the location of the

residences of the selected persons. The locations are shown in yellow if they are included in the 200m radius buffer from the bus stop, and in green if they are not included in the buffer.

There were 212 people within the 200m buffer, indicating that approximately one out of every three people used the “Higashimatsuyama City Demand Taxi” even though they had the option of taking the bus.

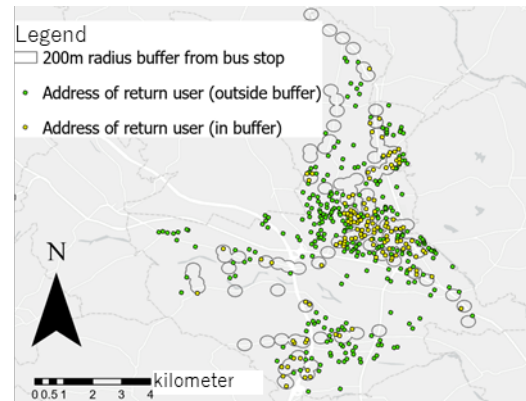


Figure 2. Spatial distribution of individuals commuting between their homes and commercial facilities

4.4 Amount of burden reduction for municipalities through promotion of appropriate use

Figure 3 shows the amount of subsidy provided by the city to users making round-trip trips between their homes and commercial facilities in each year, which was about 6.3 million yen in 2023. The city subsidy for 212 users in the buffer shown in Figure 2 was about 2.1 million yen in 2023.

If these users choose to use the bus for their outbound trip, the annual municipal subsidy amount can be expected to be reduced by approximately 1.05 million yen. Since the total municipal subsidy in 2023 is approximately 54 million yen, the estimated reduction of approximately 1.05 million yen is about 1.9% of the total subsidy.

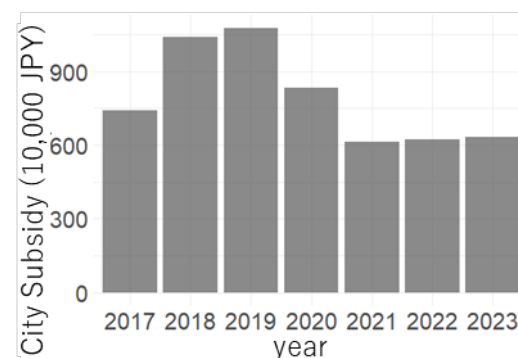


Figure 3. City subsidies for users traveling to and from home and commercial facilities

5. CONCLUSIONS

This study utilized data on the actual use of "Higashimatsuyama City Demand Taxis" to understand the current situation, define appropriate usage, and evaluate how such usage could alleviate financial burdens.

After identifying the suitable trips available, it was confirmed that many individuals rely on demand taxis to reach their destinations, even when a bus stop is nearby. One issue to address is the application of this method to areas within 200 meters of the destination, as well as estimating the potential reduction in the financial burden on local governments through appropriate demand taxi use.

Future plans include conducting a questionnaire survey and analysis to clarify how the demand for taxi services has influenced users' transportation options.

FLOW OF PEOPLE USING SENSING DEVICES IN DILI, DEMOCRATIC REPUBLIC OF TIMOR-LESTE

Y. MINEMATSU¹, M. FUJII^{2*}, Y. MORISAKI² and Y. KON³

¹School of Geosciences and Civil Engineering, Kanazawa University, Kanazawa City, Japan

²Faculty of Transdisciplinary Sciences for Innovation, Kanazawa University, Kanazawa, Japan

³Frontier Institute of Tourism Science, Kanazawa University, Kanazawa City, Japan

*Correspondence: fujii@se.kanazawa-u.ac.jp

Keywords: Timor-Leste, Mobile sensing, Movement, Disaster, Mobility, GPS logger

1. INTRODUCTION

The Democratic Republic of Timor-Leste has not yet made progress in accumulating data necessary for policy making. The collection of such data is very important for future development. It is useful for transportation, Infrastructure maintenance, and disaster prevention planning. In particular, understanding human behaviours patterns is important for urban planning, disaster management, and the promotion of economic activities. In urban planning, these data can be applied to reduce traffic jam and improve the efficiency of public transportation systems. From a disaster prevention perspective, it enables the identification of areas likely to experience high population density and to ensure the establishment of effective evacuation routes.

As above, human flow monitoring is important for urban planning and disaster prevention planning in developing countries and needs to be conducted. In addition, it is necessary to routinely monitor the situation using as simple equipment and means as possible. Therefore, the purpose of this study is to measure human flow in Timor-Leste, where the data acquisition foundation is not yet in place, by introducing sensing technology.

2. METHODOLOGY

The sensing equipment used in this study includes GPS loggers and non-contact sensing devices (model: M5STACK-K129), as shown in Figure 1. The GPS logger can acquire data such as time, latitude, longitude, and speed. Table 1 shows examples of data obtained through the GPS logger. By attaching a GPS logger to a vehicle, it is possible to measure the route and speed of the vehicle to which it is attached. Traffic jam areas and frequently travelled routes can then be identified. Next, Table 2 shows an example of data obtained through non-contact sensing devices. These devices record the passing time of persons within a radius of approximately 10-20 meters by detecting the MAC addresses from smartphones or similar devices. To ensure anonymity, the MAC addresses are hashed upon recording within the sensing device. By

installing multiple non-contact sensing devices at various locations, the number of people moving and their travel routes can be determined. As shown in Figure 2, using this equipment enables the visualization of behaviour between two points, thus supporting an understanding of human flow characteristics.

3. CONCLUSION

In this study, we used sensing equipment to acquire human flow and traffic data as a foundation for transportation and urban planning. As a result, we confirmed that it is possible to get a on human behaviour and vehicle movements and visualize these patterns, even in Timor-Leste, where data collection is difficult. Due to the limited number of sensing devices used in this study, the findings are limited to a basic understanding of human flow. In future works, we will focus on increasing the number of sensing devices and extending the observation period to enable more detailed measurement of human flow, contributing to the optimization of public transportation and the development of effective evacuation routes.

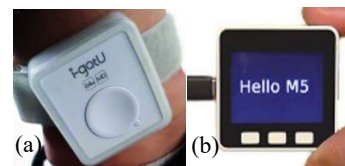


Figure 1. (a) GPS logger, (b) non-contact sensing devices

Table 1. Example of GPS logger data

Time	Local Time	Latitude	Longitude	Altitude(m)	Speed(km/h)	Course	Distance(m)
2024-01-15T23:17:36Z	2024-01-16T08:17:36+09:00	36.707188	137.837178	800.9	6.08	131.88	C
2024-01-15T23:17:39Z	2024-01-16T08:17:39+09:00	36.707155	137.837228	804.6	2.12	16.77	5.77
2024-01-15T23:17:42Z	2024-01-16T08:17:42+09:00	36.707111	137.837266	805.1	3.1	143.95	6.04
2024-01-15T23:17:45Z	2024-01-16T08:17:45+09:00	36.707086	137.837265	800.4	6.84	180.17	1.56
2024-01-15T23:17:48Z	2024-01-16T08:17:48+09:00	36.707010	137.837315	811.3	3.17	200.78	9.95
2024-01-15T23:17:51Z	2024-01-16T08:17:51+09:00	36.706906	137.837333	820.5	4.21	234.73	12.3
2024-01-15T23:17:54Z	2024-01-16T08:17:54+09:00	36.706941	137.837226	818.4	3.85	251.78	10.05
2024-01-15T23:17:57Z	2024-01-16T08:17:57+09:00	36.70698	137.837171	813.8	5.18	271.44	9.55
2024-01-15T23:18:00Z	2024-01-16T08:18:00+09:00	36.706933	137.837082	810.9	2.8	281.84	12.99

Table 2. Example of non-contact sensing devices data

Time	Lat	Long	User
2024-09-20T07:56:51	16.82568	100.2629	a53a4d344719d81a7837fbd7c0c4d858a5fmm07b5390b73c5b3c260b4170
2024-09-20T07:56:51	16.82568	100.2629	a53a4d344719d81a7837fbd7c0c4d858a5fmm07b5390b73c5b3c260b4170
2024-09-20T07:56:51	16.82568	100.2629	a53a4d344719d81a7837fbd7c0c4d858a5fmm07b5390b73c5b3c260b4170
2024-09-20T07:56:51	16.82568	100.2629	940bbca4c3cc7748cd92f1350df46ec7088802e772c4027daf4d7ad8cf9e9a
2024-09-20T07:56:55	16.82568	100.2629	19a1408f25ca35e68f566f5c136c83e9248d6d744cb43887ebd5ab8958b7f46
2024-09-20T07:56:57	16.82568	100.2629	109615752f849a93957d9e8158ed14e53bf35c73c2c04fcb5c9595e82f66d6dc
2024-09-20T07:57:11	16.82568	100.2629	940bbca4c3cc7748cd92f1350df46ec7088802e772c4027daf4d7ad8cf9e9a

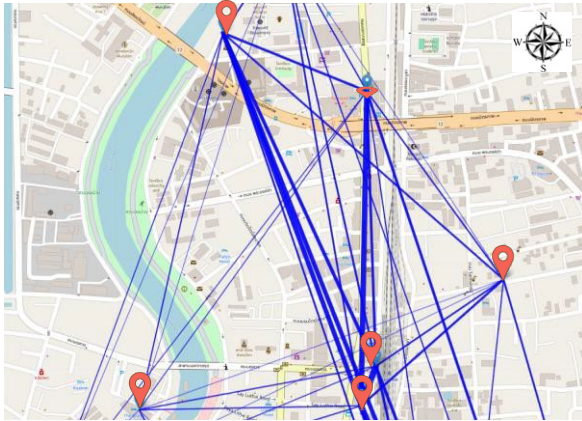


Figure 2. Amount of behavior visualized by non-contact sensing devices

INVESTIGATING THE RELATIONSHIP BETWEEN CITY COMPACTNESS AND LIVABILITY IN JAPAN

T. KONDO^{1*} and W. TAKEUCHI²

¹*Department of Civil Engineering, The University of Tokyo, Tokyo, Japan,*

²*Institute of Industrial Science, The University of Tokyo, Tokyo, Japan,*

**Correspondence: kontatsuya2000@g.ecc.u-tokyo.ac.jp*

Keywords: Sustainable Urban Development, GIS, Compact City Index, Decoupling

1. INTRODUCTION

Japan is facing many significant challenges, including a population decline, an aging population, environmental issues and an aging infrastructure. One potential solution to these social issues is the concept of the compact city. Prior research has indicated that compact cities represent a promising model for sustainable urban development, exhibiting superior attributes in terms of living convenience, environment sustainability, and financial efficiency. However, as the concept of compact city is a relatively novel one, many aspects remain unresearched. It is of great importance to gain insight into the relationship between city compactness and liveability in order to promote compact city policies effectively. However, this impact remains largely unknown.

This study examines the potential of compact cities. Specifically, this study investigated the relationship between city compactness and liveability. The study area comprised Japan's 47 prefectural capitals. Furthermore, the relationship between city compactness and sustainability was investigated, as it is essential to consider not only the liveability of cities but also their sustainability when assessing their potential.

2. METHODOLOGY

The Compact City Index (CCI) was developed using GIS data as an indicator of city compactness. This indicator, based on population distribution, can reflect both community-level compactness centered on railway stations and city-level compactness centered on city centers. CCI values were calculated from 2005 to 2025, with 2025 data being estimated. The relationship between CCI and the results of a large-scale survey on livability was analyzed. The livability data was provided by Daito Trust Construction Co, Ltd. Compactness data from 2020 and cumulative livability data from 2020 to 2024 were used. Piecewise linear regression was used to identify the relationships.

The relationship between CCI and a sustainability indicator was examined. The decoupling index was employed as a sustainability indicator. Decoupling means breaking the link

between environmental damage and economic goods [1]. The decoupling index was calculated using estimated carbon dioxide emissions data and the Financial Capability Index, defined as the rate of change in environmental impact divided by the rate of change in economic level. This analysis employed data on compactness from 2015 and decoupling from 2015 to 2020. In this section, 'High compactness' was defined as $CCI \leq 2.5\text{km}$, 'Medium compactness' as $2.5\text{km} < CCI \leq 3.5\text{km}$ and 'Low compactness' as $3.5\text{km} < CCI$.

3. RESULTS AND DISCUSSION

The relationship between CCI and liveability (Figure 1 (a)) was analyzed, and it was found that there were disparate trends between the high and low liveability groups. The CCI serves as an indicator of city form, with lower values indicating a more compact city form. In the high liveability group, higher CCI values were associated with lower liveability, while in the low liveability group there was no clear pattern. These findings indicate that the impact of compactness on liveability is negligible up to a certain threshold, beyond which it begins to exert a positive influence. One potential explanation for the absence of an influence of CCI in the lower liveability group is that people living in these cities do not rely on railways for their livelihood.

Regarding the relationship between CCI and the degree of decoupling (Figure 1 (b)), no clear relationship was identified. This suggests that CCI has a negligible effect on the extent of decoupling. One potential explanation for the absence of an impact of CCI is that the impact of urban form is relatively modest in comparison to the contribution of technological innovations and other factors to sustainability.

4. CONCLUSIONS

This study investigated the potential of compact cities. The results of this study indicated that city compactness may have a beneficial effect on liveability, yet did not reveal any obvious impact on sustainability. As the environmental data employed in the city sustainability analysis was estimated, and to extend the analysis period, satellite observation

data, which can be updated with measured data, can be used in future analysis.

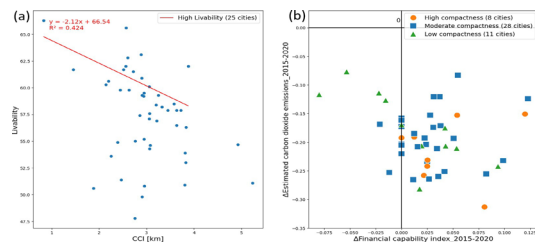


Figure 1. (a) Relationship between CCI and livability. (b) Relationship between CCI and the degree of decoupling

REFERENCES

- [1] OECD, OECD Environmental Strategy: 2004
Review of Progress, Paris, 2004

PROPOSAL OF BASE LOOP STRATEGY FOR MULTI-RETAILER AND MULTI-CUSTOMER DE LIVERY SERVICE BY AUTOMATED DELIVERY ROBOTS

MOTOYA UEDA¹, HIROYUKI HASADA², KAORI ISAWA² and YUDAI HONMA^{2*}

¹Graduate School of Engineering, The University of Tokyo, Tokyo, Japan,

²Institute of Industrial Science, The University of Tokyo, Tokyo, Japan,

*Correspondence: yudai@iis.u-tokyo.ac.jp

Keywords: Automated delivery robot, Cooperative operation, Delivery service

1. INTRODUCTION

Food delivery has evolved with the development of technology, changing the method of ordering, the means of delivery, and the form of delivery personnel. The origin of food delivery in Japan is said to have originated around 1690, when store employees would travel to customers and sell meals and food. Around 1870, store employees began using bicycles to deliver meals around town. Around 1950, landline telephones became widespread, and people began ordering delivery from neighbourhood sushi and soba restaurants over the landline telephones. In 1985, the first pizza delivery service opened in Japan, offering only delivery service without any eating and drinking space. Around 2000, with the development of the internet, orders could be placed over the internet and deliveries were made by car or motorcycle. In 2015, UverEats was founded, and deliveries were made by gig worker.

In recent years, technological developments have led to significant demonstration tests and real-world implementations of new mobility technologies, such as automated delivery robots, throughout the world. In Japan, the Road Traffic Act has been revised to allow “remotely operated small vehicles” to drive on public roads from April 2023, increasing the feasibility of their implementation in the real world.

The New Energy and Industrial Technology Development Organization (NEDO) and Kyocera Communication Systems Corporation conducted a demonstration experiment in which a single operator remotely monitored and operated multiple automated delivery robots while providing delivery services on a roadway in a portion of the Midoriendaito district of Ishikari City, Hokkaido, Japan. Uber Eats Japan has formed a business alliance with Mitsubishi Electric Corporation and Cartken of the United States to launch an AI-based food delivery service using autonomous robots in the Nihonbashi area (Figure 1). Estonian company Starship Technologies has already achieved more than 6 million autonomous deliveries.

In the food delivery market, the impact of COVID-19 in 2020 has led to a significant increase in demand for food delivery, and the market size in

2023 is expected to be 860.3 billion yen, a 106% increase from the before COVID-19 market size in 2019 [2].

The market size of food delivery is expected to continue to increase in the future.



Figure 1. Automated robotic delivery service by Uber Eats Japan in Nihonbashi, Tokyo [1]

2. PROPOSAL OF BASE LOOP STRATEGY

This study proposes “Base Loop”, governing the strategy for autonomous delivery robot waiting locations in a multi-retailer, multi-customer service. Base Loop is a generalized concept of a waiting hub, characterized by an infinitely dense distribution of waiting points along a circumference. In conventional delivery services, such as Domino's Pizza, delivery personnel use the retailer as their base and simply travel back and forth between the base and customers. In Uber Eats, there is no designated base, and delivery personnel move independently without cooperating with others.

In the delivery service considering Base Loop, an automated delivery robot receives the order and travels the shortest distance from the Base Loop to the retailer, from the retailer to the customer, and from the customer to Base Loop. It differs from conventional delivery services in that there is not a base of automatic delivery robots and the automatic delivery robots that have not received orders move in a coordinated manner to cover the pickup area of the automatic delivery robots that have received orders (Table1).

Figure 2 shows how the automatic delivery robot moves in Base Loop. The black dots represent the robot and the red dots represent the robot that received the order and the dotted circumference represents Base Loop. Base Loop is like a dedicated road for automatic delivery robots, with robots moving cooperatively on the road

The advantages of Base Loop are economic

rationality, response to demand, and operational simplicity. Since Base Loop does not require a base, it makes good economic rationality in urban areas where space is scarce, such as Tokyo, or where the number of automated delivery robots is large. Base Loop is a looped system that comprehensively covers the city, allowing you to think of the queue as one big counter to receive orders, so it can respond efficiently to demand. Furthermore, Base Loop is on a loop and is designed to be driven automatically by an automated courier robot on it, making it easy to operate.

One of the above advantages, the effectiveness of efficiently responding to demand, is demonstrated by quantitatively determining the average customer waiting time in Base Loop and Fixed Base Model using virtual circular city and Yokohama city road mesh data. Fixed Base Model assumes that the bases of the automatic delivery robots are fixed, and the automated delivery robot remains at the base if no orders are generated from the stores within the area covered by the automated delivery robot. Figure 3 shows how the automatic delivery robot moves in Fixed Base Model.

Table1. Similarities and differences between Base Loop and conventional delivery services

	Domino's Pizza	Uber Eats	Base Loop
Variable base of delivery workers	×	○	○
Cooperation between delivery workers	○	×	○

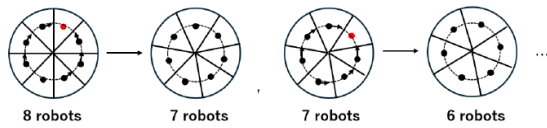


Figure 2. How the robot moves in Base Loop

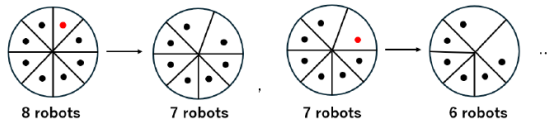


Figure 3. How the robot moves in Fixed Base Model



Figure 4. Image of Base Loop

3. NUMERICAL EXAMINATION

This study evaluates the total average customer waiting time for multiple orders in Base Loop and Fixed Base Model using virtual circular city and Yokohama city road mesh data. We assumed that retailers and customers are uniformly distributed in a virtual circular city with a radius of 10. The polar coordinates of retailers and customers are:

$$(t\cos\theta, t\sin\theta), 0 \leq t \leq 10, 0 \leq \theta \leq 2\pi$$

t denotes the linear distance from the center of the virtual circular city. θ is the angle measured counterclockwise from the line segment consisting of the center of the virtual circular city and a point on the circumference. The initial positions of automatic delivery robots in Base Loop and Fixed Base Model are assumed to be located at equally spaced positions on a circumference of radius r , where $0 \leq t \leq 10$. Then, the order coverage from a retailer with robot n is S in Base Loop is calculated as follows.

$$\bar{d}(n) = \int_0^{10} \int_{-\frac{\pi}{n}}^{\frac{\pi}{n}} d \, d\theta dt \quad (2)$$

$$d = \frac{t}{S} \sqrt{(r - t\cos\theta)^2 + (0 - t\sin\theta)^2} \quad (3)$$

The average distance from nearest robot to coverage, $\bar{d}(n)$, is

$$S = \frac{\pi 10^2}{n} \quad (1)$$

The average customer waiting time for k th order with n robots is t_k . t_k is the sum of the average distance from nearest robot to coverage and the average linear distances between two points (retailer and customer) in the virtual city [3].

$$t_k = \bar{d}(n - k + 1) + \frac{1280}{45\pi} \quad (4)$$

The total average customer waiting time in Base Loop for n consecutive orders with n robots is \bar{t} .

$$\bar{t} = \sum_{k=1}^n t_k \quad (5)$$

The r^* that minimizes \bar{t} and \bar{t} at that r^* in Base Loop were obtained by mathematical optimization. The r^* that minimizes the total average customer waiting time and the total average customer waiting time at that r^* in Fixed Base Model were calculated by the following simulation. The first step is to randomly generate one retailer point in a virtual

circular city. The second step is to calculate the linear distance from the generated retailer to the nearest automated delivery robot base. The third step is to delete the automatic delivery robot base selected in the second step and return to the first step. The first to third steps are repeated n times for the number of robots as 1 simulation. 100 simulations are performed for each r from 1 to 10 divided into 100 equal parts, and the r^* that minimizes the total average customer waiting time and the total average customer waiting time at that r^* in Fixed Base Model is obtained. Table 2 shows the r^* and The total average customer waiting time in Base Loop and Fixed Base Model with n varied from 10, 20, ..., 100.

Table2. r^* and the total average customer waiting time in Base Loop and Fixed Base Model

n	Base Loop		Fixed Base Model	
	r^*	\bar{t}	r^*	\bar{t}
10	5.93	128.21	5.36	130.97
20	6.46	241.21	5.73	252.24
30	6.65	352.56	6.18	370.53
40	6.74	463.36	6.73	485.99
50	6.81	573.91	6.73	603.70
60	6.85	684.32	6.55	717.29
70	6.88	794.64	7.36	832.44
80	6.90	904.91	7.55	948.27
90	6.92	1015.14	6.00	1058.24
100	6.93	1125.34	7.09	1174.10

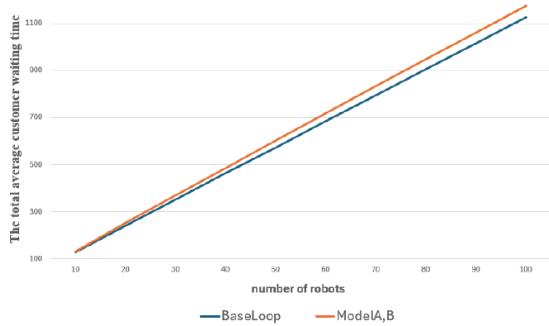


Figure 5. The total average waiting time by number of robots

Then we considered Base Loop with Yokohama city road mesh data. The Yokohama city road mesh data is generated by generating points on a grid in the city of Yokohama and moving from each point onto the nearest road (Figure 6). We assume that the blue dots shown in Figure 6 are retailers and customers. Let p denote the number of retailers and customers. We assume Base Loop for n robots be a regular n -angle, the center of the n -angle be (Cn_x, Cn_y) , the distance from the center to the base be r , and the angle from the base of the robot with the smallest angle from the x -axis counterclockwise from the x -axis be 1, 2, ..., n and the angle from the x -axis to base 1 is A (Figure 7). Let S_1, S_2, \dots, S_n be the range covered by robot base 1, 2, ..., n at n robots. The range covered

by robot base 1, 2, ..., n at n robots is determined by a Voronoi diagram with the base of the automatic delivery robot as the mother point. Let d_1, d_2, \dots, d_n be the total distance from robot base 1, 2, ..., n to the retailers in S_1, S_2, \dots, S_n . The total average distance of d_1, d_2, \dots, d_n is \bar{d}_n .

$$\bar{d}_n = \frac{\sum_{k=1}^n d_k}{p} \quad (6)$$

Assuming 10 robots and 8 consecutive orders, the total average customer waiting time is \bar{t}

$$\bar{t} = \sum_{n=3}^{10} \bar{d}_n + 11.3 \times 8 \quad (7)$$

11.3 in (7) equation is the average linear distance between the customer and the retailer. We obtained that r^* is 7.77, the optimal center is $(-17.10, -23.94)$. The \bar{t} with 10 robots and 8 consecutive orders in Fixed Base Model were calculated by the following simulation. The first step is to randomly select one retailer from the Yokohama city road mesh data. The second and third step is same as the second step in the virtual circular city. The first to third steps are repeated 8 times as 1 simulation. 1000 simulations are performed for the total average customer waiting time in Fixed Base Model is obtained. In this case, the initial position of the base of the automatic delivery robot, indicated by red crosses, is the position solved by the minsum problem (Figure 8). The total average customer waiting time in Base Loop and Fixed Base Model is shown in Table 3.

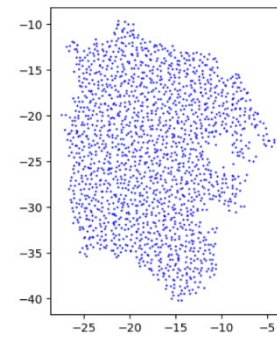


Figure 6. Yokohama city road mesh data

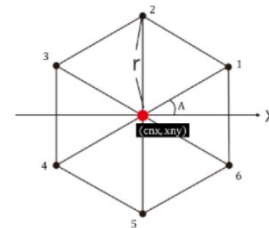


Figure 7. Shape of Base Loop

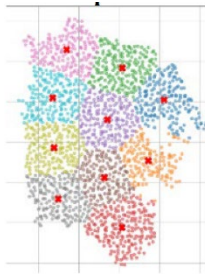


Figure 8. The initial position of the base

Table 3. The total average customer waiting time in Base Loop and Fixed Base Model

	Base Loop	Fixed Base Model
\bar{t}	146.13	149.14

4. CONCLUSIONS

In this study, we were able to quantify the effectiveness of “Base Loop” was demonstrated by comparing the total average customer waiting time for n consecutive orders with n robots in a virtual circular city and for 8 consecutive orders with 10 robots in Yokohama city road mesh data, compared to Fixed Base Model. About the total average customer waiting time for n consecutive orders with n robots in a virtual circular city, as the number of robots n increases, the difference in total average customer waiting time in Base Loop and Fixed Base Model increases. It indicates that Base Loop is more dominant with the larger number of robots. In the future, we would like to test the effectiveness of Base Loop in different shapes, such as hypotrochoid, instead of circular.

REFERENCES

- [1] Impress Watch, UberEats Robot Delivery Starts March 6 in Nihonbashi, <https://www.watch.impress.co.jp/docs/news/1573976.html>, 2024-3-5 Impress Watch, 2024-11-10.
- [2] Circana, Food Service and Restaurant Survey Report, https://www.npdjapan.com/press-releases/pr_20231218/, Circana Japan, 2024-11-10.
- [3] Osamu Kurita, The Urban Model Reader, First ed., Kyoritu Shuppan, Tokyo, 2004.

ESTIMATION OF GROUND DEFORMATION IN SUZU CITY WITH ALOS-2/PALSAR-2 DATA

YIFAN YANG^{1*}, HIDEOMI GOKON¹ AND WATARU TAKEUCHI²

¹*Division of Advanced Science and Technology, Japan Advanced Institute of Science and Technology,
Nomi, Japan*

²*Institute of Industrial Science, The University of Tokyo, Tokyo, Japan*

*Correspondence: s2320010@jaist.ac.jp

Keywords: Ground deformation, DInSAR, ALOS-2, Sentinel-2, Displacement

1. INTRODUCTION

In recent years, geological disasters such as earthquakes and landslides have become more frequent, posing challenges to ground stability. Synthetic Aperture Radar (SAR), with its all-weather capability and independence from lightning and cloud cover, enables wide-area, high-resolution monitoring [1].

Interferometric Synthetic Aperture Radar (InSAR) technology uses two SAR images to extract surface deformation information; in practice, InSAR technology is susceptible to terrain errors, resulting in less accurate results. However, Differential Interferometric Synthetic Aperture Radar (D-InSAR) can reduce the effect of topographic errors by removing topographic phase and analyzing the deformation phase between two images [2].

This study focuses on Suzu City, Japan, using D-InSAR technology and utilizing C-band data and L-band data to analyze post-earthquake surface deformation to compare their performance differences and characteristics of SAR data in monitoring ground displacement.

2. MATERIALS

Suzu City, located in the northern part of Japan's Noto Peninsula, was one of the city's most severely affected by the M_j 7.6 earthquake on January 1, 2024, which caused significant surface deformation in the area. SAR analysis was performed using C-band Sentinel-1 data and L-band ALOS-2 data, both from descending orbit.



Figure 1. Suzu City

3. METHODOLOGY

3.1 Data preprocessing:

The C-band and L-band data were pre-processed, including radiometric calibration, geometric correction, and multi-looking processing.

3.2 Interferogram generation:

Generated by co-registering SAR images from different periods.

3.3 Topographic phase removal:

The topographic phase ϕ_{topo} was removed using differential interferometry to extract the phase ϕ_{disp} caused by ground deformation only can be calculated as:

$$\phi_{diff} = \phi_{int1} - \phi_{int2}$$

where ϕ_{int1} and ϕ_{int2} are the interferometric phases of different periods are.

4. RESULTS

4.1. Interferogram Results:

The results show that the changes in Sentinel-1 are more pronounced.

4.2. Unwrapped Interferogram:

These two results are quite different, but the overall trend is consistent with decreasing values from top to bottom.

4.3. Displacement Map:

The Sentinel-1 data results range from 0.1 to -0.5, while the ALOS-2 data results range from 0.6 to -12. The differences are large, but the distribution pattern is similar, i.e. the displacement value decreases from top to bottom.

5. DISCUSSION

The differences in results are mainly attributed to the inherent characteristics of the sensors and their interaction with the ground. The L-band, with its longer wavelength (approximately 23.6cm), has a strong ability to penetrate vegetation and soil. In contrast, the C-band, with a shorter wavelength (approximately 5.6cm), is more susceptible to interference from vegetation. Additionally, differences in observation geometry and incidence angles affect the sensitivity to displacements in the

line-of-sight direction, and varying data acquisition time intervals.

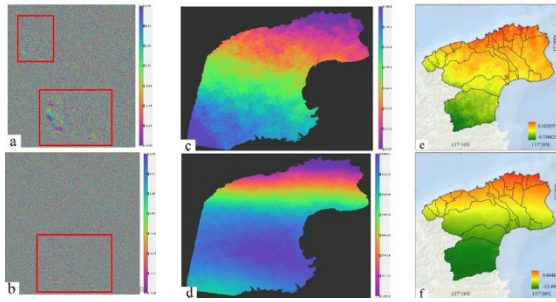


Figure 2. Results map

- a. Phase interferogram of Sentinel;
- b. Phase interferogram of ALOS-2;
- c. Unwrapped Interferogram of Sentinel-1;
- d. Unwrapped Interferogram of ALOS-2;
- e. Displacement Map of Sentienl-1;
- f. Displacement Map of ALOS-2

REFERENCES

- [1] Jiang H, Balz T, Cigna F, Tapete D, Li J, Han Y, Geo-spat. Inf. Sci. 27(5) (2024) 1424–40.
- [2] Samsonov SV, Blais-Stevens A, Remote Sens. Environ. 305 (2024) 114049.

ANALYSIS OF THE MEASUREMENT OF POPULATION FLOW BASED ON NON-CONTACT SENSING DEVICES IN PHITSANULOK PROVINCE, THAILAND

H. KAWAKAMI¹, M. FUJII^{2*}, Y. MORISAKI², Y. KON³ and JARUWAN DAENGBUPPHA⁴

¹*School of Geosciences and Civil Engineering, Kanazawa University, Kanazawa, Japan*

²*Faculty of Transdisciplinary Sciences for Innovation, Kanazawa University, Kanazawa, Japan*

³*Frontier Institute of Tourism Science, Kanazawa University, Kanazawa City, Japan*

⁴*Center of Excellence for Tourism Management Research, Naresuan University, Phitsanulok Province*

*Correspondence: fujii@se.kanazawa-u.ac.jp

Key Words: Thailand, Phitsanulok, Non-contact sensing device, Behaviour, Disaster, Evacuation

1. INTRODUCTION

One method of measuring population flow is based on non-contact sensing devices, which are small microcontroller modules. By inputting a specific program into the device, it captures the MAC addresses of smartphones owned by people passing within a 10-20 meter radius of the installed point. In this way, it is possible to get a record of the person's passage.

The purpose of this study is to clarify the population flow in the central area of Phitsanulok Province by using the data of non-contact sensing devices.

2. ANALYSIS OVERVIEW

This study measured population flows by installing non-contact sensing devices at ten locations in the central area of Phitsanulok Province on September 17, 19, and 20, 2024. Figure 1 illustrates the locations and names of these ten sites, which include stations, temples, markets, and other venues frequently visited by the public. In instances where a location was large, multiple non-contact sensing devices were installed to capture a greater number of MAC addresses.

Using the data collected from these non-contact sensing devices, origin-destination (OD) tables were created for each day of measurement. Table 2 presents the OD table for September 20, represented as a colour map, where darker colours indicate increments of 25 individuals. The analysis revealed significant movement between three key locations: Wat Phra Si Rattana Mahathat, Thani Market, and Topland Hotel. Specifically, the number of individuals traveling from Wat Phra Si Rattana Mahathat to Thani Market and Topland Hotel was recorded at 125 and 122, respectively. Conversely, movements from Topland Hotel to Thani Market and Wat Phra Si Rattana Mahathat were 167 and 121. Additionally, the number of people moving from Thani Market to Wat Phra Si Rattana Mahathat and Topland Hotel was 140 and 155.

A comparison of the OD tables across the three measurement days was conducted to identify patterns of significant movement. The results indicated notable behaviours among the three locations on September 17 and 19, as well as on September 20.

3. CONCLUSIONS

This study measured population flow in the central area of Phitsanulok Province using data from non-contact sensing devices. The findings revealed significant movement between the following locations: Wat Phra Si Rattana Mahathat and Topland Hotel, Thani Market and Wat Phra Si Rattana Mahathat, and Topland Hotel and Thani Market, in comparison to other locations.

Furthermore, the measurement of population flow via non-contact sensing devices can be applied in disaster situations. This approach enables the estimation of the exposed population at each location, facilitating assessments of congestion during evacuation scenarios.

Future work should focus on identifying potential congestion points by calculating the number of residents and the average duration of stay at each location. Additionally, increasing the number of installation sites will enhance the ability to measure population flow in greater detail.

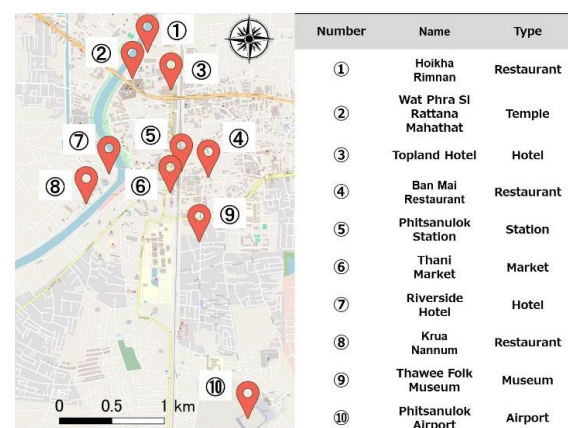


Figure 1. Locations and names of the ten places

Table 2. OD table for September 20, 2024

Origin \ Destination	Hoika	Wat Phra ...	Topland	Ban Mai	Station	Thani	Riverside	Nannum	Thawee	Airport
Holkha Rimnan		78	68	13	39	82	2	3	9	30
Wat Phra Si RattanaMahathat	70		122	30	76	125	5	8	21	64
Topland Hotel	59	121		23	69	167	10	5	37	76
Ban Mai Restaurant	15	26	27		19	42	3	3	6	20
Phitsanulok Station	27	43	55	15		65	3	0	14	42
Thani Market	73	140	155	27	114		10	4	48	84
Riverside Hotel	6	7	7	0	7	7		1	4	12
Krua Nannum	1	3	5	1	0	3	1		2	3
Thawee Folk Museum	12	19	33	6	13	44	3	7		13
Phitsanulok Airport	29	76	107	21	61	114	20	2	30	

STUDY ON AN EARLY WARNING SYSTEM FOR DISASTER MITIGATION USING GROUND-BASED SAR

Y. IZUMI^{1*} and M. SATO²

¹Graduate School of Engineering, Muroran Institute of Technology, Muroran, Japan,

²Tohoku University, Sendai, Japan,

Correspondence: yizumi@muroran-it.ac.jp

Keywords: Synthetic Aperture Radar (SAR), Ground-Based SAR, Disaster monitoring, Landslide

1. INTRODUCTION

Currently, climate change has heightened the threat of various natural disasters, including intense rainfall, super typhoons, and large-scale volcanic eruptions. These events can trigger slope-related hazards such as landslides, posing serious risks to vulnerable communities. Effectively addressing these slope disaster risks and building a resilient, adaptive society has become an urgent global challenge. A key part of this effort involves developing practical and highly accurate early warning systems.

In typical early warning systems, instruments like extensometers and Global Navigation Satellite System (GNSS) devices are installed directly at-risk sites to obtain displacement data during sliding. However, installing these instruments in areas prone to collapse carries significant safety risk. To overcome this, we present an early warning system utilizing synthetic aperture radar (SAR) technology for measuring ground surface displacement. Specifically, we introduce ground-based SAR (GB-SAR), which enables the estimation of target displacement with high temporal sampling, providing near real-time capability. This presentation will cover the latest developments in GB-SAR technique and monitoring campaigns in Japan.

2. REAL TIME MONITORING SCHEME

GB-SAR, with its advantages of high-precision displacement estimation (sub-millimeter accuracy), rapid data acquisition, all-weather capability, and long-range monitoring, shows significant potential as a tool for geo-disaster monitoring. Leveraging these capabilities, we have applied this sensor to landslide-prone areas and post-landslide slopes for early warning purposes. Figure 1 shows the GB-SAR system in operation in Japan. This system uses frequency-modulated continuous wave (FMCW) radar, operating at a Ku-band centre frequency of 17.2 GHz with a 300 MHz bandwidth. It can capture SAR images of the target every 10 seconds, allowing for the displacement map to be updated at the same interval. The maximum monitoring range is 4 km.

Figure 2 illustrates the general monitoring scheme used in our laboratory's continuous monitoring setup. The raw data collected by the GB-SAR in the field is processed into SAR images on a PC connected to the radar. These images are then transferred to a PC at the laboratory for further analysis. Using interferometric SAR (InSAR), a series of SAR images is processed to generate a time-series displacement map. InSAR analysis includes compensations to mitigate phase changes caused by atmospheric refractivity fluctuations.

The continuous observation results provide near real-time data on displacement across the observed natural slope. An early warning is issued if total displacement exceeds a pre-defined threshold or displays abnormal patterns.



Figure 1. GB-SAR operated in Japan

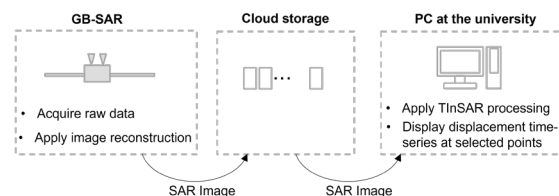


Figure 2. GB-SAR continuous monitoring scheme

3. CONCLUSIONS

GB-SAR has demonstrated its capability for monitoring land displacement with sub-millimeter accuracy. Although a few GB-SAR campaigns have successfully monitored landslides, technical and practical challenges remain in this field. If near-real-time GB-SAR data becomes more widely available, it could enable the prediction of collapse timing through machine learning. Expanding the number of

case studies and addressing existing challenges will be essential for further advancements.

REFERENCES

- [1] K. Takahashi, M. Matsumoto, and M. Sato, IEEE J. Sel. Topics Appl. Earth Observ. 6 (2013) 1286–1294.

EFFECT OF MIXING WITH STEEL SLAG ON MODIFICATION OF SIMULATED UNDER-SIEVE RESIDUE

H. HU¹ and Y. KIKUCHI²

¹Ph.D. student, Department of Civil Engineering, the University of Tokyo, Tokyo, Japan

²Counselor, Coastal Development Institute of Technology, Tokyo, Japan

Keywords: Steel slag, Under-sieve residue, Wood fiber

1. INTRODUCTION

Japan is prone to disasters caused by typhoons, torrential rains, heavy snowfalls, floods, landslides, earthquakes, tsunamis, and volcanic eruptions due to its location, topography, geology, weather, and other natural conditions. Katsumi et al. reported that, during the Great Hanshin-Awaji Earthquake, low recycling rates due to poor sorting and various environmental problems at temporary storage sites became apparent[1]. Therefore, in the Tohoku Region Pacific Ocean Offshore Earthquake that occurred on March 11, 2011, lessons and experiences from the Great Hanshin-Awaji Earthquake were used to summarize early efforts to recycle and reuse disaster waste after the earthquake, and improvements were made in various aspects. The recycling rate of the approximately 30 million tons of disaster and tsunami waste generated was 93%, more than twice as high as the 38% rate of the Great Hanshin-Awaji Earthquake [2]. However, this 13% of the disaster waste that was not recycled is called under-sieved residue, which is sediments contains a large amount of wood chips that passed through a 20 to 40 mm sieve during the sorting process. This has placed pressure on the processing capabilities of incineration facilities. In recent years, large amounts of disaster waste are expected to be generated in large-scale disasters such as Typhoon No. 19, the Kumamoto Rainstorm, the Nankai Trough Earthquake, and earthquakes directly under the Tokyo metropolitan area, making it an urgent issue to propose effective utilization methods for the under-sieve residue.

According to the Ministry of the Environment [3], the amount of disaster waste generated by a Great Nankai Trough Earthquake or a Tokyo Metropolitan Area Directly Beneath Earthquake, both of which are expected, will be significantly larger than that generated by the Great East Japan Earthquake. Therefore, there is a need to utilize the under-sieve residue.

Approximately 14 billion kg of converter steelmaking slag (hereinafter referred to as steelmaking slag) is generated annually as an industrial by-product during the production of crude steel. Steelmaking slag has properties that make it suitable as a geomaterial, such as high particle

density and exceptional abrasion resistance. Of note is its excellent hydraulic solidification, which enables it to react effectively with water [4]. It is currently widely used as a road base material and in other applications. However, the recent reduction in public works spending has posed a challenge to market expansion.

The authors are conducting research into the utilization of under-sieve residue as a high quality geomaterial by solidifying it through hydraulic solidification of steelmaking slag. According to previous studies, Yoshikawa [5] has shown that the strength of steelmaking slag increases with time, while it has been found that certain steelmaking slags do not exhibit a solidification reaction even when compacted. To promote and facilitate the hydraulic solidification reaction of steelmaking slag, the addition of binders is necessary. Based on previous studies comparing different types of subsidiary materials, blast furnace slag fine powder (BFSFP) was used in this study.

In addition, Yoshikawa [6] found that the mixture of wood chips and steel slag (hereafter referred to as the combination of steelmaking slag and BFSFP) exhibited different mechanical properties, which were influenced by the specific types of wood chips, the mixing ratios and the curing time.

However, the actual under-sieved residue consists of separated soil particles less than 20 mm in size, obtained using vibrating and rotating sieves. In this study, wood chips and sandy soil were utilised to simulate the under-sieve residue. Unconfined compaction tests were performed (according to the provisions of JIS A 1216 (JSA, 2009)). The effects of the presence, type of soil and the ratio of steel slag to simulated under-screen residue on the unconfined compressive properties were investigated.

2. MATERIALS AND TEST METHODS

Five types of materials were used in this study: steelmaking slag without aging treatment ($\rho_s = 3.40 \text{ Mg/m}^3$, hereafter steelmaking slag), BFSFP4000 ($\rho_s = 2.89 \text{ Mg/m}^3$), inland sand ($\rho_s = 2.61 \text{ Mg/m}^3$, $D_{max} = 2\text{mm}$, $F_c = 4.9\%$), mixed silica sand ($\rho_s = 2.63 \text{ Mg/m}^3$, was sieved with mesh sizes of 2mm, 0.85mm, 0.425mm, 0.25mm, 0.106mm, and 0.075mm to achieve a particle size distribution

similar to that of inland sand by utilizing 4th, 6th, 8th-grade silica sand), coconut fiber ($\rho_s = 0.53 \text{ Mg/m}^3$, average diameter $\Phi=0.27 \text{ mm}$, average length $h= 24.4 \text{ mm}$). Ion exchange water was used as pore water. Furthermore, hereafter, the mixture of steelmaking slag and BFSFP in a mass ratio of 96:4 will be referred to as steel slag.

Figure 1 shows the grain size distribution curve of the steelmaking slag and sandy soil used for this test. The target compaction density and the water content ratio of the mixed material were determined by compaction tests of the mixed material. Figure 2 shows images of each sample.

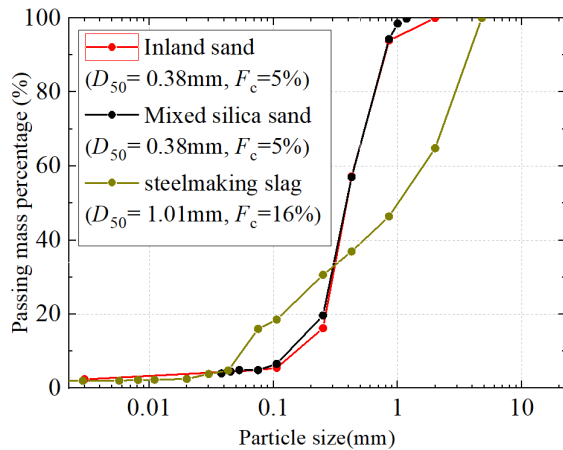


Figure 1. Grain size distribution curve of materials



Figure 2. Sample images (Steelmaking slag, BFSFP, Inland sand, Mixed silica sand, Coconut fiber)

The specimen was prepared by mixing naturally dried sandy soil (inland sand or mixed silica sand), steelmaking slag, and coconut fiber. Ion-exchanged water was then added, and finally, BFSFP was mixed into the mixture. The amount of ion-exchange water was adjusted to achieve a water content ratio just before over-compaction would occur when all the materials were mixed. The sample was placed into a hollow cylindrical mold with a diameter of 50 mm and a height of 100 mm to prepare the test specimens. Each specimen was sealed and then cured at a constant temperature of 20 °C for either 7 or 28 days. Table 1 and Table 2 present the specimen preparation conditions employed for the test sample preparation. The specimens were prepared to simulate under-sieve residues containing wood chips at a volumetric ratio of 20%. The volumetric ratio of steel slag to simulated under-sieve residues was set at three different patterns, 3:1, 1:1, and 1:3. And each pattern was further divided based on the presence or absence of sandy soil or coconut fiber.

Table 1. Specimen preparation conditions (using inland sand)

Steel slag: Under-sieve residue (By volume)	Steel slag: Inland sand: Coconut fiber (By volume)	Target dry density ρ_d (Mg/m ³)	Water content ratio w (%)
1:3	29:71:0	1.77	12.8
	25:60:15	1.48	15.6
	85:0:15	1.58	15.5
1:1	56:44:0	1.91	14.6
	50:40:10	1.65	15.6
	90:0:10	1.77	17.0
3:1	79:21:0	1.90	13.6
	75:20:5	1.85	15.6
	95:0:5	1.93	14.6

Table 2. Specimen preparation conditions (using mixed silica sand).

Steel slag: Under-sieve residue (By volume)	Steel slag: Mixed silica sand: Coconut fiber (By volume)	Target dry density ρ_d (Mg/m ³)	Water Content ratio w (%)
1:3	29:71:0	1.9	12.6
	25:60:15	1.47	15.4
	85:0:15	1.58	15.5
1:1	56:44:0	1.98	13.2
	50:40:10	1.74	15.4
	90:0:10	1.77	17.0
3:1	79:21:0	1.99	13.0
	75:20:5	1.90	14.7
	95:0:5	1.93	14.6

As indicated in Table 1, the reason for setting the volumetric ratio as 29:71 (equivalent to 75:20 assuming a total volume of 95) in cases where coconut fiber was not included was to align with the same volumetric ratio as the cases involving coconut fiber. The unconfined compression (UC) tests were conducted on the specimens by the prescribed curing durations. During the tests, each specimen was compressed at an axial strain rate of 1% per minute.

3. RESULTS AND DISCUSSIONS

Figure 4 shows the relationship between axial stress σ and axial strain ϵ_a from UC tests conducted on mixtures with or without inland sand in three different patterns. The UC tests were carried out on three specimens for each condition. The results showed minimal variation within each condition and no significant differences were observed. Therefore, a stress-strain relationship is presented for each condition. The variation in line thickness represents the variation in inland sand content. The red curves are the mixtures with inland sand and the black curves are without sand. For comparison, the slag alone is also shown as a gray dotted curve.

Figure 4 also shows that when inland sand is included, the UC strength is higher compared to the condition without sand. At the same time, the initial stiffness of the mix is also higher, suggesting that the effect of sand on the initial stiffness is effective. On the other hand, when comparing the conditions without sand, as the coconut fiber content increases, both the UC strength and the initial stiffness decrease, while the failure strain increases.

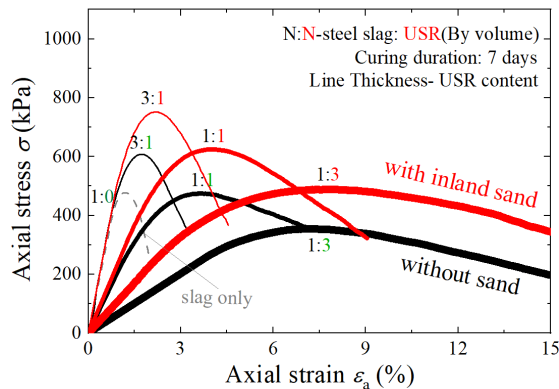


Figure 4. $\sigma - \epsilon_a$ curves through UC tests involving mixtures with or without inland sand (7 days)

Figure 5 shows the relationship between the normalized UC strength $q_u/q_{u, \text{slagonly}}$, $E_{50}/E_{50, \text{slagonly}}$ and the inland sand content. This helped explain the rate of change in q_u and E_{50} due to sand content. q_u was normalized by q_u of steel slag. The ratio $q_u/q_{u, \text{slagonly}}$ was obtained by dividing the UC strength q_u by the UC strength of steel slag in each tested condition.

E_{50} (MPa) was calculated as

$$E_{50} = (q_{u/2}) / \epsilon_{50} \quad (1)$$

As shown in Figure 5, the increase in the UC strength q_u decreases with an increase in the content of inland sand or simulated under-sieve residue. Likewise, the deformation modulus E_{50} also decreases with increasing content of simulated under-sieve residue.

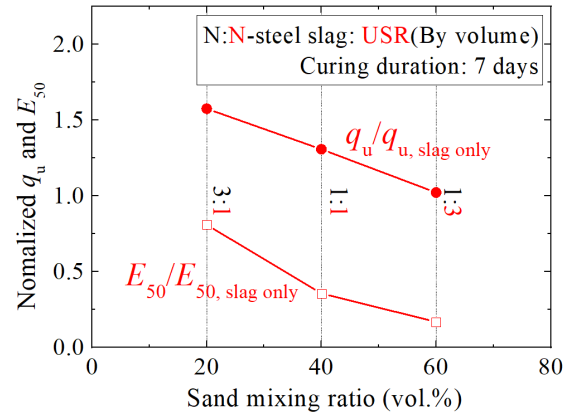


Figure 5. Relationship between $q_u/q_{u, \text{slagonly}}$, $E_{50}/E_{50, \text{slagonly}}$ only and the inland sand content (7 days)

Figure 6 shows the relationship between axial stress σ and axial strain ϵ_a from UC tests carried out on mixtures with or without inland sand in three different patterns. The variation in line thickness represents the varying inland sand content. The blue curves are the mixtures with mixed silica sand and the black curves are without sand. From Figure 6, the mixed silica sand gave the same results as the inland sand. It can be observed that when mixed silica sand is included, the UC strength is higher compared to the condition without sand.

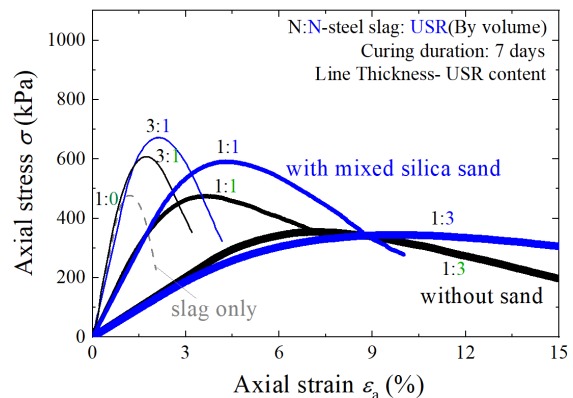


Figure 6. $\sigma - \epsilon_a$ curves through UC tests involving mixtures with or without mixed silica sand (7 days)

As previously discussed, Figure 7 shows the relationship between the normalized UC strength

$q_u/q_{u, \text{slagonly}}$, $E_{50}/E_{50, \text{slagonly}}$ and mixed silica sand content. The increase in UC strength q_u decreases as the content of mixed silica sand or simulated under-sieve residue increases. Similarly, the deformation modulus E_{50} also decreases as the content of simulated under-sieve residue increases.

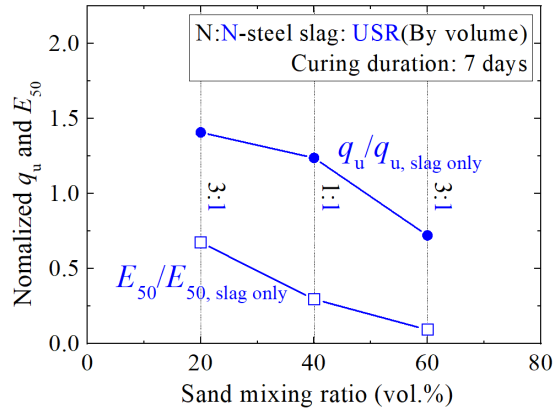


Figure 7. Relationship between $q_u/q_{u, \text{slagonly}}$, $E_{50}/E_{50, \text{slagonly}}$ and the mixed silica sand content (7 days)

After summarizing the data from the different mixtures, Figure 8 shows the UC strength at different mixing ratios of steel slag and simulated under-sieve residue. In both cases of using inland sand or mixed silica sand, the increase in the content of simulated under-sieve residue eventually leads to a decrease in the UC strength. Furthermore, both types of sand show a similar decreasing trend, and it can be observed that the UC strength of mixed silica sand is generally lower than that of inland sand in all samples. But when compared to the strength of steel slag alone, the strength of the mixtures initially increases and then gradually decreases with an increase in the content of simulated under-sieve residue.

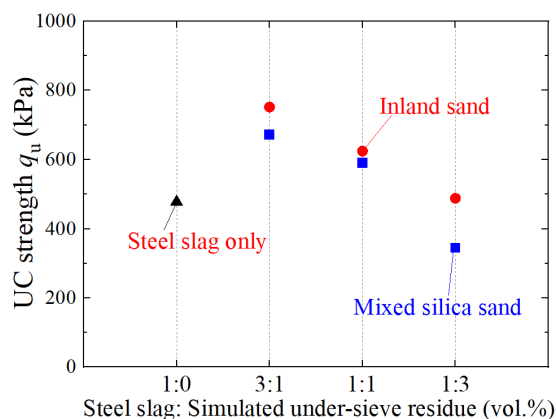


Figure 8. The UC strength in different mixing ratios of steel slag and simulated under-sieve residue (7 days)

To summarize the above results, the addition of fibrous wood chips to steel slag can reduce stiffness

and increase failure strain. Moreover, the addition of sandy soil can provide a similar level of failure strain and further increase the stiffness and strength. In other words, the addition of a suitable amount of simulated under-sieve residue can increase the UC strength of the mixture by solidifying it with steel slag.

4. CONCLUSIONS

This study considered the effects of different types and proportions of sandy soil on the properties of UC in the case of mixtures containing steel slag, sandy soil and coconut fiber. The main results are as follows:

- 1) By adding sandy soil to the mixture of steel slag and coconut fiber, it is possible to achieve higher unconfined compressive strength and initial stiffness.
- 2) Even with the same particle size distribution, the unconfined compressive strength of inland sand is higher than that of mixed silica sand.
- 3) The addition of a suitable amount of simulated under-sieved residue can increase the unconfined compressive properties of the mixture.

This study focuses on conditions with a curing period of 7 days. However, it is important to compare these results with those from longer curing periods, such as 28 and 84 days, to evaluate the hydraulic solidification of steel slag more comprehensively.

REFERENCES

- [1] T. Katsumi, K. Endo, T. Inui, Generation and Management of Disaster Waste due to the Great Hanshin-Awaji Earthquake, Annuals, Disas. Prev. Res. Inst., Kyoto Univ. 39 (1996) 37-50.
- [2] K. Ide, Treatment of disaster waste generated by the Great East Japan Earthquake, Japanese Geotechnical Society Special Publication (2016) 135-142.
- [3] M.O.E. (Ministry of the Environment, Government of Japan), Movement Over the Disaster Waste Management (2020).
- [4] T. Morishita, S. Wada, T. Kaneko, T. Kashiwabara and R. Hara, Relationship between strength and chemical property of pavement material using steelmaking slag, IDRE Journal, 296 (2015) 33-39.
- [5] T. Yoshikawa, Y. Kikuchi, T. Hyodo, the Effect of Aging Treatment on the Mechanical Properties of Steelmaking Slag Mixed with Crushed Slag, Proceedings of the 7th China-Japan Geotechnical Symposium: New Advances in Geotechnical Engineering, China Communications Press (2018) 410-415.

- [6] T. Yoshikawa, Y. Kikuchi, S. Noda, Y. Kakihara and A. Oshino, Compression Strength of Wood Chips Mixed with Steelmaking Slag, *Environmental Geotechnics* (2021)1-10.
- [7] T. Yoshikawa, Y. Kikuchi, T. Hyodo, Y. Kuroiwa, and T. Tanaka, Geomechanical Properties as Geomaterial of Wood Chips Mixed with Steelmaking Slag, *Proceedings of the 12th JGS Symposium on Environmental Geotechnics* (2017) 199-204.

ANALYSIS OF SATISFACTION EVALUATION OF FOREIGNER TO JAPAN AT RESTAURANTS IN REGIONAL SIGHTSEEING CITIES: STUDY OF THE USING REVIEWS DATA FROM TRAVEL INFORMATION WEBSITE

Y. BABA¹, M. FUJII^{2*} and Y. MORISAKI³

¹Graduate students, Division of Geosciences and Civil Engineering, Kanazawa University, Kanazawa, Japan,

²Associate Professor, Institute of Transdisciplinary Sciences, Kanazawa University, Kanazawa, Japan,

³Assistant Professor, Institute of Transdisciplinary Sciences, Kanazawa University, Kanazawa, Japan,

*Correspondence: fujii@se.kanazawa-u.ac.jp

Keywords: Inbound, Restaurant, Reviews, Text-mining, Satisfaction factor

1. INTRODUCTION

The number of foreign visitors to Japan is increasing and continues to reach the highest record from October 2023 to September 2024 [1]. Furthermore, the foreign visitors spend five times more money on their travel than Japanese tourists. Especially, foreign visitors spend more money on "food" than on anything else in Japan [2].

Because of these trends, the "food" consumption behaviours of foreign visitors has become important in Japan's inbound tourism policy. To increase the amount of money which foreign visitors spend on food, it is necessary to understand the factors which contribute to satisfaction with food. On the other hand, due to the spread of the Internet, they began to post their experiences of restaurants as reviews in real time, which is valuable data for the tourism industry.

The purpose of this study is to clarify the satisfaction factors that foreign visitors to Japan have toward restaurants by analyzing review data. Furthermore, differences and strengths in satisfaction factors of each region by comparing the restaurant satisfaction factors by region. In this analysis, eight regional sightseeing cities which have not only high tourism potential, but also significant growth opportunities in the future were selected.

2. METHODOLOGY

In this study, TripAdvisor, one of the largest travel information sites in the world [3], was utilized to collect reviews of restaurants from foreign visitors to Japan. From these reviews, only the reviews with 5-points rating, which are the highest level of rating index, are extracted and divided into sentence units. To adjust for bias in the amount of data by region, down-sampling is conducted on the reviews. Through these processes, 3,736 sentences were extracted.

Consequently, BERT-Topic, a topic modeling technique, was employed to identify satisfaction factors in regional tourist cities based on reviews. By inputting the sentences into the topic model,

sentences set with similar content are clustered. In addition, the frequent words in the clusters are output. The frequent words in the cluster are used to interpret the topics of the cluster. In this analysis, 14 clusters and frequent words in each cluster were extracted by using a combination of BERT-Topic and k-means method, which is another clustering method.

The clusters are interpreted based on frequently occurring words. Then authors selected documents included in the clusters that could be satisfaction factors for the restaurant.

Documents are cross tabulated by region and cluster to understand the differences in satisfaction factors and strengths of each region. Moreover, the percentages are calculated. The higher percentages, the stronger the contribution to satisfaction in each region. The result is shown in Figure 1.

area	Sendai	Hakodate	Beppu	Hiroshima	Nikko	Kanazawa	Nagasaki	Nagano
Satisfied factor								
food quality n = 195	8.2	13.3	11.3	10.3	13.8	12.8	12.3	17.9
sushi · sashimi n = 101	5.0	22.8	19.8	5.9	3.0	26.7	11.9	5.0
food variation n = 243	16.9	14.9	11.5	13.6	11.1	11.5	9.9	11.5
customer service n = 142	14.1	15.5	11.3	13.4	12.0	10.6	11.3	12.0
atmosphere n = 267	8.6	11.2	13.1	17.2	10.1	12.4	11.2	16.1
Drinks n = 110	14.5	9.1	10.0	17.3	15.5	11.8	10.9	10.9
price and cost performance n = 159	9.4	11.3	12.6	12.6	16.4	11.3	11.9	14.5
multilingual support n = 620	11.3	12.4	12.3	13.9	11.6	13.1	12.7	12.7
Quality of service n = 50	18.0	14.0	12.0	12.0	8.0	14.0	16.0	6.0

Figure 1. Cross-tabulation by satisfaction factor and region

3. RESULT ANALYSIS

As illustrated in Figure 1, the analysis reveals that Nagano ranks highest for "food quality," Kanazawa excels in "sashimi and sushi," Sendai leads in "food variety" and "quality of service," Hakodate is noted for "customer service," Hiroshima stands out for "atmosphere" and "drinks," and Nikko is recognized for "price and cost performance." Additionally, there are minimal regional differences in "multilingual support."

4. CONCLUSION

In conclusion, this study identified restaurant satisfaction factors as perceived by foreign visitors to Japan through reviews on travel information websites using a topic model. A regional comparison highlighted differences in satisfaction factors among various sightseeing cities. However, some interpretations remain broad in scope. To achieve a more nuanced understanding, further scrutiny of the documents within each cluster is essential.

REFERENCE

- [1] Japan National Tourism Organization, Number of foreign visitors, September 2024 Estimated
- [2] Japan Tourism Agency, Survey of Inbound Consumption Trends, Apr-Jun 2024
- [3] TripAdvisor, <https://www.tripadvisor.jp/>

AUTOMATION OF REBAR SEGMENTATION IN GPR USING BINARY IMAGES FOCUSING ON DIAGONAL CONVEXITY AND DOWNWARD OPENING SEARCH CLUSTERING ALGORITHM

S. IWAI and T. MIZUTANI*

Institute of Industrial Science, The University of Tokyo, Tokyo, Japan

*Correspondence: mizu-t@iis.u-tokyo.ac.jp

Keywords: Smartphone-equipped handheld GPR, Concrete, Rebar segmentation, Binary Image, Down word search

1. INTRODUCTION

Infrastructure inspections are supported by local government staff and the local construction industry. Despite Japan currently facing a shortage of engineers, the number of infrastructures requiring repair by local governments has not decreased.

The focus is on handheld GPR devices that emit and measure electromagnetic waves in the range of 0.7 GHz to 3.5 GHz while in motion, allowing for the acquisition of explicit depth information (Figure 1). Currently, these devices only display received images on a smartphone, requiring inspectors to visually assess internal information. This study aims to develop algorithms and software for extracting internal rebar responses and accurately segmenting each one.

Rebar in concrete appears as hyperbolic reflections in GPR images. Many researchers in previous studies have attempted to address this issue through image detection using Convolutional Neural Networks (CNN) [1]. However, to bring CNN-based image detection to practical use and create an algorithm that can adapt to all measurement conditions, a vast amount of data collection is required. Furthermore, even though the hyperbola is a fixed pattern, using CNN for such a task is inefficient.



Figure 1. Smartphone-equipped handheld GPR used in this study

2. METHODOLOGY

GPR with strong side lobes in its transmitted waves results in interference with negative values, preventing the downward opening from appearing in

the thresholder image. Therefore, we further developed the segmentation algorithm by improving the binary processing.

The proposed method is divided into two main steps: 1. Creation of a binary image that accurately captures the downward opening, and 2. Hyperbola clustering algorithm. First, hysteresis thresholding is used to create the binary image to more accurately extract signals derived from hyperbolas. Additionally, by calculating the second derivative diagonally and focusing on the convex parts, the tail of the hyperbola is extracted (Figure 2(b)).

The clustering algorithm was further generalized based on prior research [2] to adapt it to various interference conditions (Figure 2(c)). Ultimately, accurate segmentation of the rebar responses from the hyperbolas was achieved, along with the identification of the center lines (Figure 2(d)).

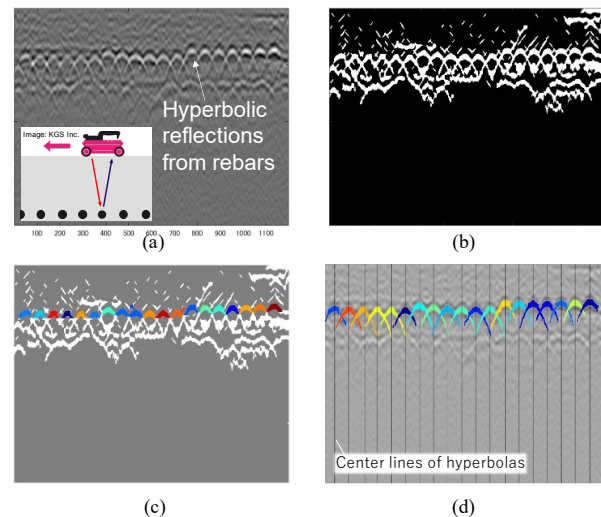


Figure 2. Automated rebar segmentation by proposed method

3. CONCLUSIONS

By leveraging the characteristics of rebar, hyperbola segmentation was achieved without the use of Deep Learning, which typically requires vast amounts of data to adapt to all conditions.

Additionally, unclear rebar responses were detected, a challenge even for Deep Learning methods.

This technology will serve as the foundation for the automation of all future GPR interpretations, including the estimation of individual rebar cover thickness and the identification of damage.

REFERENCES

- [1] H. Liu, C. Lin, Jie Cui, L. Fan, X. Xie, B. F. Spencer, Detection and localization of rebar in concrete by deep learning using ground penetrating radar, *Automation in Construction*, vol. 118, 2020, 103279.
- [2] X. Zhou, H. Chen and J. Li, An Automatic GPR B-Scan Image Interpreting Model, *IEEE Transactions on Geoscience and Remote Sensing*, vol. 56, no. 6, pp. 3398-3412, June 2018.

ESTIMATING PAVEMENT CONDITION USING PUBLICLY AVAILABLE SATELLITE IMAGERY FOR DATA-DRIVEN ROAD MAINTENANCE PLANNING

TAKUMA Ooba^{1*}, ANGELA ODERA², AZAM AMIR³, AND MICHAEL HENRY³

¹Department of Civil Engineering, Shibaura Institute of Technology, Tokyo, Japan

²Graduate School of Engineering and Science, Shibaura Institute of Technology, Tokyo, Japan

³College of Engineering, Shibaura Institute of Technology, Tokyo, Japan

*Correspondence: ah21017@shibaura-it.ac.jp

Keywords: Pavement condition, Data-driven road maintenance, Satellite imagery, Sentinel-2

1. INTRODUCTION

Road infrastructure plays a critical role globally with substantial investments. However, roads deteriorate over time due to aging and various factors, necessitating effective maintenance strategies. A key challenge in data-driven maintenance planning is the absence of pavement condition data, which may result from a variety of factors, including human error, machine error, or inadequate and incomplete data collection. This research explores the potential of using publicly available satellite imagery to estimate the Pavement Condition Index (PCI), one of the most used metrics for assessing pavement condition. The analysis aimed to determine whether a statistical correlation exists between PCI data and RGB values, which represent the intensity of red, green, and blue colours in satellite imagery. Variations in RGB values can reflect differences in surface materials, textures, and degradation levels, with darker tones often indicating new pavement overlay, while lighter shades may suggest older pavement surfaces.

2. METHODOLOGY

The PCI data, including specific coordinate locations and inspection dates, used in this study was obtained from the Kenya Roads Board Road Inventory and Condition Survey repository and consisted of 3,348 data points on the Kenyan road network. The imagery data utilized Sentinel-2 satellite imagery, which provides 13 spectral bands at a resolution of 10 to 60 meters. For each coordinate, 13 spectral bands were retrieved with filters applied for cloud cover and date, and raw values were used without additional processing. All analyses were conducted using Google Earth Engine (GEE). Specific RGB bands were extracted for analysis, as these visible light bands may correlate with PCI, which is derived from distress factors observable to human eye. This selection assumed that changes in visible band values might reflect surface condition. A correlation analysis between PCI and RGB values was then performed for entire data to assess whether any relationship exists. Furthermore, time-series data for one coordinate

point were also analyzed to examine changes in RGB values around road paving events.

3. RESULTS AND DISCUSSIONS

Figure 1 shows no significant correlation between RGB values and PCI values obtained from road inspection data. This lack of strong correlation (Pearson's $r=0.28$) suggests that surface-level satellite imagery alone may not capture nuanced changes in road condition, such as those detected by detailed on-ground assessments. These findings emphasize the complexity of road condition estimation through satellite data and point to the limitations of using only RGB values in such analyses. Similarly, Figure 2 shows a time-series analysis conducted for a single point to test the hypothesis that RGB values would change alongside the deterioration of road pavement.

However, no significant changes were observed over an eight-year period, likely due to larger variations caused by factors unrelated to road deterioration, which may have obscured any potential effects of pavement condition itself. Although RGB values are readily accessible, they may lack the sensitivity needed to accurately reflect pavement degradation, emphasizing the need for more robust data sources or advanced image processing techniques.

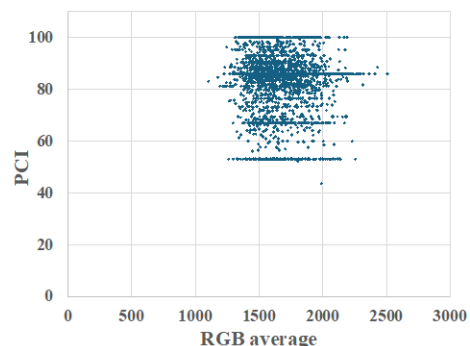


Figure 1. Correlation between RGB and PCI for all points

4. CONCLUSION

Given the importance of pavement condition data for data-driven maintenance and the need for

alternative assessment methods, this study aimed to evaluate pavement condition using publicly available Sentinel-2 satellite imagery. However, no significant correlation was found between PCI and the satellite band values. Further exploration of alternative methodologies within image processing, such as higher-resolution images or specialized classification methods, may offer viable solutions for road condition assessment.

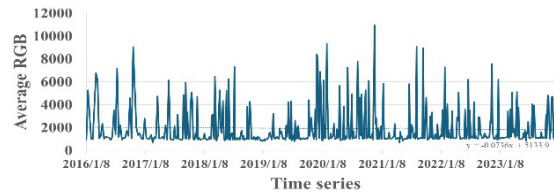


Figure 2. Time variation of RGB at one point

POTENTIAL ASSESSMENT OF VERTICAL SOLAR PV SYSTEMS FOR POWER PRODUCTION AND THERMAL PERFORMANCE IN TROPICAL BUILDING ENVELOPES

A.L. MARQUEZ^{1*}, J.A. PRINCIPE² and J.J.L. SERANILLA³

¹National Graduate School of Engineering, University of the Philippines Diliman, Quezon City, Philippines

²Department of Geodetic Engineering, University of the Philippines Diliman, Quezon City, Philippines

³Institute of Civil Engineering, University of the Philippines Diliman, Quezon City, Philippines

*Correspondence: almarquez2@up.edu.ph

Keywords: Vertical solar PV systems, GIS, Tropical buildings, Clean energy, Thermal comfort

1. INTRODUCTION

In tropical regions with warm and humid climates, balancing thermal comfort and energy efficiency is a challenge due to high cooling demands. Over the years, strategies to reduce energy use and integrate renewable energy (RE) into building design have been developed [1]. These efforts align with the United Nations' Sustainable Development Goals (SDGs), particularly SDG 7 (universal access to sustainable energy) and SDG 13 (shift to clean energy). Solar photovoltaic (PV) technology offers a practical solution, particularly in energy-intensive urban areas. Installing solar PV panels on building envelopes presents a valuable approach to maximize local energy generation and reduce heat gains. While roofs receive significant solar radiation, the space is limited by infrastructure. Vertical walls, however, offer greater installation area as buildings increase in height, while also mitigate the effects of dust deposition on solar panels.

2. METHODOLOGY

This study assessed the potential of vertical solar PV systems and their thermal performance on selected buildings at the University of the Philippines Diliman, Quezon City, Philippines. The analysis was limited to 5:00 AM to 7:00 PM on the first day of each month in 2021.

An open-source geographic information system (GIS), QGIS, was used to process spatial data. Using this data along with elevation information from LiDAR-based normalized Digital Surface Model (nDSM), a Python script was developed to produce a 3D hyper point cloud model of the building (Figure 1). A ray tracing algorithm utilizing the PySolar module was then used to model solar irradiance by casting rays from the Sun's position and mapping solar affected areas on the building envelope [2].

With the most recent publicly available local meteorological and global radiation data, alongside standard specifications for PV modules distributed in the Philippines, three scenarios were considered to evaluate PV power output: Case A

(east-facing walls), Case B (west-facing walls), and Case C (combined east- and west-facing walls). Each scenario included three subcases: (1) all surfaces facing the specified directions, (2) primary walls, and (3) designated PV installation areas.

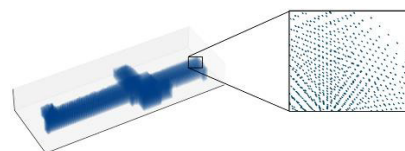


Figure 1. 3D Hyper Point Cloud Building Model

With the most recent publicly available local meteorological and global radiation data, alongside standard specifications for PV modules distributed in the Philippines, three scenarios were considered to evaluate PV power output: Case A (east-facing walls), Case B (west-facing walls), and Case C (combined east- and west-facing walls). Each scenario included three subcases: (1) all surfaces facing the specified directions, (2) primary walls, and (3) designated PV installation areas.

3. RESULTS

The area of interest, located at 14° 39' 23.38" N and 121° 4' 10.49" E, received solar irradiance levels reaching up to 1036.61 W/m². East-facing walls received the highest irradiance in the morning (60.28% at 8:00 AM), while west-facing walls received the most in the afternoon (58.98% at 4:00 PM). The average thermal load reduction, PV potential, and PV share (energy supply from solar PV) were calculated across all scenarios and subcases, as summarized in Table 1.

4. CONCLUSIONS

Vertical solar PV systems offer a promising option for RE applications in tropical urban environments. When installed on building envelopes, these systems reduce solar heat gain through shading, improving thermal comfort and, in turn, enhancing energy efficiency.

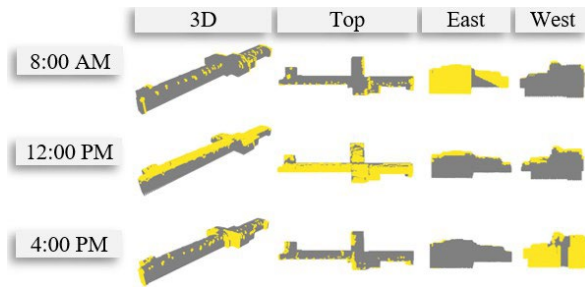


Figure 2. Building model with solar irradiance

Table 1. Thermal Load Reduction and PV Contribution

Case	Thermal Load Reduction (%)	PV Potential (kWh/day)	PV Share (%)
A	5.93 – 31.32	120.17 – 497.72	5.60 – 92.76
B	3.07 – 35.79	53.96 – 586.65	2.57 – 112.3
C	9.03 – 67.16	181.89 – 1069.0	8.57 – 413.4

REFERENCES

- [1] Chwieduk, D., Solar Energy in Buildings: Thermal Balance for Efficient Heating and Cooling, Elsevier Science, 2014.
- [2] M.L.R. Lagahit, A.C. Blanco, The International Archives of the Photogrammetry, Remote Sensing and Spatial Information Sciences, XLII-4/W19 (2019) 263–270.

ECONOMIC IMPACT ANALYSIS CONSIDERING RECONSTRUCTION FOR ASSISTANCE DURING LARGE-SCALE EARTHQUAKE DISASTER FOCUSED ON CRUISE SHIPS PASSENGERS CALLING AT KANAZAWA PORT

K. NAKABAYASHI¹, M. FUJII^{2*}, Y. MORISAKI² and Y. YAMAYA¹

¹*Division of Environmental Design, Kanazawa University, Kanazawa, Japan*

²*Associate Professor, Institute of Transdisciplinary Sciences Kanazawa University, Kanazawa, Japan*

*Correspondence: fujii@se.kanazawa-u.ac.jp

Keywords: Cruise ship, Earthquake, Hazard, Sightseeing, Questionnaire survey, Economic impact

1. INTRODUCTION

The 2024 Noto Peninsula Earthquake caused extensive damage to buildings and infrastructure, particularly in the Noto area, and had a significant negative impact on economic activities throughout Ishikawa Prefecture. Notably, while Kanazawa City experienced relatively little structural damage during the earthquake, there was a substantial decline in tourist numbers compared to previous years.

On the other hand, the number of cruise ships calling at Kanazawa Port has been on schedule since March, and cruise ship passengers have contributed to the recovery of tourism in Kanazawa. In particular, the number of passengers on large cruise ships is extremely large, approximately 4,000, and it is expected to have a large economic impact on the port of call. Also, support measures have been established in Ishikawa Prefecture from the intangible aspect, such as the sale of many products to support the reconstruction of the Noto area suffered from extensive damage. Therefore, it is considered that there are some tourists who visit Kanazawa City and spend money on tourism to support the reconstruction of the area.

This study involved conducting questionnaire surveys targeting cruise ship passengers visiting Kanazawa Port to assess their spending on sightseeing in the area. Additionally, the study evaluated the percentage of passengers who increased their expenditures due to an awareness of reconstruction assistance during their visits. The primary aim is to quantitatively assess the impact of tourists' consumption behaviours on the reconstruction of disaster-affected areas by calculating the economic effects of the reconstruction assistance provided.

2. ECONOMIC IMPACT OF RECONSTRUCTION ASSISTANCE

In this study, a questionnaire survey was conducted on 231 samples of passengers. Figure 1 shows that 93 cruise ship passengers (About 51.1%) increased their spending due to their awareness of

reconstruction assistance. The average amount spent was JPY 14,032.5 (USD 92.14). On the other hand, 89 cruise ship passengers (About 48.9%) were not aware of supporting the reconstruction, and their average spending was JPY 9,269 (USD 60.86).

Figure 2 presents the results of the economic impact of reconstruction support on consumers. In this study, the economic impact under normal conditions was calculated using the average spending of JPY 9,269 by passengers who were unaware of the reconstruction assistance, along with data from 5,568 passengers. Conversely, the economic impact for consumers aware of the reconstruction assistance was determined using an average expenditure of JPY 14,032.5 from the same number of passengers.

According to Figure 2, the economic impact during normal times amounts to JPY 95,543,000, derived from the average spending of JPY 9,269 by passengers without awareness of the reconstruction assistance. In contrast, an economic impact of JPY 14,482,000 was calculated based on the average consumption of JPY 14,032.5 from passengers aware of the assistance. This indicates that the difference of JPY 49,099,000 represents the additional economic impact attributable to the reconstruction assistance.

3. CONCLUSIONS

In this study, the economic impact of the reconstruction assistance was quantitatively evaluated. It is necessary to continue the research to investigate the effects on the reconstruction of the affected areas from the intangible aspects in more detail.

	People	Average consumption	Standard deviation
Yes	93人(51.1%)	JPY14032.5 (USD92.14)	JPY14869.0
No	89人(48.9%)	JPY9269.0 (USD60.86)	JPY11533.4

Figure1. Percentage of consumers supporting reconstruction

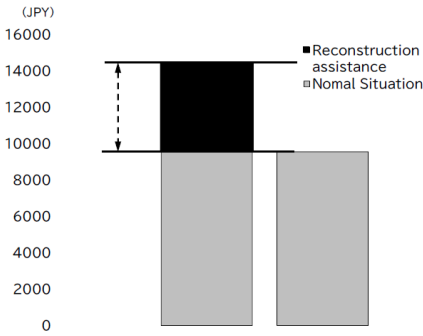


Figure 2. Economic impact

EFFECTIVE USE OF TUNNEL FACE OBSERVATION RECORDS DURING TUNNEL CONSTRUCTION FOR RENEWAL OF ABANDONED TUNNEL

Ami SHIRAI, TOMOHISA KOSEGAWA and SHINJI KONISHI*

ASANO TAISEIKISO ENGINEERING Co., Ltd, Osaka, Japan

*Correspondence: konishi-s@atk-eng.jp

Keyword: Tunnel reconstruction design, Face observation records, 3D ground model

1. OUTLINE

Increased traffic has raised concerns about safety in tunnels. For this reason, the re-use of existing disused tunnels that have been taken out of service is being planned in all over Japan. In the case of the tunnel that is the subject of this paper, plans are underway to renovate an adjacent existing tunnel that is currently not in use and increase lanes to four lanes in total with the tunnel in service in order to alleviate traffic congestion and improve safety. However, when utilizing old tunnels, some problems arise, such as the data needed for reconstruction design being outdated or non-existent. For the tunnels covered in this paper, it is also planned to renovate an adjacent existing tunnel, which is currently not in use, and convert it to four lanes in total with the tunnel in service to reduce traffic congestion and improve safety. However, in utilizing such old tunnels, problems have arisen in that the data required for the reconstruction design is outdated or does not exist.

For this reason, face observation records from the construction of the operating tunnel were made effective use. The records usually had been abandoned after construction work. Specifically, the geology and rock mass classification of the tunnel section were compiled based on previous geological surveys of the tunnel in service and tunnel face observation records during the construction of the tunnel in service.

From the created three-dimensional ground model, a geological longitudinal section of the second line location was created for the reconstruction design, and a new support pattern was set. The Autodesk's Civil 3D and GEORAMA for Civil 3D were used to create the 3D ground model. This paper describes a case in which the 3D ground model was created using face observation records from the construction of a tunnel (Phase I) that is currently in service (hereafter referred to as Phase I tunnel), and this model was then used in the reconstruction design of the adjacent old tunnel that has since been abandoned due to deterioration, to be utilized as Phase II (hereafter referred to as Phase II tunnel).

2. GEOLOGICAL OVERVIEW

The geographical feature around the subject tunnel is a narrow ridge that runs from north-northwest to south-southeast, and the tunnel runs through this ridge in a west-southwest to east-northeast direction. The ridge is 300-400m above sea level, and both slopes of the ridge are relatively steep with an average inclination of 35-45°, becoming gentler as it gets closer to the foot of the mountain.

The bedrock is composed of Sangun metamorphic rocks, which are thought to have been formed by metamorphism in the Carboniferous Period of the Paleozoic Era to the Triassic Period of the Mesozoic Era, and granites, which are thought to have intruded into the Sangun metamorphic rocks in the Cretaceous Period of the Mesozoic Era. The Sangun metamorphic rocks have been partially metamorphosed into hornfels by contact metamorphism due to contact with the granites. The Sangun metamorphic rocks are distributed on the west side of the ridge, and the granites are distributed on the east side, and the boundary between them is complex and intricate.

3. EFFECTIVE USE OF 3D GROUND MODEL

3.1 Correction of profile (Phase I) using tunnel face observation

The existing geological longitudinal section of the Phase I tunnel is an assumed cross-section of the strata created before the construction of based on the results of geological surveys such as boring, and there are some parts that differ from the geology confirmed at the time of construction. This existing geological longitudinal section of the Phase I tunnel was revised based on the face observation records, which are geological information confirmed during the construction of the tunnel section of the Phase I tunnel. Since the evaluation categories of geology and ground classification did not match between the existing geological longitudinal section created before construction and the face observation records during tunnel construction, we first examined the comparison of the geological and ground classification between the existing geological longitudinal section of the Phase I tunnel and the

face observation records during the construction of the Phase I tunnel. Geological strata distribution and support pattern of the Phase I tunnel profile were revised, and the support pattern of the Phase II tunnel profile was decided.

3.2 Setting of strata boundaries

Since the purpose of this study was to design the reconstruction project to utilize the abandoned road tunnel that will become the Phase II tunnel, it was particularly important to accurately represent the geological distribution in the tunnel area. Therefore, the face photographs were arranged three-dimensionally in the tunnel section of the Phase I tunnel, and the strata boundaries were set using the strata boundaries on the face photographs. Outside the tunnel area, the strata boundaries were set with reference to previous geological plans and topography. Outside the tunnel area, the strata boundaries were set based on previous geological maps and topography. Figure 1 shows an example of strata boundaries set on a face photograph.

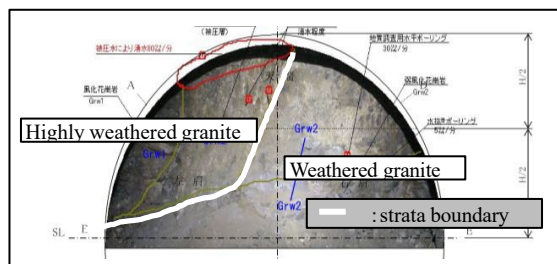


Figure 1. Strata boundary set in face observation record

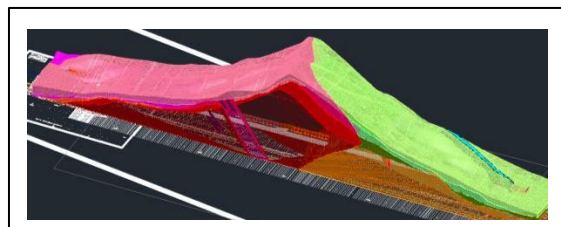


Figure 2. Solid model

Figure 3 shows profile (phase II tunnel) created from 3D ground model. The support pattern of the Phase II tunnel was set using the profile (phase II tunnel).

4. CONCLUSION

By interpreting the face observation records from the construction of the currently used tunnel (Phase I) geologically and using them to create a 3D ground model, we were able to consider the reconstruction design and support pattern for utilizing the adjacent abandoned tunnel as the Phase II tunnel without conducting additional large-scale surveys. Although information such as collapses and

spring water has been passed on as construction data for the Phase I tunnel, there are few cases where this information has been used for the construction of the Phase II tunnel. One of the reasons for this is that there was no established means or method for interpreting the face data geologically and extending it to the Phase II tunnel.

In large-scale underground rock excavation, efforts have been made to estimate the three-dimensional distribution of cracks and perform grouting, but with the development of DX (Digital Transformation) technology, it is thought that it will be possible to accurately build models with little effort even for linear structures such as tunnels. Not only geology but also spring water information can be incorporated into the model.

In dams, the use of 3D models helps to prevent errors in the evaluation of the continuity of geology and fracture distribution.

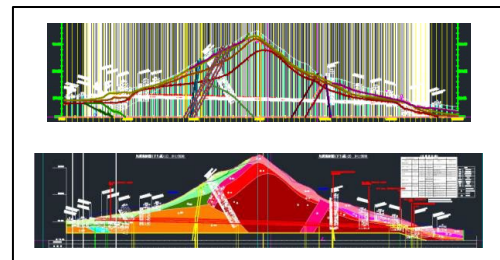


Figure 3. Profile (phase II) created from 3D ground model

5. AT THE END

Thus, reinforcing and renewing abandoned tunnels for effective utilization is an initiative that should be recommended in terms of environmental issues such as CO₂ reduction and consumption of construction materials, compared to new tunnel construction. In addition, the design of the renewal of the abandoned tunnels without large-scale additional investigations by making effective use of the face observation records from the construction of the tunnels, which had been discarded and not used after the completion of tunnel construction, was also considered to have contributed to environmental issues. This effort is considered to have established a method to develop the observation records of tunnel face into a new tunnel design in the vicinity. In the future, we would like to increase the number of case studies.

ANALYSIS OF WHAT SHOULD BE DONE AFTER A DISASTER AND THE CURRENT SITUATION IN JAPAN WHERE THIS IS DIFFICULT TO DO

TETSURO ITO

The University of Tokyo, Tokyo, Japan

Keywords: Disaster, Analysis, Verification, Extraction of lessons, Passing on experience

1. INTRODUCTION

After a disaster or other emergency has occurred and crisis management has been implemented to deal with it, what should be done after the situation is under control is to prepare for a new crisis in case a similar situation occurs again. And for this purpose, it is important to analyze and verify the state of preparedness for the emergency that has occurred and whether the crisis management response to the situation was sufficient, and to extract lessons for reflection and to prepare for the next crisis.

However, in Japan, although recovery and reconstruction activities are carried out after a crisis has occurred, there is little analysis, verification and extraction of lessons for reflection on whether these crisis preparations and the response to the crisis were sufficient, if there was anything what was lacking, and what should be done to prepare for new disasters in the future.

This is a remarkable trend compared to other countries, but this report will analyze what should be done and why this is not being done and extract the problems.

2. CURRENT DISASTER PREPAREDNESS IN JAPAN AND WHAT SHOULD BE DONE AFTER A DISASTER

In Japan, disasters such as earthquakes and floods occur every year and cause a lot of damage. The government and local authorities have spent many years preparing for possible disasters and are working on disaster preparedness measures, such as building infrastructure to make disasters less likely to occur, preparing countermeasures to be taken in the event of a disaster, securing personnel and conducting drills involving the local population.

However, disasters always come in different forms and in different places. Therefore, disaster preparedness needs to consider all possibilities. These preparations also need to be completed before the actual disaster occurs.

3. On the other hand, disasters occur suddenly and without warning. Once a disaster occurs, a large amount of personnel, equipment and materials must be deployed to save lives in a short period of time. Therefore, after a disaster questions must be asked about the nature of initial response activities, such as

whether personnel, materials and equipment were deployed to the necessary places at the necessary time, and whether disaster preparedness activities were sufficient in the first place.

After a certain period of time after a disaster, the emergency response activities for disaster relief will come to an end, and activities will begin to provide relief to victims and to restore damaged infrastructures and buildings. What is no less important than rehabilitation and reconstruction is the verification of whether the preparations taken for disasters have worked or were sufficient, and whether emergency operations during disasters have been carried out properly.

3. WHAT SHOULD BE DONE AFTER THE SITUATION IS UNDER CONTROL AND THE REASONS WHY THIS IS NOT DONE EASILY

3.1 Verification of what happened and what was done

- a. Recording is often overlooked during emergencies due to time constraints, making it essential to establish a dedicated recording team as part of the emergency response system in advance.
- b. Examination of the causes of the crisis and whether the response was good or not.
 - i. Why did the crisis occur?
 - ii. Were the measures the crisis was handled good?
 - iii. Why were response measures chosen from among the options?
 - iv. Were priorities good?

3.2 Reflection and learning of lessons Identification of problems in crisis response

Sincere reflection and preparation for the next crisis by learning lessons is important; however, these lessons are often not effectively reflected upon or applied in subsequent crises.

Reasons:

- a. The parties responded to the crisis by thinking they did their best under the circumstances at the time and did not reflect on their actions.
- b. The parties who responded to the crisis are no longer in the same post by the time the results

of the verification of the crisis response are available and are unlikely to reflect on the results of the verification.

- c. The past experiences of others are often not taken for another people as their own.

3.3 Passing on experience

Passing on past experiences to future generations and preparing for the next crisis is essential; however, effectively transferring this knowledge and experience is often challenging.

Reasons:

- a. Crisis management is an unusual task that can only be experienced once, so unlike normal work, it is not possible to learn through experience in the course of work.
- b. Crisis management requires efforts that differ from normal work - It is necessary to learn from past records, reflections and lessons learned, and to apply them to training through imagination.

3.4 Assumption of further crises and consideration of response measures

It is important not to repeat the same mistakes based on reflections and lessons learned from past crises.

- a. The importance of avoiding similar failures based on lessons learnt from past crises.
- b. The crisis will never be the same twice, but it is important to use imagination to envisage crises and build up response measures and training.
- c. The old lesson says that training is like warfare and warfare is like training is also valid in disaster response situations.

4. CONCLUSIONS

Every year in Japan, disasters occur in various parts of the country, and each time, local authorities respond to these disasters by protecting the victims and restoring the damaged infrastructure and facilities. The same mistakes and confusion can be seen every time.

One of the main reasons for this is that local authorities are not willing to learn from the experiences of other local authorities in the past and how they have responded to disasters.

There are several reasons why they do not learn from experience, including the fact that the records of each municipality's disaster response are not documented in a way that is useful to other municipalities, and that municipal officials are not willing to learn from other municipalities' experiences.

To reduce such situations in the future, disaster response records should be actively recorded in as much detail as possible in the event of a disaster,

including cases of failure, and disaster management officials should learn from the disaster response records of other municipalities and try to make them useful for their own municipal disaster response. Otherwise, the mistakes of other municipalities will often be repeated by other municipalities.

COMPREHENSIVE ASSESSMENT OF THE PERNOTE LANDSLIDE, RAMBAN DISTRICT, JAMMU & KASHMIR UNION TERRITORY (INDIA)

DEBI PRASANNA KANUNGO^{1*}, RAJESH KUMAR DASH¹ and
PRADEEP KUMAR RAMANCHARLA¹

¹CSIR-Central Building Research Institute, Roorkee – 247 667, Uttarakhand, India

*Correspondence: dpkanungo@cbri.res.in

Keywords: Landslide, Indian Himalaya, Risk assessment, Field observation

1. RESEARCH SUMMARY

Due to the changing climate and precipitation patterns in recent times, the Himalayan states of Indian territory is facing a variety of extreme disaster events. One such event occurred in the evening of April 25th, 2024, at approximately 5:00PM in the Ward No.3 (Nemnar) of Pernote- A Gram Panchayat of the Ramban district of Jammu and Kashmir, Union Territory.

The residents of Pernote noticed distress on the ground in the form of cracks and disturbances in the sub-soil of their houses. Through discussions with officials and the local affected community, it was informed that the disaster incident was visibly apparent in the evening of April 25th and continued until May 1st, 2024. As the landslide struck around 5.00pm, the first signs of impending disaster were cracks emerging on the floors and walls of local homes. Faced with the sudden realization of imminent danger, residents had no choice but to flee for their lives, leaving behind their property and possessions.

Prolonged antecedent rainfall in the area led to an increase in the pore water pressure and the active stress component, resulting in reduced shear parameters of slope-forming material. This led to the loose unconsolidated thick overburden material predominant with clay content lying on the slopes leading to failure in flow-like manner on the onset of unfavourable conditions like oversaturation due to antecedent rainfall and sub-surface natural springs, impounding pore pressure, lack of proper surface and sub-surface drainage network, etc. The area comprises of alternating layers of permeable sandstone and weak impermeable clay and silt.

Dominant clay is inherently weak and incompetent in nature and quickly swells due to the absorption and retention of water, which adds to the rise in piezometric pressure level on the free face of the slope leading to a mud flow type landslide on surpassing the threshold level. Other contributing factors included moderate average slope angle in the range of 30° - 40°, presence of sub-surface natural springs, inadequate surface and sub-surface drainage systems in the habitat area which make the area susceptible to such type of landslide.

It could be ascertained that with impounding pore pressure beyond threshold limit of the dominantly clayey overburden deposit, the landslide process started occurring gradually in the form of a slow-moving mud flow and continued for a few days. As informed, the ground cracks in different cultivated area and other terrace deposits occurred and subsequently get widened with passing of time.

This process has developed cracks in the building clusters scattered all around the affected slope and with time the buildings got completely damaged. As informed, some buildings got crumpled slowly with the landslide process and in some 3-storeyed buildings, 2 storeys got submerged in the mud with only the damaged top storey visible on the ground.

As observed, the landslide is still active with high risk without visible movement. The incident has totally damaged houses belonging to 28 families including one ashram building, agricultural fields and orchards. Critical infrastructures such as 1.2km section of the Ramban-Gool Road of the Border Roads Organisation, 0.3km section of the Pernote-Thalwa village link road, 400 KV transmission line, four transmission towers (three destroyed and one partially damaged), a power grid station, and water supply pipelines have suffered damages as well.

Houses of around 54 families in the near vicinity surrounding the landslide were assessed to be under risk by the District Administration; and hence were evacuated and shifted to temporary shelters such as the Panchayat Ghar and tents provided by the District Administration. The width of the landslide area is about 1.5 km and height from the northern side river towards the southern side crown line is approximately 3 km; therefore, the approximate coverage of the landslide affected area is 4.5km².

Based on the field observations and remote sensing image interpretation, the present paper discusses the causative factors for the landslide occurrence, future impending hazard and risk scenario and possible immediate and short-term disaster risk reduction measures.



Figure 1. Panoramic view of Pernote mud flow
(Ramban, J&K, India)



Figure 2. Damages to infrastructures due to the
landslide

ANALYSIS OF EVACUATION FACTORS FOR FAMILIES WITH INFANTS AND TODDLERS CONSIDERING PRIVACY IN EVACUATION SHELTERS: A STUDY ASSUMING A LARGE-SCALE EARTHQUAKE DISASTER

D. NAOI¹, Y. MORISAKI^{2*} and M. FUJII²

¹*Division of Geosciences and Civil Engineering, Kanazawa University, Kanazawa, Japan*

²*Faculty of Transdisciplinary Sciences for Innovation, Kanazawa University, Kanazawa, Japan*

*Correspondence: morisaki@staff.kanazawa-u.ac.jp

Keywords: Infants, Evacuation, Conjoint analysis

1. INTRODUCTION

Infants, the elderly, and people with disabilities are called vulnerable people. It is known that human damage caused by large earthquakes is greater for vulnerable people than for normal people. In fact, after the 2011 off the Pacific coast of Tohoku Earthquake and the 2016 Kumamoto Earthquake, there were many cases of delays in the supply of relief supplies within the affected areas. Among vulnerable people, infants and toddlers are physically frail and lack the ability to make decisions on their own. Therefore, infants and toddlers require the support of others. In addition, privacy issues for families with infants and toddlers include feeding the baby and worrying about their own child's crying. These issues are not found in families without infants and toddlers. Therefore, it is necessary to manage the evacuation shelter considering the privacy of families with infants and toddlers. To manage such evacuation shelters, it is important to examine the issues in privacy.

In this study, a questionnaire survey was conducted targeting parents of infants and toddlers attending kindergartens, nursery schools, and children's schools in Japan. The objective was to clarify the factors influencing the evacuation of families with infants and toddlers based on the questionnaire data. To investigate privacy factors related to evacuation, a conjoint card questionnaire was employed. Additionally, the influence of each privacy factor on the probability of evacuation was analyzed.

2. ANALYSIS RESULTS

In this analysis, a conditional logit model was used for choice-type conjoint analysis. Calculate the determined utility (V) when the seven explanatory variables (x) asked in the questionnaire are varied. The likelihood was then calculated from the coefficient of each explanatory variable. Using the calculated likelihoods, the coefficient (α) of each explanatory variable was calculated using the maximum likelihood estimation method (Equation 1).

The results are shown in Figure 1. The estimated coefficients for the presence or absence of security buzzer distribution are 1.4411 and for the presence or absence of laundry privacy considerations are 1.1813. These two factors were found to have particularly large effects.

$$V = \alpha_1 x_1 + \alpha_2 x_2 + \dots + \alpha_9 x_9 + \beta \quad (\text{Eq.1})$$

Based on the coefficients of each explanatory variable, the maximum and minimum evacuation probabilities were calculated. Based on the coefficients of each explanatory variable, the maximum and minimum evacuation probabilities were calculated. Figure 2 shows the maximum and minimum values of the evacuation probability depending on presence or absence of security buzzer distribution and privacy of laundry. The effect of each explanatory variable on the evacuation probability was clarified.

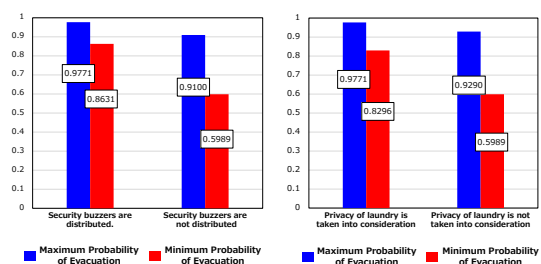


Figure 1. Estimated coefficients of each explanatory variable

3. CONCLUSIONS

In conclusion, this study utilized conjoint analysis to identify factors influencing the evacuation of families with infants and toddlers. The findings indicated that the distribution of security buzzers and the privacy of laundry facilities significantly affected evacuation decisions. The evacuation probability was calculated based on the coefficients of each explanatory variable, highlighting their respective influences. Future efforts will focus on enhancing the accuracy of the

analysis by increasing the sample size and re-evaluating the explanatory variables.

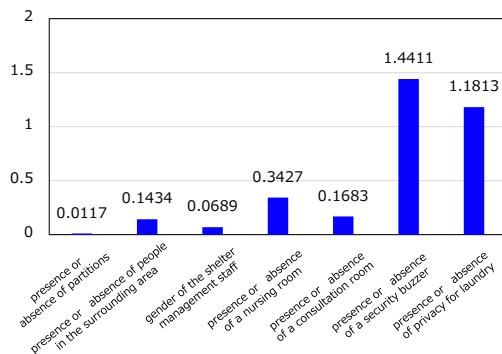


Figure 2. Evacuation probability according to presence or absence of security buzzer and privacy of laundry

GIS CHARACTERISATION FOR FOREST WEATHER INDEX (FWI) IN PEATLAND FOREST

NUREEN NATASYA MOHD SAUFI¹, ADUWATI SALI² and SHERIZA MOHD RAZALI^{1*}

¹*Institute of Tropical Forestry and Forest Products, Universiti Putra Malaysia, Serdang, Selangor*

²*Institute for Mathematical Research, Universiti Putra Malaysia, Serdang, Selangor*

**Correspondence: sheriza@upm.edu.my*

Keywords: Peatland monitoring, Fire Weather Index, GIS, Groundwater Level, Interpolation

1. INTRODUCTION

This study addresses the critical issue of fire risk in peatland ecosystems, with a specific focus on the Raja Musa Forest Reserve (RMFR) in Kuala Selangor. Peatlands are significant carbon sinks, yet they are highly susceptible to fire, which can release large amounts of carbon, exacerbating climate change. The primary objective of this study is to enhance fire monitoring and risk assessment within RMFR by integrating Groundwater Level (GWL) and Fire Weather Index (FWI) data into a Geographic Information System (GIS)-based framework. A review of pertinent literature shows that traditional methods for fire monitoring, such as manual surveys and satellite observations, often lack real-time capabilities and involve high costs, limiting their effectiveness in dynamic environments like peatlands. Previous studies highlight the utility of IoT (Internet of Things) systems combined with GIS to improve monitoring accuracy, yet few have applied GWL as a primary fire risk indicator in this context. This study aims to address these gaps by incorporating IoT-based GWL monitoring, which serves as a real-time indicator of fire risk in peatland ecosystems.

2. MATERIALS AND METHODS

The methodology involves three main stages: data collection, spatial interpolation, and integration of maps into the Peatland Monitoring System (PMS) dashboard for real-time monitoring.

2.1 Data Collection

GWL data were collected using sensor nodes deployed within RMFR. Each sensor node measured groundwater levels along with environmental parameters, transmitting the data via LoRaWAN technology to a cloud server. The collected data were exported in CSV format and processed for integration into QGIS.

2.2 GIS Layer Creation and Interpolation

Within QGIS, multiple layers were developed to represent the study area. Key layers include:

1. **Earth Surface Layer:** Visualized using OpenStreetMap (OSM) for an accurate representation of the terrain.
2. **Boundary Layer:** Created to define the study area's limits, encompassing the locations of sensor nodes.
3. **Sensor Node Layer:** This layer incorporated the geographic coordinates of each sensor node, allowing accurate localization within RMFR.
4. **Spatial Interpolation Layer:** IDW interpolation was applied to predict GWL values across unsampled areas, using known values from sensor nodes to estimate levels within the boundary. IDW assigns greater weight to points closer to the target, generating a continuous surface of predicted values.

2.3 Integration into PMS Dashboard

Once completed, the interpolated GWL map was exported as a GeoJSON file for web integration. The PMS dashboard, built with HTML and JavaScript, displayed these maps in real-time, allowing users to view updated fire risk levels. LULC data were also incorporated into the dashboard to provide a comprehensive view of the landscape, further aiding fire risk assessment.

3. RESULTS AND DISCUSSIONS

The GIS-based FWI mapping for the RMFR offers valuable insights into GWL and fire risk. Key GIS layers include the Earth Surface Layer, visualized using OSM for terrain data, highlighting features that may affect fire behavior, such as vegetation and roads. The Boundary Layer outlines the study area, focusing the analysis on regions with sensor nodes, while the Sensor Node Layer pinpoints borehole locations to provide essential GWL data. Using IDW interpolation, a Spatial Interpolation Layer was created to generate a continuous surface of predicted GWL values across unsampled locations. The IDW formula applied as below:

$$W_{BH} = \frac{1}{distance_{BH,predict}}$$

$$IDW_{predict} = \frac{W_{BH} \cdot GWL_{BH}}{W_{BH}}$$

where:

W_{BH} = Weight for each borehole

GWL_{BH} = Value of Ground water level at each borehole

$distance_{BH,predict}$ = Distance between predicted point and borehole

$IDW_{predict}$ = IDW prediction value

The final integrated map combines this interpolated GWL layer with a LULC map that classifies vegetation types and density to further assess fire susceptibility. This LULC map complements the GWL data by offering insights into how vegetation and land cover may influence fire spread within the peatland, with denser vegetation areas showing higher susceptibility.

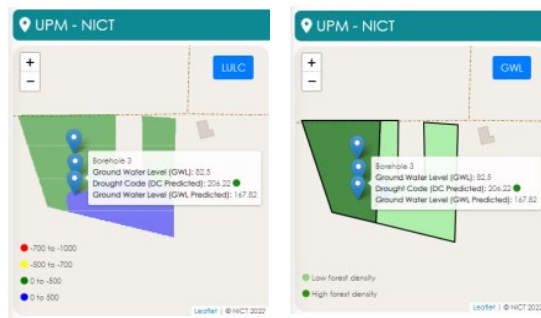


Figure 1. Map into the PMS Dashboard

These maps were then integrated into the PMS dashboard as in Figure 1. By exporting the layers from QGIS as GeoJSON files and incorporating them into the HTML-based dashboard, a dynamic, real-time visualization tool was created for monitoring fire risk. The PMS dashboard allows stakeholders to continuously assess environmental conditions, supporting proactive fire management by enabling timely intervention and informed conservation strategies.

4. CONCLUSIONS

The study demonstrates the effectiveness of GIS-based mapping and IDW interpolation for assessing fire risk in peatland ecosystems, specifically within the RMFR. Through the development of multiple layers in QGIS, this approach enables real-time monitoring of GWL and the identification of fire-prone areas where low GWL correlates with elevated fire risk. However, the accuracy of IDW interpolation is limited by the number and spatial distribution of sensor nodes, which may lead to

reduced prediction reliability in sparsely monitored areas.

Additionally, excluding factors such as soil moisture and vegetation type, which also impact fire risk, limits the model's precision. The integration of GIS and IoT in peatland monitoring offers practical implications for fire risk management, enabling proactive interventions and adaptable frameworks for conservation efforts globally. Future improvements include expanding the sensor network, incorporating more environmental variables into the model, and employing machine learning to enhance predictive accuracy and reliability in peatland fire risk monitoring.

REFERENCES

- [1] Gedefaw, A. A., Desta, M.A., & Mansberger, R. (2024). Impacts of integrated watershed management interventions on land use/land cover of Yesir watershed in northwestern Ethiopia. *Land*, 13(7), 918.
- [2] GISGeography. (n.d.). 30 Best GIS Software Applications [Rankings] - GIS Geography. Retrieved from <https://gisgeography.com/best-gis-software/>
- [3] Kamaruddin, S. A., Aziz, K.N.A., Roslani, A., Zainol, Z. E., Ahmad, A., Shaari, M. I., Nazri, R., & Tajam, J. (2022). The mapping of salinity level using the inverse distance weighted (IDW) interpolation method along the coastal area of Pulau Tuba, Langkawi. *Malaysian Journal of Sustainable Environment*, 9(1), 55–76.
- [4] Li, L., Sali, A., Liew, J.T., Saleh, N.L., Ahmad, S.M.S., Ali, A.M., Nuruddin, A.A., Aziz, N.A., Sitanggang, I. S., Syaufina, L., et al. (2022). Estimation of ground water level (GWL) for tropical peatland forest using machine learning. *IEEE Access*, 10, 126180–126187.

ANALYSIS OF CRUISE SHIP PASSENGERS' BEHAVIOR DURING EARTHQUAKE DISASTER: CASE STUDY OF KANAZAWA PORT

Y. YAMAYA¹, M. FUJIIU^{2*}, Y. MORISAKI² and K. NAKABAYASHI¹

¹Division of Geosciences and Civil Engineering, Kanazawa University, Kanazawa, Japan

²Associate Professor, Institute of Transdisciplinary Sciences, Kanazawa University, Kanazawa, Japan

*Correspondence: fujiiu@se.kanazawa-u.ac.jp

Keywords: Cruise ship, Earthquake, Disaster, Questionnaire survey

1. INTRODUCTION

Cruise ship passengers are characterized by their high average age and minimal luggage during sightseeing. As a result, they are particularly vulnerable to sudden earthquakes that may occur unexpectedly during their sightseeing activities. After the earthquake occurs, cruise ships may retreat to safer areas, potentially leaving passengers behind at tourist destinations. In such cases, passengers are advised to evacuate to nearby shelters [1].

In Kanazawa City, the study area, temporary accommodation may be provided for Cruise ship passengers who are unable to return home [2]. Some cruise ship passengers may attempt to return to the ship but could end up stranded near the port. To prepare for such situations, it is essential to examine the actions for cruise ship passengers during earthquake disaster.

In this study, questionnaire surveys were conducted to cruise ships passengers calling at Kanazawa Port. This survey consists of evacuation destinations after an earthquake, awareness of the cruise ship evacuation, and recognition of accommodation support. The purpose of this survey is to identify the characteristics of individuals who may attempt to return to the ship during an earthquake.

2. IDENTIFICATION OF INTENDED EVACUATION DESTINATIONS

In this study, respondents were asked about evacuation destinations during an earthquake with maximum intensity on Japan's 10-level seismic intensity scale. The survey considered two options: returning to the cruise ship or evacuating to nearby shelters. A total of 204 valid responses were collected, with each participant assuming being affected by the earthquake while at Kanazawa Station, a major transportation hub in Ishikawa Prefecture.

Figures 2 and Figure 3 illustrate evacuation destinations based on awareness of cruise ship evacuation and accommodation support. Results in Figure 2 indicates that respondents unaware of cruise ship evacuation were approximately 7% more

likely to choose to return to the cruise ship than those who were aware.

Similarly, Figure 3 shows that respondents unaware of accommodation support were about 15% more likely to evacuate to a cruise ship compared to those who were informed. These results suggest that cruise passengers, particularly those unaware of accommodation support, are more inclined to evacuate to the cruise ship.



Figure 1. Situation during the questionnaire survey

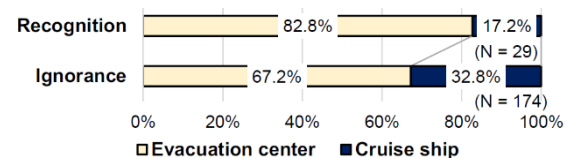


Figure 2. Evacuation destinations based on cruise ship evacuation awareness

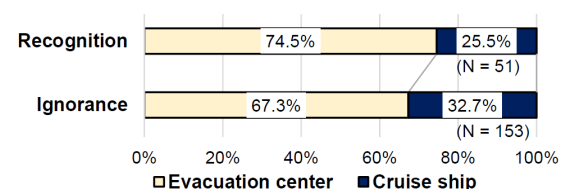


Figure 3. Evacuation destinations based on lodging support awareness

3. CONCLUSIONS

In this study, questionnaire surveys were conducted among cruise ship passengers at Kanazawa Port to examine the characteristics of those who return to the ship during an earthquake. The results indicated that passengers unaware of accommodation support are more likely to return to

the cruise ship. Future research will need to increase the sample size and explore additional variables, such as anxiety levels regarding living conditions during evacuation.

REFERENCE

- [1] Ministry of Land, Infrastructure, Transport and Tourism: Survey Report on Effective Evacuation Guidance for Foreign Visitors to Japan during a Large-Scale Disaster at Cruise Ship Berths (accessed on 13 November 2023).
- [2] Kanazawa City, Kanazawa City Regional Disaster Prevention Plan, Part 1 Earthquake Countermeasures, September 2024.

ANALYSIS OF POPULATION DYNAMICS IN THE DISASTER AREA BEFORE AND AFTER THE 2024 NOTO PENINSULA EARTHQUAKE: EXAMINATION USING KDDI LOCATION ANALYZER

T. MASHIO¹, Y. MORISAKI^{2*} and M. FUJII²

¹*Division of Geosciences and Civil Engineering, Kanazawa University, Ishikawa Prefecture, Japan*

²*Faculty of Transdisciplinary Sciences for Innovation, Kanazawa University, Ishikawa Prefecture, Japan*

Correspondence: morisaki@se.kanazawa-u.ac.jp

Keywords: Noto Peninsula earthquake, Location information, Population dynamics

1. INTRODUCTION

On January 1, 2024, the Noto Peninsula earthquake struck, with its epicenter in the Noto region of Ishikawa Prefecture. In the northern part of Ishikawa, where the earthquake was particularly severe, houses collapsed, landslides occurred, and fires spread across large areas. Consequently, over 30,000 residents were forced to evacuate. The Noto region's weak road transportation network further complicated relief efforts, delaying the transport of supplies and personnel to affected areas. As a result, recovery and reconstruction plans have not progressed as expected. During the prolonged evacuation period, some residents have chosen to leave the Noto area, making it urgent to understand the population dynamics of those affected.

This study utilized the KDDI Location Analyzer, a tool developed by KDDI Corporation, a major telecommunications company in Japan, which leverages big data from smartphone location information. The aim is to clarify population movements in the affected area before and after the disaster. This preliminary report seeks to provide insights into population dynamics in the impacted regions and offers a foundational analysis to better understand the current situation.

2. OVERVIEW OF RESEARCH METHODS

The population dynamics before and after the Noto Peninsula earthquake were examined in Wajima City, Ishikawa Prefecture, which experienced the highest number of damaged houses. This study utilized time-series data on the estimated resident population from KLA data across 26 districts in Wajima. A time-series cluster analysis was conducted to categorize demographic trends in each area.

Figure 1 presents the results of the cluster classification. Peaks in the estimated resident population were observed in clusters 1 through 5. In contrast, Cluster 6 showed no peak in the estimated population and demonstrated a consistent trend of population outmigration after the earthquake. The analysis revealed that the population returned to areas near urban centers (clusters 2 and 3) at a

relatively rapid pace, while outmigration continued in surrounding regions, such as mountainous areas. This indicates a time lag in both population outmigration and return among the various regions of Wajima City following the earthquake.

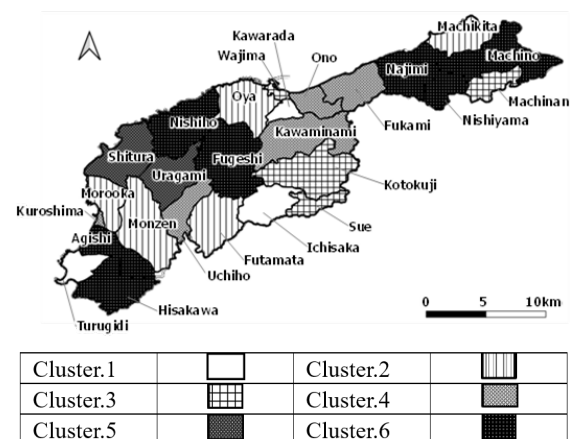


Figure 1. Results of time series cluster analysis

3. CONCLUSION

In this study, we evaluated the population dynamics in the disaster area of the Noto Peninsula earthquake using location-based big data. As a result, we succeeded in visualizing the regional characteristics of population dynamics in Wajima City. We will continue to observe population dynamics in the affected areas with regard to the restoration and reconstruction of the Noto Peninsula.

REFERENCE

- [1] KDDI Location Analyzer HP <https://k-locationanalyzer.com/> (accessed on 5 November 2024)

FIELD INVESTIGATION OF THE 30TH JULY 2024 WAYANAD DEBRIS FLOW OF WESTERN GHAT, INDIA

R.K. DASH¹, A. CHOURASIA², R. PRADEEP KUMAR³ and D.P. KANUNGO^{1*}

¹*Geotechnical Engineering & Geohazards Group, CSIR-Central Building Research Institute, Roorkee, India*

²*Structural Engineering Group, CSIR-Central Building Research Institute, Roorkee, India*

³*Director, CSIR-Central Building Research Institute, Roorkee, India*

**Correspondence: dpkanungo@cbri.res.in*

Keywords: Debris flow, Western Ghat, Rainfall, Entrainment

1. INTRODUCTION

The Western Ghat region of India is frequently affected by debris flows, and Kerala has been severely affected in the last few years [1]. Water saturation and entrainment during the flow make the debris flow more mobile and destructive [2].

2. WAYANAD DEBRIS FLOW EVENT

On 30th July 2024, a catastrophic debris flow occurred in the Wayanad region of the Western Ghats, Southern India, resulting in the tragic loss of over 200 lives. The debris flow impacted three villages namely Punchirmattam, Mundakkai and Chooralmala and destroyed many houses and other infrastructures. The major triggering factor of this debris flow was extreme rainfall, and the total runout length of the debris flow was approximately 8 km. The debris flow initiated as a landslide and the release areas are part of the Meppadi forest range (South Wayanad division) under Vellarimala vested forest.

The landslide mobilized material including rainwater, spring water, uprooted trees, tree logs, rock boulders, and debris from the release area along the channel. During its flow, entrainment along the channel and bank erosion contributed significantly to the huge quantity of material mobilization. The Chooralmala bridge initially blocked the debris, where the phase transition occurred, and the debris flow converted into hyper-concentrated flow/flash flood. This study conducts a detailed field investigation and observation of the debris flow. The findings reveal that the flow entrained a significant amount of material, and the potential for damming should not be overlooked.

3. CONCLUSIONS

The 30th July 2024 Wayanad debris flow event highlighted the need for hazard indication mapping in the debris flow susceptibility zones. In the futuristic debris flow hazard prediction, the entrainment zones and the type of materials should be considered meticulously.

REFERENCES

- [1] R. K. Dash, M. Samanta, D. P. Kanungo in: P. Thambidurai, T. N. Singh (Eds.), *Landslides: Detection, Prediction and Monitoring: Technological Developments*, Cham: Springer International Publishing., 2023, pp. 211-231.
- [2] R. K. Dash, Falae, P.O., D. P. Kanungo. *Nat. Hazards*, 111 (2022), 2011-2058.

FROM LANDSLIDE SUSCEPTIBILITY TO HAZARD & RISK MODELING: A SPACE-TIME PERSPECTIVE

S. DAS¹, D.P. KANUNGO^{2*} and S. SARKAR³

¹Geotechnical Engineering and Geo-Hazards Group, CSIR-Central Building Research Institute, Roorkee, India

²Academy of Scientific and Innovative Research (AcSIR), Ghaziabad, India

³Uttarakhand Landslide Mitigation & Management Center (ULMMC), Dehradun, India

*Correspondence: dpkanungo@cbri.res.in

Keywords: Landslide, Space-time hazard modeling, Darjeeling Himalaya

1. INTRODUCTION

Landslides are frequent geo-hazards in the Indian Himalayan region, often causing significant damage to mountain communities [1]. Therefore, hazard and risk analysis is important for landslide disaster risk reduction [2]. By integrating susceptibility (spatial prediction, P_s) with temporal (PT) and magnitude (PM) predictions, this study aims to perform landslide hazard modeling, followed by risk predictions for the Kalimpong area in Darjeeling Himalaya.

2. METHODOLOGY

First, a multi-temporal landslide inventory is prepared through visual interpretation of aerial photographs, Survey of India topographical maps, and satellite images. This inventory includes landslides that occurred over the past 51 years (1971 to 2021) and is used for subsequent hazard and risk analysis. Simultaneously, the study area is divided into slope unit (SU) based terrain segments.

For P_s prediction, the Binary Logistic Regression (BLR) model is used. For the P_T prediction, the Poisson model is applied, while the inverse-gamma function is used for P_M prediction. Hazard is then predicted for each SU by integrating the P_s , P_T , and P_M predictions over the next 5, 10, and 15 years. For risk prediction, the Resource Damage Potential (RDP) is first defined for each SU. This is then integrated with the predicted hazard values for the next 5 and 10 years to estimate the risk. The Analytic Hierarchy Process (AHP) method is used to define the RDP, and risk scores are assigned based on the socio-economic importance of the risk elements. Hazard predictions for 5 and 10 years are considered because land use patterns are expected to change over longer durations.

3. RESULTS

The prepared multi-temporal inventory contains records of approximately 3,500 landslides. Based on this data, the applied BLR model achieved a prediction accuracy of 77.9%. The Poisson model predicted mean exceedance probabilities of 0.07,

0.12, and 0.15 for the next 5, 10, and 15 years, respectively. Using the inverse- gamma function, probabilities of 0.81 and 0.17 were obtained for landslide sizes of 1,300 m² and 15,000 m², respectively. Based on this, the obtained hazard predictions are shown in the Figure 1. Next, the risk predictions are made, and obtained results are shown in the Figure 2.

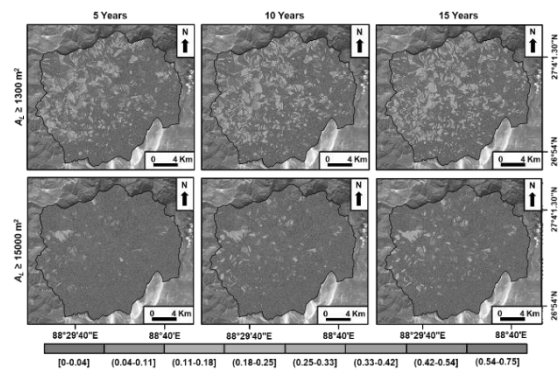


Figure 1. Landslide hazard predictions

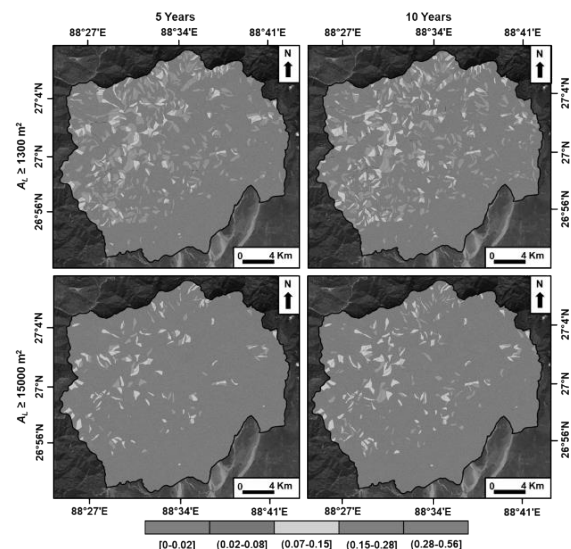


Figure 2. Landslide risk predictions

4. CONCLUSIONS

The resulting hazard and risk predictions indicate that the Kalijhora, Rambhi, Teesta Bazar, and Nimbong areas are highly vulnerable zones.

REFERENCES

- [1] National Landslide Risk Management Strategy. A publication of the National Disaster Management Authority, Govt. of India. September 2019, New Delhi
- [2] F. Guzzetti, P. Reichenbach, M. Cardinali, M. Galli, F. Aedizzzone, Geomorphology. 72 (2005) 272-299.

A FRAMEWORK FOR GEO-INTEGRATED RAINFALL THRESHOLDING AND UAV BASED LANDSLIDE MONITORING

R. PATI^{1,2}, R. DASH¹ and D.P. KANUNGO^{1,2*}

¹Geotechnical Engineering and Geo-Hazards Group, CSIR-Central Building Research Institute, Roorkee, India

²Academy of Scientific and Innovative Research (AcSIR), Ghaziabad, India

*Correspondence: dpkanungo@cbri.res.in

Keywords: Landslide, UAV, Rainfall threshold

1. INTRODUCTION

In landslide-prone regions, the need for effective monitoring and early-warning systems is critical to mitigate risks to lives, infrastructure, and ecosystems [1] This paper presents a comprehensive approach combining geospatial data analysis, rainfall thresholding, and UAV technology to enhance landslide monitoring and prediction accuracy.

2. METHODOLOGY

Landslide Mapping and Investigation involves a systematic approach to assessing and understanding landslide-prone areas along highways. The process begins with collecting historical data on landslide occurrences to identify and select unstable slopes for further study. Detailed documentation of slope geometry is then conducted to capture essential geometric parameters that characterize each slope. Following this, a comprehensive geotechnical exploration is carried out, involving both undisturbed and disturbed sampling of slope materials. Various laboratory and field tests are performed to determine the physical and mechanical properties of these materials, providing insight into their stability. Numerical Investigation focuses on a comprehensive evaluation of slope stability, aiming to assess slope vulnerability and related hazards systematically. This analysis examines the effects of rainfall on slope instability, identifying how precipitation patterns can contribute to slope failure.

By correlating rainfall data with instances of slope instability, a rainfall threshold model is developed to predict potential landslide events more accurately. Additionally, this approach integrates both the material properties of the slope and its geometric characteristics into the rainfall threshold model, addressing a previously overlooked aspect that enhances the model's predictive accuracy.

Optical Imaging for Drone-Based Mapping and Monitoring utilizes drone surveys to acquire reference data on various active and potential landslide sites. Through repeated multi-temporal data collection, drones capture and monitor surface changes over time, enabling the identification of precursor signatures that signal potential landslide

movements. This process helps define the patterns of surface displacement and provides valuable insights into the temporal progression of landslide kinematics, offering a more precise understanding of the dynamics leading to slope instability. Rainfall Threshold Model development involves setting specific rainfall thresholds along major highways to account for various types of potential landslides.

This model incorporates both the material properties and geometric characteristics of each slope, allowing for a more accurate prediction of landslide risk under different rainfall conditions. By integrating these critical slope factors, the model enhances its ability to anticipate landslide events, providing a valuable tool for early warning and risk mitigation along key transportation routes.

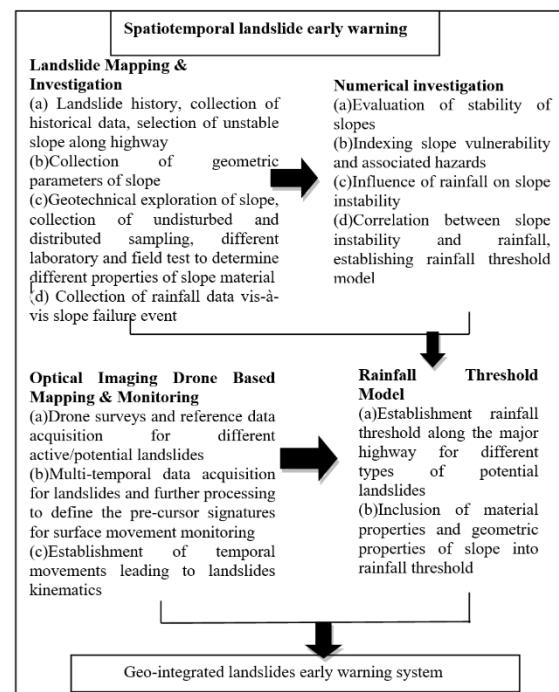


Figure 1. A framework for geo-integrated rainfall threshold and UAV based landslide monitoring

3. CONCLUSIONS

By integrating advanced data acquisition and thresholding techniques, the framework aims to improve early detection, provide real-time insights, and support decision-making processes in landslide risk management

REFERENCES

- [1] D.P.Kanungo ,S.Sharma, Landslides (2014)
11:629–638.

TSUNAMI EVACUATION RISK CHANGES IN BANDA ACEH AFTER 2004 INDIAN OCEAN TSUNAMI

O. MURAO^{1*}, M. SATO², K. SUGIYASU³, H. MIURA⁴, M. KHOIRIYAH⁵, R. SAITO⁶ and M. AFFAN⁷

¹International Research Institute of Disaster Science, Tohoku University, Sendai, Japan

²Global Environment Department, Japan International Cooperation Agency, Tokyo, Japan

³Faculty of Policy Studies, Iwate Prefectural University, Takizawa, Japan

⁴Graduate School of Advanced Science and Engineering, Hiroshima University, Higashi-hiroshima, Japan

⁵Department of Architecture and Building Science, Tohoku University, Sendai, Japan

⁶Graduate School of Information Sciences, Tohoku University, Sendai, Japan

⁷Faculty of Mathematics and Natural Science, Syiah Kuala University, Banda Aceh, Indonesia

*Correspondence: osamu.murao.a6@tohoku.ac.jp

Keywords: 2004 Indian Ocean Tsunami, Banda Aceh, Urban recovery, Population, WorldPop hub

1. INTRODUCTION

Twenty years after the 2004 Indian Ocean tsunami, it is crucial to evaluate the long-term changes in Banda Aceh considering the “Build Back Better” strategy. This study aims to apply the lessons learned from this experience to Indonesia’s future development. Recognizing the increase in population in tsunami-affected areas and the evolving lifestyle of residents, this study focuses on Banda Aceh, the region most impacted by the 2004 tsunami, to examine the changes in tsunami evacuation risk due to population growth and the capacity of existing buildings over the past two decades.

2. POTENTIAL TSUNAMI EVACUATION RISK

When assessing tsunami evacuation risks, the time required to reach a safe location from a given point in the event of a tsunami must first be determined. This calculation is independent of the population density and can be performed based on the relationship between the tsunami hazard location, route to the evacuation site, and human evacuation speed. In this study, the minimum time required for tsunami evacuation was defined as the potential tsunami evacuation risk.

To conduct the above procedure, three scenarios were established, considering the presence or absence of tsunami evacuation facilities:

(1) Scenario A: Absence of TEBs

No TEBs existed prior to the 2004 tsunami. To understand the risks before and after the construction of these buildings, this scenario considered the absence of TEBs, and the evacuation time was calculated based solely on horizontal evacuation.

(2) Scenario B: Utilizing existing TEBs

TEBs were constructed in Meuraxa district, which included those built with the support of Japan (JICA). In this scenario, the

evacuation time was calculated considering the use of these TEBs, in addition to the horizontal evacuation.

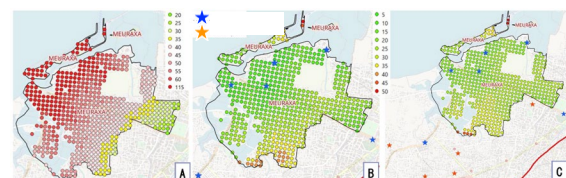
(3) Scenario C: Utilizing existing TEBs and nearby facilities

The results are presented in Figure 1. For example, in Scenario A, the number of meshes in which the evacuation was completed in the entire Meuraxa district was 86, whereas 468 meshes (approximately 84.5%) remained incomplete, as indicated in red. Evidently, the number of red dots decreased in Scenarios B and C.

3. CONCLUSIONS

While average evacuation times in scenarios A, B, and C were 49.7, 16.6, and 14.7 minutes, the construction of TEBs reduced evacuation times by over 30 minutes. However, there was an imbalance between the capacity of evacuation facilities and the number of evacuees, with some facilities receiving more than 10 times their capacity, shown in Figure 2.

Scenario D simulated more frequent, smaller tsunamis, finding that the imbalances remained unchanged. Based on these results, we proposed recommendations for improving the capacity and distribution of tsunami evacuation facilities to mitigate future tsunami risks effectively.



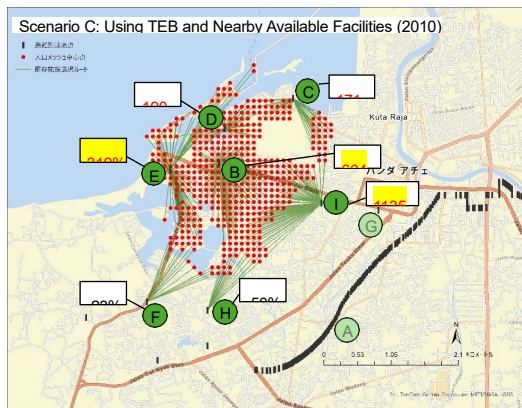


Figure 2. Shortest evacuation location from each mesh and proportion to tsunami evacuation capacity (Scenario C)

PREDICTING BUILDING RISK IN LAND SUBSIDENCE-PRONE AREAS: THE ROLE OF DECISION TREE REGRESSION MODEL IN URBAN SAFETY

K.S. KULKARNI^{1*}, S.K. NEGI¹, A. CHOURASIA² and P. K. RAMANCHARLA²

¹Architecture Planning &Energy Efficiency, CSIR-Central Building Research Institute, Roorkee, India

²CSIR-Central Building Research Institute, Roorkee, India

*Correspondence: kishorsk@cbri.res.in

Keywords: Land Subsidence, Structural damage, urban planning, disaster mitigation, predicting building vulnerability.

1. INTRODUCTION

Urban areas across the globe are increasingly facing the challenges posed by land subsidence, a gradual sinking of the ground that can lead to catastrophic structural failures. This phenomenon is often exacerbated by factors such as geological instability, groundwater extraction, and inadequate urban planning. Urban safety and disaster mitigation are critical challenges, particularly in regions susceptible to land subsidence, such as Joshimath, Uttarakhand.

In regions like Joshimath, Uttarakhand, India, where the unique interplay of topography, hydrology, and anthropogenic activities is prevalent, land subsidence has emerged as a critical issue threatening the safety and integrity of built environments. The consequences of land subsidence can be devastating, particularly in densely populated urban settings. Cracks in walls, uneven floors, and compromised foundations are common manifestations of subsidence that can render buildings unsafe or unusable.

In response to regional challenges, studies like Costa et al. (2020) proposed modular frameworks for subsidence-related building damage in the Netherlands and the Sichuan-Tibet railway region, respectively [1]. These methodologies offer crucial support for both public and private decision-making, facilitating effective awareness campaigns and risk mitigation strategies. This body of research, including Rapid Visual Screening (RVS) techniques, underscores the importance of adopting multi-faceted approaches for assessing structural vulnerabilities and improving resilience against geological hazards.

2. METHODOLOGY

The current study's goal was to assess building damage and classify it from the point of view of safety [2]. This study aims to bring about a better understanding of the structural strengths and weaknesses of these building typologies under the impact of land subsidence and provide indications of the way forward toward reducing their vulnerability in the future. The buildings' damage estimates will

be useful in analyzing the study area's urban growth regarding future development and decision-making. With over 2,300 buildings assessed in Joshimath, this research aims to understand the extent of damage and the factors contributing to structural vulnerabilities in the face of subsidence.



Figure 1. Destruction due to Land-subsidence (in Joshimath, India)

The National Disaster Management Authority (NDMA) guidelines classify building damages into four levels based on RVS [3]. This choice ensured a standardized and efficient evaluation process aligned with established protocols, enhancing the reliability and comparability of the assessment results. The photographs of the buildings were captured to record the damage as shown in Figure 1. After the field visits, analysis of the data was carried out. Based on the analysis, the buildings were classified into usable, assessed further, unusable, and demolished categories. The dataset was partitioned into two distinct subsets: one about masonry buildings and RCC buildings, comprising 8 and 9 groups of data respectively. This division encompassed building damage assessment data for Joshimath town following the 2023 land subsidence event. Specifically, groups 4 through 9 of the datasets featured binary representations of "Yes" and "No" responses [4].

The Decision Tree model is a widely used machine learning technique that excels in classification and regression tasks by breaking down complex decision-making processes into a tree-like structure of nodes and branches. Each internal node of the tree represents a decision based on a feature

(or attribute) as shown in Figure 2, while each leaf node represents an outcome or decision as shown in Figure 2. In building risk assessments, Decision Trees are particularly valuable due to their interpretability, simplicity, and ability to handle both numerical and categorical data [5].

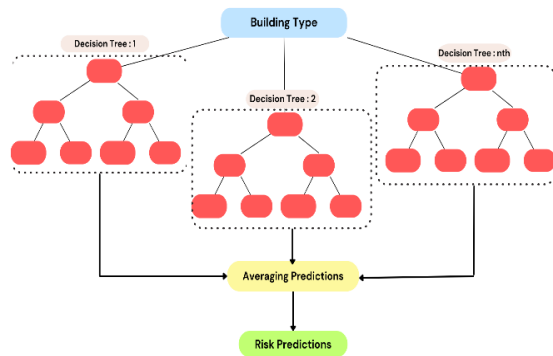


Figure 2. Working of decision tree model for both types of buildings

3. RESULTS AND DISCUSSION

The findings from the assessment of building damage in Joshimath offer critical insights into the impacts of land subsidence on the structural integrity and vulnerability of buildings. DRT model predicted between building attributes, observed damage patterns, and the spatial distribution of structural damages across different administrative zones and training and testing statistics shown in Table 1. Figure 3 shows the actual and predicted risk scores for masonry and RCC buildings. These results shed light on the mechanisms driving structural deterioration in the context of land subsidence, offering a deeper understanding of the geographic variations in building vulnerability.

The analysis underscores the significant role of building characteristics—such as construction type, age, and material—in determining susceptibility to damage. Furthermore, the spatial patterns of damage reveal a clear relationship between terrain features and the severity of structural degradation, with certain zones exhibiting a higher concentration of damaged or at-risk buildings. This information is crucial for disaster mitigation planning, as it enables authorities to prioritize interventions and focus resources on the most vulnerable areas.

The town comprises 44% masonry, 42% reinforced concrete (RCC), and 14% other construction types, including traditional timber and hybrid structures. Notably, 99% of these buildings are non-engineered, meaning they do not adhere to the provisions of the National Building Code of India 2016.

The number of stories is another critical attribute, with 38% of buildings being single-story, 43% having two stories, 14% comprising three stories,

and 5% consisting of more than four floors. These statistics highlight the structural diversity and the prevalence of non-compliant constructions, underscoring the town's vulnerability to structural damage and potential risks in the event of geological hazards like land subsidence. The assessment of 2,364 buildings in Joshimath reveals significant damage patterns, with 1% categorized as demolished, 20% as unusable, 42% requiring further assessment, and 37% deemed safe.

Table 1. Showing statistics of the DTR model

Type of Building	RCC	Masonry
Train MSE	0.0385	0.0359
Test MSE	0.0402	0.0361
Train R-squared	0.9098	0.9111
Test R-squared	0.8645	0.8545
Train RMSE	0.1963	0.1895
Test RMSE	0.2006	0.1899
Train MAE	0.1678	0.1412
Test MAE	0.175	0.1481

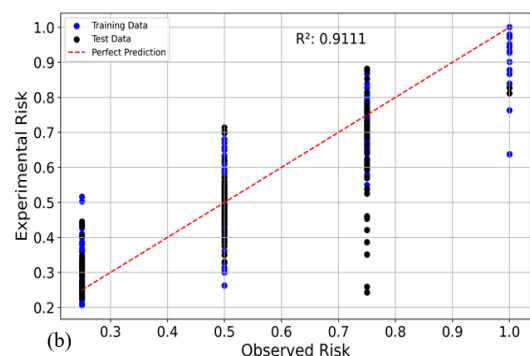
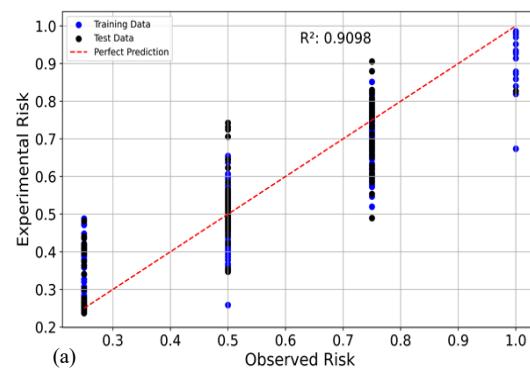


Figure 3. Actual and predicted risk score for (a) Masonry and (b) RCC

The decision tree regression model was employed to predict building risk scores, providing key insights into structural vulnerabilities. For RCC buildings, the model achieved a training MSE of 0.0385 and a testing MSE of 0.0402, with an R-squared value of 0.9098 for training and 0.8645 for

testing. Similarly, masonry buildings yielded a training MSE of 0.0359 and a testing MSE of 0.0361, with a train R-squared of 0.9111 and Test R-squared of 0.8545. The model also demonstrated promising results in terms of RMSE and MAE, with RMSE values for RCC and masonry buildings standing at 0.2006 and 0.1899, respectively, and MAE values at 0.175 and 0.1481. These results underscore the model's efficacy in identifying and quantifying building damage, facilitating risk mapping, and targeted interventions for urban safety.

The results also emphasize the importance of addressing land subsidence-related risks in disaster-prone regions, particularly where rapid urbanization and environmental factors exacerbate structural vulnerabilities. By integrating these findings into urban planning and building safety strategies, decision-makers can enhance the resilience of communities exposed to geological hazards like subsidence.

4. CONCLUSIONS

This study highlights the effectiveness of using Decision Tree Regression in assessing building vulnerability due to land subsidence in Joshimath. By analyzing over 2,300 buildings, the model successfully predicted structural damage with high accuracy, providing valuable insights into the vulnerabilities of RCC and masonry buildings. The performance metrics, including R-squared and MSE values, demonstrate the model's strong predictive capabilities. These findings are crucial for urban planners and policymakers, as they provide a data-driven foundation for disaster mitigation strategies, enabling targeted interventions to enhance urban safety and resilience in subsidence-prone regions.

REFERENCES

- [1] L. Costa, S. Kok, and M. Korff, Systematic assessment of damage to buildings due to groundwater lowering-induced subsidence: methodology for large scale application in the Netherlands, *Proc. IAHS*, vol. 382 (2020) 577–582.
- [2] B. Bera, S. Saha, and S. Bhattacharjee, Sinking and sleeping of Himalayan city Joshimath, *Quaternary Science Advances*, 12 (2023) 100100.
- [3] P. K. Ramancharla et al. A primer on rapid visual screening (RVS) consolidating earthquake safety assessment efforts in India, (2020).
- [4] L. Frédéric, J. Asté, and E. Leroi, Vulnerability assessment of elements exposed to mass-movement: Working toward a better risk perception, *Landslides*, Senneset (ed.) 1 (1996), 263–269.
- [4] R. Zhao, A. Arabameri, and M. Santosh, Land subsidence susceptibility mapping: a new

approach to improve decision stump classification (DSC) performance and combine it with four machine learning algorithms, *Environ Sci Pollut Res*, 31(10) (2024) 15443–15466.

SIMPLIFIED VULNERABILITY ASSESSMENT FOR MASONRY BUILDINGS USING FRAGILITY CURVE

A. CHOURASIA*, A. PAIN, R. PRADEEP KUMAR and A. MINHAS

CSIR-Central Building Research Institute, Roorkee, India

*Correspondence: ajayc@cbri.res.in

Keywords: Unreinforced masonry buildings, Vulnerability assessment, Fragility curves

1. INTRODUCTION

Masonry has long been a preferred construction material for low-rise buildings worldwide due to its cost-effectiveness, availability, and thermal efficiency. In India, where the demand for affordable housing and construction simplicity remains high, masonry continues to dominate in residential and small commercial building applications. However, unreinforced masonry (URM) buildings—those without reinforcement in the walls to resist lateral forces—are notably vulnerable in seismic events. Structural characteristics like the low tensile and shear strength of masonry units and mortar, variability in mortar joint thickness, weak interfacial bonding, and reliance on workmanship create significant challenges in URM buildings' seismic performance. These factors contribute to an inherent lack of uniformity and robustness, leaving such structures prone to severe damage under seismic loading.

Historically, earthquakes have demonstrated the vulnerability of URM buildings, with examples from major seismic events globally and in India highlighting the dangers associated with unreinforced masonry construction. Reports reveal extensive building collapses and high fatalities linked to URM structures, underscoring the need for accurate seismic vulnerability assessments. Despite the growing awareness of these risks, the Building Census Data reveals an increasing proportion of URM buildings in India's construction portfolio. This trend, combined with the seismically active zones across the country, underscores the urgent need for a reliable and accessible method to assess the seismic vulnerability of URM buildings.

Traditional vulnerability assessments for masonry buildings often involve complex methodologies that may not fully account for the variability in construction practices, material quality, and design approaches present in the Indian context. Therefore, a simplified and adaptable vulnerability assessment framework tailored to Indian URM buildings is crucial. Probabilistic approaches that incorporate the uncertainties in ground motion and building parameters offer a viable solution for generating realistic fragility curves. Such curves can be instrumental in

predicting the probability of structural damage under varying seismic intensities and thereby guide risk mitigation strategies for URM buildings.

The current study aims to develop fragility curves for URM buildings in India using a probabilistic framework that accommodates the diverse parameters influencing structural vulnerability. The fragility curves are calibrated based on structural characteristics unique to Indian URM buildings, enabling an accurate reflection of their seismic performance. To validate these findings, the generated curves are compared with existing vulnerability data. Additionally, this methodology is applied to a town in a high seismic zone in India, providing a practical assessment of URM building vulnerabilities in real-world settings.

The results of this research offer essential insights into risk assessment and mitigation for URM buildings, supporting informed decision-making for policymakers, engineers, and urban planners in earthquake-prone regions of India.

2. ANALYSIS METHODOLOGY

This study utilizes a structured approach to develop fragility curves for URM buildings in India, using seismic data from national codes and real earthquake ground motions. The methodology can be divided into several key steps, as shown in Figure 1.

2.1 Selection of Building Typology

Different building typologies, such as unreinforced masonry URM, reinforced masonry (RM), and confined masonry (CM), represent various construction methods and materials, each of which influences a building's response to seismic loads. In this study, the building typology selected is URM, chosen based on the structural characteristics common to the specific region under analysis, where the masonry has a compressive strength of 3.5 MPa, a Poisson's ratio of 0.1, a modulus of elasticity of 1853 MPa, and a density of 1700 kN/m³. The slab and floor components are constructed with reinforced concrete (RCC) of grade M20, having a density of 25 kN/m³, a modulus of elasticity of 200,000 MPa, a Poisson's ratio of 0.2, and a compressive strength of 20 MPa. These material

properties will be essential in assessing the seismic performance and resilience of the URM structures in the study area.

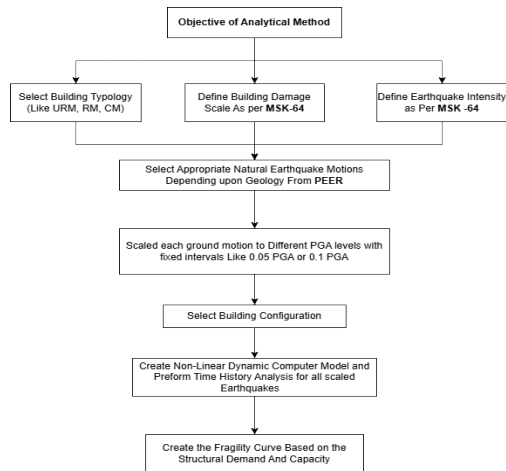


Figure 1. Flowchart for analytical vulnerability for time-history analysis-based method

2.2 Definition of Building Damage Scale (MSK-64)

The MSK-64 (Medvedev-Sponheuer-Karnik) scale is a system used to categorize building damage levels, providing a standardized approach for assessing structural impacts based on visual observations and structural deformations. This scale facilitates consistent evaluation and comparison of damage across different building types under seismic events. In this study, three specific damage states are defined: the Light Damage Limit State, which corresponds to 0.13% displacement of the total building height; the Significant Damage Limit State, which corresponds to 0.34% displacement of the total building height; and the Collapse Damage Limit State, which corresponds to 0.45% displacement of the total building height. These categories offer a structured basis for assessing levels of structural response to seismic forces [2].

2.3 Definition of Earthquake Intensity (MSK-64)

Earthquake intensity is also defined following the MSK-64 scale, which categorizes intensity based on observed effects on structures, the environment, and people. This scale helps to correlate earthquake severity with potential damage, ensuring that building performance is analysed under realistic seismic intensities.

2.4 Selection of Natural Earthquake Motions Based on Geology

To simulate realistic earthquake loading, natural earthquake records are selected from the Pacific Earthquake Engineering Research (PEER) database. Records are chosen based on geological conditions that are like the study area, ensuring that the selected

ground motions are representative of the seismic environment likely to be encountered by the building. In table 1, 11 ground motion are listed which are used in present study.

Table 1. Ground motion record from PEER database

Ground Motion Number	Record Sequence Number	Earthquake Event Name	Magnitude	Scale Factor
GM 1	RSN 4	Imperial Valley 01	5.00	0.628
GM 2	RSN 6	Imperial Valley 02	6.59	0.787
GM 3	RSN 42	Lytle Creek	5.33	2.585
GM 4	RSN 50	Lytle Creek	5.33	1.084
GM 5	RSN 57	San Fernando	6.61	0.665
GM 6	RSN 68	San Fernando	6.61	0.695
GM 7	RSN 72	San Fernando	6.61	0.864
GM 8	RSN 78	San Fernando	6.61	1.300
GM 9	RSN 130	Friuli Italy 02	5.91	1.882
GM 10	RSN 147	Coyote Lake	5.74	9.278
GM 11	RSN 172	Imperial Valley 06	6.53	0.999

2.5 Scaling of Ground Motions to Different PGA Levels

Each selected ground motion record is scaled to a range of peak ground acceleration (PGA) levels, with fixed intervals such as 0.05 PGA or 0.1 PGA. This process ensures that the analysis covers a wide range of seismic intensities, allowing for the assessment of structural response across low, moderate, and high earthquake demands. Scaling to different PGA levels facilitates a comprehensive understanding of how the building's structural integrity varies with increasing seismic load.

2.6 Selection of Building Configuration

In this step, specific building configurations are chosen, which may include variations in layout, height, structural components, and reinforcement details. This selection reflects common architectural and structural practices in the region, ensuring that the model accurately represents the actual conditions of typical buildings within the study area. Building Layout and Elevations are shown in figure 2 and 3.

2.7 Modelling of Non-Linear Dynamic Computer Model and Time History Analysis

A non-linear dynamic model of the building is developed using ETABS, and a time-history analysis is performed for each scaled ground motion. This analysis captures the building's real-time response to seismic loading, allowing for detailed evaluation of structural behaviour, including deformations, forces, and potential failure modes under various levels of earthquake intensity. From analysis maximum spectral displacement noted down and used to develop the fragility curve.

2.8 Creation of Fragility Curve Based on Structural Demand and Capacity

Based on the structural demand and capacity obtained from the time-history analysis, fragility curves are generated. These curves represent the probability of exceeding different levels of structural damage at various earthquake intensities. Fragility curves are crucial for understanding building vulnerability and provide valuable insights into the likelihood of damage under different seismic scenarios.

With the help of log normal probability density function [1] fragility curve can be obtained which is presented in Figure 4.

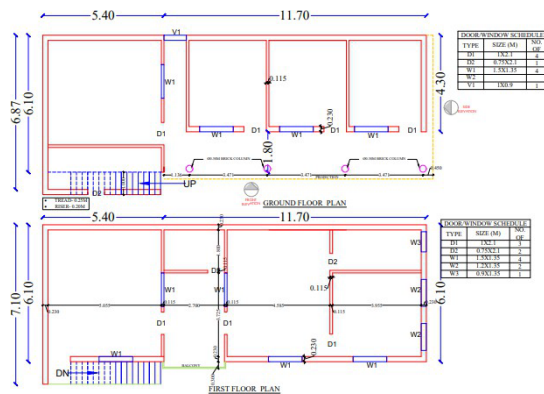


Figure 2. Ground and first floor plan

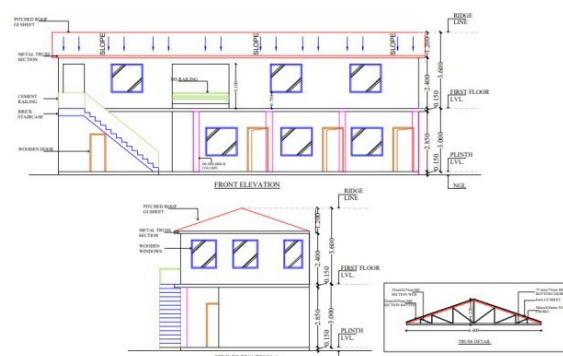


Figure 3. Front and side elevation of the building

3. CONCLUSION

This study presents a simplified and adaptable framework for assessing the seismic vulnerability of unreinforced masonry (URM) buildings in India. By using probabilistic methods and fragility curves calibrated to reflect the unique construction characteristics of Indian URM structures, this approach provides an accessible and practical tool for evaluating building resilience under seismic loads.

The methodology considers realistic ground motions, local building typologies, and construction practices, making it well-suited for widespread application across seismically active regions in

India. The results of the time-history analysis, culminating in the generation of fragility curves, offer insights into the likelihood of damage at varying seismic intensities.

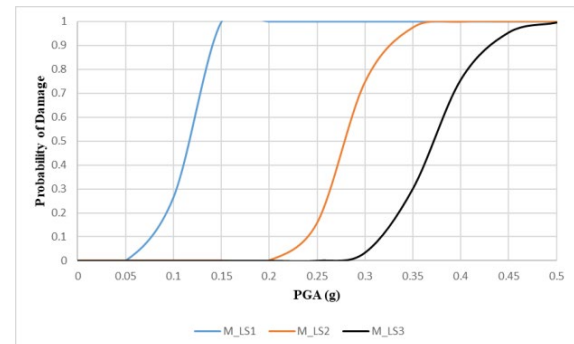


Figure 4. Fragility curve of two-story masonry building

REFERENCES

- [1] Zamiran, S., & Osouli, A. (2018). Seismic motion response and fragility analyses of cantilever retaining walls with cohesive backfill. *Soils and Foundations*, 58(2), 412-426.
- [2] Barbara Borzi, Helen Crowley, Rui Pinho (2008). Simplified Pushover-Based Earthquake Loss Assessment (SP-BELA) Method for Masonry Building.
- [3] Magenes, G. and Della Fontana, A (1998) Simplified non-linear seismic analysis of masonry buildings. *Proceedings of the British Masonry Society* 8:190-195.

DEVELOPMENT OF A POTENTIAL INDEX FOR UTILIZATION OF VACANT HOUSES CONSIDERING DISASTER RISK: A CASE STUDY OF HATOYAMA TOWN, SAITAMA PREFECTURE

A. SASAKI¹, Y. MORISAKI^{2*} and M. FUJII²

¹*Division of Geosciences and Civil Engineering, Kanazawa, University, Ishikawa Prefecture, Japan*

²*Faculty of Transdisciplinary Sciences for Innovation, Kanazawa University, Ishikawa Prefecture, Japan*

*Correspondence: morisaki@staff.kanazawa-u.ac.jp

Keywords: Vacant House, Utilization, Earthquake, Disaster Risk

1. INTRODUCTION

In recent years, due to the declining birthrate, aging population, and declining population, vacant houses in Japan have been increasing everywhere. As a measure against the problem of vacant houses, utilization of vacant houses is recommended by the national and local governments in Japan. Therefore, municipalities seek indicators to determine vacant houses that can be utilized. On the other hand, disasters occur frequently in Japan. Therefore, it is important to promote the long-term use of vacant houses by utilizing vacant houses with lower disaster risk when converting these houses.

Based on this social background in Japan, big data focused on vacant houses and estimated seismic intensity distribution data (MMI) are used in this study. Using these data, we develop an index that indicates the ease of utilizing vacant houses, considering the characteristics of vacant houses and the disaster risk particularly from earthquakes.

2. ANALYSIS OVERVIEW

In this study, we focus on Hatoyama Town, Hiki-gun, Saitama Prefecture, with vacant house problem. Therefore, we conduct the following analysis using big data focused on vacant house and MMI data from Japan Seismic Hazard Information Station [1].

In this study, the estimated seismic intensity of an earthquake occurring in the Fukaya fault zone, which is considered to cause the most damage to Hatoyama Town, is used. The seismic intensity is treated as the external force generated by the earthquake. Figure 1 shows the distribution of expected vacant houses and mesh data of estimated seismic intensity in Hatoyama Town.

The term “expected vacant house” refers to a house that was judged uninhabited during the field survey. Figure 1 shows that vacant houses are not only most concentrated in the eastern part of the town but are also relatively distributed in the southern and central parts of the town. On the other hand, the estimated seismic intensity is relatively large in the southern and northern parts of the town.

Figure 2 shows that the number of expected vacant houses to experience predicted seismic

intensity of 5.80 to 5.90 is the largest. Therefore, the estimated seismic intensity for each vacant house is extracted. Focusing on the “ease of use” of vacant houses, the potential for utilization of these houses is constructed using variables selected through a principal component analysis. Furthermore, a quantitative evaluation is conducted for each vacant house in the town to assess how easily it can be utilized.

3. CONCLUSION AND FUTURE WORKS

In this study, we focused on the ease of utilizing vacant houses using a field survey of vacant houses by local governments and Japan Seismic Hazard Information Station.

On the other hand, the large number of items in the vacant house survey has burdened local governments. In the future, it is necessary to explore approaches aimed at streamlining the survey process, such as reducing or reevaluating the survey items.

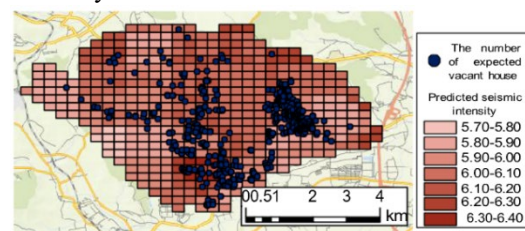


Figure 1. The distribution of expected vacant houses and predicted seismic intensity in Hatoyama Town

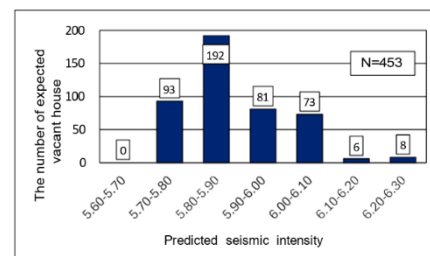


Figure 2. The number of expected vacant houses per predicted seismic intensity

REFERENCE

[1] National Research Institute for Earth Science

and Disaster Resilience, Japan Seismic Hazard
Information Station, <https://www.jshis.bosai.go.jp> (10 November 2024)

DEM STUDY ON THE STRESS DISTRIBUTION OF MUCK AND FOAM IN THE EPB SHIELD CHAMBER

J. JIANG^{1*} and R. KUWANO²

¹*Department of Civil Engineering, The University of Tokyo, Tokyo, Japan*

²*Institute of Industrial Science, The University of Tokyo, Tokyo, Japan*

Correspondence: jgg@g.ecc.u-tokyo.ac.jp

Keywords: *Muck, Foam, DEM, EPB, PFC*

1. INTRODUCTION

The Earth Pressure Balanced (EPB) shield machine is a crucial tool in the tunnel and geotechnical engineering, especially when dealing with the fine-grained soils [1]. Its operation relies on using excavated material (muck) in the shield chamber to balance the soil stress and groundwater pressure at the tunnel face, ensuring a stable advancement. However, in clay-rich soils, problems like adhesion of particles to the cutter head, blocking of the transport channel or the conveyor systems are common [2]. This imbalance in soil stress can slow down tunneling progress and lead to significant engineering issues [3].

To reduce these problems, foam, polymer suspensions and high-density slurries are frequently used in the EPB shield machine to improve the properties of soil in the chamber. These additives can improve the plasticity and fluidity of the soil, making it easier to be mixed and transported [4]. However, the amount of foam added significantly depends on the soil's mechanical properties and the specifics of the construction process. In practice, the amount of foam added to condition the soil during construction typically relies on the experience of the operator and basic on-site tests. Although foam improves the plasticity and fluidity of the soil, there is no advanced method to accurately monitor how the foam and soil mix inside the chamber or how stress is distributed within the chamber. It can lead to inefficiencies in soil condition and increase the risk of issues like clogging or pressure imbalances in the chamber.

On the other hand, due to the large scale of shield machines and the difficulty of accessing the muck-soil mixture inside the chamber, laboratory tests are often impractical for studying its behavior. But with the rapid development of computing technology, Discrete element method (DEM) simulation has become an effective solution for modeling the mechanical behavior of soil with large deformations. Many scholars have successfully used DEM to model soil-machine interactions and validate its effectiveness in simulating large deformations. Zhu et al. (2020) [5]

assessed the adaptability of an EPB shield chamber system by DEM modelling and studied the flow characteristics of soil particles inside the chamber by investigating the velocity field, motion trajectory and mass flow rate. Lee et al. (2021) [6] proposed a numerical model to simulate the tunnelling process of EPB shield machine and monitored some critical tunnelling parameters, like soil deformation in the ground and operation parameters of shield machine.

Therefore, this paper intends to use the Particles Flow Code (PFC 6.0) to evaluate the evolution of soil stress redistribution when soil and foam are mixed in the shield chamber. Through a developed DEM model, six mixtures with varying foam contents were analyzed to determine an optimal amount of foam to achieve the maximum benefit. The numerical simulation results could provide some reference to engineering practices.

2. NUMERICAL SIMULATION MODEL

2.1 Contact models

The discrete element method (DEM) follows Newton's second law to evaluate the contact force and displacement between particles [7]. Various contact models have been proposed to simulate different soil behaviors. This study applies the adhesive rolling resistance linear model to capture the viscous interactions between soil particles and foam particles. It replicates the cohesive granular material behavior by implementing a short-range attractive force that approximates van der Waals forces. A cohesive component is characterized by two main parameters: the maximum attractive force (F_0) and attraction range (D_0), as depicted in Figure 1 and Figure 2. This approach enables a relatively simple representation of cohesive forces within particle mixtures, aiding in the analysis of soil material behaviors with inter-particle attractions.

2.2 Soil-foam mixture model

A cylindrical chamber with a diameter of 0.2 m and a thickness of 0.01 m was built by using the wall element within PFC to replicate the EPB shield chamber. And two cylindrical plates (each with a

diameter of 10 mm and a thickness of 2 mm) were positioned around the chamber center to represent the stirring rods, which would rotate clockwise along the red path, as shown in Figure 3. In addition, 13 measuring spheres were distributed in the lower part of the chamber to monitor soil stress in the area.

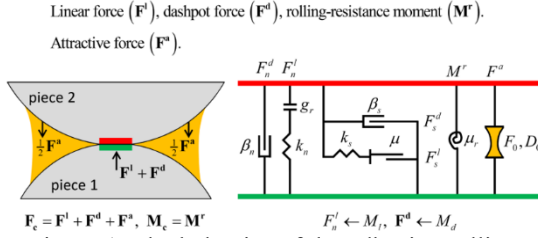


Figure 1. The behavior of the adhesive rolling resistance linear model

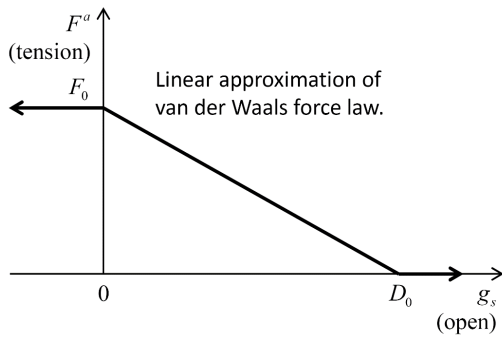


Figure 2. Attractive force versus surface gap

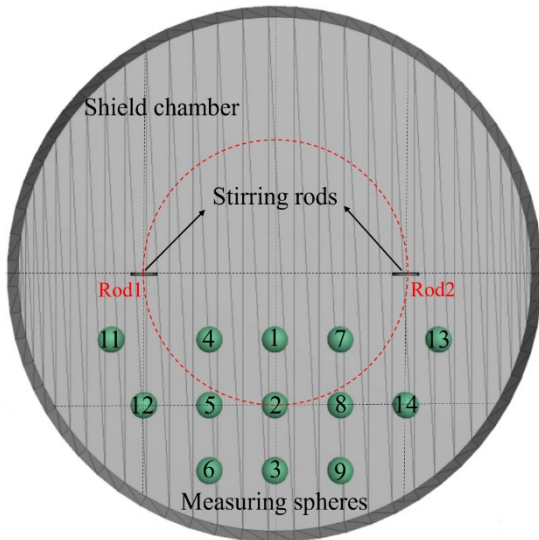


Figure 3. The schematic diagram of the shield chamber

Three steps were implemented in the stirring simulation of soil and foam mixture. In the first step, soil and foam particles of various proportions were randomly generated within the chamber, filling half of its volume. The generation method of particles followed PFC's internal particle generation algorithm, ensuring an initial even mixture. The particle size of soil and foam was set to 1 mm. And the particle density of soil and foam was 2.75 g/cm^3

and 0.125 g/cm^3 , respectively. Then, soil and foam particles were assigned with distinct contact parameters. A linear contact model was used between walls and particles. The adhesive rolling resistance linear contact model was applied for soil-soil, foam-foam and soil-foam interactions, as detailed in Table 1.

The contact parameters between soil and foam were same as foam-foam contact parameters. Finally, once the particle mixture stabilized, it was stirred at a rotation speed of $0.02^\circ/\text{s}$ under the action of stirring rods. The contact stress on the stirring rod surface and the soil stress near the measuring spheres were recorded to assess the interaction forces between rod and soil particles. It should be noted that soil particles exhibit significant higher contact stiffness and friction coefficient than foam particles.

As a kind of special material, foam particles were treated as lightweight entities with minimal adhesion and no friction. But this simplification has its limitations. One of the major limitations was that the annihilation characteristics of foam particles (dissolve) are not accounted for in this model.

Table 1. Contact model and parameters

Parameters	Value
Particle to wall contact:	Linear
Effective modulus E^* [Pa]	$1.0\text{e}6$
Normal-to-shear stiffness ratio κ^* [-]	1.0
Friction coefficient μ [-]	0.5
Soil-Soil particles:	Arrlinear
Effective modulus E^* [Pa]	$1.0\text{e}6$
Normal-to-shear stiffness ratio κ^* [-]	2.0
Friction coefficient μ [-]	0.5
Normal critical damping ratio β_n [-]	0.5
Shear critical damping ratio β_s [-]	0.5
Maximum attractive force F_0 [N]	$1.0\text{e}-4$
Attraction range D_0 [mm]	0.1
Foam-Foam particles:	Arrlinear
Effective modulus E^* [Pa]	$1.0\text{e}3$
Normal-to-shear stiffness ratio κ^* [-]	0.0
Friction coefficient μ [-]	0.0
Normal critical damping ratio β_n [-]	0.7
Shear critical damping ratio β_s [-]	0.7
Maximum attractive force F_0 [N]	$1.0\text{e}-5$
Attraction range D_0 [mm]	0.1

3. RESULTS

Soil and foam particles were randomly generated in the lower shield chamber and stirred for two cycles under the action of two stirring rods, as shown in Figure 4. Six foam contents (volume fraction) were considered in this study from 0% to 50%, with an interval of 10%. And to enhance the visibility of particle movement during mixing, the initially generated soil particles were divided into eight distinct sections, each coloured differently. During

stirring, particles visibly follow the motion imparted by the stirring rods, aligning in the stirring direction. Stress variations on the surface of the stirring rod and near the measuring spheres are continuously monitored, providing valuable data on the mechanical interactions between particles and the stirring apparatus under different foam content conditions.

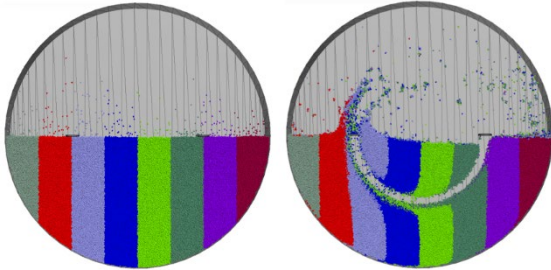


Figure 4. The initial and stirred soil-foam mixture

The contact stress on the surface of the stirring rods were shown in Figure 5. At the same foam content, the contact stress formed a regular waveform with prominent peaks. These peaks showed a gradual decline as the rotation continued. Within the initial 180-degree rotation, an increase in foam content correlated with a marked reduction in peak contact stress, after which the stress levels stabilized and showed minimal change. The trend of the contact peak stress changing with the foam content was shown in Figure 6. The peak contact stress initially decreased significantly as the foam rose, but when foam content surpassed 20%, this decreasing trend plateaued. Therefore, the 20% foam content can be interpreted as a critical threshold in this simulation, beyond which increasing foam content did not markedly impact contact stress reduction on the stirring rod within the initial 180-degree rotation. Once the rotation angle of the stirring process exceeded 180 degrees, the influence of foam content on reducing the surface contact stress becomes more pronounced. However, the impact of foam content was also affected by the first half-turn (0-180°) of stirring simultaneously.

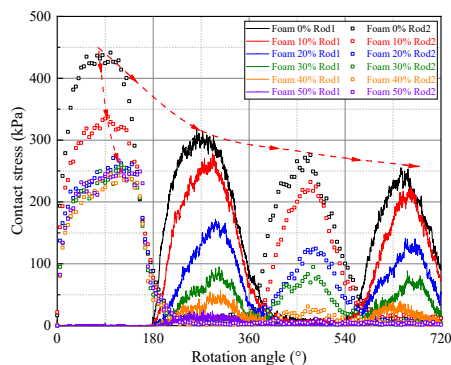


Figure 5. The contact stress on the surface of the rods

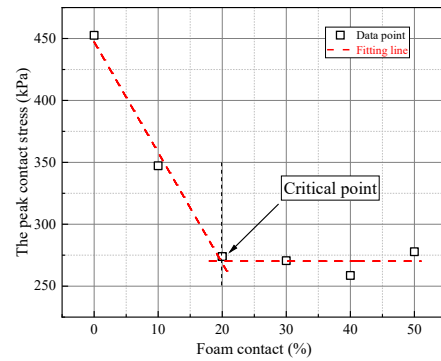


Figure 6. The peak contact stress within 180° rotation

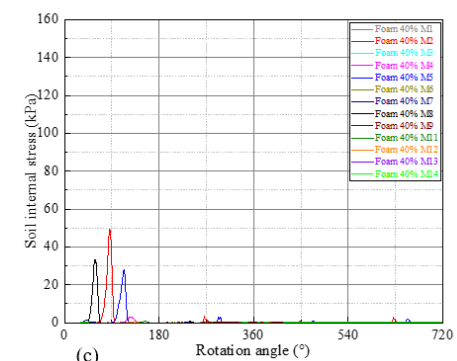
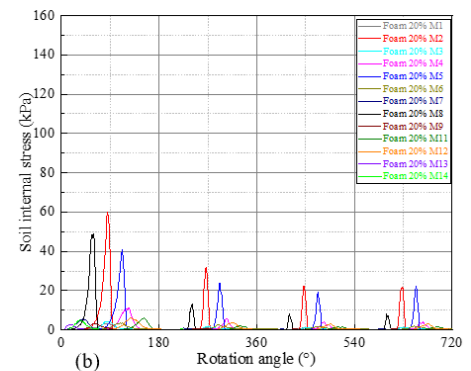
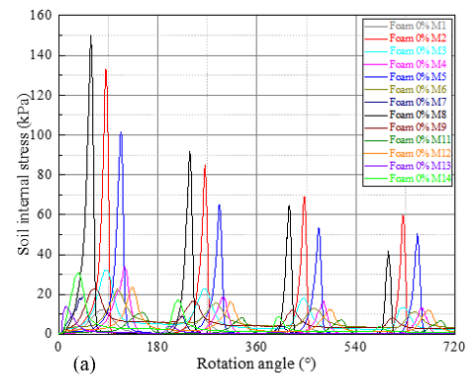


Figure 7. Soil internal stress monitored by measuring spheres with different foam contents:
(a) 0% foam content; (b) 20% foam content;
(c) 40% foam content

Figure 7 illustrated the stress variation of soil and foam mixtures in the area around the measuring spheres during stirring at the foam contents of 0%,

20% and 40%. It revealed that the stress levels along the stirring rod's rotation path were considerably higher than that in other regions, especially in the measuring spheres of 2, 5 and 8. This heightened stress was directly influenced by the stirring motion.

As stirring progressed, the overall soil internal stress gradually decreased, indicating the soil's ongoing relaxation under the stirring effect. Likewise, other mixtures containing different foam contents also exhibited this pattern. And with the increase of foam content, there was a noticeable reduction in soil internal stress in the vicinity of the measuring spheres. This indicates that higher foam content provides a more effective isolation of soil particles, leading to a decline in localized stress intensity during the mixing process.

The internal soil stress obtained from measuring spheres M2, M5 and M8 are used to analyze the effect of foam content, as shown in Figure 8. Within the first 180° rotation, the internal soil stress decreased initially and then stabilized with minimal change as the foam content increased. But once the rotation surpassed 180°, there was a pronounced drop in internal stress due to the synergistic effects of both stirring and foam content.

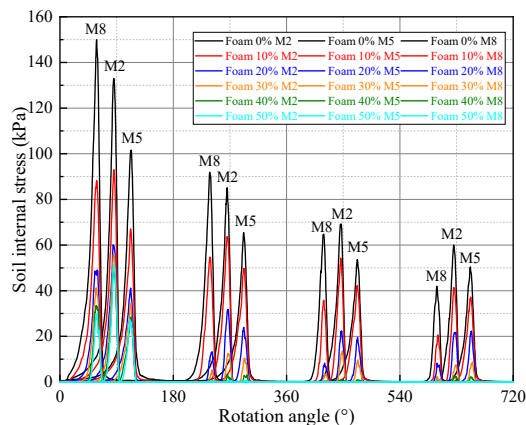


Figure 8. Soil internal stress with different foam content

Figure 9 demonstrated a clear two-stage pattern of the peak internal stress change as foam content increased within the first 180° of rotation in the measuring spheres M2, M5 and M8. With foam content up to 20%, the soil internal stress reduction was pronounced. While beyond this threshold, the stress changed gently. This 20% foam content acted as a critical threshold, marking a significant point for improving soil's mechanical properties.

4. CONCLUSIONS

In examining soil-foam mixtures in the EPB shield chamber, a DEM model based on PFC 6.0 was established to assess the impact of foam content. Stress monitoring on both the stirring rod surface

and throughout different soil regions yielded the following insights:

- 1) As the stirring rod rotated, the rod contact stress and soil internal stress gradually decreased due to the continuous stirring. The soil internal stress within rod's rotating path was significantly higher than other regions.
- 2) With the increase of foam content, both the rod surface stress and soil internal stress initially dropped rapidly, followed by a phase of slower change.
- 3) At this specific cohesion condition, a 20% foam content threshold was optimal for enhancing soil fluidity.
- 4) These findings can provide valuable guidance for optimizing soil content in soil improvement, especially in EPB applications.

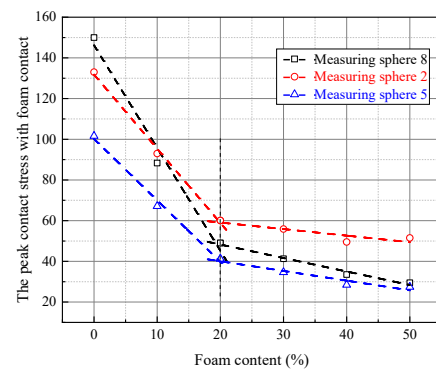


Figure 9. The peak soil internal stress within 180° rotation

REFERENCES

- [1] Q. Xu, L. Zhang, H. Zhu, Z. Gong, J. Liu, Y. Zhu, Laboratory tests on conditioning the sandy cobble soil for EPB shield tunnelling and its field application. *Tunnelling and Underground Space Technology*, 105(2020) 103512.
- [2] F. S. Hollmann, M. Thewes, Assessment method for clay clogging and disintegration of fines in mechanised tunnelling. *Tunnelling and Underground Space Technology*, 37(2013) 96-106.
- [3] Y. Alberto-Hernandez, C. Kang, Y. Yi, A. Bayat, Clogging potential of tunnel boring machine (TBM): a review. *International Journal of Geotechnical Engineering*, 12 (2018) 316-323.
- [4] V. Amirkiyaei, M.H. Kadhodaei, E. Ghasemi, Estimation of foam (surfactant) consumption in earth pressure balance tunnel boring machine using statistical and soft-computing methods. *Journal of Rock Mechanics and Geotechnical Engineering* (2024).
- [5] H. Zhu, C. Panpan, Z. Xiaoying, L. Yuanhai, L. Peinan, Assessment and structural improvement on the performance of soil chamber system of EPB shield assisted with DEM modeling.

- Tunnelling and Underground Space Technology, 96(2020) 103092.
- [6] H. Lee, H. Choi, S.W. Choi, S.H. Chang, T. H. Kang, C. Lee. "Numerical Simulation of EPB Shield Tunnelling with TBM Operational Condition Control Using Coupled DEM–FDM" *Applied Sciences* 11 (2021) 6: 2551.
- [7] P.A. Cundall, O.D.L. Strack, A discrete numerical model for granular assemblies. *Géotechnique*, 29 (1979) 47-65.

ROBUSTNESS OF TRAFFIC NETWORKS: ANALYZING DAMAGE AND RECOVERY PROCESS AGAINST REPEATED DISASTERS

T. TATEISHI¹, H. HASADA², H. WATANABE² and Y. HONMA^{2*}

¹Graduate School of Engineering, The University of Tokyo, Tokyo, Japan

²Institute of Industrial Science, The University of Tokyo, Tokyo, Japan

*Correspondence: yudai@iis.u-tokyo.ac.jp

Keywords: Robustness, Traffic network, Recovery process, Multiple damages

1. BACKGROUND

Disruptions to transportation networks due to natural disasters occur frequently and often take significant time to recover. Therefore, it is crucial to evaluate network structures and spatial configurations that can maintain functionality and recover quickly in times of disaster. However, previous studies have rarely consistently addressed assessments that not only consider the spatial configuration of networks at the time of the disaster but also consider the time required for recovery.

2. CONCEPT

It is important to consider both the spatial extent and temporal progression of disruptions and recovery in the context of natural disasters. Figure 1 illustrates the spatial location relationship of Shinkansen transport disruptions and their recovery process following the Great East Japan Earthquake on March 11, 2011. From the occurrence of the disaster to the full restoration of the network, changes in network connectivity can be observed. Therefore, this study attempts to integrate spatial disruption occurrence modeling with a time-series model.

3. MATERIALS AND METHODS

A disruption occurrence model that considers spatial relationships, as proposed by M. Tajima et al. [1], was utilized. It was assumed that disruptions occur randomly and simultaneously, represented as circular areas (referred to as disruption disks) with a specified radius R , within which routes in the internal area become unusable.

For a set of routes K^{rs} connecting two points r and s , as shown in Figure 2, we can associate each area \mathcal{R}^{rs} in space with the set of affected routes $I \in \mathcal{P}(K^{rs})$ when the center of the disruption disk is located within that area. Here, $\mathcal{P}(\bullet)$ denotes the power set of a set.

Using a spatial Poisson distribution, we calculate the probability q^{rs} that a disruption will occur within the area \mathcal{R}^{rs} . Then, the probability of a pattern $J \in \mathcal{P}(\mathcal{P}(K^{rs}))$ of unavailable routes due to disruptions is given by

$$p^{rs} = \prod_{I \in J} q^{rs} \prod_{I' \notin J} (1 - q^{rs}). \quad (1)$$

Here, we can define the evaluation value VJ^{rs} for the remaining routes, using a log-sum variable based on the C-Logit model, and the expected value of this serves as the measure of network robustness.

By extending this model to consider the time series change of unavailable route pattern J , we can evaluate network robustness with respect to temporal changes.

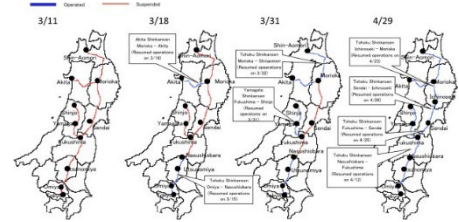


Figure 1. The occurrence and restoration of transportation disruptions on the Tohoku Shinkansen [2]

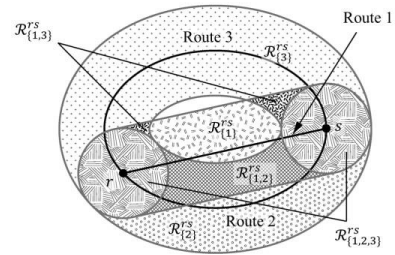


Figure 2. The area within which a disruption's center lies affects the routes [1]

4. CONCLUSIONS

The impact of disasters on transportation networks varies with spatial relationships and over time. This study finds potential in a network robustness evaluation method that focuses on the spatial configuration of disrupted transportation networks, combined with an assessment of the time taken for recovery.

REFERENCES

- [1] M. Tajima, Y. Honma, Robustness of Traffic Networks Focusing on Spatial Relationships between Multiple Routes, Journal of the City

- Planning Institute of Japan. Vol.53 No.2 (2018)
199-205.
- [2] Ministry of Land, Infrastructure, Transport and
Tourism, White paper on Land, Infrastructure,
Transport and Tourism in Japan, Tokyo, 2010,
p42.

DETECTION OF MILLIMETER-SCALE DEFORMATIONS AT JATILUHUR DAM USING PERSISTENT SCATTERER INSAR (PS-INSAR)

ARLIANDY P. ARBAD^{1*} and WATARU TAKEUCHI²

¹Department of Civil Engineering, The University of Tokyo, Tokyo, Japan,

²Institute of Industrial Science, The University of Tokyo, Tokyo, Japan,

*Correspondence: arliandyarbad@g.ecc.u-tokyo.ac.jp

Keywords: Structural health monitoring, InSAR, Subsidence, GNSS, Jatiluhur Dam

1. INTRODUCTION

Dams are vital for water management, flood control, and clean energy production [1]. The stability of dam structures is critical, as failure can lead to catastrophic consequences. Recent extreme weather events caused failures of the Derna Dam in Libya and the Arbaat Dam in Sudan. This study aims to enhance the structural health monitoring of Jatiluhur Dam using InSAR time-series analysis. Jatiluhur Dam, located on the Citarum River in Purwakarta, West Java, is Indonesia's oldest and largest concrete-faced, earth-filled dam. The dam faces challenges from sedimentation, land-use changes, and proximity to active faults, highlighted by a 5.6 earthquake near Cianjur in November 2022.

2. DATA AND METHOD

A total of 64 Sentinel-1 ascending SAR images from ESA were utilized, covering the Jatiluhur Dam area from January 2019 to June 2024. The SAR data was processed using the Persistent Scatterer Interferometry (PS-InSAR) technique in SARPROZ [2], focusing on stable ground features. GNSS data from the CPWK station, spanning January 2021 to December 2023, were obtained from the InaCORS, provided by BIG, and processed using Bernese GNSS software 5.2 to obtain daily coordinate solutions in the ITRF2014 reference frame [3] through a double-difference positioning approach. The combination of PS-InSAR and GNSS allowing cross-validation between satellite and ground-based measurements.

3. RESULT AND DISCUSSION

The processed area in Figure 1 shows extensive subsidence, with most points displayed in red to yellow on the color scale, indicating negative velocity values, especially around the main structure of Jatiluhur Dam. This analysis uses high coherence values to ensure reliable ground deformation detection. The GNSS monitoring point, marked by a red star, is strategically placed to validate the InSAR results.

As shown in Figure 2, GNSS measurements indicate an annual vertical displacement rate of -6.382 mm/year, compared to -1.5 mm/year from

LOS displacement of PS InSAR, both indicating subsidence, though GNSS reveals a more significant vertical displacement. A coordinate shift observed in the GNSS data in late 2022, likely due to data collection issues or an antenna change, was corrected using an offset technique to maintain data consistency.

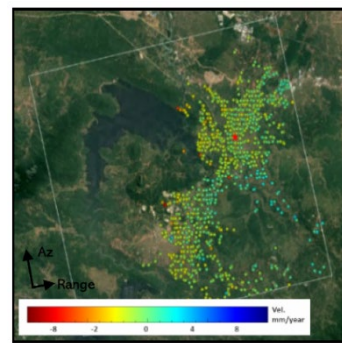


Figure 1. Ground deformation rates derived from PSI

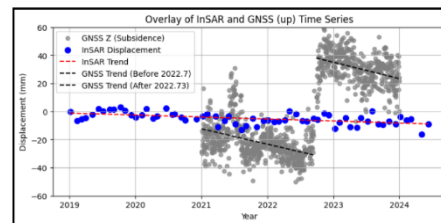


Figure 2. Comparison results between InSAR and GNSS

The detailed analysis of PS-InSAR results on the Jatiluhur Dam structure indicates significant deformation, with subsidence rates of approximately -6 mm/year on the western embankment and main spillway, as shown in Figure 3. This deformation has led to a cumulative displacement of 36.5 mm from 2019 to 2024, which may compromise the dam's structural integrity. Areas with significant subsidence require further examination, as they may indicate early instability affecting the dam's safety.

4. CONCLUSION

PSI was employed to monitor displacement in the Jatiluhur Dam, revealing significant subsidence, particularly in the embankment area. This indicates

non-uniform settlement across the structure and seasonal deformation likely influenced by rainfall, sediment load, and water levels. Future analysis will incorporate different orbital data for a more comprehensive stability assessment.

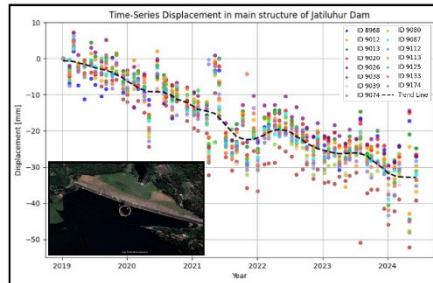


Figure 3. Time-series displacement over the main structure

REFERENCES

- [1] Wang, S., et al. (2024). Displacement observation data-based structural health monitoring of concrete dams: A state-of-art review. In Structures (Vol. 68, p. 107072). Elsevier.
- [2] Website: SARPROZ © – The SAR PROcessing tool by periZ
- [3] Alif, S. M., Ching, K. E., Sagiya, T., & Wahyuni, W. N. (2024). Determination of Euler pole parameters for Sundaland plate based on updated GNSS observations in Sumatra, Indonesia. *Geoscience Letters*, 11(1), 16.

OUT-OF-PLANE BEHAVIOUR OF MASONRY WALL STRENGTHENED USING TEXTILE REINFORCEMENT

R. SIVA CHIDAMBAARAM^{1*}, S.SARANYA¹, AJAY CHOURASIA² and R. PRADEEP KUMAR¹

¹ACSC Group, CSIR-CBRI, Roorkee, India,

²SEC Group, CSIR-CBRI, Roorkee, India

*Correspondence: schidambaram@cbri.res.in, krsinelastic@gmail.com

Keywords: Out-of-plane, flexural strength textile reinforcement, geo-grid, masonry walls

1. GENERAL INTRODUCTION

Masonry structures are durable and represent one of the oldest and most widely used construction techniques globally [1]. Masonry walls are composite in nature, with bricks being the main material bonded with mortar [2]. The wide availability of materials and easy construction processes make masonry a preferred choice worldwide. Masonry structures exhibit a box action when connected with the adjacent walls, allowing them to resist compressive loads effectively.

However, they have zero or little tension-bearing capacities [3], which disrupts the box action, especially out-of-plane, making them prone to collapse during earthquakes. Various studies have been carried out to improve the response of brick walls to seismic events. Typically, ductility is imparted to the structures by repointing or jacketing with rebars, but these methods are time-consuming and uneconomical. In new constructions, confined masonry is preferred to enhance structural response in earthquake-prone zones.

Nevertheless, retrofitting strategies using Welded Wire Meshes (WWM) and Fiber Reinforced Polymers (FRP) are employed for the existing masonry structures. FRPs are known for its high strength, high stiffness-to-weight ratio, and ease of use. Fiber Reinforced FRPs are commonly found as laminates and strips and are fixed to the masonry substrates, commonly using epoxy resins. FRP-epoxy resin combination loses adhesion in the presence of moisture, and WWMs are prone to corrosion with time.

To overcome the disadvantages of FRP and WWM, the concept of Textile Reinforced Mortar (TRM) has gained attention in masonry strengthening studies. TRM employs textiles made of different materials like carbon, aramids, glass, and polymers. embedded in a cementitious matrix. TRM is preferred due to its lightweight, cost-effectiveness, and suitability for application in wet areas, unlike FRPs. One such polymer textile is "Geo-grids," which are primarily used in non-structural applications like subsoil protection and slope stabilization [4]. Geo-grids possess higher strain than other textiles commonly used in the

strengthening process. This study replaced the commonly used textiles with uniaxial geo-grids of various grades. The effectiveness of strengthening the walls with geo-grids was analyzed using the load-deflection curve and energy dissipation behaviour after being subjected to a flexural test in a direction parallel to the load application. Strengthening the specimens with geo-grids resulted in better resistance to crack formation and improved the load-bearing capacity of the walls.

2. EXPERIMENTAL STUDY

2.1 Material properties

The single wythe wallet specimens were built using bricks of size 230mm × 110mm × 67mm. Monotonic compression tests were carried out on the bricks per the ASTM Standards in a Universal Testing Machine. The average compressive strength of the bricks was found to be 16.5 MPa. 1:4 cement sand mortar having 28-day average compressive strength of 7.9MPa was used. The tensile strength of the geo-grids is 300 kN/m and 400 kN/m respectively were used, according to ASTM D6637/D6637M-16.

2.2 Specimen configuration

Three categories of specimens have been considered for the study, with each specimen having dimensions of 800 mm × 490 mm × 140 mm. The specimens were categorized into FPL1, FPL2, and FPL3 based on the geo-grid strengthening configuration adopted and the type of test the specimens were subjected to. "FPL" refers to the Flexural Specimens Parallel to the Loading direction. The specimens in category FPL1 were cast without any external strengthening to replicate unreinforced masonry conditions, while the specimens in categories FPL2 and FPL3 were strengthened with uniaxial SGU300 and SGU400 geo-grids, respectively, only on tension sides. The unreinforced wall specimens were drilled and inserted with to 35mm long screws in a plastic sleeve to anchor the geo-grids externally. The specimen was then coated with a thin cement slurry, and the first 1:4 cement mortar layer was applied on top. Next, the specimen was U-wrapped with geo-grids,

and the anchorage setup was tightened, as shown in Figure 1, to ensure no movement.

The external strengthening process of the walls was completed by applying a second coat of cement slurry with another 1:4 cement mortar layer on top. The walls were cured for seven days before and after strengthening.



Figure 1. External strengthening of the wall with SGU300 grade geo-grid

3. EXPERIMENTAL SETUP

A four-point bending load configuration was assumed to examine the masonry walls' out-of-plane (OOP) behaviour. All the specimens were loaded parallel to the direction of the applied loading according to the ASTM E518/518-M10 standards, as depicted in Figure 2 (b). The test setup consisted of a vertically positioned actuator attached to a hydraulic jack within a 75T loading frame, as shown in Figure 2 (a). A 30T load cell and a ± 100 mm LVDT were connected to the actuator. The test was displacement-controlled at the rate of 1mm/min at the stroke level. Data collected from the load cell and the LVDT was recorded using a data acquisition system.

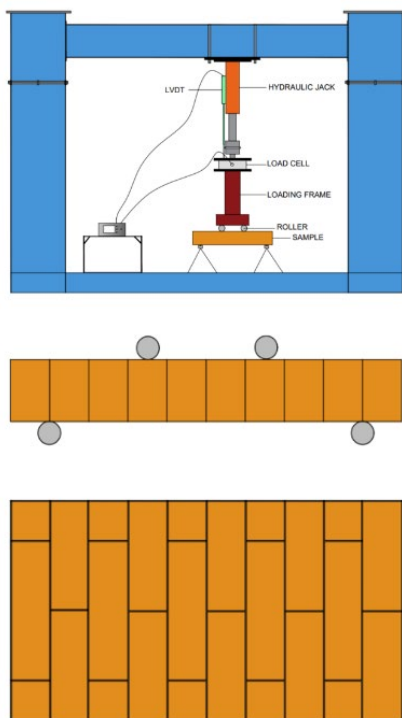


Figure 2. (a) Test setup (b) Loading pattern

4. RESULTS AND DISCUSSION

4.1 Load-deflection behaviour

The load-deflection behavior of the specimens FPL1, FPL2, and FPL3 is depicted in Figure 3. The strengthened specimens exhibited a load versus deflection pattern like the control specimen FPL1. The maximum load attained by the specimen FPL1 was 4.2 kN, after which it failed in a brittle manner.

The strengthened specimens FPL2 and FPL3 showed nearly a 350% and 550% increase in load-bearing capacity compared to FPL1, respectively, proving a more excellent performance of the walls due to external strengthening. The major crack for specimen FPL2 occurred at 21 mm deflection, followed by a rapid degradation in strength post-peak. Specimen FPL3 exhibited the highest peak load of 27.3 kN with a significant increase in residual strength compared to FPL1 and FPL2 in the post-peak region, depicting a ductile nature until failure. The primary reason for the failure was debonding in every specimen, with a flexural failure and partial rupture of geo-grids in the case of the strengthened specimens.

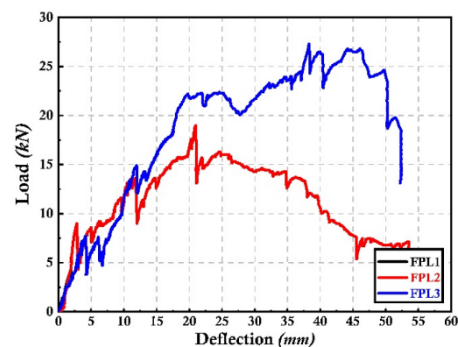


Figure 3. Load - deflection behaviour of FPL1, FPL2 and FPL3 specimens

4.2 Failure pattern

When compared to unreinforced specimens, FPL 2 and FPL 1 exhibits visible crack formation. As the deflection increases, multiple cracks formation was observed as shown in Figure 4.



Figure 4. Failure pattern of gird strengthened specimens

The higher strength of geo-grid in FPL 3, led the wall to experience higher deflection followed by spalling of cement mortar as shown in Figure 4. Both the strengthened specimens experienced ductile failure but none of the specimen experienced textile

yielding due to high strain nature of grid. It manifests that the strength plays vital role in capacity, but the strain plays crucial role in inelastic behavior and failure pattern.

4.3 Energy dissipation

The energy dissipated by a structure during the continuous action of lateral loads demonstrates the ductile nature of the specimen. Energy dissipation is calculated as the area under the load-deflection curve. The energy dissipated by the specimens in this study is presented in Figure 4. Each specimen in the study followed the same energy trend as the control specimen FPL1 in the initial stages. However, the least amount of energy was dissipated by the control specimen FPL1. The energy dissipated by the strengthened specimens increased approximately 127 times in FPL2 and 205 times in FPL3. This increased energy dissipation demonstrates the effectiveness of geo-grid strengthening in absorbing energy before collapse.

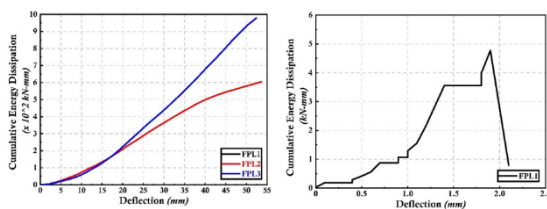


Figure 4. (left) Cumulative energy dissipation of strengthened specimens (right) Cumulative energy dissipation of control specimen

5. CONCLUSIONS

The flexural behaviour of three categories of single-wythe clay brick masonry walls was analyzed in this study. The walls under the category FPL1 were declared as control specimens, while those under FPL2 and FPL3 were strengthened with SGU300 and SGU400 grade uniaxial geo-grids only on the tension sides, respectively. The specimens were tested for flexural behaviour parallel to bending as per ASTM E518/518-M10 standards. The research compared the load versus deflection and energy dissipation characteristics of the control specimens to the strengthened specimens. The following conclusions were drawn from this study:

- External strengthening of the specimens delayed the occurrence of significant cracks and alters the failure pattern.
- The flexural behavior of the strengthened specimens exhibits better elastic and inelastic behavior over unreinforced specimen. FPL 2 & 3 have shown remarkable increase in post yield strength and deflection. It shows the efficiency of the high strain material in resisting the applied force with better inelastic resistance.

- The post yield behavior and ductile failure led the energy to dissipate higher than the unreinforced masonry. Textile having higher strength shows higher energy dissipation compared to specimen with lesser grid strength.
- Although the initial stiffness in the strengthened specimens followed the same trend, the wall strengthened with SGU400 showed increased stiffness and higher residual strength at higher deflections, indicating the robustness of the wall against lateral forces.

6. ACKNOWLEDGEMENTS

The authors express gratitude to CSIR-CBRI for granting permission to publish this work and acknowledge the financial support provided by CSIR (MLP). Appreciation is also extended to Ms. Strata Geosystems (India) Pvt. Ltd. for supplying geo-grids for the research. Special thanks are given to Mr. Vijay Tarun Kumar Moka for his support.

REFERENCES

- [1] Lourenço, P. B. et al. (2007), "Analysis of masonry structures: A review of and recent trends in homogenization techniques," *Canadian Journal of Civil Engineering*, Vol. 34, No. 11, pp. 1443–1457.
- [2] Shermi, C., and R. N. Dubey (2017) "Study on Out-of-Plane Behaviour of Unreinforced Masonry Strengthened with Welded Wire Mesh and Mortar," *Construction and Building Materials* 143: 104–20.
- [3] Thomoglou, Athanasia K., P. Jagadesh, and Maristella E. Voutetaki (2023) "Review of Out-of-Plane Strengthening Techniques of Unreinforced Masonry Walls," *Fibers* 11, no. 9: 78.
- [4] Siva Chidambaram, R., and Pankaj Agarwal. (2014) "The Confining Effect of Geo-Grid on the Mechanical Properties of Concrete Specimens with Steel Fiber under Compression and Flexure," *Construction and Building Materials* 71: 628–37.
- [5] D35 Committee. "Test Method for Determining Tensile Properties of Geogrids by the Single or Multi-Rib Tensile Method," ASTM International.
- [6] C15 Committee. "Test Methods for Flexural Bond Strength of Masonry," ASTM International.

SATELLITE IMAGERY METHOD FOR ESTIMATING CONSTRUCTION YEARS OF ROAD BRIDGES

K. MATSUMOTO¹ and B. HAMUNZALA²

¹*Division of Civil Engineering, Faculty of Engineering, Hokkaido University, Sapporo, Japan*

²*School of Engineering, Mulungushi University, Kabwe, Zambia*

*Correspondence: km312@eng.hokudai.ac.jp

Keywords: Satellite imagery, Road bridges, Construction years, NDWI_2, Cloud masking, STARS method

1. INTRODUCTION

Bridge aging is a global challenge, requiring efficient maintenance under limited budgets and personnel. Predicting future conditions based on inspection data and years since construction is effective, but many bridges lack known construction years, complicating rational maintenance efforts. Traditional methods like surveys and interviews are unreliable and labor-intensive.

Satellite data, such as from Landsat 5 and 7 (active since 1984), has been used to estimate construction years. However, challenges include noise from weather and seasonal changes and the absence of an objective determination method. This study refines these satellite-based techniques for clearer and more objective bridge construction year estimation.

2. SATELLITE IMAGERY METHOD FOR ESTIMATING CONSTRUCTION YEARS

Landsat 5 measures seven spectral bands, including visible light (blue, green, red) and infrared bands. Among various indices calculated from these bands [1], NDWI_2 (using near-infrared and mid-infrared 2) proved most effective for estimating bridge construction years, commonly used for identifying water surfaces. To minimize weather effects, data with over 30% cloud coverage was excluded using Cloud Masking, and annual averaging removed seasonal variations. The Sequential T-test Analysis of Regime Shift (STARS) method, a change-point detection technique, was introduced to objectively determine construction years (Figure 1).

3. APPLICATION TO NAGO CITY, JAPAN AND CAMBODIA

The proposed method was applied to 44 bridges in Nago City, Okinawa, Japan, with lengths of 100 meters or less, constructed between 1990 and 2006, achieving generally high accuracy in estimating construction years (Figure 2(a)). It was also applied to 423 Cambodian bridges with recorded construction years, yielding slightly lower but still reliable accuracy (Figure 2(b)). Compared to 88 bridges examined in previous research [2], the

STARS method provided more objective estimates and significantly enhanced accuracy.

4. CONCLUSIONS

A method for estimating the construction years of road bridges using satellite imagery has been developed. This method seems to enable objective estimation of construction years with a reasonable level of accuracy.

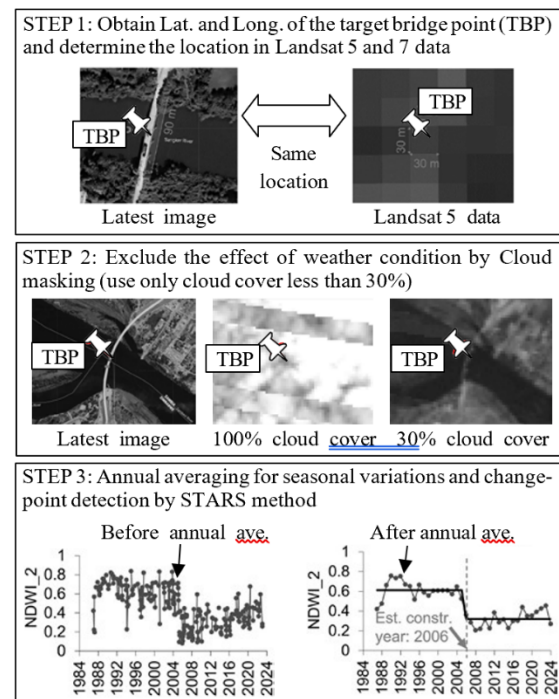


Figure 1. Procedure of construction year estimations

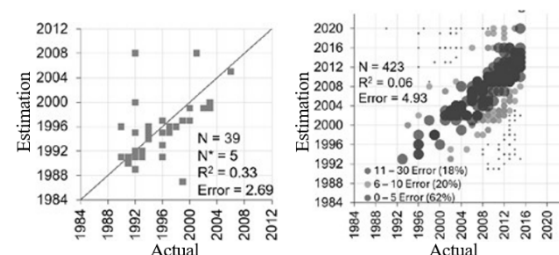


Figure 2: Validation results of (left) Nago city (right) Cambodia

REFERENCES

- [1] A.D. Prasad, P. Ganasala, Remote sensing satellite data and spectral indices: An initial evaluation for the sustainable development of an urban area, *Sustain. Water Resour., Manag.*, 2022.
- [2] E. Sovisoth, E. V.S. Kuntal, P. Misra, W. Takeuchi, K. Nagai, Estimation of Year of Construction of Bridges in Cambodia by Analyzing the Landsat Normalized Difference Water Index, *Infrastructures*, 8, 77, 2023.

DEEP LEARNING BASED APPROACHES FOR LANDSLIDE DETECTION

P. SHARMA, S. DAS, A. PAIN and D.P. KANUNGO

CSIR-Central Building Research Institute, Roorkee, India
Correspondence: priyanka.cbri20a@acsir.res.in

Keywords: Landslide inventory, Deep learning models, Sentinel-2 images, QGIS software, ResNet-50, ResU-Net

1. INTRODUCTION

Landslides have been marked as one of the major natural hazards around the globe. India is one of the major landslide hotspots and bears a loss of around 1.5 billion annually (National Landslide Risk Management Strategy 2019, Government of India). Every year, occurrence of these landslides causes losses of life and property [1,2]. Landslides are geologically complex hazards that occurs due to collective effect of slope, elevation, NDVI, fill DEM, curvature etc. [3]. To minimize landslide susceptibility, hazard and risk assessment is practiced by the researchers [4,5]. Landslide information in an inventory is critical for landslide risk assessment and mitigation. It contains information on the type of movements in the past, spatial location and total affected area [6].

To prepare a landslide inventory, experts rely on the visual inspection and cognitive interpretation of the set of optical-hyperspectral satellite images. However, it is a skill-intensive and time-consuming process, where each identified landslide is manually traced using geographic information system (GIS). Hence, to produce reliable landslide inventory researchers have been working on approaches without human intervention [5]. Researchers have developed different semi- supervised deep learning models to detect landslides from satellite images [7].

The detection process is either based on pixel-based image analysis (PBIA) or object-based image analysis (OBIA). The limitations to the already developed deep learning models are that they are studied using expensive commercial satellite images to detect landslide. Also, DL models are difficult to run on ordinary CPU aided local machines. With these considerations the objective of the study is to develop deep learning models for landslide detection by utilizing freely available open-source resources.

Two different pretrained deep learning models ResNet-50 and ResU-Net have been modified and employed for the detection. Further, the model performance is evaluated and the comparisons between the models are made. To execute this methodology, the landslides of Malappuram district of Kerala during the monsoon period of 2018-2019 have been used as training and testing samples for the DL models.

2. SITE STUDY

The present study considers the landslides of Northern hills of Malappuram district of Kerala, India that covers an area of 185 km². The area receives an average rainfall of about 2800 mm with annual temperature of 26° to 38°C. The slope of the area is with an angle of 26° and the elevation is about 82 to 2569 m. The subsurface lithology of the area belongs to Meta-volcanic rocks with abundant concentration of lineaments. In the monsoon period of year 2018 and 2019, due to extensive rainfall, many landslides had triggered and caused severe damage with fatalities. As per the landslide classification by [8] the landslides reported in this area mainly belong to debris flows and debris slides.

3. METHODOLOGY

For landslide detection, the present study considers ResNet-50 and ResU-Net models. A comparison of the model performance is done for the two models. The two models used are modified pretrained models.

The model training and implementation of these models using an ordinary computer system takes excessive time. To overcome this situation, the present attempt utilizes Google collaborator also known as Google Colab which is an open-source cloud computing servers. For the data processing and their spatial representation, the Quantum Geographic Information System (QGIS) software is used. For mapping the landslides freely available Sentinel-2 image is used (downloaded from Copernicus Open Access Hub). An RGB composite image is produced by stacking bands 2, 3 and 4.

The selected area is divided into two zones namely training and testing zones which covers an area of 117 km² and 68 km² respectively. The RGB image is used to map the identified landslides in the area in polygon-based vector format. While drawing polygons, the cognitive interpretation of colour, tone, texture, slope and association are considered.

The interpretation of landslides in these images are made considering certain assumptions such as: (1) landslides doesn't occur in flat areas (2) landslide occurrence leaves distinct signatures in the ground by removing surface cover and vegetation (3) landslides formed in general has a distinct shape typically semi elliptical.

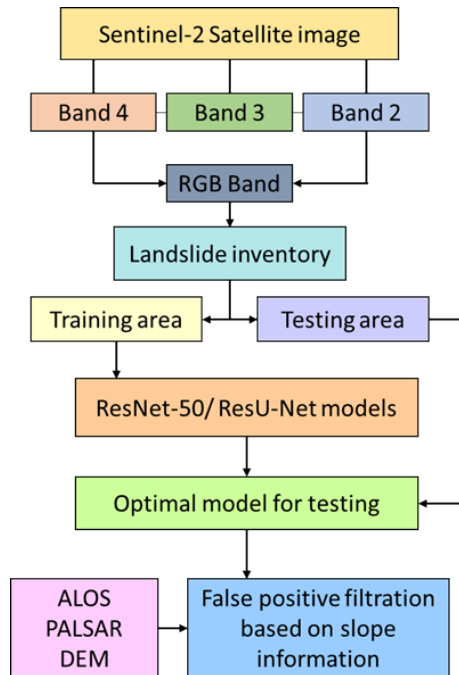


Figure 1. Flowchart of proposed methodology

The landslides in the present study are event-based landslides as they were triggered during the monsoon periods in 2018 and 2019. Figure 1. presents the adopted methodology using different DL models to detect landslides.

4. RESULTS AND DISCUSSION

4.1 Model Implementation

The landslide area drawn in the polygon format are imported in the Google Colab and used for training the different DL models. Different python libraries such as Rasterio, Geopandas, Keras, Tensorflow are used in model training. The RGB images used for model training follow certain steps to be used as information to the models. The first step is generation of binary mask images from the RGB images. This is followed by a patch generation step. Patches of size 128x128 are produced and are converted to NumPy arrays. These arrays are formed to reduce the computation time. The generated .npy file is directly used for model training.

4.2 Detection Accuracy

The accuracy assessment was done for the detected landslides in the testing area. The clip and erase analysis tools in QGIS software were used to determine the TN, TP, FN and FP rates. Figure 2. Shows the detection of landslides for the test data samples using both the models. It can be clearly observed that the results of the ResU-Net model are close to the landslides marked in the ground truth or actual image. The ResNet-50 model has been able to detect a very small area of landslide. The rest of

the area remains undetected. Based on this, the results obtained for the test dataset are shown in Table 1.

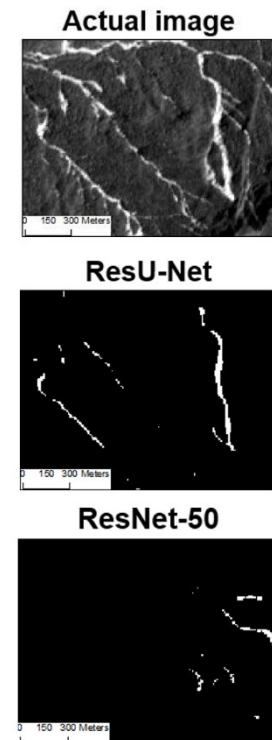


Figure 2. Landslide detection results of test dataset

Table 1. Landslide detection accuracy for different DL models

Accuracy Parameters	Models	
	ResNet-50	ResU-Net
F1 score	0.67	0.78
Precision	0.91	0.95
Recall	0.74	0.79

5. CONCLUSIONS

The landslide inventory is important to know the affected landslide areas for aiding post-disaster recovery in large areas. To generate landslide inventories for newly affected areas becomes a tedious task and needs a lot of time and skills. In this study, the application of DL models for detecting landslides using open-source resources are presented. Following are some conclusions drawn from the present study.

1. ResU-Net models have performed better detection than the ResNet-50 model.
2. Higher number of landslide samples for training may increase the model performance.
3. Images of greater resolution can also lead to better detection accuracy.

REFERENCES

- [1] Martha, Tapas R., Norman Kerle, Cees J. Van Westen, Victor Jetten, and K. Vinod Kumar.

- "Object-oriented analysis of multi-temporal panchromatic images for creation of historical landslide inventories." *ISPRS journal of photogrammetry and remote sensing* 67 (2012): 105-119.
- [2] Pain, A., D. P. Kanungo, and S. Sarkar. "Rock slope stability assessment using finite element based modelling—examples from the Indian Himalayas." *Geomechanics and Geoengineering* 9, no. 3 (2014): 215-230.
- [3] Li, Penglei, Yi Wang, Guosen Xu, and Lizhe Wang. "LandslideCL: towards robust landslide analysis guided by contrastive learning." *Landslides* 20, no. 2 (2023): 461-474.
- [4] Chen, Hesheng, Yi He, Lifeng Zhang, Sheng Yao, Wang Yang, Yumin Fang, Yaoxiang Liu, and Binghai Gao. "A landslide extraction method of channel attention mechanism U-Net network based on Sentinel-2A remote sensing images." *International Journal of Digital Earth* 16, no. 1 (2023): 552-577.
- [5] Martha, Tapas R., Norman Kerle, Victor Jetten, Cees J. van Westen, and K. Vinod Kumar. "Characterising spectral, spatial and morphometric properties of landslides for semi-automatic detection using object-oriented methods." *Geomorphology* 116, no. 1-2 (2010): 24-36.
- [6] Amatya, Pukar, Dalia Kirschbaum, and Thomas Stanley. "Rainfall-induced landslide inventories for Lower Mekong based on Planet imagery and a semi-automatic mapping method." *Geoscience Data Journal* 9.2 (2022): 315-327.
- [7] Meena, Sansar Raj, Lucas Pedrosa Soares, Carlos H. Grohmann, Cees Van Westen, Kushanav Bhuyan, Ramesh.
- [8] Cruden, David Milne. "Cruden, DM, Varnes, Dj, 1996, landslide types and processes, transportation research board, us national academy of sciences, special report, 247: 36-75." *Transp Res Board* 247 (1996): 36-57.
- [9] P. Singh, Mario Floris, and Filippo Catani. "Landslide detection in the Himalayas using machine learning algorithms and U-Net." *Landslides* 19, no. 5 (2022): 1209-1229.

Plantation Studies
Volume 1 "Proceedings of the 3rd International Symposium on One Health, One World (OHOW2024)
10-12 December 2024
Putrajaya, Malaysia"

e ISBN 978-629-95253-0-1



Institut Kajian Perladangan

(online)